ESCAPE

33RD EUROPEAN SYMPOSIUM ON COMPUTER-AIDED PROCESS ENGINEERING

GREEN AND SUSTAINABLE PROCESS SYSTEMS ENGINEERING IN THE DIGITAL AGE

ATHENS - GREECE
Royal Olympic Hotel

Extended Abstracts

18-21 JUNE 2023

ESCAPE

EFCE

www.escape33-ath.gr

THEME 1
Modelling and optimization for multi-scale integration

Paper 55	Methane decomposition in a molten-metal bubble column reactor using VOF-CFD model: Hydrodynamics and bubble determination	4
Paper 81	Automatic reformulation of nonlinear programs to reduced space for global optimization	6
Paper 97	Modeling and optimization of cascade reactions of enzymes immobilized in porous particles	8
Paper 99	One-dimensional kinetic model with axial dispersion of a molten-metal bubble column reactor for decomposition of fluorinated gases	10
Paper 108	In silico solvent Selection for optimum lignin depolymerisation process	12
Paper 169	Modelling of energetically efficient hybrid method for separation of ethanol-water mixture	14
Paper 189	Effect of electromagnetic fields on hydrodynamics of bubbles in a molten-metal bubble column reactor using CFD simulation	16
Paper 323	Graph based fault detection and root cause analysis in process manufacturing	18
Paper 374	Numerical investigation of exact designs in optimal experiment campaigns	20
Paper 424	Multi-scale integration and multi-objective optimization of the hydrogen network in an oil refinery	22
Paper 538	Computationally efficient gas flow models for energy system optimization	24
Paper 569	A Pareto aggregation approach for environmental-economic multi-objective optimization problems validated on a second-generation bioethanol production model	26
Paper 655	Open source software for flowsheet modeling of solids processes	28
Paper 677	Reaction kinetics modeling using bayesian symbolic regression	30
Paper 697	Closing the balance- the pulp industry as a prosumer in the energy	32
Paper 725	Hybridization of analytical surrogates with first principles using bayesian learning	34
Paper 830	Data embedding and hybrid modeling for industrial fluid catalytic cracking	36
Paper 866	Improvement of probability distribution estimation using method of moments with Lagrange interpolation approach	38

Methane decomposition in a molten-metal bubble column reactor using VOF-CFD model: Hydrodynamics and bubble determination

Son Ich Ngo[a], Bang Thanh Le[a], Hanh T.H. Bui[a], Mazhar Ali[a], Young-Il Lim[a]
[a]Center of Sustainable Process Engineering (CoSPE), Department of Chemical Engineering, Hankyong National University, Gyeonggi-do, Anseong-si, Jungang-ro 327, 17579 Korea

Abstract: Molten-metal bubble column reactors (MMBCR) have been used for cleaner H2 production processes from CH4 pyrolysis. A volume of fluid computational fluid dynamics (VOF-CFD) model coupled with a large eddy simulation (LES) turbulence model was employed to simulate the hydrodynamics of molten-Sn/CH4/H2 system at 900 oC and bubbling regime. The surface tension force and wall adhesion force were implemented to capture the bubble shape and size of MMBCR. An ideal gas density was applied for the gas mixture. The reactor pressure drop was about 0.21 bar. A minor effect of ideal gas density on the hydrodynamics was found compared with constant gas density in a previous study (Ngo et al., 2023).

Keywords: Molten-metal bubble column reactor, Hydrogen production, Computational fluid dynamics, Volume of fluid, Gas-liquid interfacial area.

Introduction

Besides steam methane reforming with carbon capture and storage, an alternative approach for low-carbon H2 production is non-oxidative CH4 pyrolysis using a molten metal bubble column reactor (MMBCR) (Catalan and Rezaei, 2020; Ngo et al., 2023). Separable highly economical solid carbon and H2 are obtained via CH4 pyrolysis in a MMBCR without CO2 emissions (Upham et al., 2017). However, important factors of MMBCR such as hydrodynamics, bubble size distribution, bubble velocity, and gas-liquid specific interfacial area are difficult to determine by experiments. The computational fluid dynamics volume-of-fluid (VOF-CFD) model has been used for characterizing bubbles in conventional chemical processes (Nguyen et al., 2022) as well as MMBCR (Ngo et al., 2023). The combination of the VOF-CFD model and a bubble detection algorithm provided the bubble characteristics in MMBCRs under an incompressible and isothermal condition.

This study aims to develop a non-isothermal ideal-gas VOF-CFD model coupled with a large-eddy simulation (LES) turbulence model for CH4 pyrolysis in a Sn-MMBCR. The bubble detection algorithm (Ngo et al., 2023) was applied for calculating the bubble size distribution, bubble velocity, and specific interfacial area. The effect of ideal gas density on hydrodynamics and bubble characteristics is investigated.

VOF-CFD model

The transient VOF-CFD model includes a single set of continuity and Navier-Stokes momentum equations weighted by the gas volume fraction. The LES turbulence model with wall adapting local eddy (WALE) sub-grid scale model was applied to the gas phase (CH4, H2) while the surface tension force and wall adhesion force models were considered in the liquid phase (molten Sn) (Ngo et al., 2023; Nguyen et al., 2022). A summary of the VOF-CFD model is shown in Fig. 1.

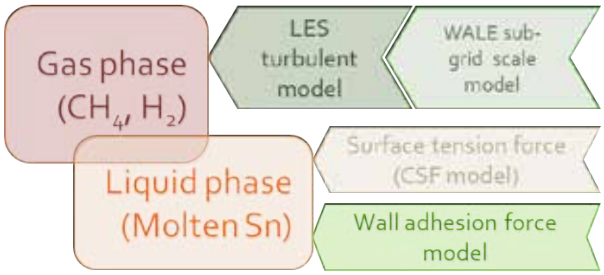

Fig. 1. VOF-CFD model description

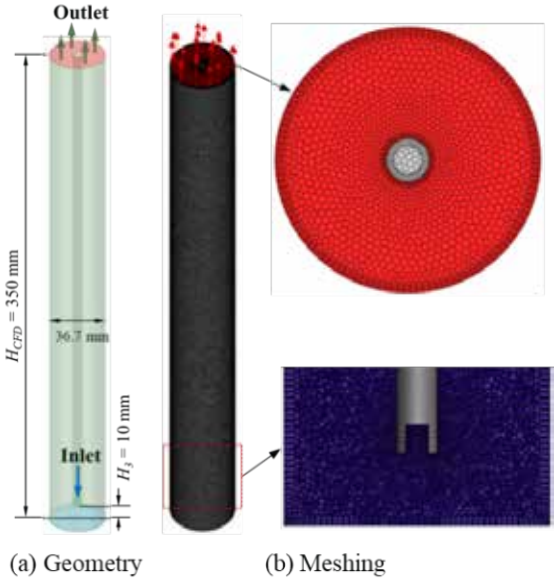

The VOF-CFD model geometry and meshing are shown in Fig. 2. A lab-scale MMBCR geometry (H = 350 mm, D = 36.7 mm) (Ngo et al., 2023) was used. The mesh number of around 1.8 million cells (mean cell size = 0.7 mm) was suitable to capture more than 80% of volume-averaged turbulence kinetic energy of direct numerical simulation (DNS).

Fig. 2. (a) Geometry and (b) meshing for VOF-CFD model.

Results and discussions

Contours of pressure, liquid velocity, flow streamline, gas volume fraction, bubble shapes, and gas density are depicted in Fig. 3. The reactor pressure drop is approximately 0.21 bar. The liquid velocity surrounding bubbles is significantly promoted. The bubble shape varies from sphere to ellipsoidal cap according to their surrounding liquid velocity. The mean gas density showed a similar value to (Ngo et al., 2023). A minor effect of ideal gas density on hydrodynamics was observed.

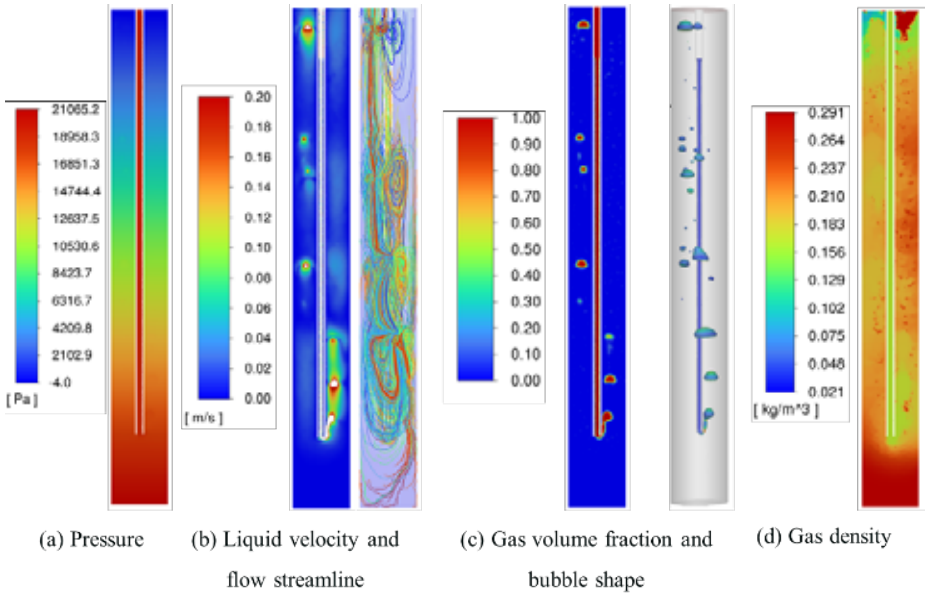

Fig. 3. Contours of (a) pressure, (b) liquid velocity, and (c) gas volume fraction.

Conclusions

A computational fluid dynamics volume-of-fluid (VOF-CFD) coupled with a large eddy simulation (LES) turbulence model was developed for a molten-metal bubble column reactor (MMBCR) to produce H2 from non-oxidative CH4 pyrolysis. Hydrodynamics and bubble characteristics such as bubble shape and size were well captured by the VOF-CFD model. A minor effect of ideal gas density on hydrodynamics was observed.

Acknowledgments

This work was supported by a National Research Foundation of Korea (NRF) grant funded by the Korean Government (MSIT; No. 2021M3I3A1084950 and 2021R1A2C1011618).

References

Catalan, L.J.J., Rezaei, E., (2020). Coupled hydrodynamic and kinetic model of liquid metal bubble reactor for hydrogen production by noncatalytic thermal decomposition of methane. Int. J. Hydrog. Energy 45(4), 2486-2503.

Ngo, S.I., Lim, Y.-I., Kwon, H.M., Lee, U.-D., (2023). Hydrodynamics of molten-metal bubble columns in the near-bubbling field using volume of fluid computational fluid dynamics. Chem. Eng. J. 454, 140073.

Nguyen, L.X., Ngo, S.I., Lim, Y.-I., Go, K.-S., Nho, N.-S., (2022). Hydrodynamics of gas-liquid bubble columns under bubbling, transient, and jetting flow regimes using volume of fluid computational fluid dynamics. Chem. Eng. Res. Des. 182, 616-628.

Upham, D.C., Agarwal, V., Khechfe, A., Snodgrass, Z.R., Gordon, M.J., Metiu, H., McFarland, E.W., (2017). Catalytic molten metals for the direct conversion of methane to hydrogen and separable carbon. Science 358(6365), 917-921.

Automatic reformulation of nonlinear programs to reduced space for global optimization

Dominik Bongartz[a,b,c], Constantinos C. Pantelides[b], Benoît Chachuat[b]
[a] Department of Chemical Engineering, KU Leuven, Belgium
[b] Sargent Centre for Process Systems Engineering, Department of Chemical Engineering, Imperial College London, United Kingdom
[c] Process Systems Engineering (AVT.SVT), RWTH Aachen University, Germany

Abstract: Reduced-space formulations have been proposed as a way of accelerating global optimization of nonconvex nonlinear programs. In these formulations, variables are eliminated from the problem using equality constraints. However, existing approaches mostly rely on manual reformulation. In this contribution, we introduce an automated approach to reduced-space reformulation. The approach builds on methods for tearing of nonlinear equation systems. It involves analyzing the computational graph of the problem regarding solvability of individual constraints, as well as analyzing the sparsity pattern of the constraints to identify in which order to evaluate equalities to eliminate variables. We demonstrate the approach on a number of case studies to evaluate its performance and discuss its benefits and limitations.

Keywords: Global optimization, Tearing, Sparsity.

Introduction

Many problems in process design and operation result in nonconvex nonlinear programs (NLPs). Guaranteeing optimal solution for such problems requires the use of deterministic global optimization methods. However, the latter are computationally expensive, and many problems of practical interest are still intractable. One way to accelerate global optimization is to make use of reduced-space formulations, which exploit equality constraints to eliminate variables from the optimization problem (Mitsos et al., 2009). These reformulations have been shown to enable drastic reductions in computational time for problems with certain special structure such as difference equations or discretized differential equations (Mitsos et al., 2009), flowsheet optimization (Byrne & Bogle, 2000; Bongartz & Mitsos, 2017), and machine-learning surrogates (Schweidtmann & Mitsos, 2019). So far, however, the reformulation needs to be implemented manually by the modeler, which is a major obstacle for broader application of the approach. In this work, we aim at automating the reformulation to reduced space through explicit elimination of variables for more general NLPs.

Method

We consider NLPs of the form

$$\begin{aligned} &\min_x f(x) \\ &s.t.\ h(x) = 0 \\ &\quad g(x) \le 0 \\ &\quad x \in [x^L, x^U] \subset R^n, \end{aligned} \tag{1}$$

where f, h, and g are factorable functions, that is, finite compositions of simple, so-called intrinsic functions (McCormick, 1976).

To construct a reduced-space formulation of Problem (1), we aim at identifying a partition of the variables x into those to be eliminated (denoted by x_{el}) and those to remain in the problem (denoted by x_{rem}), as well as a reformulation of the equality constraints such that we can express x_{el} as a factorable function of x_{rem}: $x_{el} = \hat{h}_{el}(x_{rem})$. This results in a smaller problem, with only x_{rem} as variables:

$$\begin{aligned} &\min_{x_{rem}} f\left(x_{rem}, \hat{h}_{el}(x_{rem})\right) \\ &s.t.\ \tilde{h}_{rem}\left(x_{rem}, \hat{h}_{el}(x_{rem})\right) = 0 \\ &\quad \tilde{g}\left(x_{rem}, \hat{h}_{el}(x_{rem})\right) \le 0 \\ &\quad x_{rem} \in [x^L_{rem}, x^U_{rem}] \subset R^{n_{rem}}. \end{aligned} \tag{2}$$

The elimination with a factorable function bears strong similarities with tearing of nonlinear equation systems, for which there is a large body of literature – see Baharev et al. (2016) for a recent survey. Building on these methods, we propose a four-step approach:

1. Identify which equality constraints can be solved analytically for which variables.
2. Determine the order to process the equality constraints to minimize the number of remaining variables based on the method of Hernandez & Sargent (1979).
3. Select which variables to eliminate through reordering the incidence matrix to bordered lower-triangular form.
4. Rearrange the optimization problem accordingly, and introduce new (possibly nonlinear) inequality constraints to account for the variable bounds of the eliminated variables x_{el}.

Implementation & Case Studies

The method is implemented in the open-source optimizer MAiNGO (Bongartz et al., 2018) based on the library MC++ (Chachuat et al., 2015). For Step 1, a new arithmetic is developed that evaluates the graph representation of the problem in MC++ to collect information about the occurrence of variables, and identifies which variables can be solved for analytically. This involves identifying whether a variable occurs only once in a given constraint and whether all intrinsic functions it occurs in are invertible. For Step 2, a greedy heuristic is favored due to the excessive computational demand of exact methods (Baharev et al., 2016). Step 3 performs a lexicographic selection for simplicity, since for a given evaluation order this selection does not impact the number of remaining variables. In Step 4, the graph is rearranged to yield the new problem by recursively replacing the variables with their defining expressions derived from the equality constraints. In this proof-of-concept implementation, Steps 1 and 4 are limited to eliminating variables that occur linearly in the corresponding constraint used for the elimination, but could potentially participate nonlinearly in other constraints or in the objective function.

The method is demonstrated on case studies taken from previous work on reduced-space formulations (in which these were derived manually), including flowsheet optimization (Bongartz & Mitsos, 2017) and problems with artificial neural networks (Schweidtmann & Mitsos, 2019), as well as problems from common benchmark libraries. The computational effort of solving the automatically constructed version of Problem (2) is compared to that of solving the original Problem (1) as well as solving variants of Problem (2) derived manually based on problem insight.

Conclusion & Outlook

A method automatic reformulation of NLPs into reduced space is presented with the aim of accelerating global optimization of a wide class of problems by exploiting the sparsity patterns of equalities and variables. While the current implementation demonstrates the workflow and tractability of the approach, it is still limited in the type of problem structures it is applicable to. Furthermore, alternative methods for selecting which variables to eliminate could help better balance problem size versus tightness of relaxations and allow elimination of variables beyond the single-variable-single-equation approach of tearing methods (Hernandez & Sargent, 1979).

Acknowledgments

This work was supported by a postdoc fellowship of the German Academic Exchange Service (DAAD)". Funding by the Engineering and Physical Sciences Research Council (EPSRC) under grant EP/W003317/ is gratefully acknowledged.

References

Baharev, A., Schichl, H., Neumaier, A. (2016). Tearing systems of nonlinear equations I. A survey. https://www.mat.univie.ac.at/~neum/ms/tearing_survey.pdf

Bongartz, D., Mitsos, A. (2017). Deterministic global optimization of process flowsheets in a reduced space using McCormick relaxations. J. Glob. Optim., 69, 761.

Bongartz, D., Najman, J., Sass, S., Mitsos, A. (2018). MAiNGO – McCormick-based Algorithm for mixed-integer Nonlinear Global Optimization, Process Systems Engineering (AVT.SVT), RWTH Aachen University, http://permalink.avt.rwth-aachen.de/?id=729717.

Byrne, R. P., Bogle, I. D. L. (2000). Global optimization of modular process flowsheets. Ind. Eng. Chem. Res., 39, 4296.

Chachuat, B., Houska, B., Paulen, R., Peric, N., Rajyaguru, J., Villanueva, M. E. (2015). Set-theoretic approaches in analysis, estimation and control of nonlinear systems. IFAC-POL, 48, 981. https://github.com/omega-icl/mcpp

Hernandez, R., Sargent, R. W. H. (1979). A new algorithm for process flowsheeting. Comp. Chem. Eng., 3, 363.

McCormick, G. P. (1976). Computability of global solutions to factorable nonconvex programs: Part I—Convex underestimating problems. Math. Prog., 10, 147.

Mitsos, A., Chachuat, B., Barton, P. I. (2009). McCormick-based relaxations of algorithms. SIAM J. Optim., 20, 573.

Schweidtmann, A., Mitsos, A. (2019). Deterministic global optimization with artificial neural networks embedded. J. Opt. Theo. Appl., 180, 925.

Modeling and optimization of cascade reactions of enzymes immobilized in porous particles

Leandros Paschalidis[a], Jakob Burger[b]
[a]Laboratory of Chemical Process Engineering, Technical University of Munich, Campus Straubing for Biotechnology and Sustainability, Uferstraße 53, 94315.
[b]SynBioFoundry@TUM, Technical University of Munich, Campus Straubing for Biotechnology and Sustainability, Schulgasse 22, 94315, Straubing, Germany

Abstract: Cascade reactions catalyzed by enzymes immobilized in porous particles is an emerging and environmentally friendly method to produce a variety of chemicals starting from renewable resources. Selecting an appropriate spatial immobilization strategy (SIS) inside the pores is an important step when designing such reaction processes. Model-based optimization can support the selection of a SIS. In the present work, a framework for modeling and optimizing such reaction processes was developed. This framework can be applied to simulate, optimize and select an optimal SIS for a given system of enzymes and porous particles. This is demonstrated in the present work for a selected problem.

Keywords: Enzymatic cascade, immobilization, combinatorial optimization, model-based optimization

Introduction

Enzymatic reactions are promising alternatives to complex chemical syntheses or microbial bioreactors, as they use milder reaction conditions or allow for systematic optimization of selectivity and yield. An enzymatic cascade combines two or more enzyme-catalyzed steps without isolating the intermediates. A lot of research currently aims at the co-immobilization of several enzymes of a cascade onto porous particles. This approach promises improved enzyme stability, facilitated catalyst separation, and, not least, faster kinetics through spatial clustering of different enzymes inside pores (Arana-Peña et al., 2021; Bié et al., 2022). A series of exciting questions arose and remain unsolved: When is it advantageous to co-immobilize different enzymes inside one pore compared to immobilizing them in separate pores/particles? How significant is this advantage? What is the optimal spatial distribution of the various enzymes inside the pores? Experimental studies are cumbersome and require enormous effort. Theoretical approaches that could guide experiments and improve understanding are yet missing. In the present work, we go the first steps toward such a theory. Inspired by classical approaches from chemical catalysis, we derive a quasi-steady-state, reaction-diffusion model for the porous particles and embed it into the material balances of a batch reactor with dispersed particles or a tubular reactor with a fixed bed. The model is flexible and computationally inexpensive, enabling us to evaluate and compare the performance of different immobilization strategies. E. g., we can compare the co-immobilization of two enzymes inside one pore vs. the separated immobilization in different pores. On the one hand, the developed theory provides a flexible model framework for experimental results for the kinetics of co-immobilized enzymatic cascades. On the other hand, the present work identifies general limitations of co-immobilized enzymes and guidelines for optimal spatial distribution. These general results include the maximum quantitive benefits of co-immobilization over separated immobilization as a function of reaction rate constants and diffusivities.

Methodology

We study dynamic, reaction processes in a batch reactor. A two-step enzymatic cascade takes place in the batch reactor, catalyzed by two enzymes immobilized inside the pores of porous particles. The model consists of dynamic material balances for the species in the batch reactor and material balances for the pores. The reaction macro kinetics are derived from the material balances around the pores by applying Fick's law at the beginning of the pores, following the ideas of Thiele (Thiele, 1934). Either Michaelis-Menten or first-order kinetics are used for the micro kinetic expressions. Several parameters appear in the model that can be fit to experiment or derived from literature. Parametric studies are applied to derive guidelines or general conclusions. The model equations are solved either computationally or when possible analytically to derive solutions for the macro kinetics and time profiles in the reactor.

We use the model to determine which spatial immobilization strategy (SIS), is better, between four options for a given system with known parameter values. The options are: single immobilization (each pore contains only one enzyme type), homogeneous co-immobilization (each pore contains two enzymes homogeneously distributed), heterogeneous co-immobilization with A first (enzyme A has a higher surface density at the beginning of the pore than enzyme B), and heterogeneous co-immobilization with B first (enzyme B has a higher surface density at the beginning of the pore than enzyme A).

To present results in brief, we solve a case study. The kinetics of the enzyme-catalyzed reactions are chosen to be fast compared to diffusion. The diffusivities of the educts and product are fast and the diffusivity of the intermediate is slow.

Results and discussion

The concentration profiles inside a batch reactor were calculated for all four considered options. Figure 1 shows the respective yields over time. Single immobilization performs significantly worse than all three co-immobilization SIS. This is due to the low diffusivity of the intermediate. In single immobilization SIS, the intermediate has to travel larger distances from the active site of the first enzyme to the active site of the second enzyme. Between the heterogeneous co-immobilization strategies, heterogeneous co-immobilization, with enzyme B first is the best strategy.

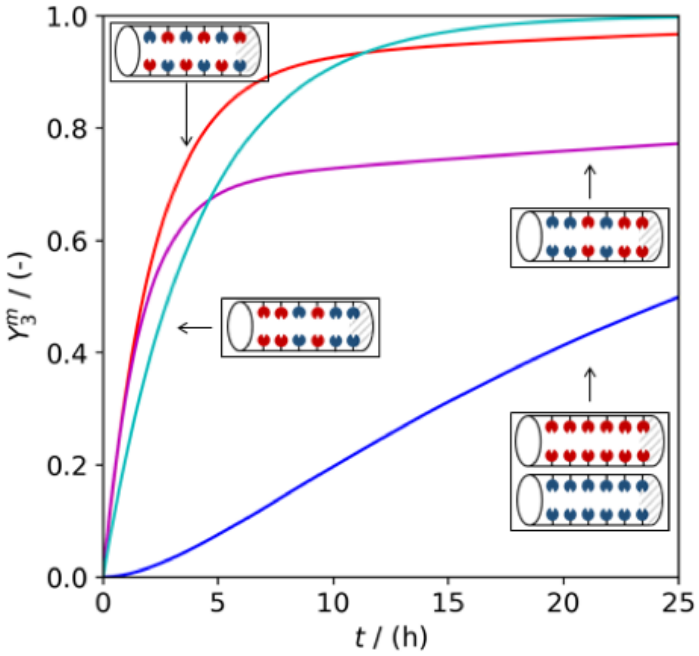

Figure 1. The yields achieved in the four studied options plotted against time.
Single immobilization,
Homogeneous co-immobilization,
Heterogeneous co-immobilization with A first,
Heterogeneous co-immobilization with B first.
Enzyme A is drawn with blue color while enzyme B is drawn with red color.

Conclusions

A modeling framework was developed for cascade reactions catalyzed by enzymes immobilized in porous particles. We demonstrated how it can be applied to select the best spatial immobilization strategy out of four options. For the studied case, heterogeneous co-immobilization with B first was found to be the optimal strategy.

References

Arana-Peña S., Carballares D., Morellon-Sterlling R., Berenguer-Murcia N., Alcántara A. R., Rodrigues R. C., Fernandez-Lafuente R. (2021), Enzyme co-immobilization: Always the biocatalyst designers' choice. . . or not?, Biotechnol. Adv. 51.

Bie J., Sepodes B., Fernandes P. C. B., Ribeiro M. H. L., (2022). Enzyme Immobilizaztion and Co-Immobilization: Main Framework, Advances and Some Applications. Processes 10, (3).

Thiele, E. W., (1934). Relation between Catalytic Activity and Size of Particle. Ind. Eng. Chem. Res., 31 (7), 916-920.

One-dimensional kinetic model with axial dispersion of a molten-metal bubble column reactor for decomposition of fluorinated gases

Bang Thanh Le[a], Son Ich Ngo[a], Hanh Thi Hong Bui[a], Mazhar Ali[a], Young-Il Lim[a], and Uen-Do Lee[b]
[a]Center of Sustainable Process Engineering (CoSPE), Department of Chemical Engineering, Hankyong National University, Republic of Korea
[b]Energy System R&D Group, Korea Institute of Industrial Technology (KITECH), Republic of Korea

Abstract: Fluorinated gases (F-gases) which have been widely used in semiconductor liquid crystal-display (LCD) industries are greenhouse gases and their potential contribution to global warming deserves our attention due to intensive infrared absorption and long lifetimes of F-gases (Kim et al. 2008). This study presents a combination of the chemical reaction kinetics model and hydrodynamic model in a molten-metal bubble column reactor (MMBCR) for SF6 destruction. The one-dimensional (1D) plug-flow reactor (PFR) model was coupled with a drift-flux velocity to represent both the chemical reactions kinetics and hydrodynamics of MMBCR. The numerical results for SF6 destruction were compared to experimental data. Maximum SF6 removal efficiency of 73.9% was achieved at 518 oC in an MMBCR with a height of 0.524 m.

Keywords: Semiconductor industry, Fluorinated gas removal, Molten-metal bubble column reactor, Axial dispersion, Reactor design

Introduction

High-toxicity fluorinated gases (F-gases) are powerful greenhouse gases (Purohit and Höglund-Isaksson 2017). It is principally produced in the electrolytic aluminum industry in the semiconductor industry. CF4 is the simplest per-fluorocarbon (PFC) having a global warming potential (GWP) of 6,630 with a lifetime of 50,000 years. The main methodologies for the PFCs removal are catalytic decomposition, plasma decomposition, adsorption, and recycling. Catalytic decomposition may be the simplest, most economical, safe method, high decomposition rate, and low-temperature operation. A molten metal bubble column reactor (MMBCR) was used to treat F-gases by catalytic decomposition at 500 – 700oC (Anus et al. 2021). A one-dimensional (1D) plug flow reactor (PFR) was used for the MMBCRs (Catalan and Rezaei 2020).

In this study, we developed a kinetic model for SF6 destruction reactions in MMBCs. The chemical reaction kinetics parameters were obtained from experimental data, whereas the hydrodynamic parameters were calculated by a drift velocity model.

Model description

The liquid metal was assumed to be at a constant temperature throughout the reactor due to the liquid recirculation and mixing. Figure 1 shows the schematic of MMBCR.

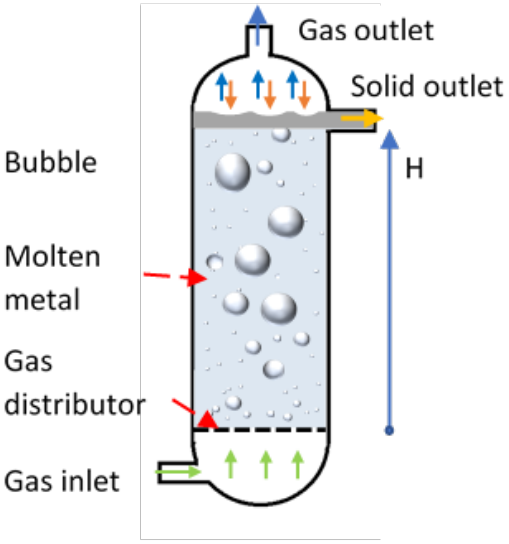

Figure 1. Schematics of MMBCR

SF6 decomposition in an MMBCR was considered in this study. The SF6 destruction reaction is

$$SF_6(g) + 4Sn(l) = 3SnF_2(s) + SnS(s) \quad (1)$$

The governing equation included the material balance for species in the gas phase and the momentum balance for pressure change of the gas along the height of the column.

$$\frac{dx_i}{dH} = -\nu_i A_R r \quad (2) \qquad \frac{dP}{dH} = -(\rho_L \alpha_G - \rho_G(1-\alpha_G))g \quad (3)$$

where x_i is the species molar fraction (-), ν_i is the stoichiometric coefficients of species i in the reaction (-), A_r is the reactor cross-sectional area (m^2), r is the net reaction rate (mol.cm^{-3}s^{-1}), ϱ_L and ϱ_G are the molten metal and gas density (kg.m^{-3}), respectively, α_G is the gas holdup in gas-molten metal mixtures, g is the gravitational acceleration (9.81 m.s^{-2}), P is the pressure (Pa).

Results and Discussions.

Fig. 2 shows a good agreement in SF6 conversion between the MMBCR model and the experimental data. The gas feed rate of 500 mL/min, which was composed of inert N2 and 1000 ppm SF6, was injected into a molten-Sn bubble column at 518 oC. The removal efficiency increases along the reactor height. 73.9% of SF6 removal efficiency was obtained at a reactor height of 0.524 m.

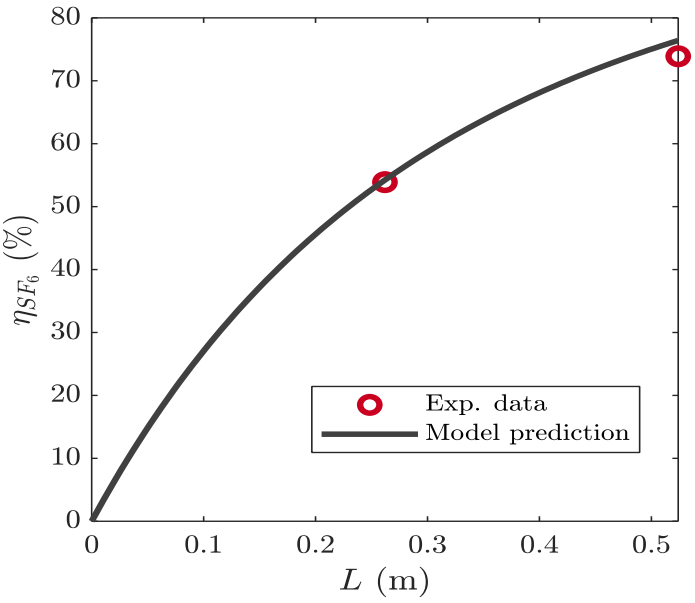

Figure 2. Comparison of experimental removal efficiency with predictions of this model

Conclusions

A one-dimensional kinetic model was developed for the SF6 removal in a molten-Sn bubble column reactor. Both reaction kinetics and bubble column hydrodynamic parameters were considered in the MMBCR model. The current model predicted well the SF6 removal efficiency. A SF6 removal efficiency of 73.9% was obtained at 518oC.

Acknowledgments

This work was financially supported by the Korea Government (KEIT: RS-2022-00155466).

References

Anus, Ali, Mahshab Sheraz, Sangjae Jeong, Eui-kun Kim, and Seungdo Kim. 2021. 'Catalytic thermal decomposition of tetrafluoromethane (CF4): A review', Journal of Analytical and Applied Pyrolysis, 156.

Catalan, Lionel J. J., and Ebrahim Rezaei. 2020. 'Coupled hydrodynamic and kinetic model of liquid metal bubble reactor for hydrogen production by noncatalytic thermal decomposition of methane', International Journal of Hydrogen Energy, 45: 2486-503.

Kim, Kwan-Tae, Young-Hoon Song, Min Suk Cha, Dae Hoon Lee, and Dong-Hyun Kim. 2008. 'Characteristics of rotating arc for CF4 removal', International Journal of Environment and Waste Management, 2: 412-22.

Purohit, Pallav, and Lena Höglund-Isaksson. 2017. 'Global emissions of fluorinated greenhouse gases 2005–2050 with abatement potentials and costs', Atmospheric Chemistry and Physics, 17: 2795-816.

In silico solvent selection for optimum lignin depolymerisation process

M. J. Jones[a,b], C. Bourmaud[b], A. Ghosh[b], M. B. Figueirêdo[c], J. Granachera, M. E. G. Ribeiro Domingos[a], J. S. Luterbacher[b], F. Maréchal[a]
[a]Industrial Energy Systems Laboratory, EPFL, 1950 Sion, Switzerland.
[b]Laboratory of Sustainable and Catalytic Processing, EPFL, 1015 Lausanne, Switzerland.
[c]Bloom Biorenewables SA, 1723 Marly, Switzerland

Abstract: The lignin polymer is the most abundant natural source of renewable aromatic molecules. Lignin depolymerization is a set of complex reactions for which kinetic modelling is challenging. The impact of the solvent on monomer yield was modelled based on limited experimental data, therefore enabling in silico testing of promising candidates from the GSK list of green solvents. Using ethanol as the solvent could decrease the CO2 emissions by 82% compared to the base case with tetrahydrofuran. The design was found to be most sensitive to coefficients linking solvent polarity and yield. By implementing a feedback loop between the lab-scale and process design, this methodology can guide experimental work with process-level considerations, therefore accelerating the development of biorefining processes.

Keywords: Lignin-first biorefinery, Chemical process design, Solvent screening

Introduction

Lignocellulosic biomass is one of the most promising feedstocks for sustainable alternatives to petroleum-based chemicals and materials. 'Lignin-first" biorefining relies on stabilization methods to deal upfront with lignin extraction rather than collecting it as a waste at the end.

Lignin depolymerization is an essential step for its valorization due to its importance for the market of renewable aromatics. However, the reaction mechanisms are complex and not yet well understood (Anderson et al., 2018). Nonetheless, optimizing reaction conditions to achieve high yield of valuable monomers is essential towards economic viability.

In this study, we aim at identifying significant cost and sustainability drivers and develop macro-models of the reactions to optimize process conditions. Those suggested conditions represent prime targets for experimental validation, which would ultimately be guided by process-level considerations.

Results and discussions

Based on process conditions and yields taken from Dick et al. (2022), we built a simulation for the hydrogenolysis of glyoxylic acid-functionalized lignin using Aspen Plus V11 (Fig. 1). Lignin is fed into the reactor, operated at 250ºC and up to 90bar, with tetrahydrofuran as solvent and reacted on a Ru/C catalyst with hydrogen at 10bar. At the outlet of the reactor, the gas is vented to be recycled, whilst the solvent is removed from the lignin oil in a column under vacuum. The monomers are then purified by evaporation at reduced pressure to minimize degradation. The operating conditions of the downstream processing units are optimized with the in-build DesignSpec function. The techno-economic analysis was performed following the methodology from Turton et al. (1985). Cradle-to-gate CO_2 emissions are indicators of the environmental impact of the process and are calculated from EcoInvent v3.9.1.

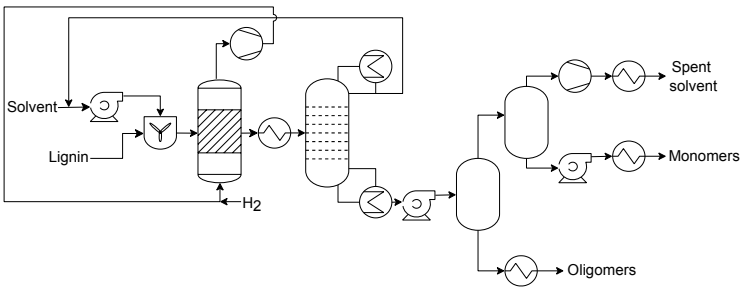

Figure 1. Process flow diagram of Aspen Plus simulation

The solvent, which needs to make up for the losses during the downstream separation of the glycolic acid by-product, is responsible for 90% of the CO_2 footprint of the process and is the second major cost burden of the process. Finding an alternative solvent is thus essential to improve the sustainability of lignin depolymerization.

The choice of solvent also greatly impacts monomer yields. Two main mechanisms are indeed involved in lignin depolymerization: first lignin solvolysis produces fragments which are then stabilized by catalytic reduction (Anderson et al., 2018). Five solvents recommended in the GSK list of green solvents (Alder et al., 2016) have been tested experimentally in the same process conditions. Monomers yields ranging from 12 to 25wt/wt% based on Klason lignin were achieved, in line with previously reported yields (Dick et al., 2022).

To investigate the relationships between the solvent's properties and the reaction performance, 50 molecular descriptors, including the Hansen solubility parameters corrected for the reaction temperature and pressure (Hansen, 2007), were retrieved from tables or calculated using open-access packages such as Clapeyron (Walker et al., 2022), RDkit and Thermo. Partial Least Square Regression (PLS-R), implemented with the Python library sklearn, was used to select the descriptors that could best explain the observed yield. The Hansen solubility parameter for polarity (δ_p) was found to be linearly correlated with the monomer yield (R2 = 0.94). The polarity of the solvent is also known to be directly correlated with the yields of cellulose solvolysis (Ghosh et al., 2015).

With this relationship, we could predict lignin monomer yields as a function of solvent polarity for reaction conditions where solvent effects are the main driver. Side reactions of the released protection aldehyde with alcohols are modelled with an equilibrium constant calculated from the Gibbs free energy of formations and matched published results (Mutschler et al., 2022).

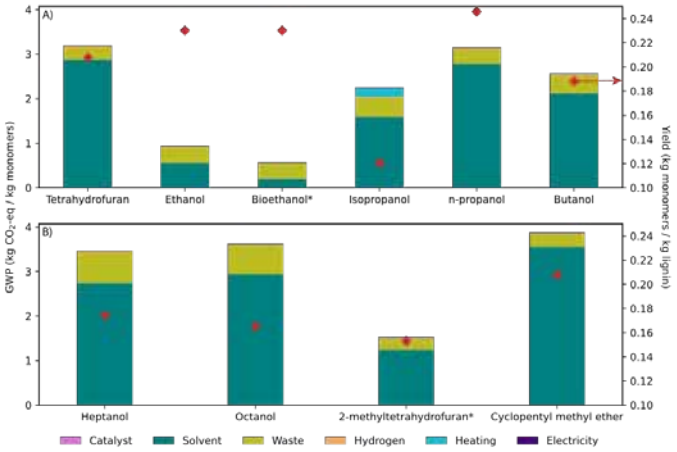

*Figure 2. Global warming potential and monomer yield from experiments (A) and predictions (B), for nine solvents. *Biobased solvent from wood*

Out of the five solvents tested experimentally, propanol achieved the highest yield (Fig. 2A) and highest profit, whilst ethanol enabled the lowest CO_2 footprint when bio-based. Four new solvents (alcohols and ethers) with high δ_p at the reaction conditions, high volatility difference with the monomers for ease of separation, and ranked as promising alternatives in the GSK list of green solvents were tested with the model (Fig. 2B). Albeit 2-methyltetrahydrofuran shows the second lowest GWP, its high price and the low monomer yield hinder its use in large scale processing. The predictions for the two alcohols show reduced yields and higher CO_2 emissions since they are more difficult to source sustainability than shorter alcohols. Experimental validation is paramount to confirm those yield predictions.

Finally, we investigated the sensitivity of the design to the coefficients used to calculate the pre-exponential factor. If the gradient relating the δ_p to yield is halved, the yield would indeed decrease by 84%. To assess the robustness of the model, those coefficients should be obtained at different pressures and temperatures.

Conclusions

From a limited number of experimental points, we were able to build a process model to optimize key parameters in lignin depolymerization. Our flowsheet indeed enables in silico testing of solvents for lignin monomer production and identified promising candidates to reduce the environmental footprint of the process. Ethanol could indeed decrease the CO_2 emissions by 82% compared to commonly used tetrahydrofuran.

The next steps of this work are three-fold: 1) experimentally validate the monomer yields predicted for new solvents, 2) expand the model by investigating the impact of the catalyst and solvent-to-lignin ratio on the monomer yield and distribution and, 3) formulate a multi-objective optimization problem to systematically identify optimum process conditions to maximize profit while minimizing the environmental impact.

Acknowledgments

This work is supported by the European Union's Horizon 2020 research and innovation programme under the Marie Skłodowska-Curie grant agreement No. 945363.

References

Alder, C. et al. (2016). Updating and further expanding GSK's solvent sustainability guide. Green Chem., 18.

Anderson, E. et al. (2018). Kinetic Studies of Lignin Solvolysis and Reduction by Reductive Catalytic Fractionation Decoupled in Flow-Through Reactors. ACS Sustainable Chem. Eng., 6.

Dick, G. et al. (2022). Controlling lignin solubility and hydrogenolysis selectivity by acetal-mediated functionalization. Green Chem., 24.

Ghosh, A. et al. (2016). Production of solubilized carbohydrate from cellulose using non-catalytic, supercritical depolymerization in polar aprotic solvents. Green Chem., 18.

Hansen, C. (2007). Hansen Solubility Parameters: A User's Handbook.

Mutschler, C. et al. (2022). Reactive Distillation of Glycolic Acid Using Heterogeneous Catalysts: Experimental Studies and Process Simulation. Front Chem., 10.

Walker, P. et al. (2022). Clapeyron.jl: An Extensible, Open-Source Fluid Thermodynamics Toolkit. Ind. Eng. Chem. Res., 61.

Modelling of energetically efficient hybrid method for separation of ethanol-water mixture

Andras Jozsef Toth, Huyen Trang Do Thi, Eniko Haaz
Department of Chemical and Environmental Process Engineering, Műegyetem rkp. 3., Budapest, 1111, Hungary

Abstract: It can be concluded that in the fine chemical industries, especially in the pharmaceutical industry, a large amount of industrial waste solvents is generated during production technology. Their management is a priority issue because their disposal often accounts for the largest share of the cost of the entire technology. Thus, it is necessary to develop regeneration procedures that are financially favourable for the factory, and it is possible, in the spirit of the circular economy, to reuse the liquid waste in the given technology or possibly elsewhere. The combination of distillation and pervaporation methods is a widely researched procedure because it can separate energetically efficient azeotropic mixtures. The hybrid process is developed in this research to separate the binary ethanol-water mixture. The separation is optimized in a professional process simulator environment. The user-added module is implemented in the case of pervaporation based on semi-empirical transport model. The bottom product of the distillation column is 99.9 weight% of water, and the ethanol content of 99.5 weight% can be reached in the retentate product of the hydrophilic pervaporation module.

Keywords: hybrid method, ethanol-water, flowsheet simulator, distillation, pervaporation

Introduction

Pervaporation is a relatively new technology, where the mixture to be treated is evaporated at low pressure on the permeate side of the membranes, and the separation of the mixtures takes place with the preferred sorption and diffusion phenomenon of the desired component through the dense membranes. Depending on the main permeation compound, the pervaporation process can be divided into two main areas: hydrophilic and organophilic pervaporation. In our case, hydrophilic pervaporation is investigated, as it is used to dewater organic solvents and separate azeotropic mixtures. Furthermore, the main advantage of hydrophilic pervaporation as follows: pollution-free, energy-saving, and high separation efficiency (Toth, 2022). These characteristic properties are difficult to achieve with other traditional technologies (Crespo and Brazinha, 2015). The aim of this study was to examine the separation of the azeotropic ethanol-water mixture with hybrid distillation and hydrophilic pervaporation method in professional flowsheet environment. Energy consumption was also determined to compare the separation with extractive distillation.

Material and methods

In the fine chemical industry, until the current separation problem, ethanol must be separated from its aqueous mixture. In the present study, the binary mixture's initial concentration was 20-weight% ethanol and 80-weight% water. The product purity to be achieved is 99.5 weight% for ethanol and 99.9 weight% for water. The feed stream was 800 kg/h. ChemCAD flowsheet simulator was applied with user-added pervaporation unit. NRTL thermodynamic method was used in the case of SCDS column type. The number of theoretical plates, reflux ratio and reboiler duty were optimized in the case of the distillation process. Figure 1 illustrates the flowsheet of the simulated hybrid method.

The pervaporation model of Szilagyi and Toth (2020) was selected to model ethanol dehydration. The main equation of this model:

$$J_i = \frac{1}{1 + \left\{ \frac{\left[\bar{D}_i \bullet exp\left(x_{i1}{}^{B}\right)\right]}{\left(Q_0 \bullet p_{i0} \bullet \bar{\gamma}_i\right)} \right\}} \bullet \frac{\left[\bar{D}_i \bullet exp\left(x_{i1}{}^{B}\right)\right]}{\bar{\gamma}_i} \bullet \left(\frac{p_{i1} - p_{i3}}{p_{i0}} \right) \qquad i = (1,\ldots,k)$$

During the optimization, the goal was to find the minimum membrane size.

Results and discussion

The results of the optimized parameters of the hybrid method can be found in Table 1. Five membrane modules with 70 m2 effective membrane transfer area was sufficient to achieve the desired product purities. The distillation column had 12 theoretical stages and the reflux ratio was 2. The calculated heat duty of the hybrid method was 605 MJ/h. In a previous study (Toth, 2018), the composition of binary mixture with 10 weight% ethanol and 90 weight% water was examined with extractive distillation, where the heat duty value of 1491 MJ/h was obtained, which is more significant. The entrainer was ethylene glycol.

	Distillation			Pervaporation	
	F	**W**	**D**	**P**	**R**
EtOH [m/m%]	20	0.1	94	1	99.5
Water [m/m%]	80	99.9	6	99	0.5

Table 1. Optimized results of the separation of ethanol-water binary mixture (F: Feed, W: Bottom product, D: Distillate, P: Permeate, R: Retentate)

Conclusions

The distillation-hydrophilic pervaporation hybrid method proved effective in ethanol-water separation, as it was possible to extract both water and ethanol with the desired purity. The energy-efficient solution can open a new perspective in research.

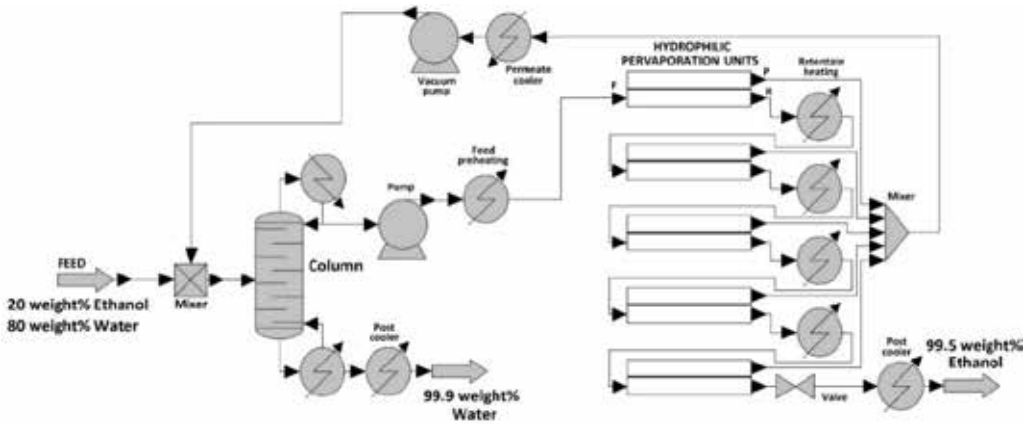

Figure 1. Simulated hybrid distillation and hydrophilic pervaporation method for separating ethanol – water binary mixture (based on Toth (2022)

Acknowledgments

This publication was supported by OTKA 131586.

References

Crespo, J. G., Brazinha, C. (2015). 1 - Fundamentals of pervaporation. In: Pervaporation, Vapour Permeation and Membrane Distillation, Oxford: Woodhead Publishing, 3.

Szilagyi, B., Toth, A. J. (2020). Improvement of Component Flux Estimating Model for Pervaporation Processes. Membranes, 10, 418.

Toth, A. J., (2022). N-Propanol Dehydration with Distillation and Pervaporation: Experiments and Modelling. Membranes, 12, 750.

Toth, A. J., (2018). Removal of ethanol from pharmaceutical process wastewater with distillation and hydrophilic pervaporation. 10th Eastern European IWA Young Water Professionals Conference, Zagreb, Croatia, 550.

Effect of electromagnetic fields on hydrodynamics of bubbles in a molten-metal bubble column reactor using CFD simulation

Hanh Thi Hong Bui, Son Ich Ngo, Young Il-Lim[a]
[a]Center of Sustainable Process Engineering (CoSPE), Department of Chemical Engineering, Hankyong National University, Gyeonggi-do, Anseong-si, Jungang-ro 327, 17579 Korea

Abstract: The use of molten-metal bubble column reactors (MMBCRs) to produce CO2-free hydrogen has gained much interest in recent years. In this study, the effect of electromagnetic fields on the hydrodynamics of bubbles was investigated using CFD simulation. A volume of fluid CFD (VOF-CFD) model coupled with a large-eddy simulation (LES) model for turbulence was used to simulate the hydrodynamics of gas-liquid two-phase flow in an MMBCR. Electromagnetic fields were applied to the MMBCR via a magnetohydrodynamic (MHD) model. The number of meshes required for the LES model was determined to obtain over 80% of resolved turbulence kinetic energy. The bubble rising velocity is investigated by CFD simulation which was validated with experimental data with and without the electromagnetic field. The terminal velocity of bubbles with a diameter of 3 mm was inhibited by a strong magnetic field. Understanding the hydrodynamics of MMBCR is useful to identify optimal operating conditions and reactor design.

Keywords: Molten-metal bubble column reactor (MMBCR), Magnetohydrodynamic (MHD) model, Volume of fraction model (VOF)

Introduction

Hydrogen is produced primarily by steam methane reforming (SMR) that emits a large amount of carbon dioxide as a product of the reaction (Msheik et al., 2021). Non-oxidative CH_4 pyrolysis in a molten-metal bubble column reactor (MMBCR) (Kudinov et al., 2021) is a promising method to produce H_2 without CO_2 emission:

$$CH_{4(g)} \rightarrow C_{(s)} + 2H_{2(g)},\ \Delta H^0_{25°C} = 74.85 \frac{kJ}{mol\ of\ CH_4} \qquad (1)$$

The hydrodynamic parameters of bubbles such as gas holdup, bubble size, bubble velocity, and bubble size distribution play a significant role in methane conversion since they affect the interfacial area and resident time of methane in MMBCRs (Leal Pérez et al., 2021). Several approaches were proposed to enhance the performance of MMBCRs such as exposing an electromagnetic field to lengthen the bubble residence time (Wang et al., 2017).

The volume-of-fluid computational fluid dynamics (VOF-CFD) is an effective tool for capturing the gas-liquid interface area (Ngo et al., 2023). A magnetohydrodynamic (MHD) model was coupled with the VOF-CFD to represent the magnetic fields and hydrodynamics (Fehling et al., 2017).

In this study, a VOF-CFD model coupled with a large eddy simulation (LES) turbulence model and an MHD model was developed for CH4 pyrolysis in an MMBCR with an electromagnetic field. The VOF-CFD model were then validated against experimental data in the literature for a GaInSn-Ar system.

VOF-CFD model

Governing equation

Equations of continuity, momentum, and electromagnetic force are described in Eq (2), (3), and (4), respectively (Ngo et al., 2023).

$$\frac{\partial \alpha_G}{\partial t} + \vec{\nabla} \bullet \left(\alpha_G \vec{u}\right) = - \vec{\nabla} \bullet \left(\alpha_G \alpha_L \vec{u}_c\right) \qquad (2)$$

$$\rho \frac{\partial \vec{u}}{\partial t} + \rho \vec{\nabla} \bullet \left(\vec{u}\,\vec{u}\right) = - \vec{\nabla} P + \vec{\nabla} \bullet \bar{\bar{\tau}} + \rho \vec{g} + F_S + F_L \qquad (3)$$

$$\frac{\partial \vec{b}}{\partial t} + \left(\vec{u} \bullet \nabla\right)\vec{b} = \frac{1}{\mu\sigma}\nabla^2 \vec{b} + \left[\left(\vec{B}_0 + \vec{b}\right) \bullet \nabla\right]\vec{u} - \left(\vec{u} \bullet \nabla\right)\vec{B}_0 \qquad (4)$$

Geometry and meshing

The 3D geometry was created based on the GaInSn-Ar system (Wang et al., 2017). Polyhedral meshes was small enough to capture all bubble diameters in the experiment. The mesh independence test was checked for at least 80% resolved turbulence kinetic energy.

Physical properties and boundary conditions

Physical properties such as the density (ϱ), viscosity (μ), and surface tension (σ) were taken from elsewhere (Wang et al., 2017). The contact angle (θ) of fluid was set to 130° in metallic nonwetting.

Results and discussion

The bubble rising velocity of a 3 mm bubble diameter at different electromagnetic strengths is depicted in Figure 1. The tendency of bubble velocity obtained from the VOF-CFD model agrees well with the experiment data (Wang et al., 2017). The bubble terminal velocity decreases as the electromagnetic field strength increases, due to the Lorentz force.

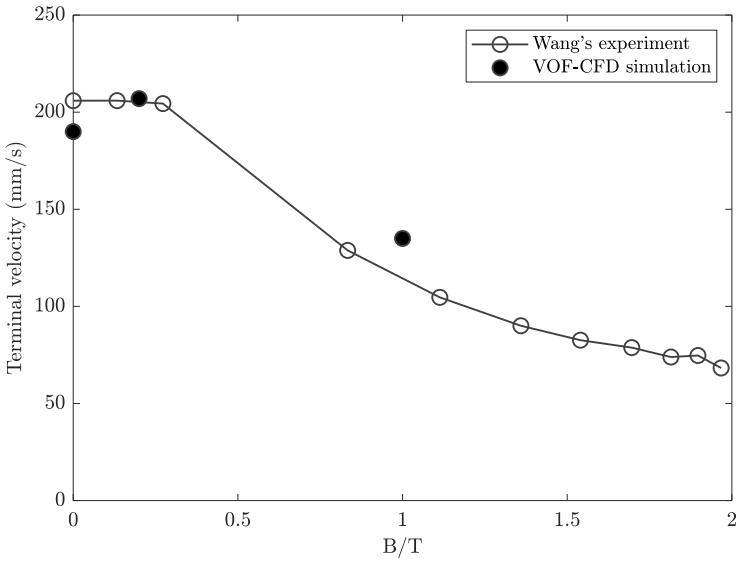

Figure 1. Bubble rising velocity (d_e=3mm) in different magnetic strength

Conclusions

A volume of fluid computational fluid dynamics (VOF-CFD) coupled with a large eddy simulation (LES) turbulence model and magnetohydrodynamics (MHD) model was developed for a molten-metal bubble column reactor (MMBCR). The VOF-CFD model was verified and validated against the experimental data of the GaInSn-Ar system. An MMBCR under electromagnetic fields showed lower bubble terminal velocities than those without electromagnetic field.

Acknowledgments

This work was supported by a National Research Foundation of Korea (NRF) grant funded by the Korean Government (MSIT; No. 2022M3J5A1051728 and 2021R1A2C1011618).

References

Fehling, T., Steinberg, T., Baake, E., (2017). Numerical modeling of bubble dynamics in liquid metal exposed to electromagnetic fields for hydrogen production. International Journal of Applied Electromagnetics and Mechanics 53, S111-S120.

Kudinov, I.V., Pimenov, A.A., Kryukov, Y.A., Mikheeva, G.V., (2021). A theoretical and experimental study on hydrodynamics, heat exchange and diffusion during methane pyrolysis in a layer of molten tin. Int. J. Hydrog. Energy 46(17), 10183-10190.

Leal Pérez, B.J., Medrano Jiménez, J.A., Bhardwaj, R., Goetheer, E., van Sint Annaland, M., Gallucci, F., (2021). Methane pyrolysis in a molten gallium bubble column reactor for sustainable hydrogen production: Proof of concept & techno-economic assessment. International Journal of Hydrogen Energy 46(7), 4917-4935.

Msheik, M., Rodat, S., Abanades, S., (2021). Methane Cracking for Hydrogen Production: A Review of Catalytic and Molten Media Pyrolysis, Energies.

Ngo, S.I., Lim, Y.-I., Kwon, H.M., Lee, U.-D., (2023). Hydrodynamics of molten-metal bubble columns in the near-bubbling field using volume of fluid computational fluid dynamics. Chem. Eng. J. 454, 140073.

Wang, Z.H., Wang, S.D., Meng, X., Ni, M.J., (2017). UDV measurements of single bubble rising in a liquid metal Galinstan with a transverse magnetic field. International Journal of Multiphase Flow 94, 201-208.

Graph based fault detection and root cause analysis in process manufacturing

Louis Allen[a], Joan Cordiner[a]
[a]Department of Chemical and Biological Engineering, University of Sheffield, Sheffield, S1 3JD, United Kingdom

Abstract: Unplanned downtime is a billion-dollar problem faced by process manufacturers across the world. Failure to prevent unplanned downtime leads to spiralling costs, including labour, part and material costs, safety issues, and concerns regarding process sustainability. Therefore, the need for an appropriate solution is desperate. Here we propose a method to detect and analyse the root cause of problems in process manufacturing environments by using advanced data driven techniques combined with domain knowledge. It is expected that the integration of this system will have a considerable impact in terms of maintenance efficiency, safety improvements and an increase in process sustainability.

Keywords: Maintenance 4.0, AI, Predictive Maintenance, GAN

Introduction

The maintenance of machines is crucial for safe and profitable operation in the process industries. Traditionally this is done using a preventative maintenance (PvM) framework in which a regular maintenance interval is set for each unit in a process. This approach does not account for fluctuations in the process conditions that might illicit premature failure in a unit before it's maintenance period has elapsed. The result is unplanned downtime of the process. Traditional root cause analysis (RCA) of these failures relies on deep, domain specific knowledge from a few experienced members of the operations and engineering This is a time consuming process that requires significant personnel input (Chemenwo et al., 2016). Furthermore, with the retirement of the aging workforce leading to a reduction in plant specific expertise, it is necessary to formulate new methods to analyse process failure (DeLong, 2004).

A potential solution could lie in the data driven techniques proposed by researchers since the advent of industry 4.0 (I4.0). However, many techniques proposed require either a knowledge of a confirmed 'normal' state of operation for a system, or a detailed knowledge of all possible failure states with datasets to match. Both of these are hard to come by, with the former varying based on external factors (shift, weather condition, product) and the latter increasing exponentially with the size of the process. Even then, the lack of process understanding of the models limits the ability to troubleshoot detected fault, offering merely as a tool to flag when an issue might occur without giving the crucial detail of why, or more importantly how can it be prevented.

This paper proposes an alternative approach which builds on a foundation of process knowledge to enhance the fault detection and troubleshooting ability of deep learning (DL) algorithms. The novelty of this work is in:

- Implementation of process knowledge graphs to enhance the fault detection capabilities of the deep learning models using novel anomaly score.
- Root cause analysis of detected faults through understanding of causal process relationships.

Methodology

We represent a manufacturing process as a network of sensors $\mathcal{G}\{V, \mathcal{E}, W\}$ containing a finite set of nodes $i \in V$ where $|V| = N$; a set of edges $e_{i,j} \in \mathcal{E}$ connecting nodes i and j based on a knowledge of causal relationships between sensors, and a weighted adjacency matrix W where $W_{i,j}$ represents the weight of the edge between node i and j, or 0 if they are not connected. Edge weights are calculated using a thresholded Gaussian kernel (Shuman et al., 2013). Each node i has an associated column vector $X_i \in \mathbb{R}^T$ where T is the length of data.

The deep learning framework shown in Figure 1 is based on a generative adversarial network (Goodfellow et al., 2020) with graph convolution. This is referred to as a graph convolutional generative adversarial network (GCGAN). A generator is trained to forecast data for each node, and a discriminator is trained to detect if the generated time series is real or fake. We divide the generator into two modules. A short term module based on a graph convolutional gated recurrent unit (GCGRU) architecture aims at capturing the spatiotemporal features of the data to predict across a shortened time period, T_S, to capture point anomalies or step changes (Deng et al., 2022). A long term module based on a long short term memory (LSTM) architecture aims at predicting each sensor across time period T_L to identify degradation or cyclical anomaly. The two outputs are combined in a graph convolutional network (GCN) layer to give the final prediction $\hat{X}_t$. This prediction is added to the generated sequence to give $\hat{S}_t$. The generator is trained using a mean squared error (MSE) loss function.

The discriminator compares the generated sequence $\hat{S}_t \in \mathbb{R}^{T\times N\times 1}$ with the real sequence $S_t \in \mathbb{R}^{T\times N\times 1}$ using a binary cross entropy (BCE) loss function. The discriminator is used in training to help the generator to observe spatiotemporal relationship. It can also be used to help detect anomaly.

Anomaly Detection

We combine both the forecasting error of the generator function, G_θ, with the score from the discriminator function, D_ϕ, to give an anomaly score Eq. (1) (Lee et al., 2018).

$$s_{total}(v,t) = \left\| G_\theta(v,\ t) - X_{v,\,t} \right\|_2 - \lambda_S \log(D_\phi(S_{v,t})) \quad (1)$$

Where λ_S is a hyper-parameter to balance the discriminator and generator detection.

Root cause analysis

The structure of the sensor network can be used to identify root causes of the faults detected. It is proposed that by observing the neighbourhood of a node, $\mathcal{N}_i$, at a time t_{A-1} for an anomaly observed at t_A we can look for raised anomaly scores in connected nodes. Say it is found node v_j is exhibiting a high anomaly score at this point, we can explore $\mathcal{N}_j$ at a time of t_{A-2}. This process can be repeated to give a path back to the true origin of the fault, enabling an early maintenance intervention by identifying and managing the root cause.

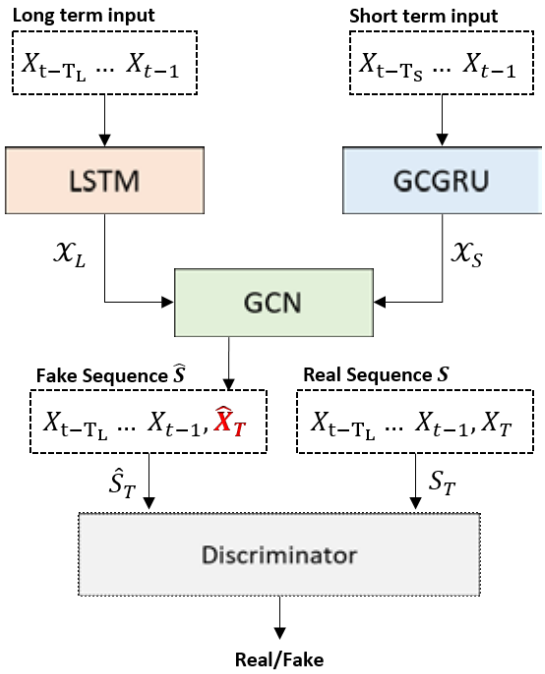

Figure 1. Framework for training a GCGAN model.

Conclusion

We propose a GCGAN framework to incorporate chemical engineering domain knowledge into deep-learning based predictive maintenance. The result can identify fault in a sensor network and use known relationships to analyse the root cause. This knowledge enables early intervention and facilitates the management of plant issues to increase maintenance efficiency

References

Chemweno, Peter, Liliane Pintelon, and Peter Muchiri. "I-RCAM: Intelligent expert system for root cause analysis in maintenance decision making." 2016 IEEE international conference on prognostics and health management (ICPHM). IEEE, 2016.

DeLong, David W. Lost knowledge: Confronting the threat of an aging workforce. Oxford University Press, 2004.

Shuman, David I., et al. "The emerging field of signal processing on graphs: Extending high-dimensional data analysis to networks and other irregular domains." IEEE signal processing magazine 30.3 (2013): 83-98.

Goodfellow, Ian, et al. "Generative adversarial networks." arXiv (2014).

Deng, Leyan, et al. "Graph convolutional adversarial networks for spatiotemporal anomaly detection." IEEE Transactions on Neural Networks and Learning Systems 33.6 (2022): 2416-2428.

Lee, Sangmin, Hak Gu Kim, and Yong Man Ro. "STAN: Spatio-temporal adversarial networks for abnormal event detection." 2018 IEEE international conference on acoustics, speech and signal processing (ICASSP). IEEE, 2018

Numerical investigation of exact designs in optimal experiment campaigns

Marco Sandrin[1,2], Benoît Chachuat[1], Constantinos C. Pantelides[1,2]
[1]Sargent Centre for Process Systems Engineering, Department of Chemical Engineering, Imperial College London, London, United Kingdom
[2]Siemens Process Systems Engineering, London, United Kingdom

Abstract: The application of model-based design of experiments presents large computational and numerical challenges when designing experimental campaigns comprising multiple parallel runs. By searching over the space of the so-called "experimental efforts", continuous-effort designs overcome said drawbacks, but require a posteriori effort rounding to integer values, which can result in large suboptimality.

This paper presents an approach to solving the exact design problem. Integer experiment replications are considered as optimisation variables, leading to pure integer programs with a convex objective function and linear constraints.

Keywords: model-based design of experiments, optimal experiment design, experiment campaign, parameter precision

Introduction

Model-based design of experiments (MBDoE) for parameter precision can greatly accelerate the development of predictive mechanistic models (Franceschini and Macchietto, 2008). A particular focus has been on sequential MBDoE, where (possibly dynamic) experiments are designed one-at-a-time using gradient-based techniques. For nonlinear models, the resulting optimisation problems are typically nonconvex, and thus prone to converging to local optima. Numerical failure caused by singular information matrices is also commonplace. Such computational challenges hinder the design of experimental campaigns comprising multiple parallel runs.

Effort-based methods (Kusumo et al., 2022; Vanaret et al., 2021) overcome these challenges by discretising the experimental space into a finite set of candidate experiments. They determine the fraction of the total number of experiments (the "effort") associated with each candidate, with the objective of selecting the combination of experiments that will generate the highest information content. Treating the efforts as continuous variables leads to a convex formulation that can be solved efficiently using convex optimisation techniques. However, the optimised efforts typically assume fractional values, which need to be rounded to integer values in a subsequent step. This a posteriori effort rounding can result in large suboptimality, especially for campaigns with a small number of experiments.

Methodology

In this study, a discrete-effort methodology for the exact design of experiment campaigns comprising a finite number of experiments is presented. Integrality constraints on the number of experiment replicates are enforced directly through pure integer programming, with a convex objective function and linear constraints. Given the generic model in Eq. (1), the experimental design space is discretised using low-discrepancy sampling (Sobol, 1967), and the Fisher information matrix $\boldsymbol{H_i}$ is computed for each candidate experiment as shown in Eq. (2). In Eqs. (1)–(2), $\boldsymbol{y}$ corresponds to experimental measurements, $\boldsymbol{f}$ to model predictions, $\boldsymbol{u}$ and $\boldsymbol{\theta}$ are experimental decision variables and model parameters, respectively, and E_y is the covariance matrix of the measurements.

$$\boldsymbol{y} = \boldsymbol{f}(\boldsymbol{u},\ \boldsymbol{\theta}) + \mathcal{N}\left(0, \Sigma_y\right) \quad (1) \qquad \boldsymbol{H_i} = \frac{\partial \boldsymbol{f}}{\partial \boldsymbol{\theta}}(\boldsymbol{u_i})^T \Sigma_y^{-1} \frac{\partial \boldsymbol{f}}{\partial \boldsymbol{\theta}}(\boldsymbol{u_i}) \quad (2)$$

The resulting optimisation problem in Eqs. (3)–(4) considers a modified D-optimal criterion on the overall information matrix $\boldsymbol{H}$; N_E and N_S are the number of experiments in the campaign and number of experiment samples, respectively, and r_i is the number of replications of candidate i.

$$\max_{r_i,\, i=1,..,N_S} \operatorname{logdet}(\boldsymbol{H}), \text{ with } \boldsymbol{H} = \sum_{i=1}^{Ns} r_i \boldsymbol{H_i} \quad (3) \text{subject to} \quad \sum_{i=1}^{N_S} r_i = N_E, r_i \in \mathbb{N}_0 \quad (4)$$

The proposed approach is implemented within the gPROMS modelling platform (Siemens Process Systems Engineering, 1997–2022). The solution of the pure integer program is obtained using a classical outer-approximation algorithm (Duran and Grossman, 1986).

Case Study

The presented methodology is applied to the semi-continuous fermentation of baker's yeast, modelled by Eqs. (5)–(6) with Monod-type kinetics.

$$\frac{dy_1}{dt} = (r - u_1 - \theta_4)y_1, \text{ with } r = \frac{\theta_1 y_2}{\theta_2 + y_2} \quad (5) \qquad \frac{dy_2}{dt} = -\frac{r y_1}{\theta_3} + u_1(u_2 - y_2) \quad (6)$$

A campaign with $N_E = 4$ parallel experiments is designed, assuming fixed experiment duration and equidistant sampling times, fixed initial conditions for the model states $y_1(0) = 7, y_2(0) = 0.1$, and constant profiles for controls $u_1 \in [0.05,\ 0.2]$, $u_2 \in [5,\ 35]$. The allowable space of the decision variables is discretised into $N_s = 50$ experiment candidates. Nominal values of the parameters are $\boldsymbol{\theta} = [0.1,\ 0.1,\ 0.1,\ 0.1]^T$.

Table 1 compares computational statistics of the continuous-effort solutions—both before and after apportionment—to those of the exact design case. The exact design approach allows designing a campaign with an improved information content with respect to the apportioned solution of the continuous-effort design. Only 3 unique candidate experiments are selected, and the most informative one is to be performed twice: $\boldsymbol{u}^* = \{(0.111,\ 32.2), (0.057,\ 13.0), (0.179,\ 33.6)\}$.

Table 1. Comparison of effort-based approaches

Methodology	$\log\det H$	CPU time [s]
Continuous design	43.77	0.35
Apportionment	43.69	–
Exact design	43.76	0.97

Conclusions

Campaigns obtained by solving the exact design case show lower degrees of suboptimality compared with approximations of the continuous-effort solutions; the method prioritises experiments with exceptional information content, while continuous-effort designs attempt to include all candidates with nonzero effort.

For the considered case study, the exact design problem is computationally tractable. In general, computational requirements are proportional to the number of experiment samples, and sensitivity calculations during the design space discretisation often represent the greatest cost (in particular for complex models).

Acknowledgments

This project has received funding from the European Union's Horizon 2020 research and innovation programme under the Marie Skłodowska-Curie grant agreement No. 955520.

References

Duran, M.A., Grossmann, I.E. (1986), "An outer-approximation algorithm for a class of mixed-integer nonlinear programs", Mathematical Programming, 36, 307–339.

Franceschini, G., Macchietto, S. (2008). Model-based design of experiments for parameter precision: State of the art, Chemical Engineering Science, 63, 4846–4872.

Kusumo, K.P., Kuriyan, K., Vaidyaraman, S., García-Muñoz, S., Shah, N., Chachuat, B. (2022). Risk mitigation in model-based experiment design: A continuous-effort approach to optimal campaigns, Computers & Chemical Engineering, 159, 107680.

Siemens Process Systems Engineering (1997–2022). gPROMS, www.psenterprise.com/products/gproms.

Sobol, I.M. (1967). On the distribution of points in a cube and the approximate evaluation of integrals, USSR Computational Mathematics and Mathematical Physics, 7, 86–112.

Vanaret, C., Seufert, P., Schwientek, J., Karpov, G., Ryzhakov, G., Oseledets, I., Asprion, N., Bortz, M. (2021). Two-phase approaches to optimal model-based design of experiments: how many experiments and which ones?, Computers & Chemical Engineering, 146, 107218.

Multi-scale integration and multi-objective optimization of the hydrogen network in an oil refinery

Yi Zhao[a], Guilherme Nascimento[a], Rafael Castro-Amoedo[a], François Maréchal[a]
[a]Industrial Process and Energy Systems Engineering Laboratory, École Polytechnique de Fédérale Lausanne, Switzerland

Abstract: In this work, a mixed integer linear programming (MILP) formulation is applied to obtain optimal hydrogen network designs in an oil refinery. Heat integration, which is frequently overlooked in the literature, is addressed using pinch analysis to evaluate the energy saving potential. A number of scenarios are analyzed considering different hydrogen production technologies. Under each scenario, multi-objective optimization is carried out to capture the unavoidable trade-off between the cost and carbon footprint. By applying our methodology to a typical refinery with a net hydrogen demand of 10.8 ton/h, the results show that the lowest cost (2.42 $/kg) and impact (4.11 kg CO2/kg) are obtained with blue hydrogen sources. This study highlights the energy savings and carbon reductions brought by optimal hydrogen network designs and could provide useful guidance for the management of hydrogen in refineries.

Keywords: Hydrogen network, Mixed integer linear programming, Energy integration, Multi-objective optimization

Introduction

Hydrogen is an essential resource in refineries. However, the current hydrogen requirement, which is largely dependent on steam methane reforming (SMR), represents a considerable energy demand, cost, and emissions for refineries. An optimal hydrogen network addresses the issue from two perspectives. On the one hand, purge gases from hydrogen processing units are important hydrogen and energy resources and making full use of them can efficiently reduce the hydrogen and heat demands of refineries; on the other hand, integrating different hydrogen suppliers, such as blue hydrogen with carbon capture and green hydrogen from electrolysis and renewables, has the potential to reduce the carbon footprints and costs at source.

In recent years, a number of studies were conducted for hydrogen network designs using mathematical programming methods and took various constraints into consideration, such as light hydrocarbon recovery (Yang et al., 2022), hydrogen turbines integration (Liu et al., 2020), CO2 mitigation (Tock and Marechal, 2012), etc. However, a holistic approach considering heat integration, environmental impacts, and alternative hydrogen utilities is still lacking. In this work, we propose a mixed integer linear programming (MILP) method to address the research gap. Compared to non-linear programming methods, the MILP method, first formulated by Kantor at al., 2020, can achieve global optimum with much fewer computation efforts given a reasonable simplification of the problem.

Methodology

As shown in Figure 1, the superstructure of a refinery hydrogen network consists of a hydrogen utility (steam methane reforming (SMR) or electrolysis), a catalytic reforming unit (CRU), hydroprocessors (hydrocrackers and hydrotreaters), a pressure swing adsorption (PSA) unit, a fuel gas sink, a natural gas boiler, and a carbon capture unit (CC). Among these units, hydroprocessors are specified by their minimum outlet flowrate and concentration to guarantee sufficient hydrogen partial pressures in the reactor. The boiler, SMR, PSA and carbon capture unit are modeled by describing their mass flows, investment cost, and heat and electricity demand. Assuming known purities at hydrogen sources, we use a MILP formula to optimize the hydrogen network and balance the trade-off between cost and environmental impacts under a multi-objective optimization framework. The market prices for different utilities are natural gas 0.0224$/kWh; electricity 0.2149 $/kWh; water 0.03 $/ton. The impact data is retrieved from Ecoinvent life cycle inventory database. The minimum energy requirement is illustrated by the approach developed by Kantor et al., 2020.

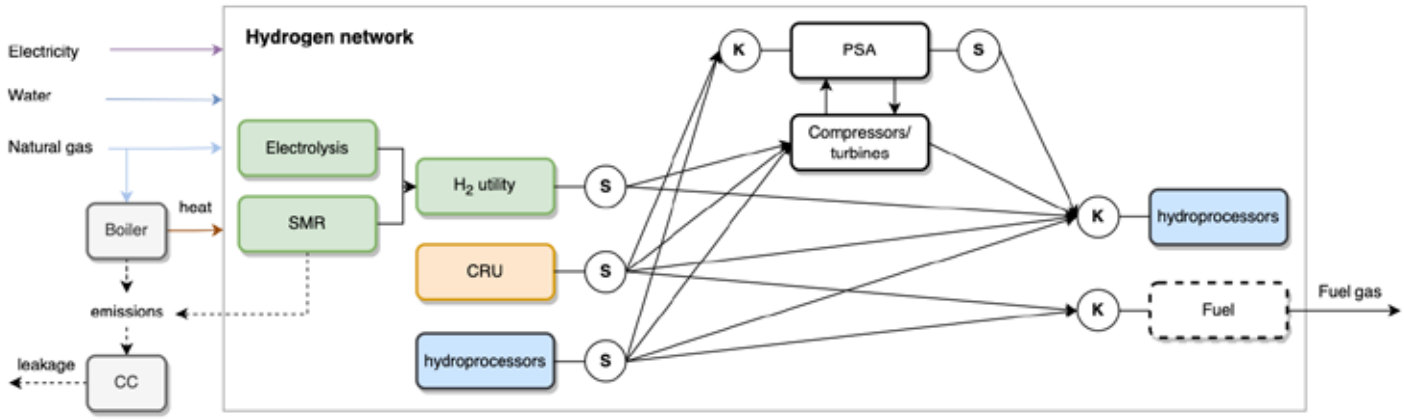

Figure 1 Superstructure of the refinery hydrogen network

Results

Under different hydrogen suppliers, four optimal configurations are identified for a typical refinery with a theoretical hydrogen demand for 10.8 t/h, and their corresponding cost and impacts are shown in Figure 2(a). Meeting the refinery hydrogen demand with blue hydrogen has the lowest impact (4.11 kg CO2/kg) and cost (2.42 $/kg), while green hydrogen and grey hydrogen have limitations either on the cost or on the impact, respectively. The minimum energy requirement, obtained using pinch analysis, is shown in Figure 2(b): Case 3 has the highest heat and cold utility demand due to the simultaneous usage of SMR and carbon capture. Figures 2(c) and 2(d) present the detailed cost and impact breakdown of the different cases. It was found that despite of a lower natural gas consumption in Case 4 owing to the usage of electrolyzers, the extremely high electricity consumption contributes to the highest cost and is responsible for considerable carbon emissions. When comparing Case 3 and Case 1, the usage of carbon capture unit (MEA) increases the consumption of natural gas and electricity thus leading to a higher cost, but it significantly reduces the direct carbon emissions from boilers and SMR.

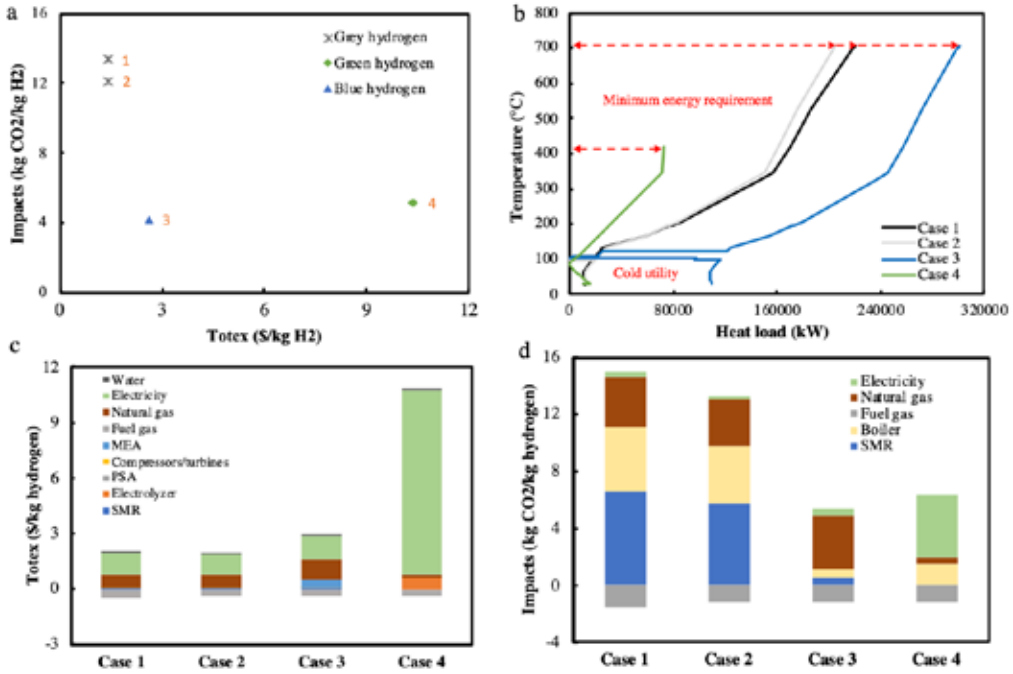

Figure 2 (a)The impacts and annualized cost of the optimal configuration with different hydrogen utilities; (b) the minimum energy requirement for different cases; (c) The cost breakdown and (d) the impact breakdown of different cases in (a).

Conclusion

This work developed a multi-scale integration approach to address the hydrogen network design problem with heat integration and alternative hydrogen utilities. A MILP model within a multi-objective framework was formulated, capturing both the economic and environmental constraints of the system. When applying the method into a typical refinery in Europe, it was found that the optimal hydrogen network design changed with hydrogen suppliers. The lowest cost (2.42 $/kg) and impact (4.11 kg CO2/kg) were achieved with blue hydrogen from steam methane reforming incorporating carbon capture. Future work will focus on improving the hydrogen network superstructure and assess the sensitivity of the optimization results to technical, environmental and economic assumptions

References

I. Kantor, J.-L. Robineau, H. Butun, and F. Marechal, 2020, A Mixed-Integer Linear Programming Formulation for Optimizing Multi-Scale Material and Energy Integration, Frontiers in Energy Research, vol. 8, 49

X. Liu, J. Liu, Chun. Deng, J. Lee, R. R. Tan, 2020, Synthesis of refinery hydrogen network integrated with hydrogen turbines for power recovery, Energy, vol. 201, pp. 117623

L. Tock, F. Maréchal, 2012, H2 processes with CO2 mitigation: Thermo-economic modeling and process integration, International Journal of Hydrogen Energy, vol. 37, 16, pp. 11785-11795

M. Yang, S, Zeng, X. Feng, L. Zhao, 2022, Simulation-based modeling and optimization for refinery hydrogen network integration with light hydrocarbon recovery, International JOurlan of Hydrogen Energy, vol. 47, pp. 4662-4673

Computationally efficient gas flow models for energy system optimization

Behnam Akbari, Paolo Gabrielli, Giovanni Sansavini
Institute of Energy and Process Engineering, ETH Zurich, Switzerland

Abstract: The nonconvex equations governing gas flow dynamics are computationally challenging to incorporate into long-term planning optimization of energy systems. This work proposes computationally efficient gas flow models that allow capturing flow dynamics in energy system optimizations with annual horizons. More specifically, the different behavior of gas pipes is described based on their length. We introduce a linear static model for short pipes and enhance a second-order cone dynamic model for long pipes by parallel pipe aggregation and fixing flow directions. Computational experiments on a single pipe and on the Belgian gas network validate the accuracy and efficiency of the models.

Keywords: Convex optimization, energy system optimization, gas flow dynamics, gas networks, transfer capacity

Introduction

Gas flow modeling is key to the optimization of energy systems with gaseous fuels, such as natural gas and hydrogen (Klatzer et al., 2022). However, the nonconvex equations governing gas flow dynamics pose a computational challenge to system optimization. Thus, techniques such as linear approximation (Correa-Posada and Sanchez-Martin, 2015) and second-order cone (SOC) relaxation (Chen et al., 2022) have been deployed to obtain dynamic flow models that remain computationally tractable for daily time horizons. In contrast, optimizations on longer time horizons usually rely on static flow models (Klatzer et al., 2022). However, static models neglect linepack flexibility, which is key to buffering gas supply against demand fluctuations. Furthermore, static models assume immediate gas delivery, which does not hold especially for long pipes due to the practical flow speed limit of 55 km/h (Kumar, 1987).

Gas Flow Models

Gas flow dynamics in the unidirectional pipe mn at time t are captured by the equations of continuity, Eq. (1), and momentum, Eq. (2), (Correa-Posada and Sanchez-Martin, 2015). Eq. (3) enforces the practical flow limit at the inlet (in) and outlet (out) of the pipe.

$$l_{mnt} - l_{mn(t-1)} = \Delta t\left(\phi^{\text{in}}_{mnt} - \phi^{\text{out}}_{mnt}\right) \tag{1a}$$

$$l_{mnt} = K^{l}_{mn}\left(\pi_{mt} + \pi_{nt}\right) \tag{1b}$$

$$\phi_{mnt} = \frac{1}{2}\left(\phi^{\text{in}}_{mnt} + \phi^{\text{out}}_{mnt}\right) \tag{1c}$$

$$\phi^{2}_{mnt} = K^{\phi}_{mn}\left(\pi^{2}_{mt} - \pi^{2}_{nt}\right) \tag{2}$$

$$\underline{\phi}^{\text{in}}_{mnt} \le \phi^{\text{in}}_{mnt} \le \overline{\phi}^{\text{in}}_{mnt}, \quad \underline{\phi}^{\text{out}}_{mnt} \le \phi^{\text{out}}_{mnt} \le \overline{\phi}^{\text{out}}_{mnt} \tag{3}$$

l_{mnt} and ϕ_{mnt} are the linepack and the mass flow rate of pipe mn, respectively. π_{mt} is the pressure at node m. K^{l}_{mn} and K^{ϕ}_{mn} are linepack and Weymouth constants. $\underline{\cdot}$ and $\overline{\cdot}$ denote lower and upper bounds. The model described by Eqs. (1)-(3) is convexified by relaxing Eq. (2) to

$$\left\| \begin{matrix} \phi_{mnt} \\ \sqrt{K^{\phi}_{mn}}\,\pi_{nt} \end{matrix} \right\|_2 \le \sqrt{K^{\phi}_{mn}}\,\pi_{mt}, \tag{4}$$

resulting in a SOC *dynamic model*. Further, a SOC *static model* decouples consecutive time steps with $K^{l}_{mn} = 0$. A penalty method enhances the relaxation quality and solution feasibility at a moderate computational cost. Bidirectional pipes can be modeled by adding integer variables denoting flow directions. To address the arising computational complexity, this work determines the flow directions using the SOC static model and fixes the corresponding integer variables in the SOC dynamic model accordingly.

We can formulate a *linear static model* without the addition of integer variables for bidirectional flows if pipes are sufficiently short, i.e., if K^{l}_{mn} and $1/K^{\phi}_{mn}$ are small. In this case, Eqs. (1) and (2) are approximated with Eqs. (5) and (6), respectively, and flow limits due to pressure bounds are represented as Eq. (7).

$$\phi_{mnt} = \phi^{\text{in}}_{mnt} = \phi^{\text{out}}_{mnt} \tag{5}$$

$$\pi_{mt} = \pi_{nt} \tag{6}$$

$$\underline{\phi}_{mn} \le \phi_{mnt} \le \overline{\phi}_{mn}, \tag{7}$$

$$\underline{\phi}_{mn} \le \phi_{mnt} \le \overline{\phi}_{mn}, \tag{7}$$

where $\underline{\phi}^{2}_{mn} = K^{\phi}_{mn}\left(\underline{\pi}^{2}_{m} - \overline{\pi}^{2}_{n}\right)$ and $\overline{\phi}^{2}_{mn} = K^{\phi}_{mn}\left(\overline{\pi}^{2}_{m} - \underline{\pi}^{2}_{n}\right)$.

Parallel pipes can be aggregated without affecting the total linepack and flow by setting the equivalent constants in Eqs. (1b) and (2) to

$$K^l_{mn} = \left\| \boldsymbol{K}^l_{mn} \right\|_1, \quad K^\phi_{mn} = \left\| \boldsymbol{K}^\phi_{mn} \right\|_{0.5}, \tag{8}$$

where $\boldsymbol{K}^l_{mn}$ and $\boldsymbol{K}^\phi_{mn}$ are the vectors containing the linepack and Weymouth constants of the parallel pipes, and $\| \cdot \|_p$ is the p-norm.

Computational Results

We maximize the outlet flow of a pipe to compute the transfer capacity as a measure of accuracy under static conditions. The linear static model accurately captures the dependence of transfer capacity on pipe length (Figure 1).

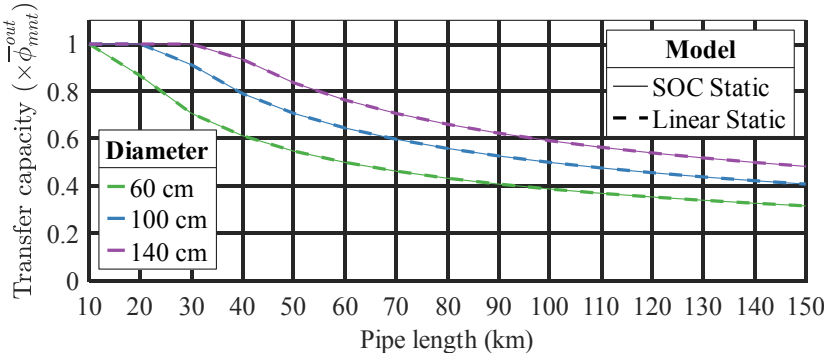

Figure 1. Pipe transfer capacity normalized by cross-section capacity ($\overline{\phi}^{out}_{mnt}$) vs. length

To assess the accuracy under dynamic conditions, we combine the linear static model for short pipes and the SOC dynamic model for long pipes in the application to the 24-pipe Belgian gas network (De Wolf and Smeers, 2000). We model an increasing number of pipes via the SOC dynamic model and minimize gas supply cost by optimizing gas supply and linepack. Figure 2 shows that 1%-2% cost saving is realized if 2-7 pipes are captured with the dynamic model, which allows linepack flexibility. While fixing the flow directions based on the SOC static model may result in minor suboptimality, it enhances the solution speed by 1-3 orders of magnitude. Because the solution time of the SOC dynamic model increases hyperlinearly with the number of pipes, parallel pipe aggregation significantly enhances solution speed. These enhancements yield accurate solutions for horizons up to 8760 hours within 300 seconds.

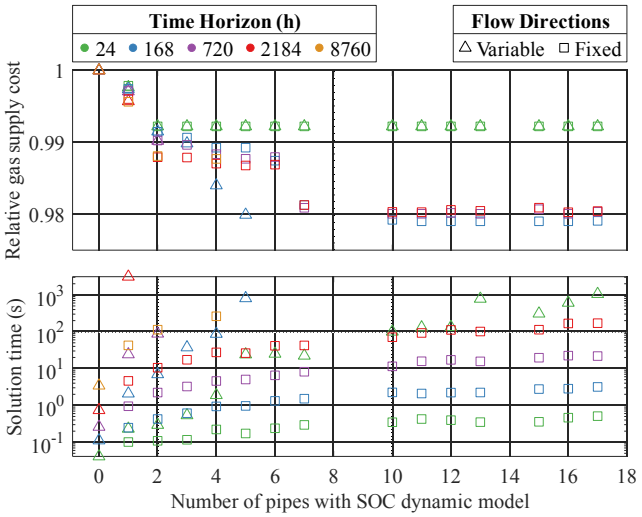

Figure 2. Application to the Belgian gas network

Conclusions

This work proposes computationally efficient gas flow models for capturing flow dynamics in long-term planning optimization of energy systems. We introduce (1) a linear static model, for short pipes, that accurately captures the transfer capacity, and (2) a SOC dynamic model for long pipes. The performance of the dynamic model is significantly enhanced by parallel pipe aggregation and fixing the flow directions using a static solution.

Acknowledgments

This work is supported by the Swiss National Science Foundation, grant no. 200021-182529, and the Swiss Federal Office of Energy as part of the SWEET PATHFNDR project.

References

Chen, Y., Xiang, J., Xie, S., Li, Y., Ni, J., Xu, Y., 2022. Optimal operation of regional meshed power–gas systems: A tightened conic relaxation based approach. Int. J. Electr. Power Energy Syst. 140, 108047.

Correa-Posada, C.M., Sanchez-Martin, P., 2015. Integrated power and natural gas model for energy adequacy in short-term operation. IEEE Trans. Power Syst. 30, 3347–3355.

De Wolf, D., Smeers, Y., 2000. The gas transmission problem solved by an extension of the simplex algorithm. Manag. Sci. 46, 1454–1465.

Klatzer, T., Bachhiesl, U., Wogrin, S., 2022. State-of-the-art expansion planning of integrated power, natural gas, and hydrogen systems. Int. J. Hydrog. Energy 47, 20585–20603.

Kumar, S., 1987. Gas production engineering, Contributions in petroleum geology & engineering. Gulf Pub. Co., Book Division, Houston.

A Pareto aggregation approach for environmental-economic multi-objective optimization problems validated on a second-generation bioethanol production model

K. Vasilakou[a,b,c] , P. Billen[b], S. Van Passel[a,c,d], P. Nimmegeers[a,b,c]
[a]Environmental Economics (EnvEcon), Department of Engineering Management, Faculty of Business and Economics, University of Antwerp, Prinsstraat 13, 2000 Antwerp, Belgium
[b]Intelligence in Processes, Advanced Catalysts and Solvents (iPRACS), Faculty of Applied Engineering, University of Antwerp, Groenenborgerlaan 171, 2020 Antwerp, Belgium
[c]VCCM Core Lab, Flanders Make, 2000 Antwerp, Belgium
[d]Nanolab Centre of Excellence, Prinsstraat 13, 2000 Antwerp, Belgium

Abstract: The increase in greenhouse gas emissions and energy demands have shifted the interest from traditional fossil fuels to biofuels, among others. Lignocellulosic biomass can be used as a renewable non-food resource for the production of advanced biofuels. In this study, a model-based multi-objective optimization approach is developed with respect to the economic and environmental performance of a second-generation bioethanol biorefinery. A method named Pareto aggregation is proposed which employs a novel multi-objective optimization based approach as an alternative for the classically used aggregation in life cycle assessment. This method identifies conflicting environmental indicators and based on decision-maker preferences, an aggregation is performed between those that require a trade-off. This aggregated environmental objective is then traded off with the economic objective function, chosen as the levelized cost of ethanol. Process parameters from a biochemical conversion pathway simulation model are chosen as optimization variables. Bioethanol production from corn stover in Belgium is used as the case study. The final Pareto optimal solutions obtained indicate the best performance possibilities for the investigated biorefinery. This research provides an insight on non-redundant objective functions while reducing the dimensionality of multi-objective environmental-economic optimization problems.

Keywords: Advanced biofuels, techno-economic assessment, environmental assessment, multi-objective optimization, Pareto front

Introduction

Life cycle assessment (LCA) is widely used to evaluate environmental impacts, by aggregating different impact categories into a single Eco-Indicator, which is normally taken as the final environmental objective function (Kalbar et al., 2017). Nevertheless, the attained solution of the problem is influenced by the weighted sum procedure. In this study, a method named Pareto aggregation is proposed which takes into consideration decision-maker preferences and identifies the most conflicting indicators and aggregates them to a final environmental objective, which is then traded-off with an economic objective. This approach is validated on a realistic and complex biorefinery case study for second-generation bioethanol production in Belgium.

Methods

Bioethanol production from corn stover is simulated in Aspen Plus v12.1, based on the model of Humbird et al. (2011). The pretreatment reactor is modelled using the kinetic model of Shi et al. (2017). The ethanol levelized production cost is calculated, while an LCA is performed in SimaPro to estimate the environmental impact. A cradle-to-gate analysis is conducted with 1kg of ethanol produced as functional unit. The life cycle inventory is based on EcoInvent database and the Midpoint ReCiPe method is used to calculate 18 environmental indicators.

The optimization variables include the pretreatment reactor temperature, acid loading and residence time. Five impact indicators, namely Global warming, Freshwater eutrophication, Marine eutrophication, Land use and Water consumption, are investigated in the Pareto aggregation, according to decision-maker preferences (Baudry et al., 2017). The multi-objective optimization problems are solved with a genetic algorithm in MATLAB, exchanging data with ASPEN Plus for the technical backbone.

Results

Ten different Pareto fronts are obtained for the five environmental indicators, which are normalized to a base case scenario. Global warming and Water consumption are conflicting indicators in contrast to Marine eutrophication and Land use, which do not require a trade-off, as the relative difference for both indicators is less than 1E-03. Based on the Pareto aggregation results, Land use indicator is not conflicting and thus is left out of the final environmental objective. The Pareto front obtained for the economic-environmental multi-objective optimization (Figure 1) indicate that there is a small trade-off to be made between the aggregated environmental and the levelized cost objectives for the studied optimization variables.

Conclusions

A novel method, named Pareto aggregation, is suggested for generating an environmental objective function, by identifying the most important and conflicting environmental indicators. This method was applied for advanced bioethanol production in an economic-environmental multi-objective optimization. A relatively small trade-off was identified for the chosen optimization variables.

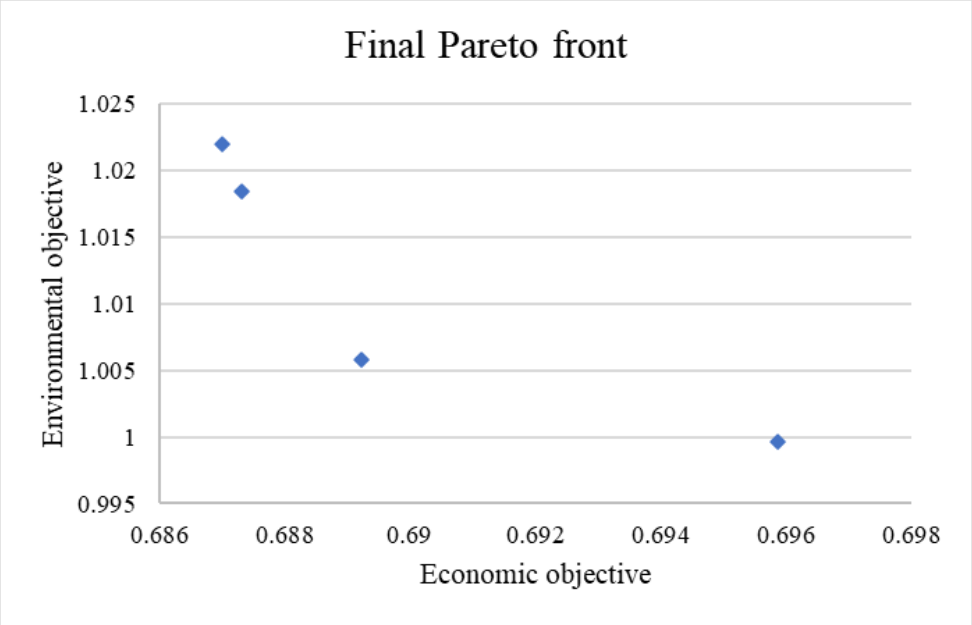

Figure 1. Economic-environmental Pareto front

Acknowledgments

This study is part of the ADV_BIO project financed by the FOD Economie - Energietransitiefonds/ SPF Économie - Fonds de Transition Energétique, call 2019-2020. Philippe Nimmegeers holds a FWO senior postdoctoral fellowship (grant number: 1215523N) granted by FWO Vlaanderen/Research Foundation Flanders.

References

Baudry, G., Delrue, F., Legrand, J., Pruvost, J., & Vallée, T. (2017). The challenge of measuring biofuel sustainability: A stakeholder-driven approach applied to the French case. In Renewable and Sustainable Energy Reviews (Vol. 69, pp. 933–947). Elsevier Ltd.

Humbird, D., Davis, R., Tao, L., Kinchin, C., Hsu, D., Aden, A., Schoen, P., Lukas, J., Olthof, B., Worley, M., Sexton, D., & Dudgeon, D. (2011). Process Design and Economics for Biochemical Conversion of Lignocellulosic Biomass to Ethanol: Dilute-Acid Pretreatment and Enzymatic Hydrolysis of Corn Stover.

Kalbar, P. P., Birkved, M., Nygaard, S. E., & Hauschild, M. (2017). Weighting and Aggregation in Life Cycle Assessment: Do Present Aggregated Single Scores Provide Correct Decision Support? Journal of Industrial Ecology, 21(6), 1591–1600.

Shi, S., Guan, W., Kang, L., & Lee, Y. Y. (2017). Reaction kinetic model of dilute acid-catalyzed hemicellulose hydrolysis of corn stover under high-solid conditions. Industrial and Engineering Chemistry Research, 56(39), 10990–10997.

Open source software for flowsheet modeling of solids processes

V. Skorych[1], C. Eichler[1,2], S. Heinrich[1]
[1]Hamburg University of Technology, Institute of Solid Process Engineering and Particle Technology, Hamburg, Germany
[2]DyssolTEC GmbH, Hamburg, Germany

Abstract: To close an existing gap in macroscale dynamic modelling of granular solids processes, the Dyssol simulation framework is being developed. This software can simulate the transient behaviour of complex process structures in the area of solids processing technology. Dyssol applies a sequential-modular approach, which allows using different calculation techniques for different units, enabling the combination of heterogeneous models in a single flowsheet. The use of the waveform relaxation method makes it possible to calculate dynamic processes fast and reliably. The used transformation matrix technique allows the correct calculation of multidimensional interdependent distributed properties of the solid phase. Both dynamic and steady-state models are supported and can be used together in the same flowsheet. The system is open-source, cross-platform and flexible, which makes it easy to add new custom modules and adjust Dyssol for each specific application.

Keywords: Flowsheet Simulation, Solids, Dynamic Processes

Introduction

Production processes of particulate materials usually have a rather complex technological structure. To obtain granular products with the desired properties, several processing steps with different types of equipment are often combined. Design, implementation, and optimization of such structures are very complex and expensive tasks due to the large number of parameters that must be considered at the same time. Numerical simulations can help solve this problem, but the variety of devices and material properties makes the simulation process very challenging when trying to combine such heterogeneous models in a single modelling environment. An additional level of complexity arises from the need to consider the transient behaviour of the processes, and from the nature of the granular matter, where every particle can have its own properties. Both significantly complicate models and simulation algorithms. The simulation system Dyssol (Skorych et al., 2017) is designed to tackle these problems, allowing dynamic flowsheet simulations of complex solids processes.

Simulation methods

There is a large diversity of models describing processes involving solids. They can use algebraic and differential equations, population balances (Skorych et al., 2019), statistical, or data-driven methods (Skorych et al., 2022), etc. To ensure the integration of such a variety of models, Dyssol applies a sequential-modular calculation approach. It assumes that every model on the flowsheet is solved independently using a suitable calculation method. This greatly increases flexibility during the model development, since now every unit can be developed disregarding the approaches applied in the rest. As a result, heterogeneous models can be used on the same flowsheet.

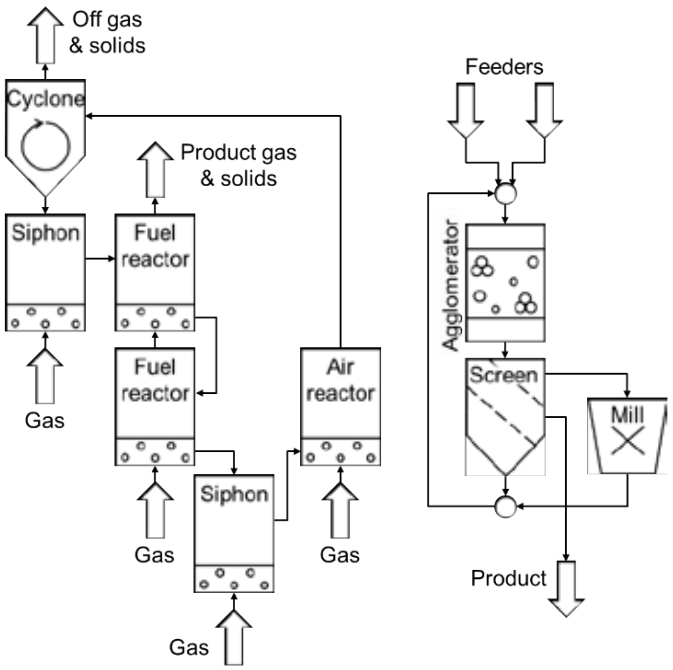

Figure 1. Process structures of chemical looping combustion (left) and agglomeration (right) processes.

One of the main drawbacks of the sequential-modular method is the complex treatment of flowsheets with recycle streams since all loops must be solved iteratively. For this, all recirculation flows are assigned initial values, and the calculation of units is repeated until a converged solution is found. Dynamic models further complicate this process, since the solution must be simultaneously found for a whole simulation interval. To overcome this, the whole interval is split into smaller time windows, and the solution is sought on each of them sequentially. This greatly reduces the number of iterations required.

Multidimensional properties of solids

One of the distinctive features of Dyssol is its advanced solids treatment. In addition to the commonly used description of bulk materials using particle size distribution, the program allows the application of additional distributed properties, like particle porosity, density, or moisture content. Moreover, they can be interdependent, forming a multidimensional set of parameters. Here, in addition to the obvious problems of storing and fast processing a large amount of data, the question arises of how to maintain the interdependency between distributions during calculations. To deal with this issue, Dyssol offers a method based on transformation matrices (Skorych et al., 2019). Here, instead of directly calculating output distributions, it is proposed to build a matrix that describes the laws of particle rearrangement between grid classes. The subsequent application of this transformation matrix allows us to calculate the target distribution and correctly maintain information about the dependent ones.

Accessibility

Dyssol has a graphical user interface that allows creating and configuring flowsheets and analyzing simulation results. It comes with extensive online documentation that includes a description of the user interface and models, explanations of the algorithms and methods used, etc. Available simulation examples and tutorials make it easier to get started with the program and develop custom models.

Dyssol and all models are written in the C++ programming language. The system provides a standardized programming interface, to allow the development of custom models. To simplify the process, preconfigured templates and examples are provided.

The source code and executables are released under the BSD license, which allows distribution, modification and use for any purpose (Skorych et al., 2020). The program runs on Linux and Windows operating systems, and its source code is available on GitHub (https://github.com/FlowsheetSimulation/Dyssol-open).

Conclusions

The developed Dyssol simulation system was designed to provide the ability to simulate the dynamic behaviour of complex production circuits built upon heterogeneous models that describe processes involving the solid phase. Advanced consideration of granular material involves its description using multidimensional distributed properties and its calculation using transformation matrices.

Thanks to its extensibility and permissive open-source software license, the program can be used without restrictions in education, science and industry for modelling a wide range of solids production processes.

Acknowledgements

The financial support of the German Research Foundation (DFG) via project HE4526/29-1 is gratefully acknowledged.

References

Skorych, V., Dosta, M., Hartge, E.-U., Heinrich, S. (2017). Novel System for Dynamic Flowsheet Simulation of Solids Processes. Powder Techn., 314, 665-679.

Skorych, V., Das, N., Dosta, M., Kumar, J., Heinrich, S. (2019). Application of Transformation Matrices to the Solution of Population Balance Equations. Processes, 7(8), 535.

Skorych, V., Dosta, M., Heinrich, S. (2020). Dyssol – An Open-Source Flowsheet Simulation Framework for Particulate Materials. SoftwareX, 12, 100572.

Skorych, V., Buchholz, M., Dosta, M., Baust, H.K., Gleiß, M., Haus, J., Weis, D., Hammerich, S., Kiedorf, G., Asprion, N., Nirschl, H., Kleine Jäger, F., Heinrich, S. (2022). Use of Multiscale Data-Driven Surrogate Models for Flowsheet Simulation of an Industrial Zeolite Production Process. Processes, 10, 2140.

Reaction kinetics modeling using bayesian symbolic regression

Daniel Vázquez, Gonzalo Guillén-Gosálbez
Department of Chemistry and Applied Biosciences, Institute for Chemical and Bioengineering. ETH Zurich, Switzerland

Abstract: Constructing accurate kinetic models can be challenging, especially when dealing with complex catalytic reactions with unknown mechanisms. This task usually requires assuming a predefined structure, e.g., a Generalized Mass Action (GMA) or a Langmuir-Hinshelwood (LH) kinetic model, and fitting the model to experimental data. In this work, we tackle the kinetic modeling of catalytic reactions using a data-driven methodology that does not assume any aprioristic structure. Specifically, we employ a symbolic regression algorithm based on Bayesian inference to automatically build kinetic expressions from data. The advantage of symbolic regression is that it returns a closed-form mathematical expression, avoiding using rigid kinetic formalisms. Our results show that our methodology can accurately describe given data while providing a more interpretable model than pure data-driven methodologies, such as artificial neural networks or Gaussian processes.

Keywords: Symbolic regression, kinetic modeling, Bayesian machine scientist

Introduction

Deriving accurate kinetic models of reaction systems is a challenging task that requires solving two nested problems, i.e., model identification and parameter estimation. First, the model structure needs to be defined, and the optimal parameter values are found next (considering some experimental data). In this work, we perform model identification for describing complex heterogeneous kinetic systems using a data-driven methodology based on symbolic regression. In essence, the idea is to apply symbolic regression to build kinetic models without any predefined structure. To this end, we employ the Bayesian Machine Scientist (BMS) (Guimerà et al., 2020) to predict reaction rates, using acrylonitrile production in propene ammoxidation over α-bismuth molybdate as a testbed (Licht et al., 2016). Usually, parameter estimation for kinetic model building is solved either sequentially or simultaneously (Michalik et al., 2009), and very often considering a given fixed mathematical structure based on first principles, such as the Generalized Mass Action (GMA) and Langmuir-Hinshelwood (LH) models. The difference lies in how the parameters of these models are fitted. During the sequential approach, integration is required at each fitting step, which is computationally costly. As for the simultaneous approach, the regression problem requires the differential equations to be reformulated using orthogonal collocation methods. This results in a complex nonlinear programming (NLP) model, where providing a good initial point might be challenging.

Here, we shall assume no aprioristic model structure concerning the kinetic expression but rather build one not constrained by any formalism using symbolic regression. Moreover, we apply an incremental approach that decouples fitting from integration (Brendel et al., 2006). This strategy avoids both the iterative integration step and solving complex NLPs while facilitating the application of symbolic regression for kinetic model building. Notably, after obtaining the species slopes analytically, we derive closed-form expressions that predict their values from the state variables using symbolic regression. This allows us to obtain a flexible analytical kinetic expression that is more interpretable than standard black-box surrogates.

Methods

We consider a general kinetic modeling problem where we are given concentration profiles of the species involved in a reaction, and the goal is to find a kinetic model encompassing a set of differential equations that accurately approximate such profiles. To illustrate the capabilities of the approach, we focus on acrylonitrile production in propene ammoxidation over α-bismuth molybdate.

Our methodology, which employs the previously mentioned BMS algorithm for symbolic regression, comprises the following general steps discussed below.

1) Reproduce isothermal isobaric kinetic experiments in silico at different temperatures. The kinetic data is obtained from Licht et al. (2016).
2) Obtain the slopes of the desired species profiles by using symbolic regression to describe them analytically. This is done by applying a one-dimensional BMS for symbolic regression and analytically differentiating the resulting expression.
3) Train a general BMS using state variables, i.e., partial pressures of all the species and temperature, to fit the previously calculated slopes.
4) Obtain the performance metric, i.e., R^2, of the integrated BMS models using in silico profiles.

We create ten training experiments, with temperatures separated uniformly from 607 K to 773 K. The initial conditions consist of a flow of C3H6, NH3, O2, H2O, and inert such that, at 273 K and with a volumetric flow of 100 mL/min, the partial pressures are respectively 8, 8, 16, and 10.5 kPa for the four reactive species assuming ideal gas behavior. The total pressure is 120 kPa. The experiments are kept isothermal and isobaric. We perform a comparison among three different cases: (1) low conversion of the main reagent, i.e., propene, without noise with extrapolation (LC), (2) complete conversion of propene with Gaussian noise and 500 equidistant points (N1), and (3) complete conversion of propene with Gaussian noise for 50 equidistant points (N2). We also compare the results from fitting the BMS equation using the true value of the rate obtained from the in silico true kinetic expression

(TV) and the approximate value from differentiating the analytical expression (AV), for a total of six different BMS models.

Results

The performance results are shown in Table 1. The integrated points to calculate the performance metric for the test experiments are chosen as 21 equidistant points between 0 and 10 m2 of the catalyst surface. Numerical problems may arise during the integration of the symbolic model. Hence, we report the results up to the point when the integrator fails in those cases.

Table 1. Test experiments for the six BMS models

Test run	T [K]	R^2_{TV} (LC/N1/N2)	R^2_{AV} (LC/N1/N2)
#1	613	**0.99**/0.99/0.89	**0.99**/0.98/0.70
#2	630	**1.00**/0.99/0.99	**0.99**/0.99/0.98
#3	646	0.99/**0.99**/0.99	0.99/**0.99**/0.97
#4	663	0.98/**0.99**/0.99	**0.99**/0.99/0.94
#5	680	0.75/**0.99**/0.99	**0.99**/0.98/0.95
#6	696	0.72*/**0.99**/0.99	0.95/**0.97**/0.96
#7	713	0.77*/**0.99**/0.99	0.91/0.91/**0.96**
#8	730	0.81*/**0.99**/0.99	0.83/0.93/**0.98**
#9	747	0.82*/**0.99**/0.98	0.71/**0.88**/-8.48
#10	763	0.83*/0.84/**0.85**	0.43/**0.70**/-12.51

**Indicates that the integration was stopped due to numerical errors.*
***Bold** signals the best model for each test run.*
An R2 value close to one implies that the BMS model correctly approximates the in silico model.

Conclusions

Here we applied symbolic regression to find analytical kinetic models of reaction systems. We found that the proposed framework can identify fairly accurate models for most test experiments. In some cases, especially at higher temperatures, the integrated result differs significantly from the in silico profiles. As expected, the best results are obtained using true slopes to train the BMS (TV), although numerical instability during extrapolation arises in the low conversion cases (LC). Therefore, iteratively adjusting the calculated slopes may improve the methodology.

Acknowledgments

This publication was created as part of NCCR Catalysis (Grant 180544), a National Centre of Competence in Research funded by the Swiss National Science Foundation.

References

Brendel, M., Bonvin, D., & Marquardt, W. (2006). Incremental identification of kinetic models for homogeneous reaction systems. Chemical Engineering Science, 61(16), 5404–5420. https://doi.org/10.1016/j.ces.2006.04.028

Guimerà, R., Reichardt, I., Aguilar-Mogas, A., Massucci, F. A., Miranda, M., Pallarès, J., & Sales-Pardo, M. (2020). A Bayesian machine scientist to aid in the solution of challenging scientific problems. Science Advances, 6(5). https://doi.org/10.1126/sciadv.aav6971

Licht, R. B., Vogt, D., & Bell, A. T. (2016). The mechanism and kinetics of propene ammoxidation over α-bismuth molybdate. Journal of Catalysis, 339, 228–241. https://doi.org/10.1016/j.jcat.2016.04.012

Michalik, C., Chachuat, B., & Marquardt, W. (2009). Incremental Global Parameter Estimation in Dynamical Systems. Industrial & Engineering Chemistry Research, 48(11), 5489–5497. https://doi.org/10.1021/ie8015472

Closing the balance- the pulp industry as a prosumer in the energy system

Julia Granacher[a], Jonas Schnidrig[a], Rafael Castro-Amoedo[a], Meire Ellen Gorete Ribeiro Domingos[a,b], François Maréchal[a]
[a]Ecole Polytechnique Fédérale de Lausanne, Rue de l'industrie 17, 1950 Sion, Switzerland

Abstract: This paper aims to analyze the potential of transforming pulp plants into integrated biorefineries, considering the conversion pathways of biomass-to-X, Power-to-X, and X-to-power as well as the capture and utilization of carbon dioxide, and operating them as part of a dynamic energy system subjected to fluctuations induced by renewable resources.

A superstructure optimization model of the integrated system is developed and analyzed under a variety of scenarios forecasting resource availability, energy demand and availability and product demand. For identified solutions, costs of internal flows between stakeholders of the system are derived, revealing that the mill operator, utility operator, and district are able to significantly improve their environmental impact at reasonable economic loads.

From the mill operator's perspective, the profitability of a configuration is largely dependent on the market profile of crude oil and electricity prices, while the mill's carbon efficiency can be increased from 50% to up to 86%, profiting from carbon capture and utilization in fuel production and mineralization. The emissions of the district can be reduced by up to 70% compared to non-integrated operation.

Keywords: pulp industry, integrated biorefineries, power-to-X, carbon capture and utilization

Introduction

Pulp and paper mills are known to convert large amounts of woody biomass, usually being a net exporter of energy in form of electricity. While not consuming significant amounts of fossil resources, the limited availability of woody biomass enhances the shift towards an intensification of resource usage in the pulp industry by co-production of pulp and other bio-based products. Simultaneously, a shift from fossil energy carriers to renewables is likely to generate uncertainties in electricity supply and related environmental impact on the energy system, causing a mismatch of demand and supply. In that regard, renewable power-to-X (P2X) is an emerging concept for storing excess electricity from intermittent renewable energy while supporting the decarbonization of transport and energy infrastructure. Furthermore, Carbon capture and utilization (CCUS) offers great potential to reduce emissions in industrial applications. In this contribution, the integration of a pulp mill biorefinery in the energy system is investigated regarding potential benefits for mill operators and districts. Besides profitable selling prices of commodities, the emission reduction and self-sufficiency potential of the different stakeholders are analyzed.

Methods

In the first step, solutions of the integrated system are generated. Then, promising configurations are analyzed regarding their implications for the stakeholders of the system.

Superstructure development and solution generation

The superstructure optimization of the integrated pulp biorefinery described by (Granacher et al., 2022) is extended with P2X and X2P options as well as CCUS technologies, and placed next to a residential district. P2X and X2P include a Solide Oxide Electrolysis /Fuel cell (SOEC/SOFC) unit operation, as well as multiple thermo-chemical-based fuel production options from bark and black liquor, as elaborated in (Granacher et al., 2022).

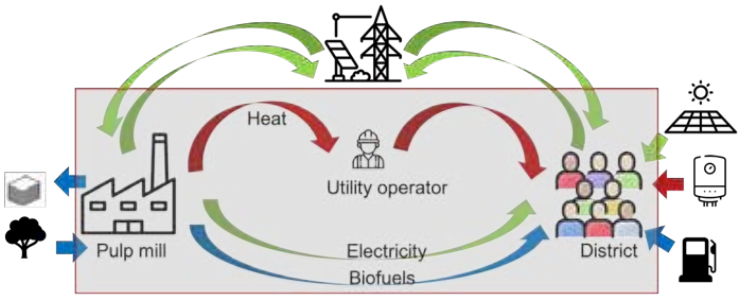

Figure 1: Simplified superstructure representation. Internal exchanges in the grey box are considered to be free of charge, everything that is exchanged with outside has a price.

CCUS includes carbon capture at all burner units in the superstructure using chemical absorption, sequestration and mineralization. The process units in the integrated mill biorefinery, consisting of the pulp mill, fuel production, CCUS, and P2X/X2P are connected via a steam network to allow for the exchange of heat and energy integration, as described in (Kantor et al., 2020). Mill and district are assumed to be able to exchange heat via a district heating network, as well as power and fuels; for everything that cannot be satisfied internally, external sources can be purchased. The temporal resolution of district demands for heating, electricity and transport, market prices, and impact factors are taken into account in the optimization formulation. Figure 1 summarizes the suggested superstructure. The defined superstructure is used in a multi-objective optimization framework to generate solutions for a multitude of market and environmental scenarios, as previously described in (Granacher et al., 2022).

Optimization of internal cost

An optimization problem is formulated that determines the cost for internal flows for the obtained configurations. For this purpose, the cost each stakeholder sees in each configuration are derived as a function of the selling prices of heat, electricity, and fuels. The flowrates of internal exchanges are fixed in each configuration and the optimal prices of commodities are determined by a parameterized Mixed Integer Linear Programming (MILP) optimization problem, that minimizes the cost of the district while setting constraints on the cost of the utility and the mill operator. Besides fixing the prices of the internal exchanges, the optimization determines the configuration that is preferable for a given constraint optimization problem.

Results

When generating configurations of the integrated system using the superstructure formulation and optimization strategy described previously, multiple configurations are identified that perform economically better than the conventional, non-integrated operation of the system. Figure 2 shows the CO2 taxes that would be needed so that a certain configuration is as profitable as conventional, non–integrated operation of the system for direct (S1), indirect (S2) and direct and indirect (S12) emissions. Negative taxes indicated that a configuration is already more profitable than the conventional operation, at least on the system perspective. However, while serving as a nice indication on emission reduction potential, the perspective of the system where internal flows are for free does not mirror the reality. Therefore, the optimization problem formulated for internal flows is used to derive preferable combinations of commodity cost. For the optimization of internal cost, the TOTEX of the mill operator is constraint to parameterized percentages of the TOTEX for conventional operation, while for the utility operator who operates a district heating network between the mill and the district, the payback period is parameterized.

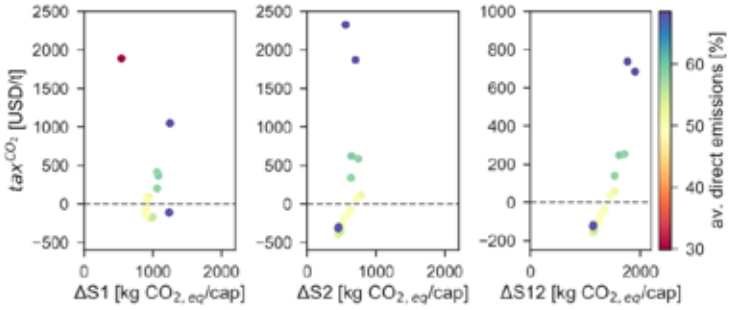

Figure 2: Required carbon taxes for system configurations to break even with the conventional operation, derived for direct (S1), indirect (S2), and direct and indirect (S12) emissions.

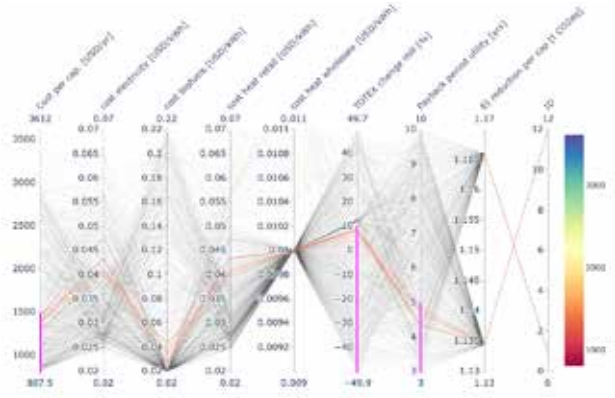

Figure 3: Results of internal optimization for the cost of mill operator, district (per capita) and utility operation, and resulting prices of commodities

Figure 3, (left) shows the TOTEX change the mill operator is subjected to, the cost per capita, and the payback period of the utility operator. Furthermore, Figure 3 (right) displays the required energy commodity prices if certain constraints on the stakeholder cost need to be met. Commodity prices stay well within the current market range, and emissions per capita can be reduced by up to 70% compared to non-integrated operations.

Conclusion

In this work, synergies between an integrated pulp biorefinery and a nearby district have been analyzed. For the mill operation, significant emission reduction potential of biogenic carbon during pulp production by means of CCUS coupled with P2X and X2P and fuel production has been identified. For the integrated system considering the district demands, large shares of the fossil emissions of the district can be avoided by replacing fossil fuels with products from the integrated pulp biorefinery. Optimization of internal flows reveals that the integration is viable for all stakeholders, suggesting that not only environmental but also economic benefits could arise from the integration.

Acknowledgments

This research has received funding from the European Union's Horizon 2020 research and innovation program under grant agreement No 81801.

References

Granacher, J., Nguyen, T.-V., Castro-Amoedo, R., McDonald, E.C., Maréchal, F., 2022. Enhancing biomass utilization by combined pulp and fuel production. Frontiers in Energy Research 10.

Kantor, I., Robineau, J.-L., Bütün, H., Maréchal, F., 2020. A Mixed-Integer Linear Programming Formulation for Optimizing Multi-Scale Material and Energy Integration. Frontiers in Energy Research 8, 49. https://doi.org/10.3389/fenrg.2020.00049

Hybridization of analytical surrogates with first principles using bayesian learning

Sachin Jog, Daniel Vázquez, Raúl Calvo-Serrano, Gonzalo Guillén-Gosálbez
Institute for Chemical and Bioengineering, Department of Chemistry and Applied Biosciences
ETH Zurich, Switzerland

Abstract: Surrogate formulations have become very popular to optimize complex process simulations, alone or combined with first principles within the framework of hybrid modeling. However, conventional surrogates like neural networks or Gaussian processes, are hard to globally optimize, particularly when combined with mechanistic equations in a hybrid model. Alternatively, analytical surrogates could be built using symbolic regression, which attempts to find an analytical equation explaining given data, giving rise to a fully analytical hybrid model integrating first principles and surrogate equations. Such a hybrid model could then be locally or globally optimized using standard optimization algorithms that would have access to accurate derivatives based on the analytical hybrid model. Following these ideas, here we explore the use of Bayesian symbolic regression to build hybrid analytical surrogate models, finding that this approach outperforms fully black-box models and the standard optimization tools available in Aspen Plus®.

Keywords: Hybrid modeling, Bayesian symbolic regression, Black-box models

Introduction

The ability of computer simulation software to mimic the real production process with sufficient accuracy has popularized their use in the modeling of chemical processes. However, the first principles models used in these simulators are often complex, and it may be challenging to estimate derivatives accurately (McBride & Sundmacher, 2019). During optimization, this can result in entrapment in local optima or failure to converge to a feasible point. To improve the numerical robustness of these first principles models, surrogate models have become popular solutions under two different approaches. The first approach is the generation of a model involving a direct mapping of the input-output relationship between the degrees of freedom and the objective function, known as a black-box surrogate model. These models present limitations, including poor extrapolation capabilities and a lack of interpretability, which have led to the development of models combining black-box and mechanistic equations, known as hybrid surrogate models. For example, Kahrs & Marquardt (2007) generated a hybrid model to maximize the ethylene glycol yield using Artificial neural networks (ANNs) complemented with mass balances and vapor-liquid equilibrium equations. Quirante & Caballero (2016) substituted complex units of a sour water stripping plant with kriging surrogate models to yield a hybrid model for process optimization. These hybrid models are hard to globally optimize, despite some recent work in the field (Schweidtmann & Mitsos, 2019). Alternatively, analytical surrogates without any predefined canonical form can be built using symbolic regression, which attempts to find an analytical equation describing the given data and the values of its parameters without assuming any predefined model structure. The use of symbolic regression to generate a closed-form analytical expression that can be combined with first-principles equations could potentially improve the numerical robustness of the optimization step by facilitating the application of derivative-based global solvers to the analytical hybrid model. Recently, Cozad & Sahinidis (2018) introduced an elegant MINLP formulation for symbolic regression which relies on the use of deterministic solvers known to lead to large CPU times. Alternatively, Guimerà et al. (2020) introduced the Bayesian machine scientist (BMS), which generates closed-form analytical expressions using Bayesian probability and Markov chain Monte Carlo (MCMC) sampling. For the first time, the BMS is used in this work for the hybrid surrogate modeling and optimization of process flowsheets.

Methodology

A propylene glycol production process is simulated in Aspen Plus® v11, which consists of a single continuous stirred tank reactor (CSTR) and a distillation column. The calculations are implemented in an Intel® Core i7-10700 CPU @ 2.90 GHz computer. The first step is to use Latin hypercube sampling (LHS) to generate values for the degrees of freedom of the process units within allowable ranges. Python 3.7 sends these values to Aspen Plus® and reads the required outputs. These inputs and outputs are then used to construct surrogate models using the BMS. Here we explore three different approaches. The first method (BB) is to construct one black-box surrogate model that calculates the unitary production cost (in $/kg), i.e., the objective function (OF) to minimize. The second method (H1) is to construct separate surrogate models to predict the output variables of the CSTR and the distillation column, complementing them with mass balances of the flowsheet (e.g., the stream mixer and recycle stream), resulting in a hybrid surrogate model. The third method (H2) uses the same surrogate models of the CSTR and distillation column generated in H1 and inserts them into the Aspen Custom Modeler® (ACM) v11, thus substituting only these two units in Aspen Plus® to generate a hybrid surrogate model. The optimization of BB and H1 is carried out in the algebraic modeling system, GAMS v35.2.0, using BARON (Tawarmalani & Sahinidis, 2005) v21.1.13, while the in-built optimizer in Aspen Plus® is used for H2. The optimal OF obtained from the three methods and the deviation in the OF between the surrogate models and the rigorous simulation is computed by inserting the optimized design variables back into the rigorous simulation. The termination criteria set for BARON are a maximum CPU time of 14,400 seconds and a relative optimality gap of 10-9.

Results and Conclusions

Table 1 shows the numerical results obtained from the optimization of the three methods:

Table 1. Results obtained from the three methods, where the optimal solutions are evaluated in Aspen Plus®

Method	CPU time (s)	OF Surrogate model ($/kg)	OF Aspen Plus® ($/kg)	Deviation (%)
BB	14400.00	3.52	3.55	-0.77
H1	0.20	3.56	3.55	0.45
H2	5.00	3.61	3.60	0.11

The deviation between the optimal OF values from the surrogate model and rigorous simulation is less than 1% in all three cases. However, when the actual values of the OF are compared, it can be seen that H2 performs 1.41% worse than the other methods, while BB and H1 return the same value (i.e., 3.55 $/kg). Comparing BB and H1 further, it is observed that the former does not close the optimality gap fully, while the latter does so in just 0.2 seconds. Thus, the hybrid surrogate model (H1) in GAMS returns the global minimum of the hybrid model in only 0.2 seconds, with a relative optimality gap of 10-9, and a 0.45% deviation between the surrogate model and rigorous simulation.

Therefore, the hybrid surrogate model (H1), consisting of surrogate models complemented with mass balances and optimized in GAMS, presents the best performance. Overall, this work shows that hybrid surrogate modeling based on Bayesian learning can effectively improve the optimization performance of process flowsheets.

References

Cozad, A., & Sahinidis, N. V. (2018). A global MINLP approach to symbolic regression. Mathematical Programming, 170(1), 97–119.

Guimerà, R., Reichardt, I., Aguilar-Mogas, A., Massucci, F. A., Miranda, M., Pallarès, J., & Sales-Pardo, M. (2020). A Bayesian machine scientist to aid in the solution of challenging scientific problems. Science Advances, 6(5).

Kahrs, O., & Marquardt, W. (2007). The validity domain of hybrid models and its application in process optimization. Chemical Engineering and Processing: Process Intensification, 46(11), 1054–1066.

McBride, K., & Sundmacher, K. (2019). Overview of Surrogate Modeling in Chemical Process Engineering. Chemie-Ingenieur-Technik, 91(3), 228–239.

Quirante, N., & Caballero, J. A. (2016). Large scale optimization of a sour water stripping plant using surrogate models. Computers and Chemical Engineering, 92, 143–162.

Schweidtmann, A. M., & Mitsos, A. (2019). Deterministic Global Optimization with Artificial Neural Networks Embedded. Journal of Optimization Theory and Applications, 180(3), 925–948.

Tawarmalani, M., & Sahinidis, N. V. (2005). A polyhedral branch-and-cut approach to global optimization. Math. Program., Ser. B, 103, 225–249.

Data embedding and hybrid modeling for industrial fluid catalytic cracking

Dimitrios Blitas, Antonis Kokossis
School of Chemical Engineering
National Technical University of Athens, Greece

Abstract: Fluid catalytic cracking is a both a critical and complex operation for refineries. Furthermore, the nature of the process (complex feedstock, complex sets of reactions and products) bears similarity with the complexity of emerging technologies in bio-renewables such as pyrolysis or hydrothermal liquefaction. FCC models are either linear and bilinear models adapted by regression or data-driven models. Instead, the paper explores machine-learning technologies to combine first-principle based models by embedding operational data from a real process. This artificial data, derived from equation-based models acts directly on neural network parameters, steering them in the right direction without the formation of new or updated input-output equations. The embedding provides for a systematic use of measurements form the plant while the first-principle based models offer a basis to explain the performance of the model. Early results illustrate very satisfactory accuracy, faster times and the opportunity to reduce the complexity of the process.

Keywords: Fluid catalytic cracking, neural networks, data embedding

Introduction

Fluid catalytic cracking (FCC) is the most economically important refinery operation currently in use. The process contributes about 35% of total gasoline production, as well as other valuable refined products. The process itself is markedly complex. FCC units make use of high temperatures, as well as specialized catalysts which continuously circulate, to break down complex hydrocarbons into simpler compounds.

To tackle the complexity of the FCC process, various approaches to modeling have been proposed. The earliest papers in FCC modeling relied on lumped kinetics and is widely used to this day. In lumped kinetic (LK) models, feed and product components are grouped into pseudo-components by means of clusters. Criteria for sorting feed or product components into lumps (boiling point range, chemical structure, etc.) may vary. Feed lumps are connected to product lumps by arrows, which represent cracking reactions and set up the basis for equation-based analysis. Models are derived from first principles and simplified with the use of empirical assumptions. Other than simplifying the process, LK models offer important means to both understand and manipulate the FCC process. Further model reduction is always possible but at the peril to compromise understanding of the process and model accuracy.

Data-driven models are able to abstain from first principles as they apply systems analysis to infer input-output relationships using multi-parametric models that range from simple linear models to deep learning developments trained out of data from daily operations. Such models can be used to monitor the FCC performance in design, off-line and on-line control applications. They are less demanding computationally, can make full use of plant data and are reported to monitor performance quite accurately. However, they fail to offer proper insights for the process and are prone to significant errors whenever in use outside the particular remit of data space they have been trained for.

Motivation and approach

There is an apparent motivation to upgrade first-principle-based models towards hybrid models that make systematic use of operational data, thus combining merits of available approaches currently in use. Rather than directly inferring input-output relationships, data embedding may infer model parameters used in the first-principle-based models. Training could alternatively use a superset of data comprised by curated simulations and operational data. Data include then: (a) sets of curated (simulation) data from constitutional equations of first-principle based models in the FCC; and (b) operational data from the process. A simple diagram for the data flows is illustrated in Figure 1.

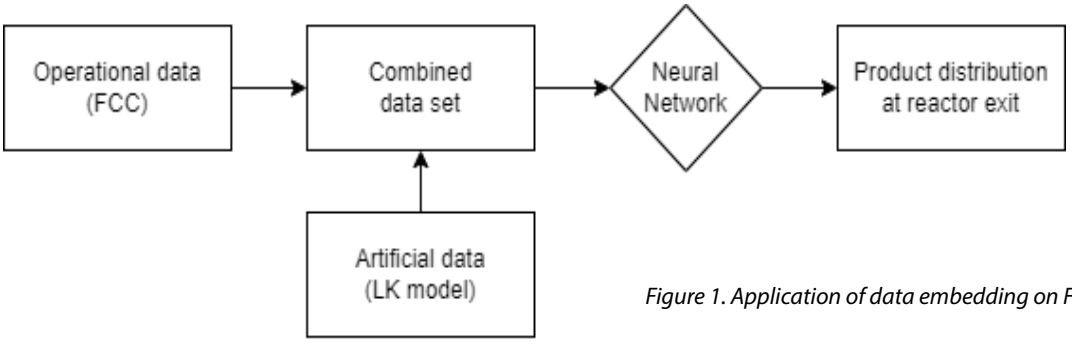

Figure 1. Application of data embedding on FCC model

Methodology and implementation

The approach addresses the importance of merging data from two different resources (plant data, curated data) assessing the potential of the merged approach to improve the accuracy of the LK model as well as the ability of the data-based model to generalize outside the remit of the training set used.

Table 1: Proposed model input and output variables

Input variables	Output (yields)
Feed volume flow (m^3/h)	Slurry
Feed temperature (°C)	LCO
Reactor temperature (oC)	Total Naptha
Regenerator temperature (oC)	Coke
Regenerator air flow (kNm3/h)	LPG
	Sour Gas

The methodology involves a staged approach that is applied as follows: (i) a curated model is developed based on a LK method (deterministic model) to produce datasets ds1, and predict the FCC output, (ii) data streams ds2 from the real process are increasingly merged and hybridize ds1 to predict (neural network) new FCC outputs, and (iii) the process continues measuring the level of improvement achieved as each stage by reporting improvements in the accuracy of predictions for each one of the output streams of the system. Aspen HYSYS was used to produce an LK model; the ANN was developed in Python: ds1 consists of 55 rows of data, generated by use of the case study function in HYSYS. ds2 consists of 70 rows of operational data from the HELPE FCC unit at the Aspropyrgos refinery, of which 15 were randomly selected to be used as the test set and 55 as the initial training set. Data from ds2 was introduced in increments of 10% to form the hybridized ds1, which ultimately consisted of equal parts real and curated data. The ANN underwent 100 instances of training at each step, of 1000 epochs each. The best results achieved through training at each 10% step were used as the basis for analysis.

Results and conclusions

Data embedding significantly improved the prediction accuracy of the initial model (Fig.2). In the case of naptha and LPG average prediction errors were markedly reduced (Table 1). Good predictions were already achieved at 10% hybridization for certain products and rapidly improved at 20% and beyond for the overall model.

Table 2: Relative error of predictions at various ratios of data embedding

Relative Pred. error	0%	20%	50%
Naptha	0.032	0.023	0.022
LPG	0.054	0.051	0.022

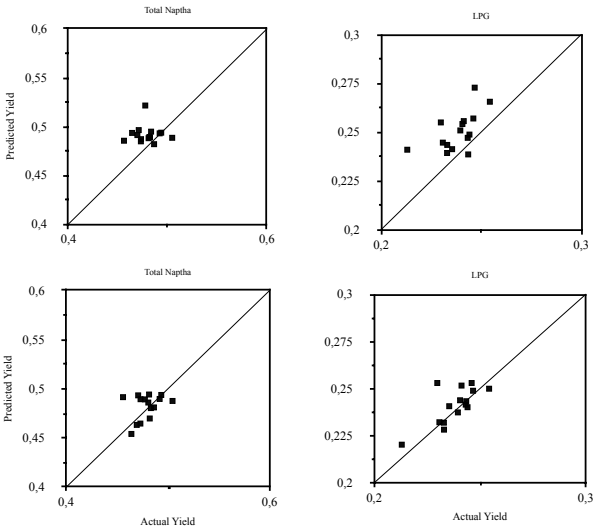

Figure 2. Model fit diagrams for naptha and LPG product (top-0% hybridization, bottom-50% hybridization)

Acknowledgments

We are grateful to Athanasios Stefanakis and Dimitra Kolokotsa of HELPE for providing operational data and constant support and guidance throughout the project.

References

G.M. Bollas, 2003, Chemical Engineering and Processing, 42, 8, 697-713

E. Kawai, 2020, J. Adv. Manuf. Process. 2022, 4, 3

C. Pinheiro, 2012, Fluid Catalytic Cracking (FCC) Process Modeling, Simulation and Control, Ind. Eng. Chem. Res, 51, 1, 1-29

F. Yang, 2020, Chemical Engineering Research and Design,Volume 155, 202-210

Improvement of probability distribution estimation using method of moments with Lagrange interpolation approach

Meltem Turan[a], Joakim Munkhammar[b], Abhishek Dutta[c]
[a]Department of Mathematics, Ege University, Izmir 35180, Turkey
[b]BEESG, Department of Engineering Sciences/Uppsala University, Uppsala, Sweden
[c]Department of Chemical Engineering, Izmir Institute of Technology, Gulbahce Campus, Izmir 35430, Turkey

Abstract: Moment-based determination of a probability density function (PDF) is widely used in chemical and process engineering applications. In this study, a procedure is suggested for estimating interpolation approximation to unknown (or known) PDFs. The procedure is based on the reconstruction of a distribution knowing only a finite number of moments using Lagrange interpolation. To show the improvement through this approach, test cases have been solved with complex integro-differential equation such as Smoluchowski coalescence equation (SCE) with both linear and product kernels. The results are then compared using the polynomial approach for estimating probability distributions using moment-based determination and analytic solutions where possible.

Keywords: method of moments, probability density function, Lagrange interpolation, population balance equation

Introduction

Determination of a probability density function (PDF) by using moments is an active research area in chemical and process engineering. Although various moment-based methods have been proposed in the literature, in all these methods only a finite number of moments associated with the real distribution are ultimately determined. A more recent procedure was proposed by Munkhammar et al. (2017) for estimating N-order polynomial approximation of a PDF based on N statistical moments. However, the procedure has certain limitations such as experimentally determining the interval and the degree of approximation polynomial where the convergence is best, and using the goodness-of-fit test which is not always reliable (Goldman and David, 2018) as a stopping criterion. This leads to increase in error, rise in the number of arithmetic operations and the loss of time. The above-mentioned shortcomings in the moment-based determination of a PDF are the primary motivation of this study.

This study focuses on estimating interpolation approximation to a complex integro-differential population balance equation (PBE). To overcome the above-mentioned shortcomings, a procedure based on the reconstruction of a distribution knowing only a finite number of its moments by Lagrange interpolation is proposed. As an example, two cases of Smoluchowski coalescence equation (SCE) with both linear and product kernel (Aldous, 1999) whose solutions are probability density distributions has been solved using the approach of Munkhammar et al. (2017) and the approach proposed in this study.

Case 1: Smoluchowski coalescence equation (SCE) with linear kernel from Aldous (1999)

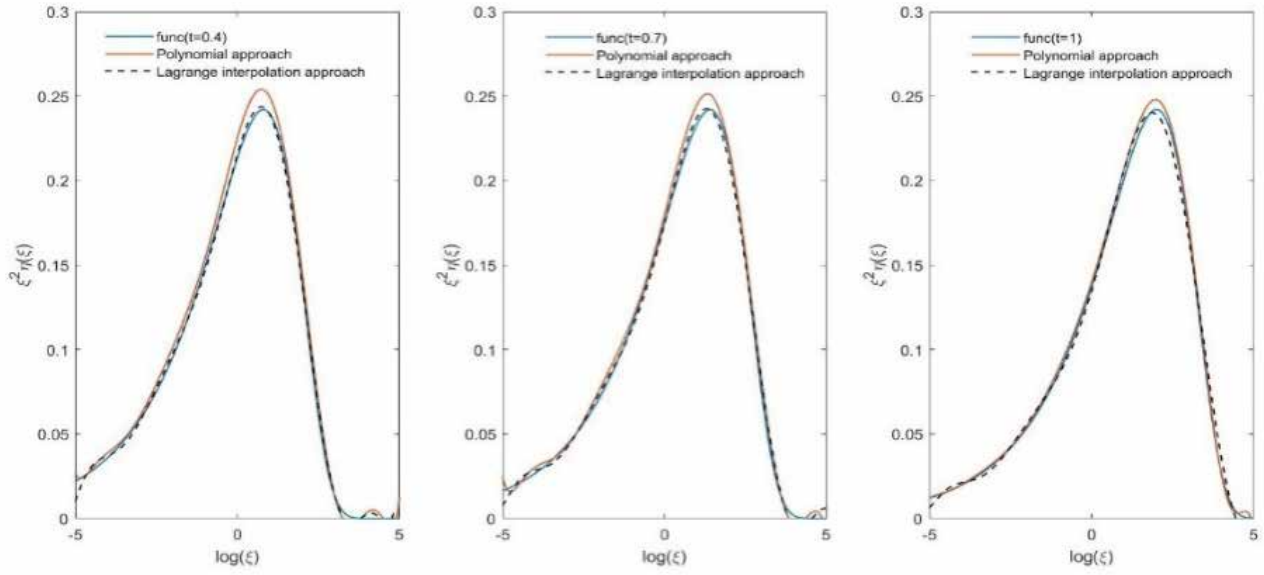

Fig. 1. Approximate solutions with the analytic solution (blue) obtained by polynomial approach (red) and Lagrange interpolation approach (black) with t = (a) 0.4, (b) 0.7 and (c) 1

Case 2: Smoluchowski coalescence equation (SCE) with product kernel from Aldous (1999)

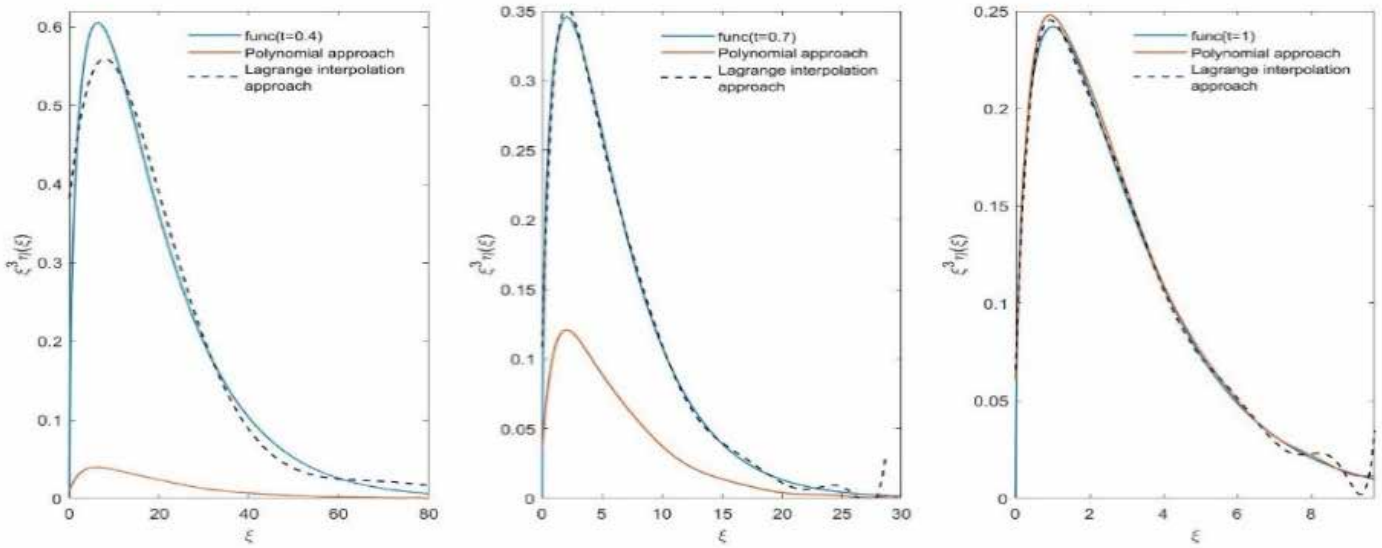

Fig. 2. Approximate solutions with the analytic solution (blue) obtained by polynomial approach (red) and Lagrange interpolation approach (black) with t = (a) 0.4, (b) 0.7 and (c) 1.

Table 1. Root mean square error (RMSE) values for the two cases used in this study using polynomial approach, Lagrange interpolation approach with the corresponding analytic solution.

Cases	RMSE using polynomial approach	RMSE using Lagrange interpolation approach	Improvement (%)
Smoluchowski coalescence equation linear kernel (t=0.4, 0.7, 1)	0.1930 0.1517 0.0868	0.0687 0.0922 0.0860	64 39 0.9
Smoluchowski coalescence equation product kernel (t=0.4, 0.7, 1)	23.1967 5.1011 0.0642	1.7096 0.1314 0.0534	> 90 > 90 16

Conclusions

As seen in the results, the modified Lagrange interpolation approach shows an improvement from the polynomial approach for narrow distributions. For the SCE, there is a clear improvement using the modified approach by 64 % for linear kernel and by 90% for product kernel. This is mainly because equal distance points are used in the polynomial approach while Chebyshev polynomial roots are used in Lagrange interpolation approach. It is also concluded that the polynomial approximation shown in this study is a reasonable fit to the analytically obtained results for N = 11.

References

Aldous, D.J. (1999). Deterministic and stochastic models for coalescence (aggregation and coagulation): a review of the mean-field theory for probabilists. Bernoulli, 5, 1.

Munkhammar, J., Lars M., Jesper R. (2017). Polynomial probability distribution estimation using the method of moments. PloS One, 12, 4.

Goldman, M, David M.K. (2018). Comparing distributions by multiple testing across quantiles or CDF values. Journal of Econometrics, 206, 1.

THEME 2
Modelling and optimization for multi-scale integration

Paper 610 | Comparative Analysis and Improved Scheduling Model for MULTI-STAGE Biopharmaceutical Processes | 42

Comparative Analysis and Improved Scheduling Model for MULTI-STAGE Biopharmaceutical Processes

Vaibhav Kumar, Munawar A. Shaik
Department of Chemical and Petroleum Engineering, College of Engineering
UAE University, Al Ain, United Arab Emirates

Abstract: In this study, we present a general analysis of relevant literature models for continuous manufacturing of biopharmaceuticals, along with a critical discussion on some of the deficiencies that were observed. The proposed model extends an earlier unit-specific event-based model with additional features including modeling of shelf-life and minimum campaign length to continue over multiple events, in contrast to the literature models. We also present different scenarios based on whether early delivery of products is allowed or not. These improved features lead to better modeling, and the performance of the proposed model is evaluated on selected examples based on industrial data adopted from the literature giving higher profit.

Keywords: Mathematical modelling, Optimization, Scheduling, Biopharmaceuticals.

Introduction

The biopharmaceutical industry has been developing significantly with growing demand for therapeutic drugs. The concerned challenges associated with drug development and cost-effective manufacturing require a decision support system for improving resource utilization. Several deterministic and stochastic/evolutionary approaches have been reported in the literature to schedule a multiproduct facility for the batch and continuous manufacturing of biopharmaceuticals using discrete-time and continuous-time representations.

Lakhdar et al. (2005) presented a midterm planning model based on discrete time representation for continuous manufacturing of biopharmaceuticals. Kabra et al. (2013) developed a unit-specific event based model, while Vieira et al. (2016, 2017) proposed global-event based model for the same problem including maintenance scheduling with performance decay. Kumar et al. (2022) extended the work of Kabra et al. (2013) and proposed modifications to remove several model inconsistencies arising in the literature such as: no initial setup time (Kabra et al., 2013), real-time storage violation (Lakhdar et al., 2005; Vieira et al., 2016; Vieira et al., 2017), early product delivery (Lakhdar et al., 2005; Kabra et al., 2013; Vieira et al., 2016; Vieira et al., 2017), lack of adequate mapping in the upstream and downstream tasks (Lakhdar et al., 2005; Kabra et al., 2013; Vieira et al., 2017), incomplete sequencing of storage tasks (Lakhdar et al., 2005; Kabra et al., 2013; Vieira et al., 2016; Vieira et al., 2017), and overestimated objective values (Lakhdar et al., 2005; Kabra et al., 2013; Vieira et al., 2016; Vieira et al., 2017). The present study extends the work of Kumar et al. (2022) by improving their model to address several additional features including modeling of shelf-life and minimum campaign length to continue over multiple events, with different scenarios based on whether early delivery of products is allowed or not.

Modeling

We present different scenarios based on whether early delivery of products is allowed or not. A three-index binary variable is used for handling initial setup time in each unit. Four index binary variables are introduced to handle modeling of shelf-life and minimum campaign length to continue over multiple events, in contrast to the literature models. The proposed modeling equations are not provided here due to limited space for an extended abstract but will be covered during the conference presentation.

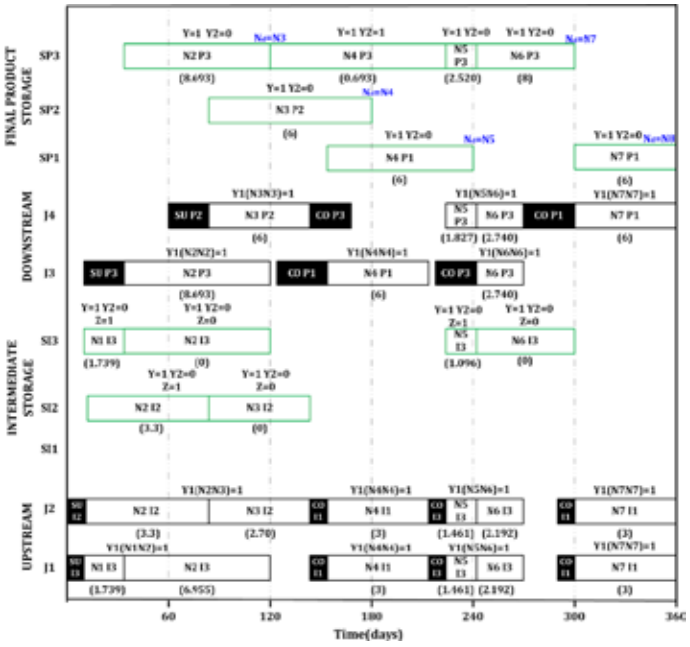

Figure 1. Gantt chart of the proposed model

Results and Discussion

The performance of the proposed model is evaluated for a multi-stage biopharmaceutical manufacturing facility with a finite and unknown product delivery rate and based on whether early delivery is allowed or not allowed.

The example is taken from Lakhdar et al. (2005), where a two-stage biopharmaceutical manufacturing facility produces three mammalian cell products with a multi-period demand specified over 360 days. The resulting Gantt chart is shown in Figure 1.

The model statistics and the profit structure are reported in Tables 1 and 2 and compared with the literature. The proposed model has a larger problem size in terms of the number of variables and constraints due to the enhanced modeling of additional features. The profit value obtained using the proposed improved model is 460.67 rmu for the case when early delivery is not allowed, unlike most of the literature models which allowed early delivery of products, in contrast to the original problem requirement, leading to lower storage costs and a higher profit, which is not realizable due to the restriction on early delivery.

Table 1. Model statistics

Model statistics	Kumar et al. (2022)	Proposed work
Constraints	4538	7119
Continuous variables	638	847
Binary variables	229	1365
Profit (rmu)	491.22	460.67

Table 2. Profit structure

Profit structure (rmu)	Kumar et al. (2022)	Proposed work
Sales revenue	680	680
Manufacturing cost	136	136
Changeover cost	10	10
Initial setup cost	4	4
Storage cost	38.78	69.27
Late delivery cost	0	0
Waste disposal cost	0	0
Profit	491.22	460.67

Acknowledgments
The authors gratefully acknowledge funding received from UAE University Research Start-up (Grant #G00003355).

References
Lakhdar, K., Zhou, Y., Savery, J., Titchener-Hooker, N. J., Papageorgiou, L. G. (2005). Medium Term Planning of Biopharmaceutical Manufacture using Mathematical Programming. Biotech. Prog., 21, 1478.

Kabra, S., Shaik, M. A., Rathore, A. S. (2013). Multiperiod Scheduling of a Multistage Multiproduct Bio-Pharmaceutical Process. Comput. Chem. Eng., 57, 95.

Kumar, V., Shaik, M. A., Jain, A. (2022). Analysis of Commonly used Scheduling Models for Multistage Biopharmaceutical Processes. Can. J. Chem. Eng., 100, 3635.

Vieira, M., Pinto-Varela, T., Moniz, S., Barbosa-Póvoa, A. P., Papageorgiou, L. G. (2016). Optimal Planning and Campaign Scheduling of Biopharmaceutical Processes using a Continuous-Time Formulation. Comput. Chem. Eng., 91, 422.

Vieira, M., Pinto-Varela, T., Barbosa-Póvoa, A. P. (2017). Production and Maintenance Planning Optimisation in Biopharmaceutical Processes under Performance Decay using a Continuous-time Formulation: A Multi-objective Approach. Comput. Chem. Eng., 107, 111.

THEME 3
Safe and sustainable products by design

Paper 364	Integrating environmental impacts into the screening of metal-organic frameworks for carbon capture	46
Paper 561	Molecule design beyond group counts – Integrated design of processes and molecule superstructures	48
Paper 631	Computer-aided design of magnetophoretic microfluidic systems for enhanced recovery of target products	50
Paper 708	Screening and modeling tools for optimal design of safe and sustainable chemicals	52
Paper 711	A Solar-Driven Integrated Adsorption Desalination and Direct Contact Membrane Distillation System for A Net-Zero Fuel Consumption	54

Integrating environmental impacts into the screening of metal-organic frameworks for carbon capture

Johannes Schilling[a], Eva Sanchez-Fernandez[b], Charithea Charalambous[c], Elias Moubarak[d], Kevin Jablonka[d], Berend Smit[d], Susana Garcia[c], André Bardow[a]
[a] ETH Zurich, 8092 Zurich, Switzerland
[b] Solverlo limited, EH42 1TL Dunbar, United Kingdom
[c] Heriot-Watt University, EH14 4AS Edinburgh, United Kingdom
[d] École Polytechnique Fédérale de Lausanne (EPFL), 1951 Sion, Valais, Switzerland

Abstract: Novel materials such as metal-organic frameworks (MOFs) provide access to an almost unlimited chemical design space and thus have great potential to improve carbon capture processes. Since carbon capture aims to mitigate climate change, technologies need to ensure environmental benefits. However, proper life-cycle assessment (LCA) is challenging for novel materials that mostly exist only in silico. This work, therefore, presents a framework for high-throughput screening of MOFs for carbon capture based on their environmental performance. To estimate the environmental impacts of MOFs at an early design stage, we developed a predictive LCA model covering the synthesis, use, and disposal of the MOFs. A temperature-vacuum swing adsorption process is considered with a detailed accounting of utilities and economics. We use the predictive framework to assess the environmental impacts of hundreds of MOFs in high-throughput screening for carbon capture and storage from a natural gas combined cycle power plant in Great Britain. The results highlight that material rankings differ enormously depending on the assessment criterion. The high-throughput screening allows us to derive guidelines for developing sustainable MOFs.

Keywords: CCS, adsorption, environmental impacts, life-cycle assessment, MOF.

Introduction

Carbon capture is crucial for climate change mitigation by enabling both storage and utilization of CO2. Promising technologies for carbon capture are adsorption processes that rely on solid adsorbents to separate CO2 from flue gases or air. The vast chemical design space allows for selecting the best adsorbent but also renders the selection challenging. Today, new materials for CO2 adsorption are commonly evaluated in high-throughput screenings based on their material properties or energy requirements (Farmahini et al., 2021). However, to identify sustainable materials, the environmental impacts must additionally be considered during the entire life cycle of the material.

In pioneering work, Hu et al. (2021) presented a screening framework integrating life cycle assessment (LCA) for 50 adsorbents. The LCA combined inventory data from the literature with proxy data. The results highlight the importance of integrating environmental impacts into screening adsorbent materials for carbon capture. However, because the screening framework relies on literature LCA data for each material, applying the framework to more extensive adsorbent databases is challenging.

Here, we present a framework for high-throughput screening of metal-organic frameworks (MOF) for carbon capture, considering a predictive LCA model to assess materials based on their environmental impacts.

Method

Our high-throughput screening framework integrates predictive LCA with detailed models of the process and techno-economic analysis (TEA), and Grand-Canonical Monte Carlo simulations. We focus this study on MOFs, promising materials to reduce energy requirements, cost, and environmental impacts. Due to limited data availability for LCA in the early design phase, we developed a predictive LCA model that estimates the environmental impacts of an adsorbent-based carbon capture process solely from the foreground data of the capture process and the structure of the material. We perform a cradle-to-gate assessment to capture 1 kg of CO2 that thus includes the environmental impacts of the carbon capture plant, the materials synthesis, and disposal. Due to the diversity of MOF synthesis, we have developed a simplified, predictive LCA model for MOF synthesis based on proxy data from the literature for solvent and organic linkers.

The foreground data of the LCA model is calculated using an equilibrium shortcut model for a temperature-vacuum swing adsorption process combined with detailed models for sizing, utility systems, and costing (Charalambous et al., 2022). The adsorption thermodynamics required for the process modeling are calculated based on molecular simulations. Beyond material, process, and economic key performance indicators (KPI), the overall framework assesses adsorbent materials for carbon capture based on their environmental impact (e.g., climate change or metal depletion) using the Environmental Footprint 3.0 (EC-JRC, 2022).

Results

Our high-throughput screening framework is applied to screen over 900 MOFs for CO2 capture from the flue gas (4 mol-% of CO2) of a natural gas combined cycle power plant in Great Britain. The crystal structures are a subset of the CoRE MOF open-source database (Chung et al., 2019).

Over 100 MOFs outperform an amine-based benchmark in almost all environmental impact categories, including climate change (up to 53% lower) but also "material resources: metals/minerals" (up to 61% lower) (Figure 1). Generally, the material rankings strongly depend on the assessment criterion. For example, rankings based on LCA criteria strongly differ from rankings based on selectivity, a material KPI commonly used in the literature for material selection. The results highlight the importance of assessing environmental impacts in material selection frameworks to ensure overall optimal solutions. Our screening results can guide the development of more sustainable MOFs, e.g., replacing a rather rare metal in a promising MOF with an abundant metal with similar thermodynamic performance.

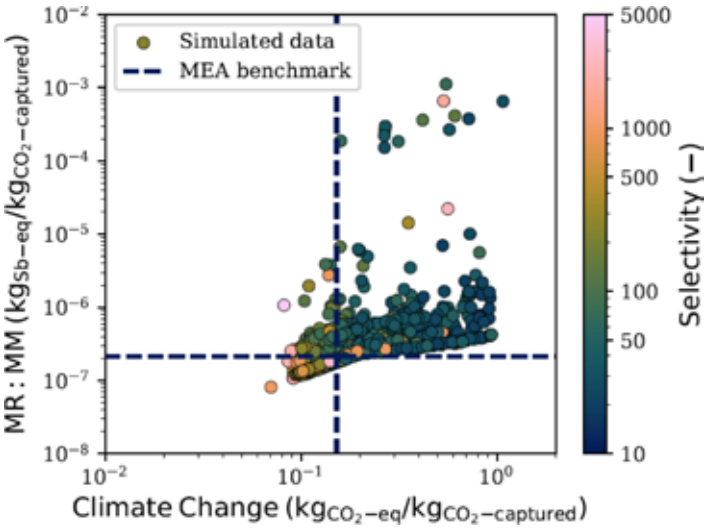

Figure 1: Materials screening for LCA KPI climate change and material resources: metals/minerals (MR:MM) vs. the material KPI selectivity and an amine-based benchmark process (MEA).

Conclusions

This work presents a high-throughput screening framework to screen MOFs for material, process, TEA, and LCA criteria. Our screening of over 900 MOFs identifies materials that outperform an amine-based benchmark process in environmental impacts. The results highlight that the material rankings can enormously differ depending on the assessment criterion. Thus, a MOF selection based on material KPIs, e.g., selectivity, can be misleading regarding environmental impacts.

Acknowledgments

This work is part of the PrISMa Project (No. 299659), funded through the ACT program (Accelerating CCS Technologies, Horizon 2020 Project No. 294766).

References

Charalambous, C. et al. (2022), Can we systematically rank the performance of any existing material for sorbent-based carbon capture? Proceedings of the 16th Greenhouse Gas Control Technologies Conference, 23-24 Oct 2022.

Chung, Y. G. et al. (2019), Advances, Updates, and Analytics for the Computation-Ready, Experimental Metal-Organic Framework Database: CoRE MOF 2019. J. Chem. Eng. Data 64, 5985−5998.

European Commission-Joint Research Centre (EC-JRC), Environmental Footprint reference package 3.0 (EF 3.0). 2018; www.eplca.jrc.ec.europa.eu/LCDN/developerEF.xhtml (Accessed 2022 June).

Farmahini, A. H. et al. (2021). Performance-based screening of porous materials for carbon capture. Chemical Reviews, 121(17), 10666-10741.

Hu, J. et al. (2021). Toward Sustainable Metal-Organic Frameworks for Post-Combustion Carbon Capture by Life Cycle Assessment and Molecular Simulation. ACS Sustainable Chemistry & Engineering, 9(36), 12132-12141.

Molecule design beyond group counts – Integrated design of processes and molecule superstructures

P. Rehner, J. Schilling, A. Bardow
Energy and Process Systems Engineering
ETH Zurich, Switzerland

Abstract: Integrated molecular and process design optimizes process variables together with molecules as an additional degree of freedom. The integrated design needs to represent the molecule in a machine-readable way that can be operated on by an optimization algorithm. For this purpose, group-contribution (GC) methods have been established as property models in molecular design. Thereby, the molecular degrees of freedom are group counts. However, the group counts omit information about the structure of the molecule and thus limit the molecular detail available during design. In this work, we present a graph-based molecular representation that encodes the full structure of the molecule during optimization. This so-called molecule superstructure unlocks property prediction methods with higher fidelity than GC methods for integrated molecular and process design while still allowing the use of gradient-based optimization algorithms. The resulting framework is applied in a case study to design the working fluid for an organic Rankine cycle using the heterosegmented gc-PC-SAFT equation of state as property prediction model. The molecular superstructure representation is shown to enable the efficient integration of advanced property models into molecular design.

Keywords: CAMPD, molecular design, PC-SAFT, group-contribution method

Introduction

Many industrial processes require auxiliary materials that are not part of the feed or product streams but still influence the process efficiency significantly. An example is the working fluid in a heat pump or organic Rankine cycle. Likewise, separation processes, such as gas absorption, require choosing a solvent. The identification of a suitable auxiliary material is often key to process performance.

Suitable auxiliary materials can be identified using computer-aided molecular and process design (CAMPD) (Papadopoulos et al., 2018). The goal of CAMPD is to determine the optimal molecule with respect to a target function and constraints specified in a process model. To make the molecular design problem solvable, the structure of the molecules needs to be featurized, i.e., transformed into a machine-readable format. Molecules are commonly featurized by splitting them into functional groups. Properties of the molecules are then calculated from the number of occurrences of each group. These so-called group contribution methods can directly estimate properties like critical data but also parameters for equations of state like PC-SAFT. However, the most common first-order group contribution methods cannot account for bonds or higher-order structures in the molecule.

Therefore, in this work, we present a CAMPD method based on molecule superstructures that describe the entire molecular graph from a small input of integer variables. The approach can be coupled with fast, gradient-based optimization algorithms and reduces the combinatorial complexity of the molecular design problem so that it can be used together with nonlinear process models. With the presented approach, we use for the first time the heterosegmented gc-PC-SAFT equation of state in an integrated molecular and process design. Sauer et al. (2014) showed that the heterosegmented approach is more accurate than the homosegmented GC method. The proposed method is demonstrated for the integrated design of an organic Rankine cycle (ORC) to assess the capability of the method.

Molecule Superstructures

Molecule superstructures represent molecules as graphs in which every node is associated with a non-hydrogen atom and a binary structure variable. The binary structure variable indicates whether the atom is part of the actual molecule or not. An example of a small molecule superstructure is shown in Figure 1.

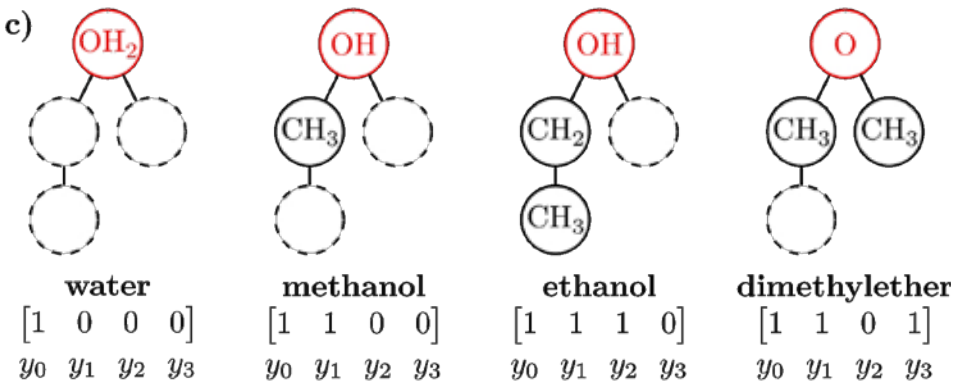

Figure 1. The four valid molecules that can be represented by an alcohol/ether superstructure of size 3 and their corresponding structure variables.

The structure variables can be translated to group and bond counts to parametrize property models like the heterosegmented gc-PC-SAFT equation of state. Linear structural constraints guarantee that the found molecules are fully connected and unique with respect to symmetries. A key feature of the molecule superstructure is that the structure variables can be relaxed, i.e., the model produces meaningful results for structure variables that vary continuously between 0 and 1. This relaxation allows the use of fast gradient-based optimization algorithms.

Case Study: Organic Rankine Cycle

The proposed CAMPD method based on molecule superstructures is applied to identify the optimal working fluid for a small-scale high-temperature organic Rankine cycle (Lampe et al., 2019). A ranking of the 50 most promising working fluids is calculated by repeatedly solving the CAMPD problem while disallowing already found solutions via integer cut constraints.
A comparison with the homosegmented group contribution PC-SAFT model used in previous studies (see, e.g., Schilling et al., 2017) shows that for both property prediction methods propanal is identified as the working fluid leading to the highest net power output for the given operation conditions. For the remaining molecules in the ranking, the order varies between the two models but the difference in net power is small, and many molecules appear in the top 50 for both models. For the fluids in the ranking, the process optimization is repeated using PC-SAFT with parameters fitted to individual components. For the molecules found in this study, both group contribution methods compare well to the reference calculations.

Conclusions

The molecule superstructures introduced in this work enable gradient-based CAMPD using high-fidelity property prediction methods by considering the full structural information of molecules during the design. The output of the introduced CAMPD approach is the full molecular graph which can be represented, e.g., as a SMILES code. Therefore, the (possibly ambiguous) translation of group counts to structures is avoided.
For the first time, the heterosegmented gc-PC-SAFT equation of state is used as a property prediction method in CAMPD. While the benefits have been modest for the studied pure component design, we regard the heterosegmented group contribution models particularly promising for mixtures, because these GC models describe interactions between segments rather than entire molecules and hence, corrections for unlike segments on different molecules can be included directly in the perturbation terms. With the extension to mixtures in mind, the proposed molecule superstructure optimization strategy can contribute to increasing the accuracy of property prediction methods used in integrated molecular and process design.

Acknowledgments

PR acknowledges funding by the Deutsche Forschungsgemeinschaft (DFG, German Research Foundation) – 497566159.

References

Lampe, M., De Servi, C., Schilling, J., Bardow, A., Colonna, P. (2019). J. Eng. Gas Turbines Power, 141(11): 111009

Papadopoulos, A. I., Tsivintzelis, I., Linke, P. (2018). Reference Module in Chemistry, Molecular Sciences and Chemical Engineering, Elsevier, Walthm, MA, USA

Sauer, E., Stavrou, M., Gross, J. (2014). Ind. Eng. Chem. Res., 53, 38, 14854-14864

Schilling, J., Lampe, M., Gross, J., Bardow, A. (2017). Chem. Eng. Sci., 159, 23, 217-230

Computer-aided design of magnetophoretic microfluidic systems for enhanced recovery of target products

Cristina González-Fernández[1], Jenifer Gómez-Pastora[2], Eugenio Bringas[1], Inmaculada Ortiz[1]
[1]Departamento de Ingenierías Química y Biomolecular, Universidad de Cantabria, Avda. Los Castros, s/n, 39005 Santander, Spain
[2]Department of Chemical Engineering, Texas Tech University, Tx, USA

Abstract: Magnetophoretic microfluidic devices (MMDs), which exploit the outstanding properties of magnetic separation, magnetic beads, and microfluidics, offer promising possibilities to be used in downstream processing of target products. From the different MMDs, it has been demonstrated that quadrupole magnetic sorters (QMSs), which consist of an annular channel with quadrupolar-oriented permanent magnets, exhibit a notably enhanced performance compared to Y-Y shaped microseparators, which comprise a rectangular channel with a single permanent magnet. Despite their great potential, these QMSs need to be further optimized since the processing of relatively high flow rates has only been achieved for completely retrieving micron-sized beads. Nevertheless, the unique properties of magnetic nanoparticles, such as their high specific surface area, call for the development of magnetophoretic microseparators able to capture them while treating high flow rates. In this context, we propose the computer-aided optimization of QMSs, using an experimentally validated computational fluid dynamics (CFD) numerical model, by increasing the magnetic force applied to the beads via changing the channel diameter, as well as the maximum magnetic field produced by the quadrupolar-oriented magnets. Overall, this study highlights the improved performance of QMSs and foresees promising possibilities of these magnetophoretic microseparators.

Keywords: CFD, Magnetophoretic microfluidic devices, Magnetic separation

Introduction

The use of magnetophoretic microfluidic devices (MMDs) for retrieving magnetically-labelled compounds from complex media has attracted great attention. This fact stems from the unique benefits that the coupling of magnetic separation, microfluidics and magnetic beads offers. Hence, the design of MMDs has been the focus of intense research in order to develop systems that efficiently retrieve the target products. (Gómez-Pastora et al., 2017) Particularly, interest has been devoted to the design of MMDs that provide complete bead recovery while processing relatively high flow rates, since the reduced dimensions of microchannels causes that they are only able to process small flow rates. (González-Fernández et al., 2020; González-Fernández et al., 2021)

Different strategies have been pursued in the literature to recover the target compounds at high volumetric throughputs. It has been demonstrated that increasing the driving force for the separation, that is the magnetic force exerted on the target compound-bead complexes, represents an attractive strategy. (González-Fernández et al., 2020; González-Fernández et al., 2021) In this context, the performance of two typically used MMDs for particle retrieval, namely quadrupole magnetic sorter (QMS) and Y-Y shaped microseparator, that have similar geometrical features but differ in the magnetic force applied to the particles, has been compared. Particularly, QMSs consist of an annular channel with a quadrupolar orientation of the permanent magnets, whereas Y-Y shaped microseparators, which represent the standard configuration, comprise a rectangular channel with a single permanent magnet. (González-Fernández et al., 2021)

Despite their promising possibilities for recovering target products, QMSs need to be further optimized since the processing of relatively high flow rates has only been achieved for completely retrieving micron-sized beads. Nevertheless, reducing the beads dose that is required for the recovery of the target solute represents a potential strategy for meeting process intensification and reducing the process cost. (González-Fernández et al., 2021) In this regard, the higher specific surface area of magnetic nanoparticles, which enhances the adsorption of the target compound on the bead surface, calls for the development of MMDs able to capture magnetic nanoparticles while processing high sample flow rates. (Gómez-Pastora et al., 2017)

Ongoing research

We propose the computer-aided optimization of QMSs by changing the channel diameter, as well as the maximum magnetic field produced by the quadrupolar-oriented magnets in order to increase the magnetic force applied to the beads, thus enabling the recovery of smaller particles. These strategies for increasing the driving force for particle retrieval derive from the work of Gómez-Pastora et al. (2022), who demonstrated how the magnetic field gradient inside the QMS is influenced by the column diameter and the quadrupole magnetic field applied on the separator walls (see Figure 1). For conducting this research, our experimentally validated computational fluid dynamics (CFD) numerical model, which is solved in FLOW-3D, can be employed. Briefly, this model predicts bead trajectory through an Eulerian-Lagrangian approach and considers the dominant forces (i.e., magnetic and hydrodynamic forces) acting on the beads. The magnetic force is calculated in an external Fortran subroutine compiled in Visual Studio, that is linked to the FLOW-3D hydrodynamics solver during running. (Gómez-Pastora et al. 2018; González-Fernández et al. 2021)

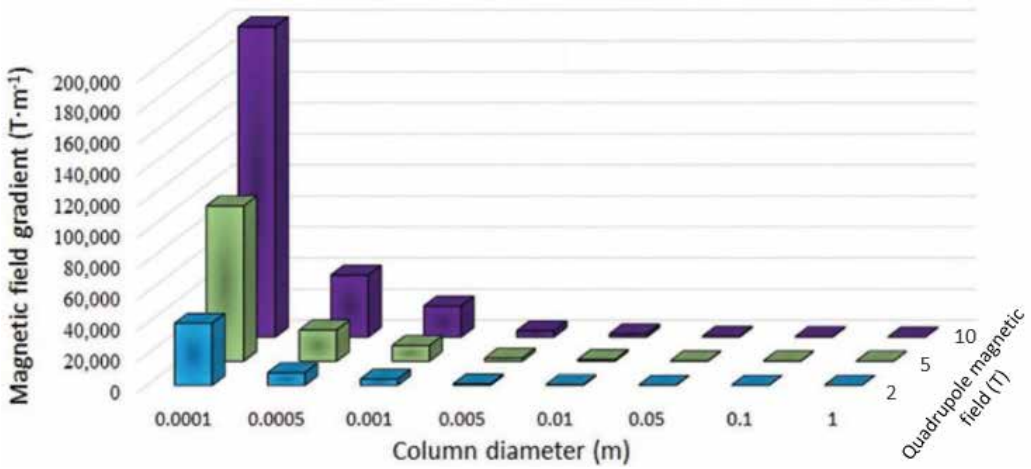

Figure 1. Dependence of the magnetic field gradient inside a QMS with the column diameter and the quadrupole magnetic fields applied on the separator walls (adapted from Gómez-Pastora et al. 2022)

Conclusions

In light of the above-mentioned insights, this study emphasizes the improved performance of QMSs and provides guidelines for designing more efficient QMSs (i.e., those able to recover smaller beads). Additionally, promising possibilities of QMSs for nanoparticle retrieval are foreseen.

Acknowledgments

Financial support from the Spanish Ministry of Science, Innovation and Universities under the project RTI2018-093310-B-I00 is gratefully acknowledged.

References

Gómez-Pastora, J., Wu, X., Chalmers, J. J. (2022). Magnetic separations of micro- and nanoparticles for water treatment process. In Solid-liquid separation technologies. CRC Press, Broken Sound Parkway NW, Boca Raton, 211-232.

Gómez-Pastora, J., González-Fernández, C., Real, E., Iles, A., Bringas, E., Furlani, E. P., Ortiz, I. (2018). Computational modeling and fluorescence microscopy characterization of a two-phase magnetophoretic microsystem for continuous-flow blood detoxification. Lab Chip, 18, 1593-1606.

Gómez-Pastora, J., Xue, X., Karampelas, I. H., Bringas, E., Furlani, E. P., Ortiz, I. (2017). Analysis of separators for magnetic beads recovery: From large systems to multifunctional microdevices. Sep. Purif. Technol., 172, 16-31.

González-Fernández, C., Gómez-Pastora, J., Basauri, A., Fallanza, M., Bringas E., Chalmers, J. J., Ortiz, I. (2020). Continuous-flow separation of magnetic particles from biofluids: How does the microdevice geometry determine the separation performance? Sensors, 20, 3030.

González-Fernández, C., Gómez-Pastora, J., Bringas E., Zborowski, M., Chalmers, J. J., Ortiz, I. (2021). Recovery of magnetic catalysts: advanced design for process intensification. Ind. Eng. Chem. Res., 60, 16780-16790.

Screening and modeling tools for optimal design of safe and sustainable chemicals

Effie Marcoulaki[a], Antonis Kokossis[b]
[a]System Reliability and Industrial Safety Laboratory, National Centre for Scientific Research "Demokritos", Greece.
[b]School of Chemical Engineering, National Technical University of Athens, Greece

Abstract: Ex-ante consideration of safety and sustainability aspects at the early stages of material or process design, promotes the concept of safe and sustainable by-design (SSbD) and reduces the need to mitigate impacts on human health and the environment in later product development stages. Computer Aided Molecular Design (CAMD) tools can be used to screen for SSbD chemicals and implement strategies for sustainability.

Keywords: LCA, Computer Aided Molecular Design, optimization, QSPR, Group Contribution models.

Introduction

The European chemicals strategy for sustainability aims to consider safety and sustainability aspects as early as possible product development design chain [1]. The resulting substances, materials, products or processes are safe and sustainable by-design (SSbD), reducing the need for retroactive measures to mitigate impacts on human health and the environment in later product development stages [2].
The concept of SSbD integrates safety, circularity and functionality throughout the entire life cycle, and minimizes the environmental footprint. The EC-JRC proposed implementation strategies for SSbD, with focus on safety and environmental dimensions, and the availability of tools to assess life-cycle impacts on climate change, resource use, ecosystems and biodiversity. Social and economic dimensions were not overlooked, on the contrary, occupational risks can be considered under the social risks [3]. CAMD tools can apply a preliminary screening to reverse-engineer molecular configurations featuring optimal or/and desirable properties and process conditions. This could also include safety and sustainability.

Methodology

The CAMD optimization tool considered here was originally demonstrated on the design of refrigerants [4] and separation-enhancing organic materials [5]. The optimizer was extended and used extensively since then on a variety of material design applications, including solvents for reactive separation processes [6], organic Rankine cycle [7], CO2 capture [8] etc. Applications of the above CAMD optimizer are only limited by the availability of Quantitative Structure-Property Models (QSPR), like group-contribution (GC) models, for fast and efficient property predictions. A general statement to describe the problem of optimal design of novel materials as considered here would be:

Optimize {performance} = f{structure}
Subject to {properties} = f{structure} &
{process conditions} = f{properties}

Safety and sustainability can be considered ex-ante, in addition to the functionality requirements, if Life Cycle Analysis (LCA) or Health, Safety and Environment (HSE) indicators are evaluated using materials in databases [9] or appropriate QSPR-type models able to consider any given molecular structure [10]. This work integrated the GC-LCA models developed by [10] in the CAMD optimization tool. These GC models are for the following climate change indicators: Global Warming Potential (GWP), Cumulative Energy Demand (CED) and EcoIndicator 99 (EI99). Safety features were also considered in the property constraints.

Results

The CAMD optimizer was then applied to the design of safe and sustainable phase change materials (PCMs) and extractive fermentation solvents for the production of biofuels.
For the design of PCMs, the optimizer was linked to a simple metamodel predicting the total annual required heat for a given residence. The applied constraints on the thermo-physical properties were based on the properties of materials traditionally used for such applications. The obtained results were either similar or outperformed traditional materials in terms of functionality. However, since the compliance to HSE/LCA requirements was integrated in the optimal search, the obtained designs were additionally SSbD [11].
The extractive fermentation process combines fermentation with a primary liquid–liquid extractive separation stage to increase the ethanol productivity. Though promising, the process is still not practical for industrial application, also due to the lack of suitable extraction solvents. The optimizer was linked to a simple simulator to model the process performance of the candidate designs and improve their assessment. The obtained designs provided significant insights on the kind of molecular structures that satisfy the process objectives and constraints, as well the desired requirements for the solvent sustainability and safety [12].

Conclusions

This paper discusses the current strategies for sustainability and how they can be implemented using available CAMD optimization tools to propose designs, which are also safe and sustainable, at the early stages of material / process development. The optimal search can consider various HSE/LCA criteria, depending on specific needs and the availability of GC models for the evaluation of relevant indicators. In total, the obtained material designs for two case studies feature improved functionality, safety and sustainability. This work also demonstrates that the proposed approach can promote novel processing options, not practically feasible using tabulated materials.

References

1. European Commission (2020). EU Chemicals Strategy for Sustainability Towards a Toxic-Free Environment. https://ec.europa.eu/environment/pdf/chemicals/2020/10/Strategy.pdf
2. Shandilya, N., Marcoulaki, E., Barruetabena, L., Llopis, I.R., Noorlander, C., Jiménez, A.S., Oudart, Y., Puelles, R.C., Pérez-Fernández, M., Falk, A. and Resch, S., (2020). Perspective on a risk-based roadmap towards the implementation of the safe innovation approach for industry. NanoImpact, 20, p.100258. https://doi.org/10.1016/j.impact.2020.100258
3. Caldeira, C., Farcal, R., Moretti, C., Mancini, L., Rauscher, H., Riego Sintes, J., Sala, S., Rasmussen, K. (2022). Safe and sustainable by design chemicals and materials: review of safety and sustainability dimensions, aspects, methods, indicators, and tools, JRC127109 (EU). https://publications.jrc.ec.europa.eu/repository/handle/JRC127109
4. Marcoulaki, E.C., Kokossis, A.C. (2000a). On the development of novel chemicals using a systematic synthesis approach. I–Optimisation framework. Chem. Eng. Sci. 55, 2529. https://doi.org/10.1016/S0009-2509(99)00522-9
5. Marcoulaki, E.C., Kokossis, A.C. (2000b). On the development of novel chemicals using a systematic optimisation approach. II–Solvent design. Chem. Eng. Sci. 55, 2547. https://doi.org/10.1016/S0009-2509(99)00523-0
6. Papadopoulos, A.I., Linke, P. (2009). Integrated solvent and process selection for separation and reactive separation systems. Chem. Eng. Process. Process. Intensif. 48, 1047–1060. https://doi.org/10.1016/j.cep.2009.02.004
7. Papadopoulos, A.I., Stijepovic, M., Linke, P., Seferlis, P., Voutetakis, S. (2013). Toward optimum working fluid mixtures for organic Rankine cycles using molecular design and sensitivity analysis. Ind. Eng. Chem. Res. 52, 12116–12133. https://doi.org/10.1021/ie400968j
8. Papadopoulos, A. I., Zarogiannis, T., & Seferlis, P. (2017). Computer-aided molecular design of CO2 capture solvents and mixtures. In Process Systems and Materials for CO2 Capture: Modelling, Design, Control and Integration, John Wiley & Sons Ltd., pp. 173-201. https://doi.org/10.1002/9781119106418.ch7
9. Papadopoulos, A.I., Shavalieva, G., Papadokonstantakis, S., Seferlis, P., Perdomo, F.A., Galindo, A., Jackson, G. and Adjiman, C.S., (2020). An approach for simultaneous computer-aided molecular design with holistic sustainability assessment: Application to phase-change CO2 capture solvents. Comput. Chem. Eng. 135, 106769. https://doi.org/10.1016/j.compchemeng.2020.106769
10. Baxevanidis, P., Papadokonstantakis, S., Kokossis, A., Marcoulaki, E. (2022). Group Contribution-based LCA models to enable screening for environmentally benign novel chemicals in CAMD applications. AIChE Journal, e17544. https://doi.org/10.1002/aic.17544
11. Geroulis, I., Kokossis, A., Marcoulaki, E. (2022). Ex-ante optimal design of sustainable phase change materials for latent heat storage. Chemie Ingenieur Technik, special issue on Computer-Aided Molecular and Process Design, in press. https://doi.org/10.1002/cite.202200099
12. Marcoulaki, E., Baxevanidis, P. (2022). Screening for new efficient and sustainable -by-design solvents to assist the extractive fermentation of glucose to bioethanol fuels, Separations 9(3): 60. https://doi.org/10.1002/cite.202200099

A Solar-Driven Integrated Adsorption Desalination and Direct Contact Membrane Distillation System for A Net-Zero Fuel Consumption

Ayman A. Alazab[a], Naef A.A. Qasem[b,c], Hassan Baaqeel[a,d]
[a]Department of Chemical Engineering, King Fahd University of Petroleum & Minerals, Dhahran 31261, Saudi Arabia
[b]Department of Aerospace Engineering, King Fahd University of Petroleum & Minerals, Dhahran 31261, Saudi Arabia
[c]Interdisciplinary Research Center for Membranes and Water Security, King Fahd University of Petroleum & Minerals, Dhahran 31261, Saudi Arabia
[d]Interdisciplinary Research Center for Renewable Energy and Power Systems, King Fahd University of Petroleum & Minerals, Dhahran 31261, Saudi Arabia

Abstract: This paper demonstrates the synergistic integration of direct contact membrane distillation system (DCMD), adsorption desalination system (AD), and evacuated tube solar collector (ETSC), referred to as S-MDAD. The performance of S-MDAD was analyzed using a mathematical model of each component and compared to that of the standalone AD system. Specific daily water production (SDWP), gain output ratio (GOR), coefficient of performance (COP), and freshwater cost were investigated as primary performance indicators. Based on the findings, we can conclude that GOR values can approach 1.59, which is greater than the standalone AD system by more than 133%. The SDWP reaches 60.1 m^3/ton per day, which is 157.3% more than the AD system. Moreover, the cost of freshwater produced from S-MDAD system is calculated to be around 0.001 $/L, with a reduction of around 97.9% from the standalone AD system.

Keywords: Net-zero energy; solar-driven; integrated system; DCMD; Adsorption desalination.

Nomenclature

AD	adsorption desalination	SDWP	specific daily water production (m^3/ton.day)
COP	coefficient of performance		
c_p	specific heat (kJ/kg K)	T	temperature (K)
DCMD	direct contact membrane distillation	η	efficiency
ETSC	evacuated tube solar collector		Subscripts
GOR	gain output ratio	w	water
$\dot{m}$	mass flow rate (kg/s)	s	solar collector

Introduction

The increasing demand for energy and the scarcity of freshwater resources confront researchers with the challenge of finding ways to conserve energy in water desalination systems. High energy consumption from fossil fuels and electricity is a problem for traditional desalination systems such as multi-stage flash (MSF), Reverse Osmosis (RO), and Multi-effect Distillation (MED), which all add to climate change and exacerbate ecological threats (Do Thi et al., 2021; Olabi et al., 2020). Additionally, these systems involve expensive operating costs and require regular maintenance (Ghazy et al., 2022). The adsorption desalination (AD) system is a potentially useful technology that could effectively address the interconnected water-energy problem. It can use solar energy or waste heat as a heat source, making it an excellent representative of the renewable energy market's current attractiveness (Hoseinzadeh et al., 2020). It also has the capability of concurrently producing freshwater and cooling power. Additionally, the system's ease of use, low corrosion, and lack of fouling all contribute to a lower cost of operation (Mohammed & Askalany, 2019).

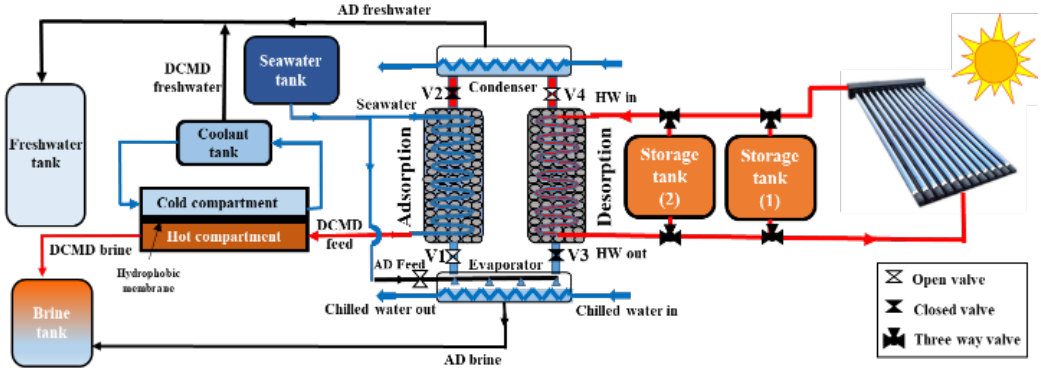

Fig. 1. Schematic diagrams of S-MDAD hybrid system.

Due to its low productivity and hence low efficiency, the adsorption cycle is still not widely available on the market. Therefore, its performance (SDWP, GOR, and COP) can be improved using different adsorbents, different configurations, or integrating it with another system. Efficiency can be further enhanced by utilizing a renewable energy source, such as solar energy (Abo-Elfadl et al., 2020). One solar energy technology that performs well in low radiation, cloudy, or cold weather is the evacuated tube solar collector (ETSC), which can be utilized throughout the year (Sharafeldin & Gróf, 2018). With its vacuum insulation, selective surface coating, and tubular absorber, this collector has reduced operating costs and lower heat loss through convection than flat plates collectors. Additionally, the broken tubes can be easily replaced, so the entire system doesn't have to be shut down for maintenance (Ayompe et al., 2011).
In order to improve GOR and freshwater production while minimizing freshwater cost, this research proposes a solar-assisted hybrid DCMD and AD desalination system. Since adsorption is exothermic, the waste heat it produces in the adsorption bed can drive the DCMD. The DCMD system is fed by the seawater used to collect the waste heat from the AD system. An increase in SDWP and GOR, as well as a decrease in freshwater costs have been observed in the designed hybrid S-MDAD system. S-MDAD also produces a cooling effect as a byproduct. Notably, the DCMD system is added to enhance the performance of the AD system, which has a relatively poor performance, by utilizing its waste heat.

System description

As can be seen in Fig. 1, the proposed hybrid system consists of DCMD system, AD system, evacuated tube solar collector (ETSC), and two water storage tanks. The DCMD and AD systems are integrated synergistically where the DCMD seawater feed passes through the adsorption bed to utilize the waste heat that would otherwise be lost during cooling. Meanwhile, a desorption process using hot water is carried out on the desorption bed. ETSC system is implemented to produce hot water, which is stored in the tanks. In order to maintain homogenous hot water temperature in Tank1, the hot water is circulated between tank 1 and the ETSC.
The secondary cycle transports the heated water from Tank1 to Tank2. The second cycle improves the hybrid MDAD's performance by reducing the temperature fluctuations of the driving hot water and producing more stable input heating water temperature (HWT). This is due to the fact that, as mentioned by (Ali et al., 2017), systems with hot water storage tanks have less fluctuating potable water product and cooling energy than systems without storage tanks.

Mathematical modeling

We, here, specifically concentrate on changes in solar irradiance and ambient temperature in Dhahran city (26.2361° N, 50.0393° E), which locates in the eastern region of Saudi Arabia. The software Homer (HOMER - Hybrid Renewable and Distributed Generation System Design Software) was used to extract the meteorological weather data. Water that will be used during the desorption periods was heated in two tanks using evacuated tube solar collectors (ETSCs). ETSCs were used to heat water stored in two tanks to be used during the desorption periods. The driving thermal power for the present solar-powered hybrid desalination system is determined as (Ali et al., 2017):
where T_{amb} is the ambient temperature, I_s is the solar intensity, A_{sc} is the area of the solar collector, and a_0, a_1 and a_2 are coefficients which are taken as 0.7, 10.0, and 0.03, respectively (Ali et al., 2017).

$$Q_{th} = \eta * A_{sc} * I_s = \dot{m}_{w,s} * c_{pw} * (T_{s,out} - T_{s,in}) \quad (1)$$

$$\eta = a_0 - a_1 * \frac{(T_{s,in} - T_{amb})}{I_s} - a_2 * \frac{(T_{s,in} - T_{amb})^2}{I_s} \quad (2)$$

The mathematical models with validation of AD, DCMD, and the integrated AD-DCMD systems were published in our previous work (Alazab et al., 2022). The key parameters, the performance, and the economic analysis of the integrated AD-DCMD system were also determined using the same models.
The beds used in the AD system are regarded the same as those described in the published experiment (Alsaman et al., 2017). The operating parameters of the DCMD system and the two identical beds, the condenser, and the evaporator are stated in our previous work (Alazab et al., 2022). REFPROP software was used to obtain the thermodynamic properties of water (REFPROP | NIST). The simulation is carried out using the MATLAB software with a computational tolerance error of $<10^{-6}$.

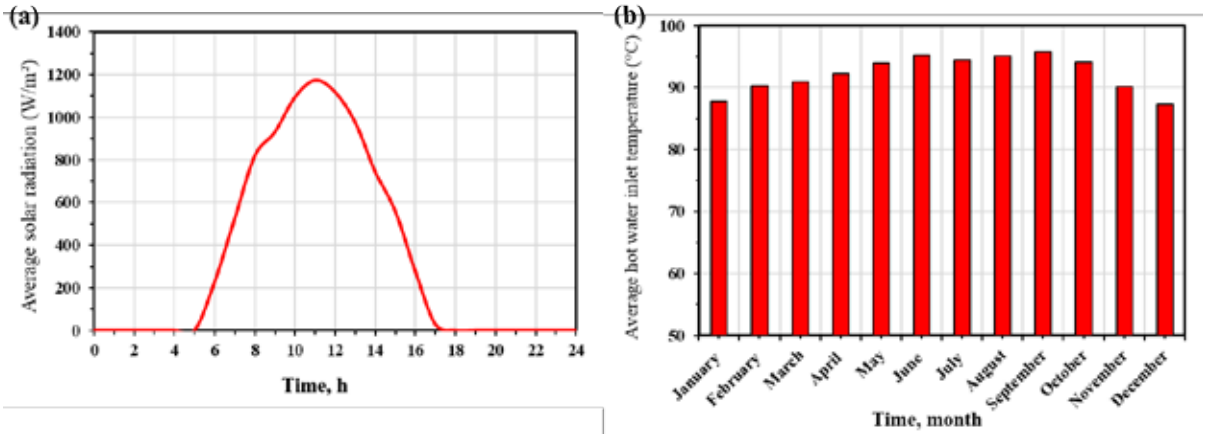

Fig. 2. (a) Hourly presentation of solar radiation profile for Dhahran in 19 September. (b) Average hot water inlet temperature record during the year for Dhahran.

Results and discussion

Here, we reveal the hybrid S-MDAD's simulation outcomes. For the most part, May marks the beginning of Saudi Arabia's warm season, which typically lasts until October. September is the warmest month in Dhahran, with average T_{amb} and SR of around 34.5 °C and 311.4 W/ m^2, respectively. The hourly display of SR for Dhahran on September 19 is shown in Fig. 2(a). While solar radiation is completely absent at night, it progressively rises throughout the day. The intake HWT to S-MDAD varies throughout the year, as seen in Fig. 2(b). The temperature of the hot water exiting the collector varies with the weather conditions.

As shown in Fig. 3(a), the hot water from the insulated storage tank that heats the desorption bed during the desorption process significantly affects the SDWP of the S-MDAD hybrid system. The quantity of freshwater given from the DCMD and AD systems, and consequently from the hybrid system, constantly increases as the regeneration/driving temperature rises. For instance, the SDWP of the whole system rise from about 48.5 to 60.1 m^3/ton.day (~24% improvement) when the desorption temperature goes from 87.3 to 95.9 °C through January to September in Dhahran, Saudi Arabia.

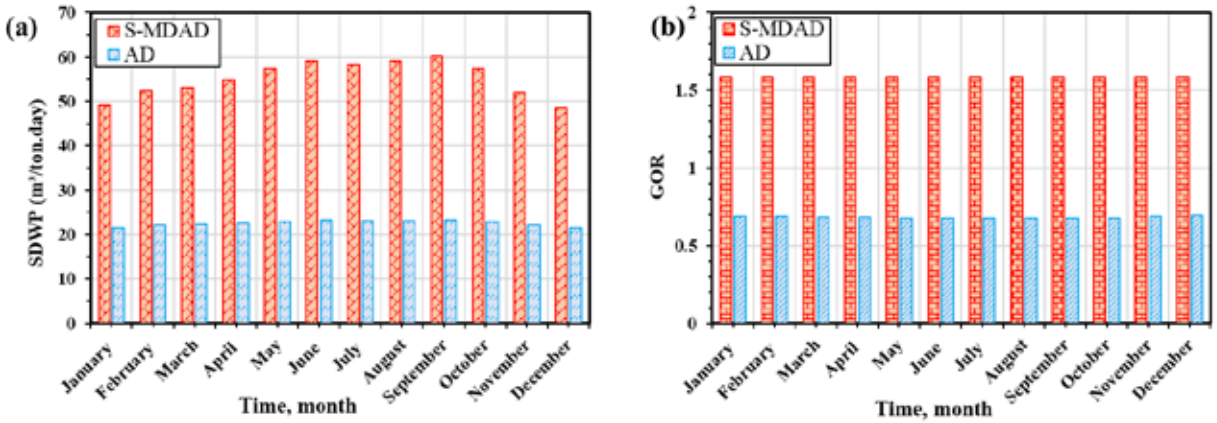

Fig. 3. (a) Average SDWP of AD and S-MDAD during the year for Dhahran.
(b) Average GOR of AD and S-MDAD systems during the year for Dhahran

The monthly average GOR variation over the year is illustrated in Fig. 3(b). It is also shown that, using the same amount of energy, GOR of the of the hybrid S-MDAD system is much higher than that for standalone AD system. For instance, in September, GOR of stand-alone AD, S-MDAD systems are 0.68 and 1.59, respectively. This mean a 133% increase in GOR was achieved with integration.

As indicated in Fig. 4(a), cooling effect is produced as a secondary product. The optimal cooling effects is in January and December, with COP values of 0.275 and 0.305 respectively, which are higher than some standalone AD refrigeration systems (e.g. (Lattieff et al., 2021)) at similar operating conditions.

The economic model was used to determine the S-MDAD integrated system's overall capital investment cost. Fig. 4(b) compares the results of standalone AD, MDAD, and S-MDAD systems. It is obvious that integrating a DCMD system with the adsorption cycle lowers the specific cost of freshwater. The cost of produced water is further significantly reduced when a solar system is added to the collection. For instance, the proposed S-MDAD system produces potable water at a specific cost of around 0.001 $/L throughout the year. This particular cost of water is about 97.9% less than that of standalone AD system using the same amount of energy.

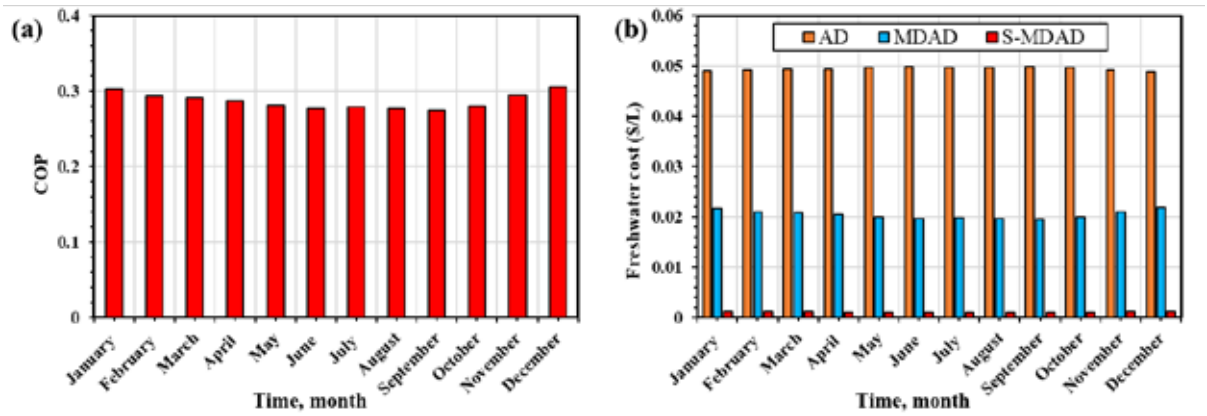

Fig. 4. (a) Average COP of S-MDAD during the year for Dhahran.
(b) Average freshwater costs of AD, MDAD, and S-MDAD during the year for Dhahran

Conclusion

It is proposed to combine the solar-powered adsorption desalination (AD) cycle with the direct contact membrane distillation (DCMD) system. The thermodynamic performance and economic feasibility of this hybrid system are analyzed using mathematical models. The proposed system (S-MDAD) outperforms the standalone AD system in terms of both freshwater production and GOR. The proposed system's SDWP and GOR improved by 157.3% and 133%, respectively. The cost analysis indicates that the specific cost of freshwater produced from the hybrid MDAD system reduces from 0.02 $/L to 0.001 $/L when solar system is used. The S-MDAD has a 97.9% lower cost per letter of potable water produced compared to the standalone AD system.

Acknowledgment

The authors thank the support from the Deanship of Research Oversight and Coordination (DROC), King Fahd University of Petroleum & Minerals (KFUPM), Dhahran, Saudi Arabia, under Project INRE2213.

References

Abo-Elfadl, S., Hassan, H., & El-Dosoky, M. F. (2020). Energy and exergy assessment of integrating reflectors on thermal energy storage of evacuated tube solar collector-heat pipe system. Solar Energy, 209, 470–484. https://doi.org/10.1016/J.SOLENER.2020.09.009

Alazab, A. A., Qasem, N. A. A., & Baaqeel, H. (2022). Performance Evaluation of a Novel Integrated Adsorption Desalination System with Direct Contact Membrane Distillation Plant. SSRN Electronic Journal. https://doi.org/10.2139/SSRN.4263783

Ali, E. S., Harby, K., Askalany, A. A., Diab, M. R., & Alsaman, A. S. (2017). Weather effect on a solar powered hybrid adsorption desalination-cooling system: A case study of Egypt's climate. Applied Thermal Engineering, 124, 663–672. https://doi.org/10.1016/J.APPLTHERMALENG.2017.06.048

Alsaman, A. S., Askalany, A. A., Harby, K., & Ahmed, M. S. (2017). Performance evaluation of a solar-driven adsorption desalination-cooling system. Energy, 128, 196–207. https://doi.org/10.1016/J.ENERGY.2017.04.010

Ayompe, L. M., Duffy, A., Mc Keever, M., Conlon, M., & McCormack, S. J. (2011). Comparative field performance study of flat plate and heat pipe evacuated tube collectors (ETCs) for domestic water heating systems in a temperate climate. Energy, 36(5), 3370–3378. https://doi.org/10.1016/J.ENERGY.2011.03.034

Do Thi, H. T., Pasztor, T., Fozer, D., Manenti, F., & Toth, A. J. (2021). Comparison of Desalination Technologies Using Renewable Energy Sources with Life Cycle, PESTLE, and Multi-Criteria Decision Analyses. Water 2021, Vol. 13, Page 3023, 13(21), 3023. https://doi.org/10.3390/W13213023

Ghazy, M., Askalany, A. A., Ibrahim, E. M. M., Mohamed, A. S. A., Ali, E. S., & AL-Dadah, R. (2022). Solar powered adsorption desalination system employing CPO-27(Ni). Journal of Energy Storage, 53, 105174. https://doi.org/10.1016/J.EST.2022.105174

HOMER - Hybrid Renewable and Distributed Generation System Design Software. (n.d.). Retrieved December 2, 2022, from https://www.homerenergy.com/

Hoseinzadeh, S., Ghasemi, M. H., & Heyns, S. (2020). Application of hybrid systems in solution of low power generation at hot seasons for micro hydro systems. Renewable Energy, 160, 323–332. https://doi.org/10.1016/J.RENENE.2020.06.149

Lattieff, F. A., Atiya, M. A., Mahdi, J. M., Majdi, H. S., Talebizadehsardari, P., & Yaïci, W. (2021). Performance Analysis of a Solar Cooling System with Equal and Unequal Adsorption/Desorption Operating Time. Energies 2021, Vol. 14, Page 6749, 14(20), 6749. https://doi.org/10.3390/EN14206749

Mohammed, R. H., & Askalany, A. A. (2019). Productivity improvements of adsorption desalination systems. Green Energy and Technology, 325–357. https://doi.org/10.1007/978-981-13-6887-5_15/FIGURES/33

Olabi, A. G., Elsaid, K., Rabaia, M. K. H., Askalany, A. A., & Abdelkareem, M. A. (2020). Waste heat-driven desalination systems: Perspective. Energy, 209, 118373. https://doi.org/10.1016/J.ENERGY.2020.118373

REFPROP | NIST. (n.d.). Retrieved April 2, 2022, from https://www.nist.gov/srd/refprop

Sharafeldin, M. A., & Gróf, G. (2018). Evacuated tube solar collector performance using CeO2/water nanofluid. Journal of Cleaner Production, 185, 347–356. https://doi.org/10.1016/J.JCLEPRO.2018.03.054

THEME 4
Green and sustainable processes for the circular economy

Paper 33	Optimal design of refineries for low-density polyethylene (ldpe) waste upcycling	60
Paper 36	GWI- and cost-Minimal retrofitting of cement production by superstructure optimization	62
Paper 40	Economic feasibility of bio-diesel production plants from animal fat wastes	64
Paper 105	One-dimensional kinetic model with axial dispersion of a molten-metal bubble column reactor for decomposition of fluorinated gases	66
Paper 274	Optimizing energy exchanges for decarbonizing industries through industrial ecology concepts	68
Paper 415	Study of lithium recovery from desalination concentrates BY MEANS OF Density Functional Theory (DFT)	70
Paper 417	Circular economy in the management of spent acids: modelling of the adsorption process for the copper recovery	72
Paper 673	Planetary Environmental benefits of CO2-to-Ethylene Direct bifunctional catalytic Synthesis	74
Paper 786	Evaluating the potential of current and emerging alternatives to enable a Sustainable Circular Economy	76
Paper 865	Economic feasibility of hydrometallurgical process in LiBs metal recycling	78
Paper 867	Techno-Economic Analysis and Environmental Assessment of Synthetic Fuel Production from Green H2 and INDUSTRIAL CO2 using Fischer-Tropsch synthesis	80
Paper 869	Process development for hydrogen production using LNG cold energy	82
Paper 870	Microkinetic Modelling of CO2 Conversion to Methanol and Catalyst Deactivation Description for a Rugged Operation Control	84

Optimal design of refineries for low-density polyethylene (ldpe) waste upcycling

Borja Hernández, Dionisios G. Vlachos, Marianthi G. Ierapetritou
Department of Chemical and Biomolecular Engineering.
University of Delaware, Newark, Delaware, United States

Abstract: In this work, we propose a superstructure optimization study to determine the products and processes for plastic depolymerization and upgrading that minimize the generation of CO2 emissions while ensuring economic feasibility. The processes studied have been modeled using Aspen Plus® and custom models with Python that have been later reduced and considered within a Mixed-Integer-Lineal Programming optimization problem (MILP). The MILP has been solved following the ε-constraint method obtaining a pareto set of solution with the most profitable and environmentally friendly technologies. Chemical recycling based on solvents is the technology that avoids the highest release of CO2 emissions. The most profitable path is obtained for a multi-product refinery where plastic is first pyrolyzed, obtaining naphtha that is used to produce aldehydes. Other alternative solutions also suggest pyrolysis as depolymerization technology but with different final products.

Keywords: Superstructure optimization, plastic waste, recycling, upcycling, multi-objective optimization.

Introduction

Global plastic production is estimated at 350 million tons per year and is projected to increase by over 1200 million tons by 2050 (Rochman, 2013). Most of these plastics are discarded after their first use, with their characteristics nearly intact, permitting easy recycling. However, due to the cost associated with the collection and revalorization, only 9% of the total plastics produced in the United States are recycled, and 16% are incinerated (U.S. EPA, 2019). The remaining 75% is disposed into landfills without obtaining any value.

Mechanical recycling has been the most widely implemented technique due to its lower capital cost. However, it generates plastic that can only be recycled up to 3 times (Dogu et al. 2021). As an alternative, chemical and thermochemical recycling techniques have been proposed due to the ability to recover polymers with intact properties or generate added-value products. Chemical techniques based on the combination of solvents and antisolvents have been demonstrated to be very effective, with recovery yields of around 90% (Walker et al., 2020). Thermochemical recycling based on pyrolysis is the most extended thermochemical method with industrial scale plants, but other technologies such as gasification, hydrothermal liquefaction (HTL), hydrocracking (Dogu et al. 2021) or hydrogenolysis (Wang et al., 2021) have started to cover attention last years. Techno-economic and life cycle assessments have evaluated these technologies for some specific products. For example, pyrolysis has been studied to produce LDPE (Somoza-Tornos et al. 2020), or gasification has been investigated to produce methanol (Singh et al. 2022). However, these technologies may result in other alternative products. The naphtha in pyrolysis obtained contains a high fraction of olefins that can be transformed into a wide range of final products such as lubricants by oligomerization, detergents by alkylation, aldehydes by mean of the oxo-process, virgin polymers like LDPE or polypropylene or polystyrene, alcohols by oxidation, etc. In a similar way, gasification also results in syngas that can be transformed into methanol, ethanol, or Fischer-Tropsch fuels. Other technologies have more restricted applications, such as hydrocracking or hydrothermal liquefaction, since they result in paraffins that are of lower value. Understanding, which technology provides the highest value-added product, can be critical to engage companies in treating this waste. In a similar way, it is also interesting to determine the most environmentally friendly technology and product generated. In this context, the optimization framework described here can provide significant insights for determining the desired products and pathways.

Methodology

In this work, we propose a superstructure formulation to determine the optimal products and processes. Due to its high contribution to the market, 24% (U.S. EPA, 2019), LDPE is selected as a reference waste. The superstructure formulation has been developed as described in the following paragraphs.

First, process models have been developed for all the technologies. Most of the processes have been modeled with Aspen Plus®. However, specific processes (e.g., mechanical recycling, sorting) and processing units (e.g., extruder after solvent-based recycling or polymerization of the ethylene obtained in pyrolysis) are not available in Aspen Plus®, and they have been evaluated with custom models. A summary of all the processes considered is provided in Figure 1. Once the models with mass and energy balances have been developed for all the processes, techno-economic (TEA) and life cycle analyses (LCA) are performed. The cost of raw materials, utilities, and amortization due to investment are considered in the economic analysis. A recovery period of 10 years is considered for the life of the plant. LCA assessment is performed from cradle to gate in each process to determine the emissions generated by the raw materials and utilities. Other emissions generated by the construction of the catalyst production are not considered in the analysis. The emissions are computed following Traci method with the emission factors from Ecoinvent v3.8. The yields obtained in each of the processes, the costs involved, and the emissions generated are modeled with linear and parametric models that are included in each of the blocks of the superstructure formulation. The capital costs are addressed following a piecewise linear model. To evaluate technology integration (e.g., syngas can be used in parallel with pyrolysis to produce aldehydes), some sections of the code consider the composition of the stream as a variable. This requires the use of McCormick relaxations (Misener,R. and Floudas,C. 2009) for the bilineal product used in computing the resultant composition of a mixer. Another relaxation technique used in the selection of multiple alternatives is a big-M formulation to avoid the definition of a large set of binary variables. This allows reducing the number of discrete variables, resulting in a problem with a final size of 1,522 continuous variables and 428 discrete variables. The problem is formulated as a mixed integer linear programming (MILP) problem that is solved in GAMS using CPLEX. The ε-constraint method is followed for solving the problem considering multiple objectives, the profitability, and the CO2 emissions generated. Profitability is computed as defined in Eq. (1), where corresponds to the costs involved in all the processes, and the revenue generated by selling all the finished products. The emissions are computed as in Eq. (2), where the emissions for each process, are computed as defined in the previous paragraph and the refer to the discount generated by each of the final products when they substitute the same product based on conventional processes and fossil sources.

1.

$$Pr = \sum_{j=1}^{j\ Products} R_j - \sum_{i=1}^{i\ Process} C_i$$

2.

$$CO_{2_{Net}} = \sum_{i=1}^{i\ Process} CO_{2_i} - \sum_{j=1}^{j\ Products} Credits_j$$

Results

The solution of the optimization problem with the ε-constraint method results in a Pareto chart that provides the most profitable and environmentally friendly solutions as well as the intermediate solutions see Figure 2. Chemical recycling based on the use of solvents is the technology that avoids the highest release of CO2 emissions. This technology does not require high energy intensive methods, which generate high emissions. Furthermore, compared to mechanical recycling, it results in a polymer with nearly intact properties that can be recycled more times.

The most profitable path is obtained for a multi-product refinery where plastic is first pyrolyzed obtaining naphtha with a wide range of carbon olefins (C2 to ~C20). Light olefins (C2 to C4) are suggested to be oligomerized to increase the amount of α-olefins. These α-olefins are separated in two parts, the ones from C5 to C8 are separated in detail and used to produce aldehydes by the oxo-processes. The α-olefins with a carbon number higher than C8 are suggested to be oligomerized to produce olefins with a carbon number higher than C20 that can be used as lubricant. The paraffins of the naphtha in the process are assumed as inert in the oligomerization and they are separated by distillation from the lubricants. Apart from the most profitable and environmentally friendly solution, ε-constraint method also allows for obtaining intermediate alternative solutions that try to balance the two objectives. As can be seen from the Pareto chart presented in Figure 2, there are two other suggested alternatives. These two intermediate cases also suggest the use of pyrolysis as depolymerization technology. At the same time, fractions higher than C8 are desired to produce lubricants.

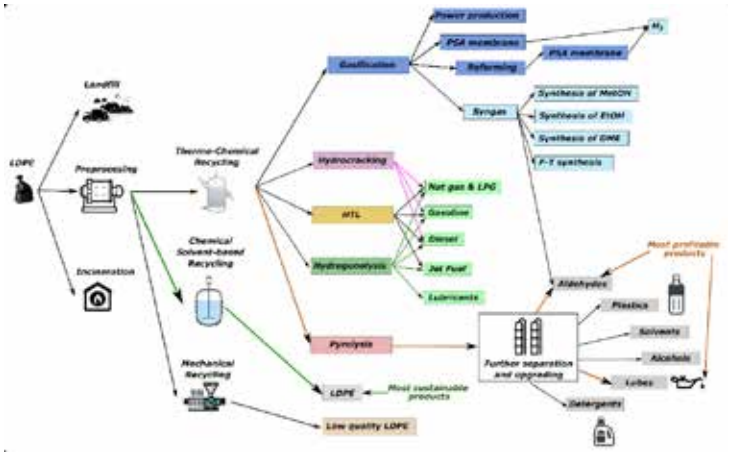

Figure 1. Summary of alternatives considered in the superstructure.

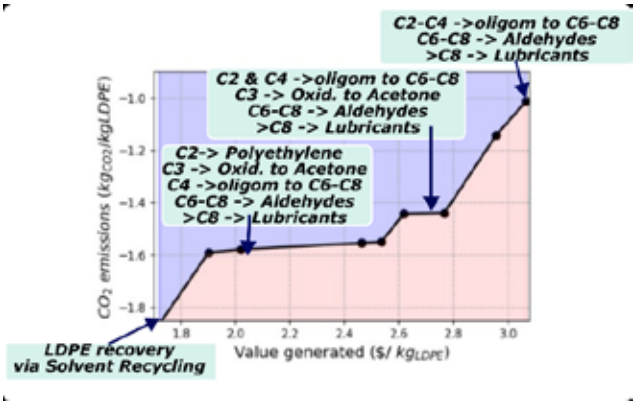

Figure 2. Pareto chart obtained by solving the MILP optimization problem.

Conclusions

The presented optimization formulation can support decisions for future technology implementation where plastic waste is considered as an alternative resource to fossil sources to produce valuable chemicals. Decisions are presented considering economic and environmental criteria, but they can be extended to other objectives including social impact. The work can also be extended to consider important components related to the supply chain of chemicals and collection of plastic waste.

Acknowledgments

This work is financially supported by the National Science Foundation, grants No. OIA – 2119754 and No. 2134471.

References

Dogu, O. Pelucchi, M. Van de Vijver, R. Van Steenberge, P.H.M. D'hooge, D.R. Cuoci, A. Mehl, M. Frassoldati, A. Faravelli, T. Van Geem, K.M. (2021) The chemistry of chemical recycling of solid plastic waste via pyrolysis and gasification: State-of-the-art, challenges, and future directions. Progress in Energy & Combustion Research, 84.

Misener, R. Floudas, C.A. (2009) Advances for the pooling problem: Modeling, global optimization, and computational studies. Appl. Comp. Math. 8, 1, 3-22.

Rochman, C.M. Browne, M.A. Halpern, B.S. Hentschel, B.T. Hoh, E. Karapanagioti, H.K. Rios-Mendoza, L.M. Takada, H. The, S. Thompson, R.C. (2013) Classify plastic waste as hazardous. Nature, 494, 169-171.

Singh, A. Afzal, S. Nicholson, S. Beckam, G.T. (2022) Techno-Economic Analysis of Waste Plastic Gasification to Methanol Process. Avalilable in: https://www.nrel.gov/docs/fy22osti/82636.pdf

Somoza-Tornos, A. Gonzalez-Garay, A. Pozo, C. Graells, M. Espuña, A. Guillén-Gosalbez, G. (2020) Realizing the potential high benefits of circular economy in the chemical industry: ethylene monomer recovery via polyethylene pyrolysis. ACS Sustainable Chemistry & Engineering, 8,9, 3561-3572.

United States Environmental Protection Agency. (2019) Advancing Sustainable Materials Management: 2017 Fact Sheet. Available in: https://www.epa.gov/sites/default/files/2019-11/documents/2017_facts_and_figures_fact_sheet_final.pdf

Wang, C. Xie,T. Kots, P. Vance, B. Yu, K. Kumar, P. Fu, J. Liu, S. Tsilomelekis, G. Stach, E.A. Zheng, W. Vlachos, D. (2021) Polyethylene hydrogenolysis at mild conditions over ruthenium on tungstated zirconia. JACS Au, 1, 9, 1422-1434.

GWI- and cost-Minimal retrofitting of cement production by superstructure optimization

Ariana Y. Ojeda P.[a,b], Alexander Mitsos[c,a,d], Manuel Dahmen[a]
[a]Forschungszentrum Jülich GmbH, Institute of Energy and Climate Research, Energy Systems Engineering (IEK-10), Jülich 52425, Germany
[b]RWTH Aachen University, Aachen 52062, Germany
[c]JARA-ENERGY, Jülich 52425, Germany
[d]RWTH Aachen University, Process Systems Engineering (AVT.SVT), Aachen 52074, Germany

Abstract: Cement production is an energy-intensive process and a major contributor of greenhouse emissions (GHG). To strongly reduce its global warming impact (GWI), it is essential to retrofit conventional cement production with carbon capture utilization or storage technologies and an energy supply system based on renewable energies. We present a superstructure optimization approach that enhances a well-established conventional route of cement production with various alternative options for carbon capture and utilization (CCU), carbon capture and storage (CCS), as well as power-to-gas technologies for provisioning of process heat. Applying bi-objective optimization, we assess the economic and environmental impact of optimal retrofits with minimal GWI and total annualized costs. Our results show that the installation of electricity-powered retrofit units, air separation and alkaline electrolysis, and the substitution of a fraction of fossil fuels by H2 can reduce the amount of GWI by 38% at an additional cost of 113 €/t cement. However, a strong GWI reduction is only possible by complementing with CCU technologies, raising the added costs to 406 €/t cement. The increase in operating costs is due to much higher electricity consumption, therefore the use of renewable electricity is crucial to achieve a large GWI and employ CCU technologies.

Keywords: Cement production, Superstructure optimization, Bi-objective optimization

Introduction

Carbon capture, utilization or storage (CCUS) technologies are necessary for the retrofit of cement plants with the aim of abating CO2 emissions (Karlsson et al., 2020). According to technology readiness level (IEA, 2020), one of the most mature technologies is oxyfuel combustion, which is between the large prototype and pre-demonstration stage. Power-to methane technology can utilize the captured CO2 and transform it into synthetic natural gas that can be sold for the residential sector and power generation (Ghaib and Ben-Fares, 2017) or used to supply thermal energy in the cement production process itself.

Since most of the retrofit technologies developed for cement production have been investigated separately, our contribution focuses on a holistic assessment that considers the different options in a process-wide optimization. A particular challenge is to find the optimal combination and sizing of available technologies to identify process designs with minimum global warming impact (GWI) and total annualized costs (TAC).

Problem Formulation

We propose a superstructure that adapts a well-established conventional route of cement production by including one or more of: oxyfuel combustion, alkaline or polymer electrolyte membrane electrolysis, catalytic or biological methanation, air separation, carbon purification, and carbon capture and storage. We develop a model consisting of mass and energy balances combined with nonlinear cost correlations and implement it in our open-source energy system optimization framework COMANDO (Langiu et al., 2021). After automatic linearization, we obtain a bi-objective mixed integer linear program (MILP) formulation, with an economic objective function (min TAC) accounting for investment and operating costs of each unit and the variable cost of consumed commodities, and a global warming impact objective function (min GWI) considering direct process emissions and indirect emissions from the use of electricity and commodities. In the bi-objective optimization problem, the TAC and GWI are repeatedly solved. The resulting MILPs are solved using Gurobi 9.5.1 with a relative optimality tolerance of 1%.

Results

With respect to the status quo of electricity production in Germany with a GWI of 375 gCO2/kWh (Icha and Lauf, 2022), assuming a CO2 tax of 54.17 EUR/t CO2 (EEX, 2021) and an electricity price of 50 EUR/MWh (Bundesnetzagentur - SMARD.de, 2022) there is no trade-off between the two objectives, as the optimal design is a conventional process that burns coal and emits CO2 to the atmosphere (red rhombus in Fig. 1).

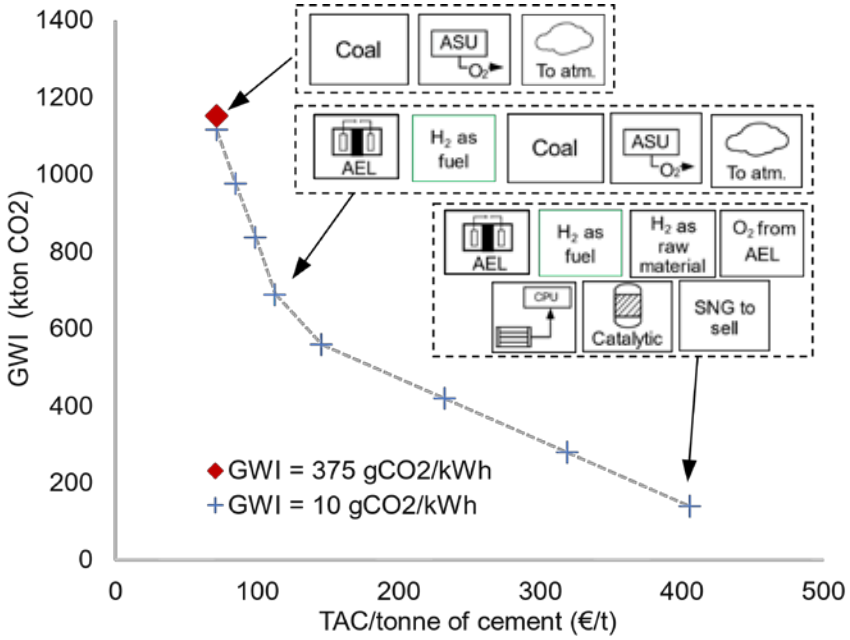

Figure 1. Pareto-front of retrofits with minimal TAC and GWI

Considering an electricity supply from the Norwegian grid with a GWI of 10 gCO2/kWh (IEA, 2022), 8 Pareto front design points are generated, and interpolated lines between the optimal solutions are added to guide the reader. All evaluated points show a trade-off between the economic and environmental objectives, with one objective improving while the other worsening. The fourth design point from left on the dashed gray line in Fig. 1 shows that initially coal for provisioning of process heat is substituted by H2, decreasing the GWI by 38%. Further reduction of GWI requires significantly more expensive options, as the implementation of carbon capture and power-to-gas technologies is needed (8th design point in Fig. 1).

Conclusions

The results demonstrate that strong reductions in GWI can be achieved, but only with expensive technologies for carbon capture and utilization, e.g., power-to-gas, as solely eliminating fossil fuel combustion is not sufficient.
In the next step, we will expand the considered superstructure to include further options for carbon capture technologies, i.e., chemical absorption, direct separation, and calcium looping.

Acknowledgments

This work was funded by the Helmholtz Association of German Research Centers through program-oriented funding and the Innovation Pool project "Energiewende und Kreislaufwirtschaft".

References

Bundesnetzagentur | SMARD.de. (2022). SMARD Strommarktdaten. Web page. Bundesnetzagentur. URL: https://www.smard.de/ (accessed on: 22-08-2022)

EEX. (2021). Emission spot primary market auction report 2021. Report. European Energy Exchange. URL: https://www.eex.com/en/market-data/environmental-markets/eua-primary-auction-spot-download (accessed on: 22-08-2022)

Ghaib, K., Ben-Fares, F. (2017), Power-to-Methane: A state-of-the-art review. Renew. Sustain. Energy. Rev., 81, 433

Icha, P., Lauf, T. (2022). Entwicklung der spezifischen Treibhausgas-Emissionen des deutschen Strommix in den Jahren 1990 – 2021. URL: https://www.umweltbundesamt.de/en/publikationen/entwicklung-der-spezifischen-kohlendioxid-8 (accessed on: 21-11-2022)

IEA. (2020). CCUS technology innovation. URL: https://www.iea.org/reports/ccus-in-clean-energy-transitions/ccus-technology-innovation (accessed on: 22-08-2022)

IEA. (2022). Norway 2022. Energy Policy Review. URL: https://www.iea.org/reports/norway-2022/executive-summary (accessed on: 21-11-2022)

Karlsson, I., Toltarova, A., Rootzén, J., Odenberger, M. (2020). Technical roadmap cement industry. URL: https://www.mistracarbonexit.com/news/2020/5/19/technical-roadmap-cement-industry (accessed on: 21-11-2022)

Langiu, M., Shu, D. Y., Baader, F. J., Hering, D., Bau, U., Xhonneux, A., Müller, D., Bardow, A., Mitsos, A., Dahmen, M. (2021). COMANDO: A Next-Generation Open-Source Framework for Energy Systems Optimization. Comput. Chem. Eng., 152, 107366.

Economic feasibility of bio-diesel production plants from animal fat wastes

Semie Kima, Pyeong-gon Jung[a], Young-Il Lim[a], Ki Eun Shin[b], Youn Kim[c], Youngdo Yang[c]
[a]Center of Sustainable Process Engineering (CoSPE), Department of Chemical Engineering, Hankyong National University, 327, Jungang-ro, Anseong-si, Gyeonggi-do, Republic of Korea
[b]SBK, 49, Sandan-ro, Gunsan-si, Jeollabuk-do, Republic of Korea
[c]Emax solutions, 63, Gombaemi-gil, Seo-myeon, Suncheon-si, Jeollanam-do, Republic of Korea

Abstract: In order to reduce petroleum diesel produced from fossil fuels to cope with climate change, interest in producing bio-diesel from waste-residues is increasing. Bio-diesel is produced from vegetables, animal fat wastes, and waste oils generated after food production such as fried foods. Animal fat waste and used cooking oil contain 10-50% free fatty acid (FFA), which reduces bio-diesel yield. Therefore, it is necessary to remove FFA before the trans-esterification reaction, which produces glycerol and fatty acid methyl esters (FAME) from triglyceride and alcohol.

The techno-economic analysis (TEA) of a bio-diesel production process including pre-treatment, pre-ester or neutralization reaction, offensive odor treatment, and wastewater treatment was presented for economic feasibility. The bio-diesel production cost from animal waste oil with high and medium acid value was 1.68 $/l and 1.12 $/l, respectively.

Keywords: Biodiesel production, Animal fat waste (AFW), Free fatty acid (FFA), Process modeling, Techno-economic analysis (TEA)

Introduction

Demand of biofuels is increasing to reduce carbon dioxide emissions from transport to achieve carbon neutrality in 2050 (IEA, 2020). Recently, the demand for electric (or hydrogen) vehicles has increased, and biofuels are interested in replacing fossil fuels as a fuel for aircraft and ships (IEA, 2021., Elgharbawy et al., 2021). The biodiesel in biofuels is produced from renewable bio-sources such as vegetables and animal fat wastes (De Araújo et al., 2013., Gebremariam et al., 2018). Attention is paid to inedible feedstock such as animal fat waste and used cooking oil as feedstocks to produce biodiesel, because edible raw materials have food security and ethical issues (Kumar et al., 2022., Adewale et al., 2015). However, animal fat waste and used cooking oil contain a high free fatty acid (FFA) in oils (Gnanaprakasam et al., 2013). The acid value is a mass of potassium hydroxide (KOH) required to neutralize 1 g of chemical substance, and a high acid value deteriorates the quality of oil (Odoom et al., 2014). When bio-diesel is produced using animal fat wastes, the cetane number is higher than vegetable oils due to high ratio of saturated fatty acids in animal waste fats (Adewale et al., 2015). A high cetane value has the advantage of lowering NOx by lowering the initial temperature of the combustion process, which leads to lower NOx (Alleman et al., 2016). Oil containing a high FFA generates soap emulsion during bio-diesel production and reduces safety (Susilowati et al., 2019., Kuleasan et al., 2008). Because FFA contained in animal fat waste interferes with the ester exchange reaction and reduces the biodiesel yield, a pre-treatment process to remove FFA is required (Susilowati et al., 2019., Leung et al., 2010).
In this study, process modeling was conducted for biodiesel production from animal waste oil with medium and high acid values. Economic feasibility was performed based on the simulation of the process flow diagram (PFD).

Raw bio-diesel production processes

The 1,250 kg/hr (or 4,170 kg/hr) of animal fat waste containing 13 wt% (or 25 wt%) of FFA is purified below an acid value of 5 using pre-transesterification, neutralization reactions. The raw bio-diesel production process used two scrubbers for offensive odor treatment and included a process for wastewater treatment from water washing, as shown in Figure 1.

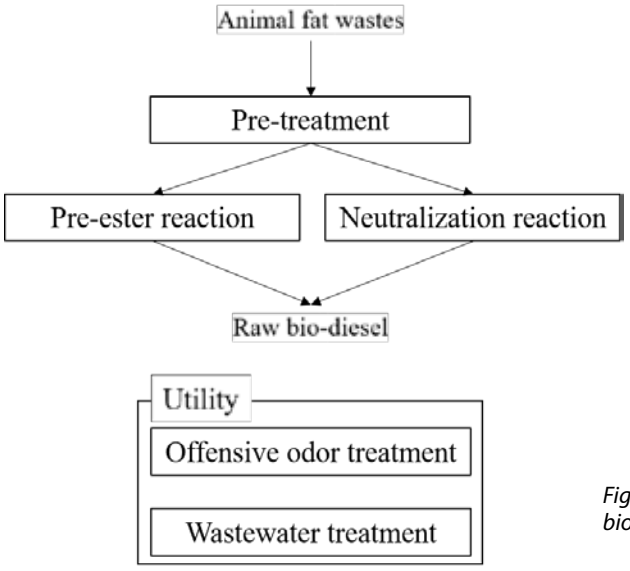

Figure 1. Block flow diagram (BFD) of raw bio-diesel production

Results

As a result of process simulation using ASPEN Plus (ASPEN Tech, USA), 1,000 kg/hr (or 4,000 kg/hr) of raw bio-diesel was produced from animal fat wastes with a high and medium acid values. The production cost was calculated as 1.68 $/ and 1.12 $/ , respectively.

Acknowledgments

This work was supported by the Korea Institute of Energy Technology Evaluation and Planning (KETEP) grant funded by the Korea government (MOTIE) (No. 2021010000001B).

References

IEA. (2020). World Energy Outlook 2020.

IEA. (2021). Transport Biofuels.

Elgharbawy, A. S., Sadik, W., Sadek, O. M., Kasaby, M. A. (2021). A review on biodiesel feedstocks and production technologies. Journal of the Chilean Chemical Society, 66(1), 5098-5109.

De Araújo, C. D. M., de Andrade, C. C., e Silva, E. D. S., Dupas, F. A. (2013). Biodiesel production from used cooking oil: A review. Renewable and sustainable energy reviews, 27, 445-452.

Gebremariam, S. N., Marchetti, J. M. (2018). Economics of biodiesel production. Energy Conversion and Management, 168, 74-84.

Kumar, R., Sexana, L., Kumar, R., Sonkar, R., & Katiyar, P. (2022). A REVIEW-Biodiesel Production, and Properties. International Journal of Research in Engineering and Science, 10, 1-11.

Adewale, P., Dumont, M. J., Ngadi, M. (2015). Recent trends of biodiesel production from animal fat wastes and associated production techniques. Renewable and Sustainable Energy Reviews, 45, 574-588.

Gnanaprakasam, A., Sivakumar, V. M., Surendhar, A., Thirumarimurugan, M., Kannadasan, T. (2013). Recent strategy of biodiesel production from waste cooking oil and process influencing parameters: a review. Journal of Energy.

Odoom, W., Bart-Plange, A. Darko, J. O., Addo, A. (2014). Quality assessment of moisture content, free fatty acids and acid value of coconut oil produced in the Jomoro District of the Western Region of Ghana. Journal of Research in Agriculture. Journal of Research in Agriculture, 3.

Alleman, T. L., McCormick, R. L., Christensen, E. D., Fioroni, G., Moriarty, K., & Yanowitz, J. (2016). Biodiesel handling and use guide (No. NREL/BK-5400-66521; DOE/GO-FEN102016-4875). National Renewable Energy Lab. (NREL), Golden, CO (United States).

Susilowati, E., Hasan, A., & Syarif, A. (2019). Free fatty acid reduction in a waste cooking oil as a raw material for biodiesel with activated coal ash adsorbent. In Journal of Physics: Conference Series, 1167.

Leung, D. Y., Wu, X., & Leung, M. K. H. (2010). A review on biodiesel production using catalyzed transesterification. Applied energy, 87(4), 1083-1095.

Kuleasan, S., & Tekin, A. (2008). Alkaline neutralization of crude soybean oil by various adsorbents. European journal of lipid science and technology, 110(3), 261-265.

Machine-learning-powered process design for the recycling of waste polyurethane

Luca Bosetti, Benedikt Alexander Winter, Johanna Lindfeld, André Bardow
Energy and Process System Engineering
ETH Zurich, 8092 Zurich, Switzerland

Abstract: A fully circular economy for the plastics industry needs both mechanical and chemical recycling. Some polymers, such as polyurethane rigid foams (PUR), can only be recycled chemically. The resulting multi-step process involves depolymerization, which leads to complex mixtures and thus challenging separations of the valuable monomers, e.g., aniline. To minimize the energy demand for separation, extraction seems promising. However, extraction requires a solvent with specific thermodynamic properties. Here, we present a machine-learning-based framework to screen solvents for the chemical recycling processes of PUR foams. The in-house machine learning model SPT is used to calculate the partition coefficients of the target component in the two phases resulting from the extraction process. The predicted properties allow us to efficiently rank solvents suitable for the separation of aniline in the chemical recycling of PUR.

Keywords: Machine Learning, Polyurethane Waste Recycling, Computer-aided Process Design

Introduction

A net-zero CO2 future seems unfeasible without a circular economy for the chemical industry (Meys et al. 2020). Many studies agree that this circular economy would need both mechanical and chemical recycling. Recycling's contribution is twofold: first, substituting fossil-based feedstocks, and second, avoiding plastic pollution and carbon emissions due to waste combustion at the end of life.

The recycling of Polyurethane rigid foams (PUR) is limited to chemical recycling due to its physical and chemical structure, which prohibits mechanical recycling. Chemical recycling often results in complex mixtures that require energy-intensive separation processes, which challenges the sustainability of the recycling process. Additionally, these mixtures are difficult to characterize thermodynamically, making it difficult to design systematic recycling processes.

In this work, we develop low-energy separation pathways for the chemical recycling of PUR by exploiting predictive thermodynamic models based on machine learning.

Method

Our analysis considers that end-of-life PUR is processed in a catalytic process, resulting in a mixture of aniline, a polyol, e.g., propylene glycol (PG), and other by-products, e.g., acetone. This mixture simplifies the expected pyrolysis output but is a suitable approximation to develop a method for aniline recovery. In the most straightforward downstream, a series of distillation columns separates aniline from the rest of the products. However, the energy demand and total cost of the separation plant could potentially be reduced by an extraction unit at close to ambient temperature, which exploits the formation of a liquid-liquid equilibrium between the main component in the mixture, e.g., aniline and a solvent (Green and Southard 2019).

The main challenge in extraction is identifying a solvent, which requires accurate thermodynamic properties. However, these thermodynamic properties are often not available, leading to the need for predictive thermodynamic models, e.g., COSMO-RS (Polte et al. 2022). Recently, some of the authors developed a machine learning approach that can be more accurate and computationally efficient to calculate activity coefficients for a broad range of molecules (Winter et al. 2022a). Here, we embed the machine learning model into a framework to determine the solvents' thermodynamic properties. Thereby, we can explore a large solvent database at a reduced computational cost.

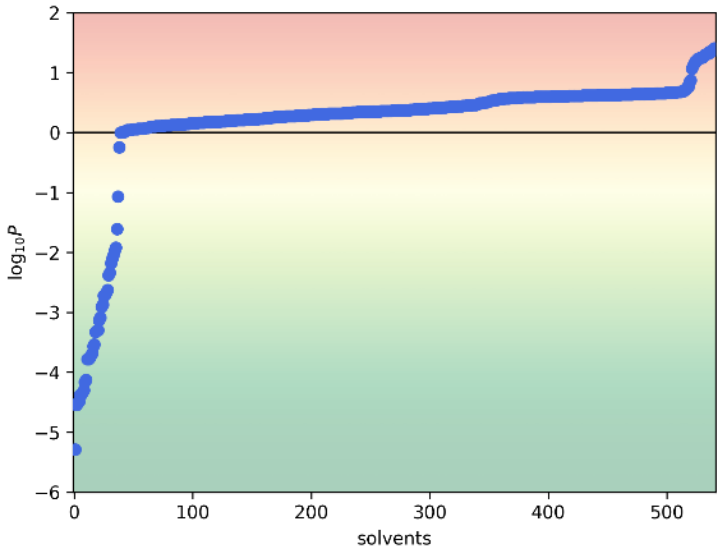

Figure 1. Partition coefficients of acetone between aniline and around 550 candidate solvents (each represented by a blue dot) forming an LLE with aniline identified by a database screening of 10000 compounds; around 50 solvents show $\log_{10}P_{\text{acetone}}<0$*, making them suitable for the extraction of acetone from aniline*

Results and discussion

The machine learning model (SMILES to Properties Transformer, SPT) is based on natural language processing and takes SMILES code as input. SPT was originally trained to estimate activity coefficients (Winter et al. 2022b). Here, we further trained SPT to estimate properties relevant to the extraction process: first, we limited the training to only solvents forming a liquid-liquid equilibrium (LLE) with aniline; second, properties such as boiling point, melting temperature, etc., have been calculated to ensure that the extraction process would be able to operate seamlessly. Finally, the screened solvents have been ranked according to an optimality indicator, which can be a heuristic quantity like the partition coefficient, defined in equation 1, or an indicator resulting from a more thorough analysis of the operation of the extraction unit, e.g., the solvent use or the energy demand for the entire column. In this study, we limit the analysis to the partition coefficient, defined as

$$\log_{10} P_i = \log_{10} \frac{\gamma_i^{II}}{\gamma_i^{I}} \qquad (1)$$

where γ_i is the activity coefficient of compound i, calculated with SPT, and phases I and II are the raffinate and the extract outlet flows of the extraction column, respectively. A value of $\log p_i$ close to 0 means that the compound i would split equally into both phases. Values of the partition coefficients lower than 0 indicate a solvent able to extract compound i from the original solvent, thus achieving the desired separation.
By screening a large database of around 10000 candidates, the model found around 550 solvents forming an LLE with aniline. For these 550 solvents, the value of $\log_{10} P$ for acetone has been calculated and used to rank the solvent candidates (Figure 1). For around 50 solvents, the $\log_{10} P$ is lower than 0, thus making these solvents potential candidates to extract acetone from aniline in the context of chemical recycling of PUR.

Conclusions

Machine-learning models are shown to support the conceptual design of the separation of a reaction mixture coming from PUR foam recycling. The presented design method allows us to screen rapidly a very large number of solvents for which the thermodynamic properties are not experimentally available but are instead predicted with SPT. Further constraints specific to extraction can also be considered. The approach can be extended to include process-level optimality indicators, like reducing energy demand and solvent use, which are not reported in this contribution. Moreover, this method can be applied to design solvents, making it an integrated solution for computer-aided molecular and process design (CAMPD).

Acknowledgments

The project leading to this application has received funding from the European Union's Horizon 2020 research and innovation program under grant agreement No 101036854 and from NCCR Catalysis (grant number 180544) a National Centre of Competence in Research funded by the Swiss National Science Foundation.

References

Green, D. W., Southard, M. Z. (2019). Perry's chemical engineers' handbook. McGraw-Hill Education.

Meys, R., Kätelhön, A., Bachmann, M., Winter, B., Zibunas, C., Suh, S., Bardow, A. Achieving net-zero greenhouse gas emission plastics by a circular carbon economy. Science 2021, 374(6563), 71-76. DOI: 10.1126/science.abg9853

Polte, L.; Raßpe-Lange, L.; Latz, F.; Jupke, A.; Leonhard, K. COSMO-CAMPED – Solvent design for an extraction distillation considering molecular, process, equipment, and economic optimization. 2023, No. 3, 1–12. https://doi.org/10.1002/cite.202200144.

Winter, B., Winter, C., Schilling, J., Bardow, A. A SMILE is all you need: Predicting limiting activity coefficients from SMILES with natural language processing. Digital Discovery, 2022a. https://doi.org/10.1039/D2DD00058J

Winter, B., Winter, C., Esper, T., Schilling, J., Bardow, A. SPT-NRTL: A physics-guided machine learning model to predict thermodynamically consistent activity coefficients. arXiv preprint, 2022b.

https://doi.org/10.48550/arXiv.2209.04135

Optimizing energy exchanges for decarbonizing industries through industrial ecology concepts

Marianne Boix, Stéphane Négny, Ludovic Montastruc
Laboratoire de Génie Chimique, UMR5503,
Toulouse INP/CNRS/UPS, 4 Allée Emile Monso,
31432 TOULOUSE Cedex 4, FRANCE

Abstract: Regarding the current environmental context, the production systems need to be highly transformed and modified in order to fit with the polluting norms. Industrial ecology consists in the gathering of companies on a geographical area that are able to share services, energy flows, network structure or equipment to reduce the environmental footprint of the industrial complex. These symbiotic relations also lead to a decrease of economic cost. The aim of the paper is to propose an optimization procedure to take into account environmental footprint, total cost aqof the network and the flexibility at a design stage to overcome the different barriers encountered in the practice. One of the main bottleneck is the ability of the network to adapt to fluctuations of inlet flows in a crisis context, or to different level of production of partners if the economic situation is changing. It is shown that the flexibility at a design stage has an investment cost that we are able to define and that an increase of the cooperation leads to reduce carbon emissions of the site.

Keywords: Decarbonation, industrial ecology

Introduction and scientific context

The National Low Carbon Strategy (SNBC) sets out objectives for reducing greenhouse gas emissions in France in the short/medium term. It has two ambitions: to achieve carbon neutrality, i.e., net-zero emissions by 2050 (an objective introduced by the July 2017 climate plan and enshrined in law), and to reduce the carbon footprint of the French people. French industry (chemical industry, steel industry, cement industry...) is one of the main emitting sectors, responsible in 2018 for the emission of 70 Mt CO2/year, i.e., 20% of French emissions (Directive 2018/2001). Transforming industries towards decarbonization and sustainability can be achieved by enforcing industrial ecology (IE) through the development of eco-industrial parks (EIP) (Boix et al., 2015). The concept of Industrial Ecology has emerged in scientific literature in the early 90's (Frosch and Gallopoulos, 1989). This concept, which is directly linked to sustainable development, aims at engaging separate industries, geographically closed enough, in a collective approach so that exchanges of raw materials, by-products, energy and utilities are maximized (Chertow, 2000). Indeed, the most widespread manifestations of these kinds of industrial symbiosis are eco-industrial parks. A definition widely
accepted for EIP is "an industrial system of planned materials and energy exchanges that seeks to minimize energy and raw materials use, minimize waste, and build sustainable economic, ecological and social relationships" (Montastruc et al., 2013). Despite some successful proofs of concept that they reduce economic, environmental and social impacts, the implementation of EIP is often limited to dedicated hubs, industrial zones or maritime ports, in France (maritime ports (Rhône valley- France, SOGEBI Lacq, Kalundborg's EIP in Denmark, PIICTO Fos- Marseille-9 France, Grand Port Maritime de Nantes Saint- Nazaire-Fance, Grand Port de Dunkerque-France, Port de Strasbourg-France...). Among the barriers already identified, the notion of interdependence and flexibility of the networks between industrial actors has a prohibitive effect. Moreover, the last few years have provided numerous examples of the uncertain nature of the production domain, whether due to pandemics, geopolitical conflicts or raw material shortages. This work aims at developing a robust methodology to take into account the flexibility that an exchange network can assume during its design. Flexibility refers to the ability of a given system to operate in a fluctuating context, actively or passively, with or without modification of the system in question (Hoch and Eliceche, 1996). The flexibility of an EIP will thus be zero if at least one of the enterprises can no longer operate when its input parameters vary. Boix et al. (2023) has recently shown that the development of a new optimization procedure can lead to anticipate the cost of the flexibility. The aim is to show the ability of industrial symbioses to be key elements for the decarbonization of production systems by reducing their carbon footprint.

Methodology

A superstructure has been developed in Boix et al. (2022) to model the multi-energy network (vapor of different levels of pressure, electricity from renewable sources and from the grid) of an eco-industrial park. A Mixed Integer Linear Program (MILP) is formulated to model the energy exchanges in both each company and inter-companies simultaneously. The objective function is the net global emissions of CO2 related to the energy consumption of the EIP as a function of the connections between companies. The flexibility is used to evaluate the different optimal networks among the Pareto front. The case study chosen (Kim et al., 2010) involves 15 companies, each one encompasses four energy demands over four time periods. The impacts are evaluated through an indicator based on Life Cycle Assessment approach. An impact factor is used to convert the energy consumptions into carbon emissions obtained with EcoInvent database through SIMAPRO software.

Results and discussion

During the iterations of the optimization procedure, connections between companies are allowed step-by-step what increases the level of cooperation of companies in the EIP. According to figure 1, if the level of cooperation increases in the symbiosis, then, a carbon emission reduction could be effective.

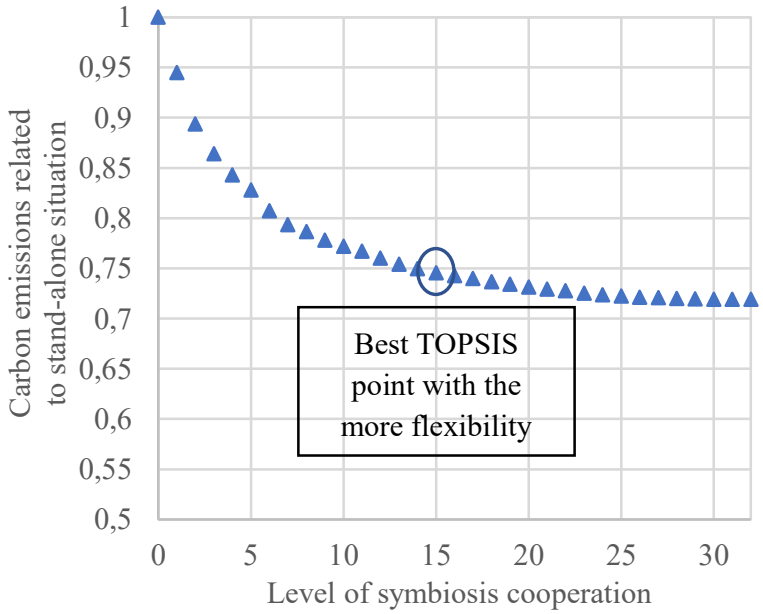

Figure 1. Decrease of carbon emissions with the increase of cooperation in the EIP

A 30% reduction of carbon footprint can be achieved by increasing the number of exchanged flows in the EIP. By the way, the procedure developed in Boix et al. (2023) for taking into account the flexibility of the network leads to an optimal solution with 20% of flexibility with a network involving 15 connections in the total EIP between the different companies. This solution is the same as the one chosen by TOPSIS as a multicriteria decision making tool (Figure 1). Indeed, increasing the number of flows exchanged (going from 15 to 30) will not lead to a great decrease of carbon emissions but a great loss of flexibility will be measured.

Conclusion and perspectives

The results obtained are generic enough to be applied to other cases study and can help to reduce carbon footprint of industrial production. Indeed, if the networks are flexible enough with a measured cost, a generalization of industrial ecology at a territorial scale could help to reach the carbon emissions objectives while maintaining production of goods and services. A perspective of this work is the application of the methodologies deployed to the territory scale with a management of energy flows between the different actors, as the problematics of nexus (Cansino-Loeza, 2022).

References

Boix, M., Négny, S., Montastruc, L., Mousqué, F, 2023. Flexible networks to promote the development of industrial symbioses: A new optimization procedure. Comput. Chem. Eng., 169, 108082.

Boix, M., Montastruc, L., Azzaro-Pantel, C., Domenech, S., 2015. Optimization methods applied to the design of eco- industrial parks: a literature review. J. Clean Prod., 22, 85-97.

Directive (EU) 2018/2001 of the European Parliament and of the Council of 11 December 2018 on the promotion of the use of energy from renewable sources (OJ L 328, 21.12.2018, p. 82).

Cansino-Loeza, B., Munguía-López, A., Ponce-Ortega, J.-M., 2022. Optimizing the allocation of resources for the security of the water-energy-food nexus, Computer Aided Chemical Engineering, 51, pp. 1579-1584

Chertow, M.R., 2000. Industrial symbiosis: Literature and taxonomy. Annu. Rev. Energy Environ. 25, 313–337.

Frosch, R.A., Gallopoulos, N.E., 1989. Strategies for Manufacturing. Sci. Am. 261, 144–152.

Hoch and Eliceche, 1996. Flexibility analysis leads to a sizing strategy in distillation columns. Comput. Chem. Eng., 20 (4).

Kim Kim, S.H., Yoon, S.G., Chae, S.H., Park, S., 2010. Economic and environmental optimization of a multi-site utility network for an industrial complex. J. Environ. Manage. 91, 690–705.

Montastruc, L., Boix, M., Pibouleau, L., Azzaro-Pantel, C., Domenech, S., 2013. On the flexibility of an eco- industrial park (EIP) for managing industrial water. J. Clean. Prod. 43, 1–11.

Study of lithium recovery from desalination concentrates BY MEANS OF Density Functional Theory (DFT)

E. Fernández-Escalante, R. Ibañez, Ma.-F. San-Román
Departamento de Ingenierías Química y Biomolecular, ETSIIyT
Universidad de Cantabria, Avda. de los Castros, 46, Santander, 39005, Cantabria, Spain

Abstract: Lithium, declared "Critical Raw Material" by the European Union in 2020, is a competitor to hydrogen as an alternative to petroleum. While its use is increasing, the natural reserves are decreasing, encouraging new sources of supply, such as seawater desalination concentrates. This work aims at the computational study of the selectivity of lithium extraction with regard to other cations present in high concentrations in seawater desalination concentrates such as Na+, K+, Mg2+, Ca2+ and Sr2+. For this purpose, the calculated coefficients of extraction K, cation•(β-diketones or organo-phosphates), were calculated. These calculations were carried out by molecular simulation using ab initio Density Functional Theory (DFT), to determine the geometries, reaction energies, and thermodynamic parameters. The results show, on the one hand, that the complexation reaction energies of the systems have negative ΔG values, indicating stable complexes and spontaneous reactions, and, on the other hand, that the synergistic effect of the extractants allows obtaining a high selectivity Li+ with respect to the other cations, for the systems DBM•TOPO•HFDOD and DBM•TOPO•HBTA.

Keywords: Lithium, Desalination Concentrates, Extraction, Selectivity, Molecular Simulation, DFT

Introduction

Lithium was considered for the first time as one of the raw materials declared critical by the European Union in 2020. The development of electric vehicles and the use of portable electronic devices will increase Li+ consumption, estimated at 56,000 tons in 2020 (U.G. Geological Survey, 2021). In the context of the Circular Economy, new lithium sources such as seawater reverse osmosis (SWRO) desalination concentrates show increasing potential. Currently, seawater desalination plants are generating concentrated brine discharges about of 100×106 m3 each day, with the rejects being 10 to 15 times more concentrated than seawater. Thus, it is a challenge to incorporate technologies capable of extracting Li+ from SWRO brines due to its still low concentration and competition with the rest of the ions. So, liquid-liquid extraction has demonstrated numerous advantages for the separation and purification of metals from different matrices.

The state of art describes the use of a number of extractants of different natures, mostly used in model solutions containing just one single cation. The need to selectively extract lithium in complex mixtures can lead to extraordinarily high experimental effort. To avoid inefficient experimental work, a computational study has been carried out on the selective extraction of lithium in presence of the metal ions found in higher concentrations in the brines, such as Na^+, K^+, Mg^{2+}, Ca^{2+} and Sr^{2+}, using the β-diketones DBM, TTA, FTA, BTA, FDOD and LIX54 and the organophosphates TOPO, TBP, TRIS and BIS. The systems Li+•DBM•TOPO and Li+•LIX54•TOPO were used for Li+ extraction, which was obtained in previous work (Coterillo et al., 2022). Equilibrium and thermodynamic properties, and structural optimizations were carried out using the ORCA 4.2.1 quantum chemistry package at the B3LYP/def2-SVP level of theory.

Computational methodology

Selectivity model (S)

The extraction capacity of extractants for metal ions was studied on the basis of reaction energies as a measure of the stability of the cation-extractant system, i.e. as a measure of the stability of the final complex according to the complexation reaction of the form:

$$A^{m+} + L \Longleftrightarrow [A \bullet L]^{m+} \qquad (1)$$

Where Am+ is the cation (Na^+, K^+, Mg^{2+}, Ca^{2+} or Sr^{2+}) and L is the selected extractant (DBM, TTA, FTA, BTA, FDOD, LIX54, TOPO, TBP, TRIS and BIS). In this sense, the reaction energy can also be understood as the binding energy between the cation and the extractant. On the other hand, the hydration process of the cations was also considered, as they are the competing reactions in the extraction processes. The hydration reaction between a cation and the n water molecules within its coordination shell can be written as (n=4 for this work):

$$A^{m+} + nH_2O \Longleftrightarrow [A(H_2O)_n]^{m+} \qquad (2)$$

The extraction was characterized by defining an extraction coefficient K, defined as the ratio between the equilibrium constants of the complexation (kec) and hydration (keh) reactions:

$$K = \frac{k_{ec}}{k_{eh}} \qquad (3)$$

Finally, the selectivity model was evaluated to assess the feasibility of extracting Li+ over the other cations present in the seawater desalination concentrates:

$$S_{Li^+/A_i^{m+}} = \frac{K_{Li^+}}{\sum K_{A_i^{m+}}} \qquad (4)$$

Where A_i^{m+} is the rest of the metal ions present in the aqueous solution, i.e., Na^+, K^+, Mg^{2+}, Ca^{2+} or Sr^{2+}.

Computational tools

The starting structures of the extractant and cation-extractant complexes were hand-crafted using the Avogadro chemical editor and the UFF force field potential was incorporated. Structure optimization was carried out using the ORCA 4.2.1 quantum chemistry package at the B3LYP/def2-SVP level of theory. This includes both the optimization process and the subsequent frequency calculation.

The effects of the solvation media -i.e. the kerosene-based organic phase on the binding process were considered by including of the Solvation Model based on Density (SMD) in the final energy calculations of the cation-extractant reactions. However, geometry optimizations and frequency calculations were performed without the implicit solvent model, as tests indicated that the final geometries remained largely unaffected and the numerical noise introduced by this approach would render the molecular PES too unstable to find reliable minima, partly due to the large size of the systems. It was also omitted in the case of the hydration reactions, as the solvent is explicitly in the reaction considered in the reaction itself.

Results

Selectivity Li^+ from seawater desalination concentrates

Figure 1 shows the selectivity of lithium with respect to the rest of the cations present in high concentrations in desalination concentrates. The selectivity has been calculated according to Eq. (4) for the Li^+•DBM•TOPO and Li^+•LIX54•TOPO systems. Those conditions where the extractant is repeated, e.g., in the case of LIX54, TOPO or DBM, have not been taken into account. As can be observed, the Li^+•DBM•TOPO system gives higher selectivity values in all cases, where HBTA and HFDOD extractants providing the highest selectivity values, 520 and 660 respectively.

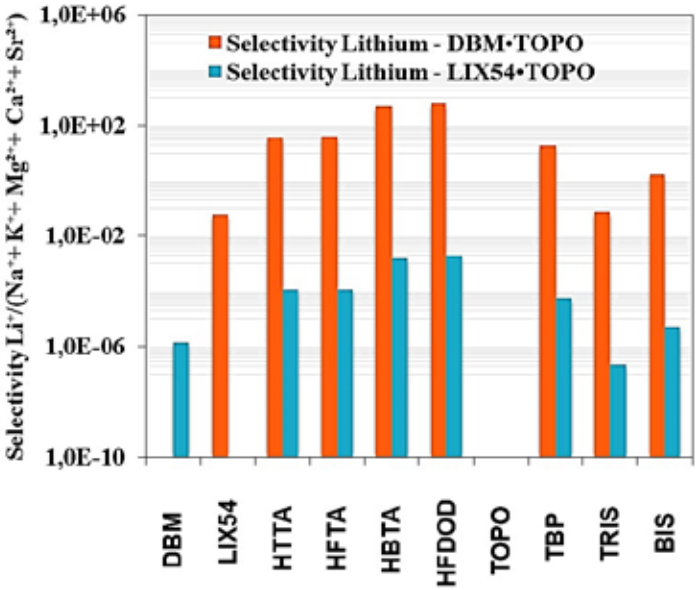

Figure 1. Selectivity of Li^+ respect to Na^+, K^+, Mg^{2+}, Ca^{2+} and Sr^{2+} (log. scale)

Conclusions

The results obtained after these simulations will contribute to increase the knowledge regarding the selective extraction of Li^+ in desalination concentrates, thus, reducing the experimental work required in these studies. Considering the results obtained in this work, it is expected, that the ternary mixtures DBM•TOPO•HFDOD and DBM•TOPO•HBTA will provide the highest selectivity of Li^+.

Acknowledgments

This research was developed in the framework of the project PID2020-115409RB-I00 (MCIN/AEI) financed by the Spanish Ministry of Science and Innovation.

References

Coterillo, R., Gallart, L.-E., Fernández-Escalante, E., Junquera, J., García- Fernández, P., Ortiz, I., Ibañez, R., San-Román, M.-F. (2022). Selective extraction of lithium from seawater desalination concentrates: Study of thermodynamic and equilibrium properties using Density Functional Theory (DFT). Desalination, 532, 115704.

U.S. Geological Survey, Mineral Commodity Summaries 2021, https://doi. org/10.3133/mcs2021.

Circular economy in the management of spent acids: modelling of the adsorption process for the copper recovery

A. Bringas, E. Bringas, R. Ibañez, Ma.-F. San-Román
Departamento de Ingenierías Química y Biomolecular, ETSIIyT
Universidad de Cantabria, Avda. de los Castros, 46, Santander, 39005, Cantabria, Spain

Abstract: Hazardous industrial wastes with a high metal and acid content such as spent acids (SP) can be considered secondary sources of raw materials and they should be managed following the principles of Circular Economy. Chelating resins have received considerable attention as separation agents due to their high efficiency and selectivity toward toxic metal cations. In this work, SP effluents containing Ni2+ (≈12 g L−1), Cu2+ (≈2 g L−1) and Fe2+ (≈30 g L−1) in sulphuric acid were treated with the commercial chelating resin Puromet™ MTS9600 with bis-picolylamine moieties (Bis-PMA) in order to allow the selective recovery of copper. At pH=1.0, 80% of Cu2+ was selectively adsorbed with low separation of Ni2+ and Fe2+ (≈10%). Finally, the mathematical model to describe the adsorption of Cu2+ was proposed, considering as the controlling stage the metal diffusion through the pore. The parametric estimation was carried out by Aspen Custom Modeler software, obtaining the mass transport apparent coefficient solid phase kS = 0.12 h-1, with a relative error lower of 15.0%.

Keywords: Spent acids, Chelating resins, Copper, Mathematical Modelling

Introduction

Today, demanded metals are affected in some cases by scarcity and continuous increases in cost; therefore novel strategies to carry out their recovery from secondary sources should be designed in the framework of the Circular Economy that aims at minimization of waste generation and raw materials consumption.

Industrial wastewaters containing heavy metals in acid medium, give rise to hazardous waste streams with complex and varied compositions. Therefore, the removal and recovery of metals from spent acids has received considerable attention from the scientific community. Among different technologies, solid-phase separation with materials functionalized with chelating ligands has reported, high efficiency and selectivity in the removal of metals (Ulloa et al., 2020a).

In previous works, spent acidic effluents containing nickel (≈12 g L^{-1}), copper (≈2 g L^{-1}) and iron (≈30 g L^{-1}) in sulphuric acid media were treated with commercial chelating resin Puromet™MTS9600 functionalized with Bis-PMA groups in order to generate two streams enriched in copper and nickel, respectively. At pH 1.0, this resin is able to obtain excellent separation results with removal percentages of copper≈80% versus nickel and iron (≈10%). Subsequently, the adsorption equilibrium of copper was described by the Langmuir isotherm (Ulloa et al., 2020a).
In this work, the mathematical model to describe the adsorption of Cu^{2+} with the MTS9600 chelating resin in a fixed bed column is reported. The model that includes the microscopic and macroscopic mass balances in the column, considers that the kinetic controlling step was the diffusion of the metal through the pore. The model parameters were calculated with mass transport and fluid-flow correlations. The mass transport apparent coefficient solid phase kS was mathematically estimated by the comparison of simulated and experimental data using Aspen Custom Modeler (Aspen Tech).

Experimental section

Materials

Adsorption with chelating resins was applied to treat real industrial exhausted sulphuric acid-based baths with the following characteristics: Ni^{2+} (≈12 g L^{-1}), Cu^{2+} (≈2 g L−1), Fe^{2+} (≈30 g L^{-1}) and pH≈1.0. The chelating resin used for the recovery of copper was Puromet™ MTS9600 functionalized with Bis-PMA supplied by Purolite.

Experimental methods

Adsorption experiments were performed in a column (effective length of 0.19 m and an inner diameter of 0.03 m) to describe the kinetics of the selective adsorption of copper against nickel. The feed solution was circulated through the column in a continuous and downward mode with a flow rate of 3.4·10-4 m3 h-1 using a peristaltic pump (Watson Marlow). Samples were taken during the treatment at column exit and the copper content was determined by Microwave Plasma-Atomic Emission Spectrometry (Agilent, Spain).

Results

Adsorption kinetics of Cu^{2+}

As shown in Figure 1, only, the copper adsorption is described by a breakthrough curve since Ni and Fe removal is expected to be negligible; Cu^{2+} concentration increases, achieving an asymptotic concentration of 80% of the initial concentration after 20 operating hours. Nevertheless, Ni^{2+} and Fe^{2+} were adsorbed minimally, around 10%, as was expected, since working at pH values lower than 2.0, where their adsorption is not favoured.

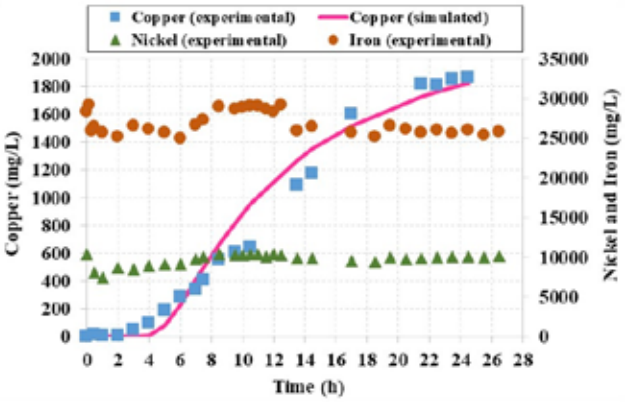

Figure 1. Breakthrough curves of Cu^{2+}. Adsorption of Ni^{2+} and Fe^{2+}

Modelling of Cu^{2+} adsorption in fixed bed

The mathematical model that describes the breakthrough curve of Cu^{2+} consists of: i) the mass balance equation of the column (Eq. (1)), ii) the equilibrium equation and iii) a set of equations describing external and internal mass transfer phenomena. Based on previous results (Ulloa et al., 2020a) it was concluded: i) equilibrium data for Cu^{2+} adsorption with Puromet™ MTS9600 resin are described by the Langmuir model (Eq. (2)), ii) the dispersion term in the fixed mass balance should be taken into account due to the operation at low flow rates, iii) diffusion in the liquid film should be considered as a controlling stage (Eq. (3)), and iv) diffusion in the pore (internal diffusion) in the controlling step (Eq. (4))

$$\varepsilon_B \frac{\partial C}{\partial t} + \rho_F \frac{\partial q}{\partial t} + v_F \frac{\partial C}{\partial t} = D_{ax}\, \varepsilon_B \frac{\partial^2 C}{\partial z^2} \qquad (1)$$

Where C is Cu^{2+} concentration, mg L-1; q is Cu^{2+} concentration in the resin, mg kg^{-1} (resin); εB=0.5 is bed porosity; ρF=1.100 kg m-3 is fluid density; vF=0.45 m3 h-1 is linear velocity; Dax=1.16 10-3 is axial dispersion.

$$q_{eq} = \frac{q_m K_{Lg} C_{eq}}{1 + K_{Lg} C_{eq}} \qquad (2)$$

Where Ceq is Cu^{+2} concentration in the equilibrium; qeq is Cu^{+2} concentration in the resin in equilibrium; qm=48,000 mg kg^{-1}_dry resin; KLg=9.1 10^{-2} L mg^{-1}.

$$\rho_F \frac{\partial q}{\partial t} = k_L A_P \left(C - C_{eq}\right) \qquad (3)$$

Being A_p=8,425 m^2 m^{-3} external surface area; k_L=5.5 10^{-2} m h^{-1} mass transport coefficient liquid phase.

$$\frac{\partial q}{\partial t} = k_S \left(q - q_{eq}\right) \qquad (4)$$

Where k_s is the mass transport apparent coefficient solid phase to estimate.

The mathematical model was solved using the software Aspen Custom Modeler V12.1 (Aspen Tech) and solver options: Estimator=Least Squares, Solver=NL2SOL, maximum iterations=100, relative function tolerance=1.0 10-4 absolute function tolerance=1.0 10-20 and solution convergence tolerance=1.0 104. Finally, ks estimated was 0.12 h-1. The fitting between experimental and simulated data is shown in Figure 1.

Conclusions

This study reported the mathematical modelling of an adsorption process to remove Cu2+ from SP using Bis-PMA chelating resins. The process was limited by the mass transfer resistance in the pores of the resin. In a further step, the separation of nickel and iron and the process scale up will be studied.

Acknowledgments

This research was developed in the framework of the project PID2020-115409RB-I00 (MCIN/AEI) financed by the Spanish Ministry of Science and Innovation.

References

Ulloa, L., Bringas, E. San-Román, Mª-F. (2020a). Simultaneous separation of nickel and copper from sulfuric acid using chelating weak base resins. J. Chem. Technol. Biotechnol., 95, 1906.

Ulloa, L., Martinez, M., Bringas, E. Cobo, A., San-Román, Mª-F. (2020b). Split regeneration of chelating resins for the selective recovery of nickel and copper. Sep. Purif. Technol., 95, 1906.

Planetary Environmental benefits of CO2-to-Ethylene Direct bifunctional catalytic Synthesis

Cecilia Salah[a], Iasonas Ioannou[a], Stavroula Batsolaki[a], Gonzalo Guillén-Gosálbez[a]
[a]Institute for Chemical and Bioengineering,
Department of Chemistry and Applied Biosciences
ETH Zürich, Switzerland

Abstract: In view of meeting the Paris Agreement, it is important to decarbonize current technologies, particularly in the petrochemical industry. Carbon capture and utilization (CCU) has gained attention in recent years because it has the potential to reduce emissions whilst generating valuable chemicals, such as methanol and olefins. Within the general field of CCU, this work performs an absolute environmental sustainability assessment (AESA) based on the planetary boundaries (PBs) framework to quantify the environmental benefits of producing ethylene through the direct synthesis of CO2 using renewable H2 (dSyn). The results show that the direct catalytic route has the potential to decarbonize the olefins market, as it significantly reduces the pressure applied on the climate change-related PBs. Moreover, it is possible to meet the global demand for ethylene within PBs via dSyn deploying H2 from electrolysis powered by nuclear.

Keywords: Direct ethylene synthesis, carbon capture and utilization, planetary boundaries, life cycle assessment

Introduction

Carbon capture and utilization (CCU) has the potential to reduce emissions whilst generating valuable chemicals. Ioannou et al. (2020) discussed the environmental benefits of employing CCU for the production of light-olefins (C2-C5) via CO2-to-methanol and methanol-to-olefins (MTO), showing that this route enables a drastic reduction in environmental impacts with respect to naphtha steam cracking, the business-as-usual (BAU) route.

Although effective, the MTO comes with two main limitations. Catalysts require frequent regeneration due to coke formation, and the equilibrium limited methanol synthesis from CO2 hydrogenation. Studies of bifunctional catalysts have progressed in recent years, in order to simplify this two-step process, allowing for in situ synthesis of olefins from syngas, which could overcome both limitations (DeWilde et al. 2021).

Here we assess for the first time the environmental feasibility of the direct synthesis of CO2-to-olefins (dSyn) deploying electrolytic H2, against planetary boundaries.

Methodology

Process description – direct synthesis of olefins from CO2

A simulation was carried out in Aspen Plus V12. CO2 and H2 are fed (ratio 3:1) to the dSyn reactor, which operates at 390 ^{0}C and 21 bar. The direct synthesis was modeled in a plug flow reactor, with kinetic data for a bifunctional catalytic bed consisting of the conventional Cu–ZnO–Al2O3 catalyst, typically used for CO2 hydrogenation to methanol, and the SAPO-34 catalyst, widely used for MTO. The subsequent separation steps were modeled as in DeWilde et al. (2021).

Absolute environmental sustainability assessment (AESA)

The environmental assessment followed the guidelines of the ISO 14040 (2006), using data of global activities from Ecoinvent 3.5 (Wernet et al. 2016) in Simapro 9.2. The assessment follows a cradle-to-gate approach, using the "cut-off by classification" allocation method.

The life cycle impacts were calculated with the absolute environmental sustainability assessment (AESA) method based on the planetary boundaries (PBs) framework (Rockström et al. 2009 and Steffen et al. 2015), using the characterization factors developed by Ryberg et al. (2018) and Galán-Martín et al. (2021). The framework introduces boundaries for nine control variables linked to seven Earth-systems: climate change (CC), quantified via the atmosphe-ric CO2 concentration (CCCO2), and the energy imbalance at the top of the atmosphere (CCEI), stratospheric ozone depletion (SOD), ocean acidification (OA), biogeochemical flows of nitrogen (BGFN) and phosphorus (BGFP), land-system change (LSC), freshwater use (FWU) and changes in biosphere integrity (CBI).

The transgression level of each scenario s from PB b ($TL_{b,s}$) was calculated with respect to the downscaled safe operating space attributed to ethylene production ($SOS_{eth,b}$) and the scenario's total environmental impact ($EI_{b,s}$). $EI_{b,s}$ and $TL_{b,s}$ were calculated according to Eq. (1) and (2) respectively, where $I_{s,f}$ is the quantity of elementary flow f associated with the production of 1 kg of ethylene, CF_b are the characterization factors defined for each PB b, and FU the functional unit (the global demand of ethylene).

$$EI_{b,s} = \sum_{f \in F} I_{s,f} \cdot CF_b \cdot FU \quad \forall\, b, s \qquad (1)$$

$$TL_{b,s} = \frac{EI_{b,s}}{SOS_{eth,b}} \quad \forall\, b, s \qquad (2)$$

The $SOS_{eth,b}$ was downscaled following the utilitarian principle (Ryberg et al. 2020), using the gross value added (GVA) of ethylene, and the global GVA.

$$SOS_{eth,b} = SOS_{GLO,b} \frac{GVA_{eth}}{GVA_{GLO}} \forall b \qquad (3)$$

The life cycle inventories considered impacts from raw materials, electricity, process utilities, products, and direct emissions, disregarding the end-of-life of the plant infrastructure and use phase of the produced ethylene. Five technologies were assessed: the BAU route, fossil-MTO from conventional methanol, and dSyn deploying CO2 captured from a natural gas power plant and H2 obtained via electrolysis powered by solar, wind and nuclear power.

Results and Discussion

The results show that utilizing renewable H2 and CO2 from CCU in the dSyn route enables a significant reduction of the impacts of ethylene production on CC related PBs, notably in the CC related Earth-system processes. Indeed, the fossil routes (fossil-MTO and BAU) transgress CC-CO2 and CC-EI (TL>1) whilst the dSyn routes operate within these boundaries (TL<1). Deploying CCU leads to negative emissions in the ethylene synthesis, as opposed to fossil routes, which exert high pressure on the corresponding carrying capacities, thereby transgressing these PBs.

dSyn-nuclear is found to operate within PBs, as it does not transgress any of the boundaries. Burden shifting can be observed for dSyn-solar and dSyn-wind due to the impacts related to the energy source used in the H2 production. Indeed, both transgress BGF-N and dSyn-solar CBI as well.

Ethylene from dSyn could contribute to decarbonizing the petrochemical sector, notably in the production of polymers for packaging. In fact, ethylene from CCU and nuclear-H2 operates within PBs.

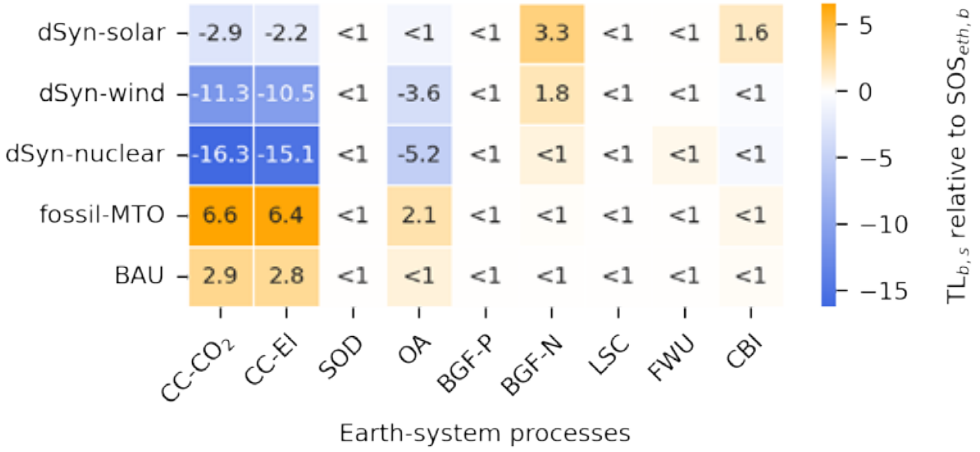

Figure 1. Transgression level relative to the SOSeth of the assessed scenarios of ethylene production

Acknowledgments

This publication was created as part of NCCR Catalysis (grant 180544), a National Centre of Competence in Research funded by the Swiss National Science Foundation.

References

DeWilde, J.F., et al. (2021) Kinetics of Direct Olefin Synthesis from Syngas over Mixed Beds of Zn-Zr Oxides and SAPO-34, Ind. Eng. Chem. Res., 60, 39.

Galán-Martín, Á., et al. (2021) Sustainability Footprints of a Renewable Caron Transition for the Petrochemical Sector within Planetary Boundaries, One Earth, 4, 4.

Ioannou, I., et al. (2020) Hybridization of Fossil- and CO2-Based Routes for Ethylene Production using Renewable Energy, ChemSusChem, 13, 23.

ISO (2006), ISO 14040:2006(E): Environmental Management – Life Cycle Assessment – Principles and Framework, International Standards Organization.

Rockström J., et al. (2009) Planetary Boundaries: Exploring the Safe Operating Space for Humanity, Ecol. Soc, 14, 2:32.

Ryberg, M.W., et al. (2018) Development of a Life-Cycle Impact Assessment Methodology Linked to the Planetary Boundaries Framework, Ecol. Indic., 88, 250-262.

Ryberg, M.W., et al. (2020) Downscaling the planetary boundaries in absolute environmental sustainability assessments – A review, J. Clean, 276, 123287.

Steffen, W., et al. (2015) Planetary boundaries: Guiding human development on a changing planet, Science, 347, 6223.

Wernet, G., et al. (2016) The ecoinvent database version 3 (part I): overview and methodology, Int J Life Cycle Assess, 21, 9.

Evaluating the potential of current and emerging alternatives to enable a Sustainable Circular Economy

Vyom Thakker[1], Amrita Sen[1], George Stephanopoulos[2,3], Bhavik R. Bakshi[1]
[1]William G. Lowrie Department of Chemical and Biomolecular Engineering, The Ohio State University, Columbus, Ohio, 43201
[2]The Global KAITEKI Center, Arizona State University, Tempe, Arizona 85287, USA
[3]Department of Chemical Engineering, Massachusetts Institute of Technology, Cambridge, MA 02139, USA

Abstract: Industry and governments are pledging to achieve sustainability and circularity targets to mitigate climate change and pollution by as early as 2030, without a clear indication of a concrete plan of action. This is partly due to the oversight of potential innovations, emerging technologies and policy interventions. The objective of this work is to guide future investment strategies in eco-innovations, based on quantitative criteria and holistic environmental impact assessment of cradle-to-cradle life cycles. A novel framework to screen and rank conceptual eco-innovations is developed, which relies on hot-spot and sensitivity analyses to identify promising sectors for screening eco-innovations and formulates a metric based on multi-objective optimization and technology readiness for adoption to rank the screened eco-innovations. The developed ranking can be used to guide future investment strategies based on holistic impact estimation, trade-offs between environmental and economic objectives, and innovation readiness.

Keywords: Sustainable Circular Economy, Anticipatory Life Cycle Assessment, Net-Zero Emissions, Circularity

Introduction

Current value-chains of several products need to be reformed to meet sustainability and circularity targets set by corporations and governments, such as The Climate Pledge, US Plastics Pact, Paris Agreement, etc. These reforms are expected to occur through development and adoption of eco-innovations such as new technologies, electrification, policies. and supply-chains. This work is dedicated to guiding such reforms and sustainability transitions through a quantitative methodology that relies on optimization and holistic environmental impact assessment methods such as Life Cycle Assessment (LCA). Notably, there are numerous considerations while guiding sustainability transitions, including economics, climate change mitigation potential, resource use and circularity. Thus, a multi-objective optimization is needed to capture trade-offs between these indicators while identifying optimal synergies between eco-innovations and current value-chains. This work highlights a novel framework developed to sequentially guide eco-innovations by screening from a large list of alternatives and ranking them based on their potential to improve the aforementioned objectives and reduce trade-offs. It also considers the technology readiness levels (TRL) of several eco-innovations and identifies potential synergies between them. As a result, industrial stakeholders can understand which eco-innovations can help them achieve their net-zero emissions and circularity targets, and at what expense. This framework is demonstrated for the value-chain of grocery bags, with eco-innovations from the packaging domain, sustainability programs/policy and supply-chain reforms.

Motivating Case Study

Grocery bags are a ubiquitous boon and bane in the society, and each household in USA requires ~4000 liters of volume carrying capacity in a year. The value-chain of these bags has several alternatives not only in the type of bags, but also collection methods, and end-of-life treatment alternatives at the Material Recovery Facility (MRF) as shown in Figure 1. The previously developed Sustainable Circular Economy (SCE) framework can identify Pareto-optimal SCE pathways in the conventional value-chain network (Thakker and Bakshi 2021a, b), as presented in Figure 2. Notably, the Pareto-front with alternatives in the conventional value-chain fail to achieve net-zero GHG emissions, and there is a need for eco-innovations to achieve targets by extending to the infeasible space of the Pareto-front. The developed framework screens and rank eco-innovations from the entire value chain using a systematic and holistic methodology.

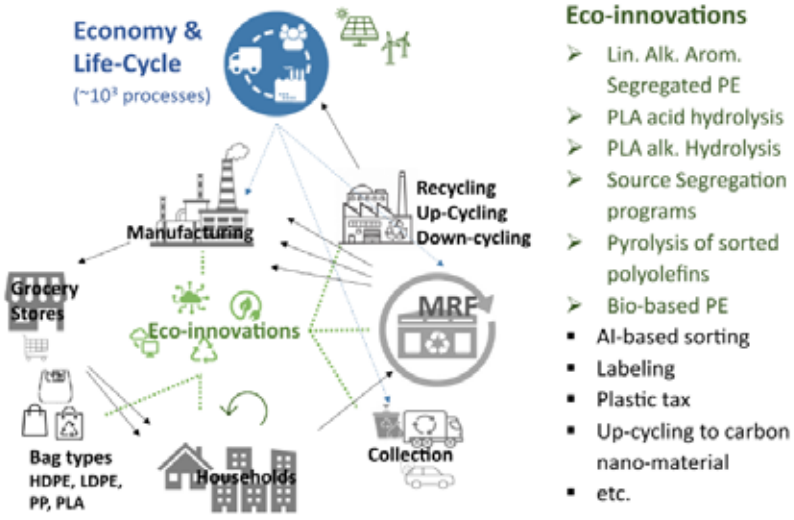

Figure 1. Case Study: The Grocery Bags Value-chain alternatives (multiple arrows), quantified using LCA datasets

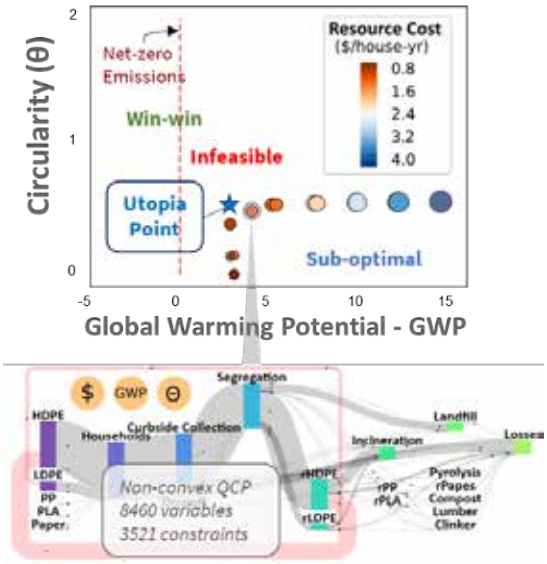

Figure 2: SCE optimal solutions as Pareto-optimal points for the conventional value-chain alternatives

Screening and Ranking Methodology

Since there are thousands of conceptual innovations in different parts of the value-chain to promote SCE and help meet corporate targets, it is essential to have a screening step to perform skillful vetting of these alternatives. The two approaches used for screening are (1) retrospective hot-spot analysis of current value-chains, and (2) prospective sensitivity-based optimization to identify optimal perturbations of LCI data to pinpoint promising sectors.

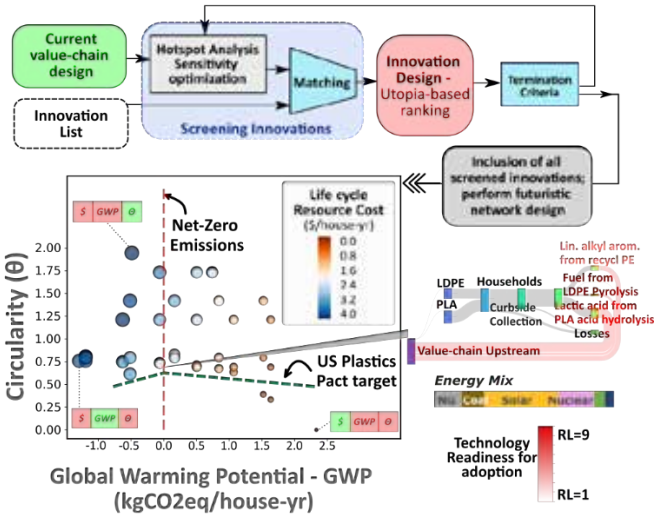

Figure 3: Screening and Ranking Methodology (top), and futuristic Pareto-front (bottom) shows that environmental pledges can be met in the future with a subset of innovations (right)

This screening step provides a manageable subset of eco-innovations for progressive addition into the superstructure of alternatives. Optimizing each innovative superstructure network, yields a new Pareto-front with an improved 'Utopia point', representing the best independently obtainable objective values. The shift in Utopia point in the win-win space, along with the TRL of the innovation is considered as a ranking criterion, thereby guiding future investment strategies. Next, multiple innovations are combinatorically added to the superstructure to identify potential synergies and scope of achieving targets under these futuristic scenarios.

Conclusions

The methodology is established in Thakker and Bakshi, 2023, and is implemented for the motivating grocery bags case study with 10 screened eco-innovations from the packaging domain. The findings are briefly summarized in Figure 3 of this proceeding. Notably, for the case study, chemical recycling of biomass-derived polylactic acid bags and pyrolysis of polyethylene-based innovations can lead the grocery bags value-chain to net-zero emissions and meeting of plastic circularity pledges. The framework can therefore guide synergistic development of infrastructure to support eco-innovations.

References

Thakker, V., & Bakshi, B. R. (2021a). Toward sustainable circular economies: A computational framework for assessment and design. Journal of Cleaner Production, 295, 126353.

Thakker, V., & Bakshi, B. R. (2021b). Designing Value Chains of Plastic and Paper Carrier Bags for a Sustainable and Circular Economy. ACS Sustainable Chemistry & Engineering, 9(49), 16687-16698.

Thakker, V., & Bakshi, B. R. (2023). Ranking Eco-Innovations to Enable a Sustainable Circular Economy with Net-Zero Emissions. ACS Sustainable Chemistry & Engineering, 11, 4, 1363–1374.

Economic feasibility of hydrometallurgical process in LiBs metal recycling

Thang Toan Vu, Junhyung Seo, Daesung Song
School of Chemical Engineering
Chonnam National University, Republic of Korea

Abstract: LiBs production has risen rapidly in recent years and become an important power storage source. It encourages the demand for valuable metals such as Co, Ni and Li. However, the metal resource is limited and requires high energy consumption and human source to exploit. Thus, the recycling of valuable metals in waste LiBs is a critical topic. There are many studies on this topic but most of them are on a lab scale and do not cover the real situation in the industry. This study provides a detailed techno-economic analysis of the hydrometallurgy process application for metal recovery from LiBs on a commercial scale. The NCM622 is chosen as the feed of the plant and is handled through all necessary sections: pre-treatment, leaching, solvent extraction and purification. The mass and energy balance is calculated by the commercial tool Aspen Plus. Based on the process simulation result, the economic feasibility of this process is evaluated. In the context of the USA industry zone, the process shows good economic feasibility, represented by a return on investment (ROI) of 15% and an internal rate return (IRR) of 18%. This work would provide a basis for an investment decision in this industry.

Keywords: Waste battery recycling, LiBs, hydrometallurgical process, techno-economic analysis.

Introduction

Due to their beneficial characteristics, such as high energy density and minimal self-discharge, lithium-ion batteries (LIBs) have dominated the market for batteries during the past three decades. LIBs are currently the preferred energy storage medium for portable consumer devices such as laptops, cell phones, and industrial applications such as electric vehicle production, stationary storage, etc. (Neumann et al., 2022). The increasing usage of LIBs leads to the development of reuse and recycling solutions aimed at minimizing the LIB technology's environmental impact and advancing the circular economy objective (Cerrillo-Gonzalez et al., 2020).

Several recycling technologies for LIBs have been developed. Among them, pyrometallurgical and hydrometallurgical techniques are the most used today (Mossali et al., 2020). Hydrometallurgy is advantageous to pyrometallurgical processes in terms of recovery efficiency, energy consumption, and gaseous emissions (Larouche et al., 2020). Recently, the majority of research efforts have concentrated on identifying a variety of extractants with high extraction efficiency to improve the hydrometallurgical process. Nevertheless, these investigations were conducted on a laboratory size and addressed just a part of the processes, not the entire process, on a commercial scale. Thus, we investigated the whole recycling process of all valuable metals using hydrometallurgy technology. The economic feasibility is evaluated in the context of the USA industrial market.

Methodology

In this study, the process is simulated by the commercial tool Aspen Plus. The proposed process contains six units: pre-treatment (discharging, crushing, and pyrolysis), leaching by H_2SO_4 and H_2O_2, Mn extraction by D2EHPA, Co extraction by Cyanex272, Ni extraction by PC-88A, and Li precipitation with Na_2CO_3. The metals are recovered under battery-grade form as MnO_2, $CoSO_4$, $NiSO_4$. and Li_2CO_3. The process is designed to treat approximately 3.9 t/h of NCM622 battery pack. The cathode material is obtained from Yang et al. (Yang et al., 2020) and showed in Table 1.

Table 1. The element composition of NCM622 (%wt)

Li	Ni	Co	Mn	Al	C
5.97	34.69	11.61	11.65	8.67	2.45

The mass and energy balance result from the model was used to estimate economic indicators. The equipment cost was estimated by the capacity ratio method (Vu et al., 2021; Vu et al., 2020) by Eq. 1. The base size and base cost are collected from public data and literature (Qiang Dai, 2019).

$$New\ cost\ at\ the\ current\ year = base\ cost \times \left(\frac{new\ size}{base\ size}\right)^{scaling\ factor} \times \frac{CEPCI\ at\ the\ current\ year}{CEPCI\ at\ the\ base\ year} \quad (1)$$

In consideration of maintenance and repair time, the operation time of the process is expected to be 8000h per year. The projected lifetime of the process was 20 years, which is the average lifetime of a process. The discount rate is 2.0% and an installation cost is assumed as 25% of the equipment cost. Based on the above parameters, the net present value (NPV) calculation was applied as Eq. 2. A positive NPV indicates that the investment yields a bigger return than the discounted cash flow; hence, the firm is deemed economically successful

$$NPV = \sum_{t=1}^{T} \frac{C_t}{(1+r)^t} - C_0 \quad (2)$$

T is the lifetime of the process, C0 is the initial investment cost, Ct is the net cash flow over the period T and r is the discount rate. Ct is determined by subtracting the amount of tax, material cost, utility cost, etc. from the annual income. The ROI value is measured as the ratio of profit to investment followed the Eq. 3.

$$ROI = \frac{Net\,profit}{Investiment\,value} \qquad (3)$$

Result

In this section, we considered a detailed calculation for the equipment cost and economic possibilities parameter. The summary of the equipment cost is shown in Figure 1. The total cost of major equipment is approximately 80 M$. Around 80% of the principal equipment expenditures are attributable to the separation of Mn, Co, and Ni sections. The solvent extraction segment is primarily responsible for the majority of the capital costs due to its high liquid flow rate treatment. Figure 1 indicates the progressive increase in equipment costs for Mn, Co, and Ni extraction, which is a significant factor. As Ni extraction is the final extraction step, the volume of aqueous input entering the reactor is the largest compared to previous extraction processes.

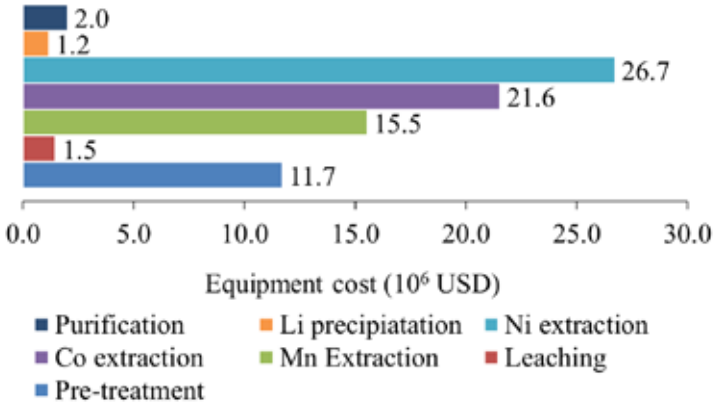

Figure 1. Equipment cost of the process

The ROI, IRR, and NPV of the proposed method are 14.8 percent, 18.4 percent, and 474.1 million dollars, respectively. There is a lack of research to assess these economic indicators, thus, similar project economic outcome is compared. According to China Everbright Securities, the ROI for recycling LFP batteries ranges from 6.1 to 16.2, depending on the price of the battery (Lima et al., 2022). According to McKinsey analysis, the investment in a new market with new technology typically accepts 8-12% of IRR, while for most chemical plants IRR is 9-12%. The ROI of 14.8% and the IRR of 18.4 years indicate that this approach has great potential.

Conclusion

This research estimated the techno-economic feasibility of hydrometallurgical technology in the specified case of commercial NCM622 batteries. The analysis figured out that the series of solvent extraction units could recycle valuable metals of battery-grade quality while the return on investment is acceptable. At the capacity of 3.9 t/h of the battery pack, this process cost 80 million dollars. However, the process can get 474 million dollars of NPV and achieve 15% of ROI. In the context of the declining supply of the main metals (Ni, Co, Li) from mines, it is expected that the high possibility result will encourage the commercialization of this process.

Acknowledgments

This research was conducted with the support of the National Research Foundation of Korea (NRF) grant funded by the Korea government (MSIT) (No. 2021R1F1A1048416).

References

Cerrillo-Gonzalez, M.d.M., Villen-Guzman, M., Acedo-Bueno, L.F., Rodriguez-Maroto, J.M., Paz-Garcia, J.M., 2020. Hydrometallurgical Extraction of Li and Co from LiCoO2 Particles–Experimental and Modeling. Applied Sciences 10(18).

Larouche, F., Tedjar, F., Amouzegar, K., Houlachi, G., Bouchard, P., Demopoulos, G.P., Zaghib, K., 2020. Progress and Status of Hydrometallurgical and Direct Recycling of Li-Ion Batteries and Beyond. Materials (Basel) 13(3).

Lima, M.C.C., Pontes, L.P., Vasconcelos, A.S.M., de Araujo Silva Junior, W., Wu, K., 2022. Economic Aspects for Recycling of Used Lithium-Ion Batteries from Electric Vehicles. Energies 15(6).

Neumann, J., Petranikova, M., Meeus, M., Gamarra, J.D., Younesi, R., Winter, M., Nowak, S., 2022. Recycling of Lithium-Ion Batteries—Current State of the Art, Circular Economy, and Next Generation Recycling. Advanced Energy Materials 12(17).

Qiang Dai, J.S., Shabbir Ahmed, Linda Gaines, Jarod C. Kelly, and Michael Wang, 2019. EverBatt: A Closed-loop Battery Recycling Cost and Environmental Impacts Model. Argonne National Laboratory.

Vu, T.T., Lim, Y.-I., Song, D., Hwang, K.-R., Kim, D.-K., 2021. Economic analysis of vanillin production from Kraft lignin using alkaline oxidation and regeneration. Biomass Conversion and Biorefinery.

Vu, T.T., Lim, Y.-I., Song, D., Mun, T.-Y., Moon, J.-H., Sun, D., Hwang, Y.-T., Lee, J.-G., Park, Y.C., 2020. Techno-economic analysis of ultra-supercritical power plants using air- and oxy-combustion circulating fluidized bed with and without CO2 capture. Energy 194, 116855.

Yang, X., Dong, P., Hao, T., Zhang, Y., Meng, Q., Li, Q., Zhou, S., 2020. A Combined Method of Leaching and Co-Precipitation for Recycling Spent Lini0.6Co0.2Mn0.202 Cathode Materials: Process Optimization and Performance Aspects. Jom 72(11), 3843-3852.

Techno-Economic Analysis and Environmental Assessment of Synthetic Fuel Production from Green H_2 and INDUSTRIAL CO_2 using Fischer-Tropsch synthesis

Marcelino Artur. L. Fernandes[2,3], Frederico S. Coelho[1], Gustavo P. Rangel[1,2,3], Mariana G. Domingos[1], José Carlos B. Lopes[1], Fernando G. Martins[2,3]

[1]CoLAB NET4CO2, Rua Júlio de Matos, 828-882, 4200-355 Porto, Portugal

[2]LEPABE - Laboratory for Process Engineering, Environment, Biotechnology and Energy, Faculty of Engineering, University of Porto, Rua Dr. Roberto Frias, 4200-465 Porto, Portugal

[3]ALiCE - Associate Laboratory in Chemical Engineering, Faculty of Engineering, University of Porto, Rua Dr. Roberto Frias, 4200-465 Porto, Portugal

Abstract: This work simulates a Power-to-Liquid (PtL) process to produce synthetic crude (syncrude) via Fischer-Tropsch (FT) synthesis, from CO2 emitted from an industrial source combined with renewable H2. The introduction of CO2 and H2 recycling streams, with the additional equipment and utilities for the separation steps, has been proved advantageous from an economic and environmental perspective, for the electricity, medium pressure steam, and hydrogen prices considered. Compared to conventional fossil crude, economically, the PtL process led to higher costs than the typical price of Brent crude oil, but could have a less environmental impact, if by-product valorization is considered.

Keywords: Synthetic Fuels, Power-to-Liquid Process, Techno-Economic Analysis and Environmental Assessment

Introduction

Synthetic fuels are expected to play a relevant role in energy transition: they can be obtained from CO2 that would otherwise be emitted to the atmosphere; they act as an important renewable energy storage medium, if Green Hydrogen is used for their synthesis; and they require no change to the existent infrastructures. Indeed, the International Energy Agency estimates around 7.5 Mton of CO2 per year would be used for synthetic fuel production in a NetZero by 2030 scenario (IEA,2022), and in 2022, the European Parliament markedly increased its ambition regarding aviation decarbonization, amending the ReFuelEU Aviation proposal to introduce a minimum share of 50% by 2050.

In the literature, techno-economic analysis (TEA) indicates that PtL pathways lead to syncrude productions more expensive than fossil crudes, with the main cost driver being the H2 price, even at the target price is of 2 €/kg (Zang, 2021).

Regarding the environmental assessment (EA) of PtL applications, CO2 is usually modelled as being captured from a Direct Air Capture unit (Micheli, 2022), which ultimately leads to significant life cycle benefits since the GHG emissions of combustion are neutral. Therefore, the potential of PtL in utilizing industrial CO2 utilization from industry to simultaneously reduce those industries' emissions and the transport sector is often overlooked (CSI ECRA, 2017). Thus, this paper addresses such gaps by assuming CO2 capture from a refinery and by modelling the process assuming state-of-the-art conversions and thermodynamic limitations of each process unit.

The PtL process consists of 3 main stages; 1) Reverse Water Gas Shift Reaction (RWGS), to transform CO2 into CO; 2) Fischer Tropsch (FT) reaction, a polymerization reaction, in which CO and H2 react to produce heavier hydrocarbons; 3) Syncrude separation to separate long chain from short-chain hydrocarbons. To maximize syncrude production, three recycling streams can be considered 1) the unreacted CO2 from the RWGS reaction; 2) the CO2 emitted from the light gases combustion; 3) the H2 remaining after the FT reaction.

The processes were simulated in Aspen Plus ® using the Peng-Robinson property model, recommended when hydrocarbons and light gases are present, and the NRTL-RK model for process sections containing electrolytes. For the RWGS, a kinetic model developed by (Vázquez, 2017) was used, the CO2 conversion was set to 70% and the feed ratio of H2/CO2 was adjusted to approximately 2 at reactor outlet. For the FT reaction, the kinetic model presented in the work of (Pandey, 2021) was implemented, considering the production of paraffins (CnH2n+2) and olefins (CnH2n) within the range C1-C30, assuming a CO conversion of 70 %. For the case where recycling is considered, the CO2 is separated by chemical absorption, where Monoethanolamineis used as an absorbent, whereas H2 is separated by a Pressure Swing Adsorption. A heat exchanger network, capable of integrating process heat and minimizing energy consumption, was also developed in Aspen Energy AnalyzerTM through Pinch analysis, and the heat released from the exothermic FT reaction was used to produce medium pressure steam (MPS), at 8.6 bar and 175 °C.

Both simulations started with a CO2 flow rate of 17 ton/h, typical of a medium size refinery fixed source. The results indicate that the introduction of recycle streams increases production per day by nearly 3 times, from 371 to 1000 bpd, whereas the energy content of the barrel has only a slight increase, from 34.5 to 36.1 MJ/kg. This was expected since the FT parameters depend on the reactants relative amount, which was fixed and kept very similar for both cases simulated.

The TEA proved the case with recycling streams is always more cost effective, both at the current green H2 price (7 €/kg, 725 vs 646 €/barrel) and the target green H2 price (2 €/kg, 188 vs 172 €/barrel), while considering an electricity price of 82 €/MWh, and a steam price of 25 €/ton. However, even at the target green H2 price, the process is still more expensive than the conventional crude (80-100 €/barrel) .

For the EA, the functional unit, system boundaries and impact allocation between co-products followed the same framework as the TEA. Excess steam and electricity produced were credited with avoided burdens. Electricity is co-produced exclusively in the case study with recycling streams, in a Rankine Cycle and via expansion of the high-pressure steam generated in a turbine. Global Warming Potential (GWP) impact results yielded between -0.1 to 0.6 and between 0.6 to 1.3 ton CO2 eq / barrel for the case with and without recycling streams. The range obtained expresses the impact change depending on whether co-product steam and electricity are valorized. Impacts are reduced significantly when recycling is considered because of the 97% lower direct emissions. Compared to fossil crude, which has a GWP of 0.07 kg CO2 eq / barrel (Rangel, 2022), the GWP advantage of producing synthetic crude depends on the existence of recycling streams and co-product valorization.

Conclusions

In this work, the economical and environmental assessment of a Fischer-Tropsch PtL pathway is given. Economically, the process is more expensive than the conventional crude. Environmentally, the process can be less impactful than the conventional crude, when by products valorization is considered.

Acknowledgments

This work was financially supported by: LA/P/0045/2020 (ALiCE), UIDB/00511/2020 and UIDP/00511/2020 (LEPABE), funded by national funds through FCT/MCTES (PIDDAC). Also, funding from project POCI-01-0247-FEDER-069953, funded by the European Regional Development Fund - FEDER, through the Competitiveness and Internationalization Operational Program (POCI). Frederico S. Coelho, Mariana G. Domingos and José Carlos B. Lopes acknowledge funding from NORTE-06-3559-FSE-000069 – Highly Qualified Human Resources for CoLAB NET4CO2 – Network for a Sustainable CO2 Economy – funded by the European Social Fund (FSE). Gustavo P. Rangel was also funding by FCT, Foundation for Science and Technology, through the individual research grant BD 2022.14621.BDANA.

References

Brooke, A., et. al (1992). GAMS- A User's Guide (Release 2.25). The Scientific Press. San Francisco, CA.

European Cement Research Academy; Cement Sustainability Initiative, Ed. Development of State of the Art-Techniques in Cement Manufacturing: Trying to Look Ahead; CSI/ECRATechnology Papers 2017. Duesseldorf, Geneva, 2017 Available at: http://www.wbcsdcement.org/technology

https://www.exchangerates.org.uk/commodities/live-oil-prices/BRT-EUR.html

IEA, 2022. https://www.iea.org/reports/co2-capture-and-utilisation

Pandey, U., et al. (2021), "Modeling Fischer–Tropsch kinetics and product distribution over a cobalt catalyst." AIChE Journal 67(7)

Rangel, G., et. al (2022). Life Cycle Flaring Emissions Mitigation Potential of a novel Fischer-Tropsch gas-to-liquid microreactor technology for synthetic crude oil production. Science of the Total Environmental, 822,153647

Vidal Vázquez, F., et al. (2017). "Catalyst Screening and Kinetic Modeling for CO Production by High Pressure and Temperature Reverse Water Gas Shift for Fischer–Tropsch Applications." Industrial & Engineering Chemistry Research 56(45): 13262-13272.

Process development for hydrogen production using LNG cold energy

Bomin Choe[a], J. Jay Liu[b], Wangyun Won[a]
[a]Department of Chemical Engineering (Integrated Engineering), Kyung Hee University, 1732 Deogyeong-dearo, Giheung-gu, Yongin-si, Gyeonggi-do 17104, Republic of Korea
[b]Department of Chemical Engineering, Pukyoung National University, 45 Yongso-ro, Nam-gu, Busan 48513, Republic of Korea

Abstract: Renewable energy-powered water electricity for hydrogen production is know as "green hydrogen", which is considered as an environmentally friendly method among various hydrogen production technologies. However, green hydrogen can only be produced using renewable energy sources. Among them, liquefied natural gas (LNG) cold energy is a potential resource that has been recently explored for utilization. Traditionally, the LG cold energy is wasted during the vaporization process using seawater. However, studies have been conducted to utilized this energy in the organic Rankine cycle (ORC) as a refrigerant to generate electricity. This study proposes a process for green hydrogen production using the eco-friendly generated from ORC with LNG cold energy. The efficiency of ORC process varies depending on the type of working fluid used. Therefore, three strategies using C1-C3 as working fluids were developed, and a case study was conducted through techno-economic analysis (TEA) and life cycle assessment (LCA). The TEA was performed using the minimum selling price of hydrogen as an economic index, while the environmental impacts were evaluated using LCA.

Keywords: Renewable energy, Case study, Economic evaluation, Environmental evaluation.

Introduction

The increasing demand for renewable energy sources has led to the exploration of various technologies for sustainable energy production. One promising technology is the use of liquefied natural gas (LNG) cold energy to generate electricity and produce green hydrogen through on organic Rankine cycle (ORC) system. The ORC system uses a working fluid to convert the thermal energy of the LNG cold energy into electricity, which can then be used to produce green hydrogen.

The selection of the working fluid (WF) in the ORC system is critical, as it has a significant impact on the system's efficiency and overall performance. In this study, we investigated the effect of different WFs on the ORC efficiency and propose three strategies using methane (CH_4), ethane (C_2H_6), and propane (C_3H_{10}) as working fluids.

Method

In this study, after the simulation of process using the Aspen plus, the techno-economic analysis (TEA) and life cycle assessment (LCA) are performed to evaluate the economics and environmental impact of the process.

TEA is a method of evaluating the economic efficiency of a technology or a production process when introducing new technology or designing a production process. In this study, the capital and operating costs of the process are calculated based on the mass and energy balance from the process simulation result, and the economic evaluation of the process is performed using the minimum selling price (MSP) as an economic indicator (Davis et al., 2018).

LCA is a comprehensive environmental evaluation method that assesses the environmental impact of the process to provide the improve point in terms of environmental impact. In this study, LCA is performed based on the ISO 14040 and 14044 standards and using the Ecoinvent 3.6 database, ReCiPe midpoint method and Hierarachist version of SimaPro (Kim et al., 2020; Artz et al., 2018).

Process development

The proposed process uses LNG as a refrigerant in the ORC system to generate electricity, which is then used to produce green hydrogen by the electrolysis. Strategies A-C is developed, each using a different WF (CH4, C2H6, and C3H10) in the ORC system.

Strategy A: CH_4 is used as a WF in the ORC system.

Strategy B: C_2H_6 is used as a WF in the ORC system.

Strategy C: C_3H_{10} is used as a WF in the ORC system.

LNG is partially vaporized through heat exchange with the WF of ORC system and completely vaporized to NG through heat exchange with seawater (SW).

The WF of the ORC system is pressurized by the pump, and then completely vaporized through heat exchange with seawater. The vaporized working fluid is used to turn the turbine and generate electricity. The WF in the gas state after passing through the turbine is liquefied through heat exchange with LNG, and the circulated through the ORC system to generate electricity.

The produced electricity from ORC system is supplied to the electrolysis stack, and ultimately, green hydrogen is produced through water electrolysis in the electrolysis stack.

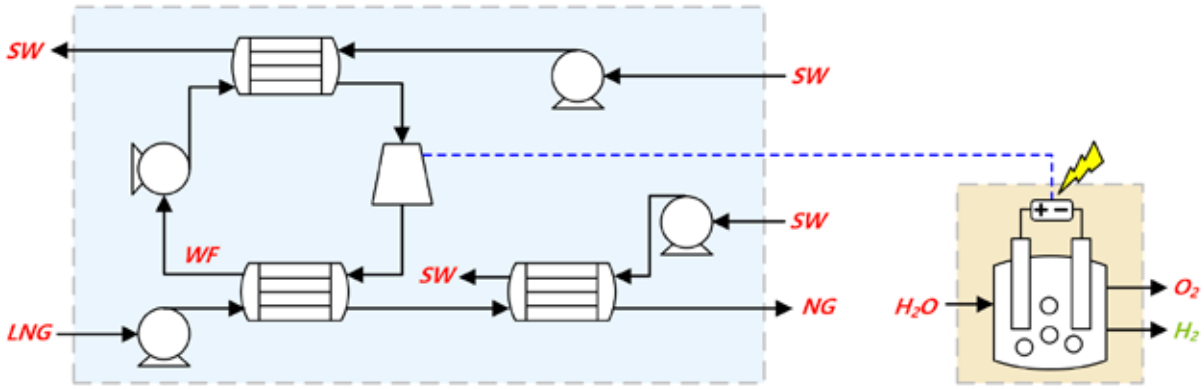

Figure 1. Process flow diagram for Strategies A-C.

Conclusion

In this study, a process for producing green hydrogen using LNG cold energy as a renewable energy was proposed. In particular, taking into account the characteristics of ORC system, which is influenced by the WF, different strategies A-C using CH4, C2H6, and C3H10 as working fluids were designed and case study was conducted. TEA and LCA were conducted for each strategy, and the contributing factors were analyzed from each perspective. Additionally, the strategies A-C were compared to determine the most economically and environmentally viable process.

References

Artz J., MüllerOrcid T.E., Thenert K., Kleinekorte J., Meys R., Sternberg A., Bardow A., Leitner W. (2018). Sustainable conversion of carbon dioxide: an integrated review of catalysis and life cycle assessment. Chem. Rev., 118, 434-504.

Davis R., Grundl N., Tao L., Biddy M.J., Tan E.C.D., Beckham G.T., Humbird D., Thompson D.N., Roni M.S. (2018)., Process design and economics for the conversion of lignocellulosic biomass to hydrocarbon fuels and coproducts: 2018 biochemical design case update. NREL Report., NREL/TP-5100-71949.

Kim H., Lee S., Ahn Y., Lee J., Won W. (2020). Sustainable production of bioplastics from lignocellulosic biomass: technoeconomic analysis and life-cycle assessment. ACS Sustainable Chem. Eng., 8, 12419-12429

Microkinetic Modelling of CO_2 Conversion to Methanol and Catalyst Deactivation Description for a Rugged Operation Control

Anže Prašnikara, Damjan Lašič Jurkovića, Andraž Pavlišića, David Bajeca, Matic Groma, Blaž Likozara

[a]Department of Catalysis and Chemical Reaction Engineering, National Institute of Chemistry, Hajdrihova 19, Ljubljana 1001, Slovenia

Abstract: Increasing effect of CO2 emissions on the environment is pushing humanity to close the carbon loop. Since there are so many unavoidable or hard-to-eliminate CO2 sources, methanol synthesis is one of the most important ways of carbon reuse. For this reason, we investigated crucial differences between conventional methanol synthesis (from CO-rich gas) to synthesis from CO2 (which are a larger quantity of CO2 and H2O and active sites on the catalyst). Specifically, what are they and how catalyst structure changes. We correlated reaction conditions with catalyst structure changes and further those with catalytic activity. Microkinetic model was developed which accounts for different active sites, which can be used for a more robust operation control.

Keywords: Methanol synthesis, CO2 utilization, microkinetic modelling, catalyst deactivation.

Introduction

Reducing CO2 emissions is crucial to achieving a carbon-neutral future, with a possibility of sequestering a fraction of it in saline aquifers. CO2 can (and will have to) be used to close the carbon loop by producing methanol using renewable sources and nuclear energy. Methanol is a versatile product that can be used as a biofuel and can be produced from CO2 using 3 H2 molecules in a single step. Although other products such as formaldehyde, ethylene, formic acid, and elemental carbon can also be produced from CO2, large scale methanol synthesis appears to be the most developed and the product, generally, the most useful. Due to performance reasons, the thermocatalytic CO2 conversion is currently preferred over electrocatalytic or photocatalytic routes for methanol production. Developing better software tools and increasing computation power will lead to more precise control and more economical production of methanol.

There is an extensive community focused in mechanistic experimental-based descriptions of catalytic conversion of CO2, especially on Cu/ZnO/Al2O3 catalytic system (Fujitani et al., 1995; Huš et al., 2017 a; Kattel et al., 2017). It appears that the rate methanol synthesis is heavily dependent of catalyst structure, such as Cu nanoparticle size (Karelovic et al., 2015; van den Berg et al., 2016), crystallite termination (Palomino et al., 2018) and Zn-Cu contact (Fujitani et al., 1995; Kuld et al., 2016). The structure of Cu/ZnO/Al2O3 structure is very dynamic during reaction conditions, which in the end affects catalytic performance. Detailed modeling by combining descriptions of the main catalytic activity-affecting processes would be therefore highly beneficial.

A lot of work has been performed on prediction of catalytic activity on various structures. Theoretical modeling using density functional theory assumed different active site structures, initially starting from pure Cu(111) (Grabow et al., 2011) to Cu/ZnO(10-10) (Tang et al., 2015), to alloy-based descriptions ZnCu(211)(Studt et al., 2015) and CuZn/ZnAl2O4(110) (Huš et al., 2017 a) with a possibility of Zn being (partially) oxidized, (i.e. inverse catalyst) ZnO/Cu(111) (Huš et al., 2017 b; Kattel et al., 2017; Liu et al., 2022; Shi et al., 2022). Experimental identification together with the theoretical simulations of the most abundant and most active site structure is necessary, since too many factors effects the activity.

Methods

We tested commercial catalyst (Cu/ZnO/Al2O3) in a parallel packed bed reactor and expose it to various gas compositions. The samples were then characterized with scanning transmission electron microscopy (STEM), X-ray powder diffraction (XRD), and several others techniques to understand the mechanisms of structural and activity changes. We then performed long-term catalytic tests with a variation of pressure and temperature and short-term catalytic tests for model development in the packed bed reaction. A model of catalyst deactivation was developed. In addition, a microkinetic model based on structure-activity relationships and ab initio kinetic constants by Kattel et al. (2017) was developed to obtain a robust process description.

Findings

Through long-term catalyst ageing and characterization, we observed a correlation between copper particle sintering and steam partial pressure (Prašnikar et al., 2019). This mechanistic insight was used to develop the first catalyst deactivation model that considers gas composition, pressure and temperature (Prašnikar et al., 2022). From structure-activity relationships, we determined that Zn coverage over Cu phase is the most important indicator of activity along the exposed copper surface area. Zn is very mobile in the Cu/ZnO/Al2O3 catalyst; it dissolves in Cu (alloying), it starts to cover Cu particles, while also ZnO nanoparticles grow (coarsen) when exposed to reaction conditions. Based on this, we developed a microkinetic model of CO2 conversion to MeOH and CO with the concentration of Cu sites and Zn sites and an input (Prašnikar et al., 2021).

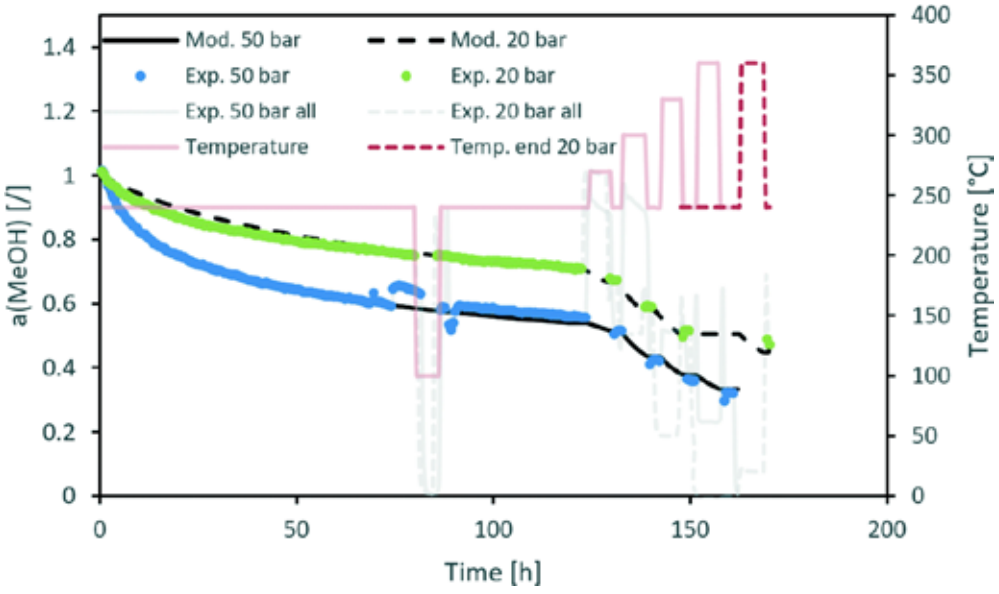

Figure 1 (Top): A catalyst activity decrease model validation based on temperature and pressure of operation. (Bottom): Effect of Zn coverage on catalyst activity.

Conclusion

Current research is important in a way that it exposes critical points of commercial methanol synthesis catalysts for the future process of CO2 hydrogenation. In addition, the models developed here consider more parameters than in current ones, which is especially important for large-scale systems, such as methanol synthesis. Although microkinetic models are more robust than conventional models, there is a slow adoption due to the higher computational power needed. Therefore, some sort of simplification or better software is needed for an easier transition in the industry.

Acknowledgments

This research was supported by project FReSMe No 727504.

References

Fujitani, T. et al. (1995). Methanol synthesis by the hydrogenation of CO2 over Zn-deposited Cu(111) and Cu(110) surfaces. Catal. Letters., 35, 297.

Grabow, L. C.; Mavrikakis, M. (2011). Mechanism of methanol synthesis on Cu through CO2 and CO hydrogenation. ACS Catal., 1, 365.

Huš, M. et al. (2017)a. Mechanism, kinetics and thermodynamics of carbon dioxide hydrogenation to methanol on Cu/ZnAl2O4 spinel-type heterogeneous catalysts. Appl. Catal. B Environ., 207, 267.

Huš, M, et al. (2017)b. Unravelling the mechanisms of CO2 hydrogenation to methanol on Cu-based catalysts using first-principles multiscale modelling and experiments. Catal. Sci. Technol., 7, 5900.

Karelovic, A.; Ruiz, P. (2015). The role of copper particle size in low pressure methanol synthesis via CO2 hydrogenation over Cu/ZnO catalysts. Catal. Sci. Technol., 5, 869.

Kattel, S et al. (2017). Active sites for CO2 hydrogenation to methanol on Cu/ZnO catalysts. Science (80-.)., 355, 1296.

Kuld, S et al. (2016). Quantifying the promotion of Cu catalysts by ZnO for methanol. Science (80)., 352, 969.

Liu, X et al. (2022). In Situ Spectroscopic Characterization and Theoretical Calculations Identify Partially Reduced ZnO 1– x /Cu Interfaces for Methanol Synthesis from CO 2 . Angew. Chemie., 134.

Palomino, R. et al. (2018). Hydrogenation of CO_2 on ZnO/Cu(100) and ZnO/Cu(111) Catalysts: Role of Copper Structure and Metal – Oxide Interface in Methanol Synthesis. J. Phys. Chem. B., 122, 794.

Prašnikar, A. et al. (2019). Mechanisms of Copper-Based Catalyst Deactivation during CO2 Reduction to Methanol. Ind. Eng. Chem. Res., 58, 13021.

Prašnikar, A. et al. (2021). Reaction Path Analysis of CO2 Reduction to Methanol through Multisite Microkinetic Modelling over Cu/ZnO/Al2O3 Catalysts. Appl. Catal. B Environ., 292, 120190.

Prašnikar, Likozar, B. (2022). Sulphur Poisoning, Water Vapour and Nitrogen Dilution Effects on Copper-based Catalyst Dynamics, Stability and Deactivation during CO2 Reduction Reactions to Methanol. Reac. Chem. Eng., 7, 1073.

Shi, Y. F. et al. (2022). Methanol Synthesis from CO2/CO Mixture on Cu-Zn Catalysts from Microkinetics-Guided Machine Learning Pathway Search. J. Am. Chem. Soc., 144, 13401.

Studt, F. et al. (2015). The mechanism of CO and CO 2 hydrogenation to methanol over Cu based catalysts. ChemCatChem., 7, 1105.

Tang, Q. L. et al. (2015). Effect of the components' interface on the synthesis of methanol over Cu/ZnO from CO2/H2 : a microkinetic analysis based on DFT + U calculations. Phys. Chem. Chem. Phys., 17, 7317.

van den Berg, R. et al. (2016). Structure sensitivity of Cu and CuZn catalysts relevant to industrial methanol synthesis. Nat. Commun., 7, 13057.

THEME 5

Systems methods in industrial biotechnology and biomedical applications economy

Paper 6	Modeling the Progression of Fibrosis Regulated by TGF-B in COVID19 Patients	88
Paper 578	Computational analysis of human ovarian cancer metabolism	90
Paper 583	Analysis of Salmonella Typhimurium growth in the murine intestine using metabolic network reconstruction	92
Paper 607	A computational workflow to reconstruct microbial interaction networks	94
Paper 641	A Systematic Mixed-integer linear programming approach for the solution of large-scale metabolism and protein expression (ME-models)	96
Paper 775	Dynamic studies of metabolism empowered by AI	98
Paper 776	Overcoming combinatorial explosion – A Strain Design Framework Based on Nonlinear Kinetic Models	100
Paper 851	A process systems engineering approach for the parallel generation of multiple condition-specific genome-scale metabolic models by integrating relative multi-omics data	102

Modeling the Progression of Fibrosis Regulated by TGF-B in COVID19 Patients

Mohammad Aminul Islam, Ashlee N. Ford Versypt
Department of Chemical and Biological Engineering
University at Buffalo, The State University of New York, Buffalo, NY, USA

Abstract: The COVID19 pandemic has created an emerging need to investigate the long-term effects of infection on patients, many of which suffer from pulmonary fibrosis due to impairment in the lung healing mechanism. Fibroblasts are the central mediators of extracellular matrix deposition during tissue regeneration, regulated by anti-inflammatory cytokines, including TGF-β. The TGF-β dependent accumulation of fibroblasts in the damaged site and excess collagen deposition lead to fibrosis. Here, we focused on modeling the mechanisms of the fibrotic process in the lung tissue during SARS-CoV-2 infection and the role of TGF-β in the progression of lung fibrosis. We outline our hybrid approach where continuous partial differential equations are used to represent the spatial dynamics of cytokines and collagen and discrete agent-based modeling is used to capture the stochastic evolution of cell populations involved in the immune response to infection.

Keywords: reaction-diffusion equations, agent-based modeling, partial differential equations, healthcare.

Introduction

In response to the COVID19 pandemic, the SARS-CoV-2 Tissue Simulation Coalition was founded with the goal of developing a tissue simulator for the human lung subject to respiratory virus infection (Figure 1). The coalition has built a multiscale tissue simulator that models multiple scales of physiological processes involved in the infection that leads to COVID19 and the associated immune response in the lung (Getz et al., 2021). The tissue simulator (Figure 1) focuses on an agent-based (discrete, stochastic) model of the epithelial surface of lung alveoli and considers epithelial cells and fibroblasts of different states and rules for their interactions with immune cells such as macrophages and dendritic cells. The intracellular scale considers infection and viral replication, and the continuum scale includes reaction and diffusion of chemical species that signal between the various cells and processes. The most recent preprint version of the model (Getz et al., 2021) yields various immune responses for disease severity, but most have extensive tissue damage and loss as a result. Rather than seeing tissue loss clinically, fibrosis is observed in COVID19 patients (Li et al., 2021). Our objective here is to add a submodel for the progression of fibrosis in the lung.

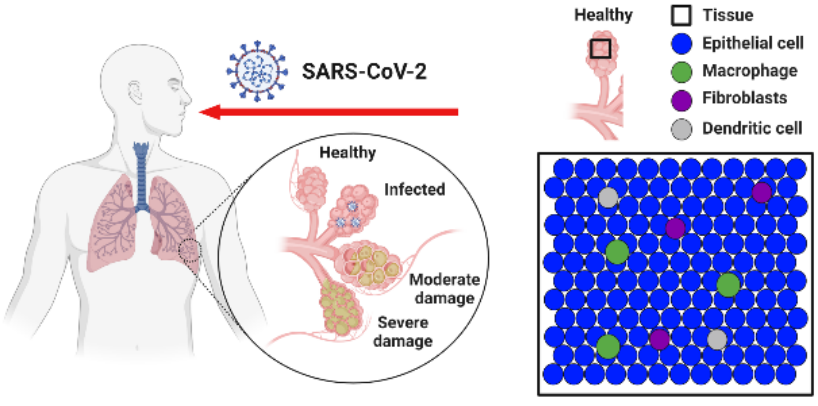

Figure 1. (Left) The SARS-CoV-2 virus can lead to different levels of severity of lung damage in COVID19. (Right) Simplified sketch of the tissue simulator for the epithelial surface of lung alveoli and some of the cell types considered in the agent-based model.

Methods Summary

The signaling molecule TGF-β from multiple sources is a key regulator of fibroblasts (cells that produce collagen and induce fibrosis). Here, we consider two TGF-β sources (Figure 2): (1) stationary: latent TGF-β released from the tissue when an infected cell is removed by the immune response and (2) mobile: anti-inflammatory macrophages patrolling the tissue to suppress inflammation release TGF-β in a dispersed fashion. For this submodel (Figure 2), rules for the secretion and diffusion of TGF-β from the two sources and subsequent interactions with fibroblasts (resident and recruited by the immune response) are layered onto the larger agent-based model via if statements based on the locations of cell removal and mobile macrophages. We consider collagen to be the main extracellular matrix insoluble fibrous component that the fibroblasts deposit, contributing to net fibrosis of the tissue when this fibrotic process does not resolve after a short healing period.

Figure 2. The main concepts in the fibrosis submodel: two different sources of TGF-β stimulate fibroblasts to produce excess collagen. The fibroblasts and macrophages are subject to the agent-based model rules, and TGF-β is modeled through a reaction-diffusion PDE. The collagen is considered to accumulate wherever it is secreted by fibroblasts that continue to migrate throughout the domain subject to various stochastic rules influencing their homing towards TGF-β gradients.

Preliminary Results

For each stochastic simulation scenario, we ran the multiscale tissue simulator and then connect the fibrosis submodel. We explored the effects of many parameters influenced by literature values for various biological processes and the sensitivity to those approximated in the absence of clinical data. We quantified the populations of various cells and concentrations of cytokines over time, but the most salient results are the spatial patterns of and intensity of fibrotic collagen deposition under various conditions (Figure 3). We superimposed the dynamic cell population results from the tissue simulator onto the spatial contour map of the collagen concentration at different time points (Figure 3). We summarized these patterns by the area fraction of the domain covered by collagen above some baseline threshold and by the maximum of collagen concentration. These metrics correspond to metrics clinically reported for fibrosis. High values of both of these metrics result when the second of the TGF-β sources (mobile macrophages) is strongly activated and sustained over longer periods of time before being resolved or de-activated. The relative abundance of fibroblasts is higher than macrophages in COVID19 patients, also observed in the simulation cases we considered.

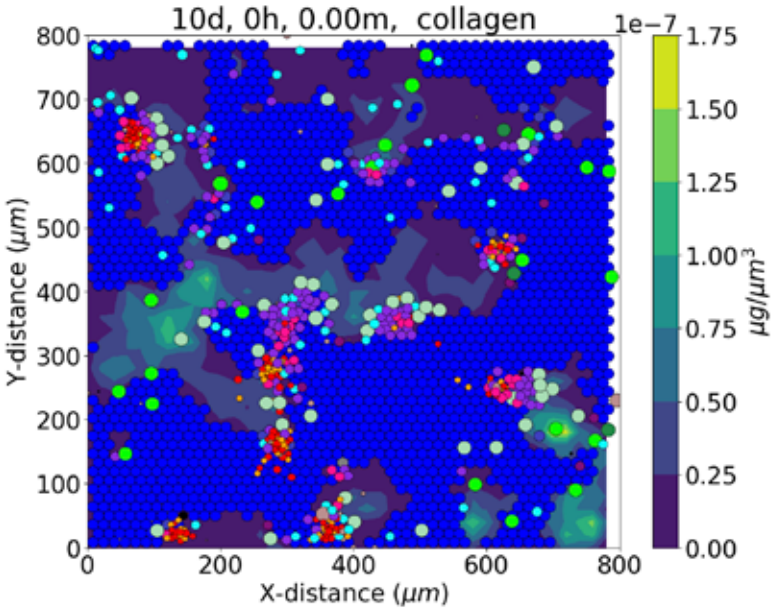

Figure 3. Representative model result for the agent-based model (cells are circles of various sizes and colors) superimposed on the corresponding collagen field showing the accumulated collagen concentration from the fibrosis submodel at 10 days post-infection.

Conclusions

Quantification of collagen using the fibrosis submodel could help characterize the evolution of fibrosis in COVID19 survivors. Treatment strategies controlling TGF-β synthesis could also be benefited from this model. This model may also be extended to long COVID via considering chronic pulmonary fibrosis (Dinnon et al., 2022). The model results are an application of a multiscale hybrid continuum differential equations-based and discrete agent-based modeling approach that may be broadly of interest to the Computer Aided Process Engineering community.

Acknowledgments

Research reported in this extended abstract was supported by US National Institutes of Health R35GM133763 and the University at Buffalo.

References

Dinnon, K. H., III, Leist, S. R., Okuda, K., et al. (2022) SARS-CoV-2 Infection Produces Chronic Pulmonary Epithelial and Immune Dysfunction with Fibrosis in Mice. Sci. Transl. Med., 14, eabo5070.

Getz, M., Wang, Y., An, G., et al. (2021). Iterative Community-Driven Development of a SARS-CoV-2 Tissue Simulator. bioRxiv, 2020.04.02.019075v5.

Li, X., Shen, C., Wang, L., et al. (2021). Pulmonary fibrosis and its related factors in discharged patients with new corona virus pneumonia: a cohort study. Respiratory Res., 22, 1-11.

Computational analysis of human ovarian cancer metabolism

I. Toumpe[a], M. Masid[a,b], B. Narayanan[a], L. Miskovic[a], V. Hatzimanikatis[a]
[a]Laboratory of Computational Systems Biotechnology, Ecole Polytechnique Federale de Lausanne (EPFL), CH 1015 Lausanne, Switzerland
[b]Ludwig Institute for Cancer Research, Department of Oncology, University of Lausanne, and Centre Hospitalier Universitaire Vaudois (CHUV), Switzerland

Abstract: Cancer is a leading cause of death worldwide, accounting for nearly 10 million deaths in 2020 (WHO Cancer fact-sheet). To accelerate the otherwise slow and expensive cancer drug development cycle, several computational tools have been developed to help with drug discovery and optimization. In this work, we present metabolic kinetic modelling, a method that uses a metabolic network structure, along with multi-omics data, to study the physiology of cancer cells. We used a representative model of ovarian cancer metabolism constrained with thermodynamic curations and multi-omics data to produce a large-scale kinetic model with 494 mass balances parameterized by more than 12798 kinetic parameters. We created populations of kinetic parameters and estimated promising drug targets that were aligned with the current experimental and clinical trials. Overall, the developed pipeline allowed us to create the first kinetic model of a metabolic network of this scale, which was used to describe the physiology of ovarian cancer cells reliably.

Keywords: Metabolic networks, Kinetic modelling, Cancer

Introduction

Cancer is a leading cause of death worldwide, accounting for nearly 10 million deaths in 2020, and the number of cancer cases is expected to grow in the years to come (WHO Cancer fact-sheet). Ovarian cancer (OC) is the most lethal form of gynecological cancer; on average, only 40% of patients survive five years after the diagnosis when considering all types and stages of the disease (Jayde and Boughton, 2012). While many general and cancer-specific drugs exist, the drug development cycle is slow and contains high economic risks (Graham Patrick, 2017). For this reason, several computational tools have been developed to provide some early estimations about promising drug targets and early drug candidates. Examples include gene regulatory networks (Madhamshettiwar et al., 2012), which simulate different regulatory genes and their interactions, and gene essentiality methods (Pacheco et al., 2019), which simulate the active metabolic subsystems in the cell. However, gene regulatory networks can only provide binary information, i.e., whether a gene is a possible drug target. At the same time, gene essentiality methods only provide steady-state flux profiles, disregarding the dynamic responses that occur when the original perturbation (drug administration/gene knockout) is imposed. In this work, we present metabolic kinetic modelling, a method that uses a metabolic network structure, along with multi-omics data, to study the physiology of cancer cells. The kinetic modeling capabilities include the identification of drug targets for cancer elimination, calculating responses of organism's or cell line's metabolic network, and quantifying the effects of candidate drug targets on cancer proliferation.

Results

In a previous study, a representative model of ovarian cancer metabolism was produced using redHUMAN (Masid et al., 2020) to curate the model's size and REMI (Pandey et al., 2019) to integrate transcriptomic, metabolomic, and fluxomic data along with thermodynamic constraints. This model consisted of 1724 reactions and 614 metabolites spanning 57 subsystems, including glycolysis, citric acid cycle, amino acid metabolism, and lipid and nucleotide metabolism. The model was used in this work as a scaffold to produce with ORACLE (Miskovic and Hatzimanikatis, 2010; Hameri et al., 2019, 2021; Tokic et al., 2020), a large-scale kinetic model with 494 mass balances and 12798 kinetic parameters. We estimated populations of kinetic parameters and utilized MCA (Wang et al., 2004; Miskovic et al., 2019; Tsouka et al., 2021) to estimate promising drug targets that were further validated by literature, and we studied the effects of the drug administration on cancer cell growth (Figure 1).

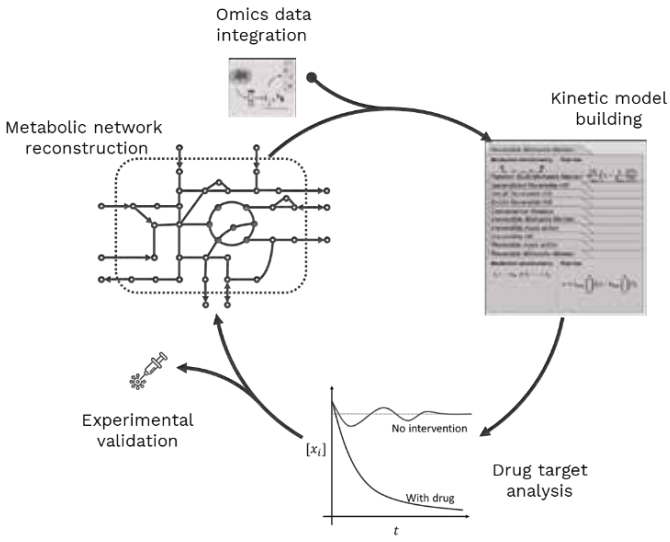

Figure 1. The workflow for the drug target discovery using metabolic kinetic modelling

MCA results suggest that glycolysis, nucleotide metabolism fatty-acid synthesis and lipid metabolism show altered levels of activity and are essential for the OC cell's survival. It was also shown that ATP levels of the system significantly affect OC cell growth, indicating that cancer's fast proliferation demands high levels of energy.

Conclusions

Overall, the developed pipeline allowed us to create the first kinetic model of a metabolic network of this scale, which was used to describe the physiology of ovarian cancer cells reliably. The model can be utilized to identify novel drugs for targeting cancer cells and give insight into the overall network effects of already existing drug targets. Further refinement of the pipeline will pave the way for advancing researchers' understanding of cancer metabolism and allow for the development of models of other types of cancers.

Acknowledgments

This work was executed within an inter-university research collaboration project between the National Technical University of Athens and École Polytechnique Fédérale de Lausanne. It was supported by the Master Thesis Grant funded by Zeno Karl Schindler Foundation.

References

Graham Patrick, (2017). An Introduction to Medicinal Chemistry.

Hameri, T. , Fengos, G. , Ataman, M. et al., (2019). Kinetic models of metabolism that consider alternative steady-state solutions of intracellular fluxes and concentrations. Metabolic Engineering., 52, 29–41.

Hameri, T. , Fengos, G. , Hatzimanikatis, V., (2021). The effects of model complexity and size on metabolic flux distribution and control: case study in Escherichia coli. BMC Bioinformatics., 22, 1–25.

Jayde, V. , Boughton, M., (2012), April. The diagnostic journey of ovarian cancer: A review of the literature and suggestions for practice. Contemporary Nurse.

Madhamshettiwar, P. B. , Maetschke, S. R. , Davis, M. J. et al., (2012). Gene regulatory network inference: evaluation and application to ovarian cancer allows the prioritization of drug targets. Genome Medicine., 4, 41.

Masid, M. , Ataman, M. , Hatzimanikatis, V., (2020). Analysis of human metabolism by reducing the complexity of the genome-scale models using redHUMAN. Nature Communications., 11, 1–12.

Miskovic, L. , Hatzimanikatis, V., (2010). Production of biofuels and biochemicals: In need of an ORACLE. Trends in Biotechnology., 28, 391–397.

Miskovic, L. , Tokic, M. , Savoglidis, G. et al., (2019). Control Theory Concepts for Modeling Uncertainty in Enzyme Kinetics of Biochemical Networks. Industrial and Engineering Chemistry Research., 58, 13544–13554.

Pacheco, M. P. , Bintener, T. , Ternes, D. et al., (2019). Identifying and targeting cancer-specific metabolism with network-based drug target prediction. EBioMedicine., 43, 98–106.

Pandey, V. , Hadadi, N. , Hatzimanikatis, V., (2019). Enhanced flux prediction by integrating relative expression and relative metabolite abundance into thermodynamically consistent metabolic models. PLoS Computational Biology., 15, 1–23.

Tokic, M. , Hatzimanikatis, V. , Miskovic, L., (2020). Large-scale kinetic metabolic models of Pseudomonas putida KT2440 for consistent design of metabolic engineering strategies. Biotechnology for Biofuels., 13, 1–19.

Tsouka, S. , Ataman, M. , Hameri, T. et al., (2021). Constraint-based metabolic control analysis for rational strain engineering. Metabolic Engineering., 66, 191–203.

Wang, L. , Birol, I. , Hatzimanikatis, V., (2004). Metabolic control analysis under uncertainty: Framework development and case studies. Biophysical Journal., 87, 3750–3763.

Analysis of Salmonella Typhimurium growth in the murine intestine using metabolic network reconstruction

E. Vayena[a], L. Fuchs[b], H. Mohammadi Peyhani[a,c], B. Nguyen[b], W. D. Hardt[b], V. Hatzimanikatis[a]
[a]Laboratory of Computational Systems Biotechnology, EPFL, 1015, Lausanne, CH
[b]Institute of Microbiology, D-BIOL, ETH Zurich, 8093 Zurich, CH
[c]Present address: pRED, Roche Glycart AG, 8952 Schlieren, CH

Abstract: Nontyphoidal Salmonellae (NTS) are foodborne pathogens responsible for 95 million cases of gastroenteritis, bacteremia, and subsequent focal infections and over 50,000 deaths yearly worldwide, imposing a significant burden on the health care system. The increasing antibiotic resistance of NTS bacteria requires a better understanding of their complex metabolism during infection. Genome-scale metabolic models (GEMs) and constraint-based optimization methods constitute powerful tools for studying metabolism. In this study, we reconstructed a thermodynamically constrained GEM for S. Typhimurium SL1344 and curated it with experimental data. We used the curated network and optimization-based computational methods to explore the metabolic pathway usage of NTS bacteria in the murine gut environment and gain insight into the essential metabolism of S. Typhimurium. Our work expands our knowledge about the biochemical capabilities of SL1344 beyond the information from the conventional sequence annotation and can guide further experimental studies to facilitate a better understanding of the NTS metabolism and, thus, the identification of targets for efficient treatment.

Keywords: Salmonella, Genome-scale model, Constrained-based optimization

Introduction

Throughout the world, even the most common pathogenic bacteria are becoming increasingly resistant to antibiotics, posing a significant threat to human health. Salmonella is one of the most ubiquitous enteropathogens (Stanaway et al., 2019) and is a major cause of global morbidity and mortality, and imposes a substantial burden on global health (Kirk et al., 2015). Current antibiotic therapies have been proven ineffective; thus, new treatment strategies are needed.

S. Typhimurium faces a dense microbial community in the lower gut. This community offers health benefits to the host including the prevention of enteropathogen growth, a phenomenon called colonization resistance (CR) (Wotzka et al., 2017). And while CR prevents S. Typhimurium growth in the intestine of most exposed hosts (Simonsen et al., 2009), in some cases, the pathogen can grow in the gut and cause enteric disease. Identifying the key factors that allow NTS invasion will help to find ways to fight S. Typhimurium and possibly other enteropathogens that employ similar mechanisms. NTS bacteria pathogenicity is typically studied in vitro and in vivo in animal model systems. However, the complex environment of the gut lumen and the complex metabolism of NTS bacteria make the employment of computational studies necessary to accelerate research in the field.

Genome-scale metabolic models (GEMs) are mathematical representations of all known metabolic capabilities of a strain. GEMs have been widely used to study metabolism and identify metabolic interactions, drug targets, and metabolic engineering strategies (Gu et al., 2019). They, thus, represent a powerful framework to study NTS growth in the gut and identify new drug and therapeutic strategies targets.

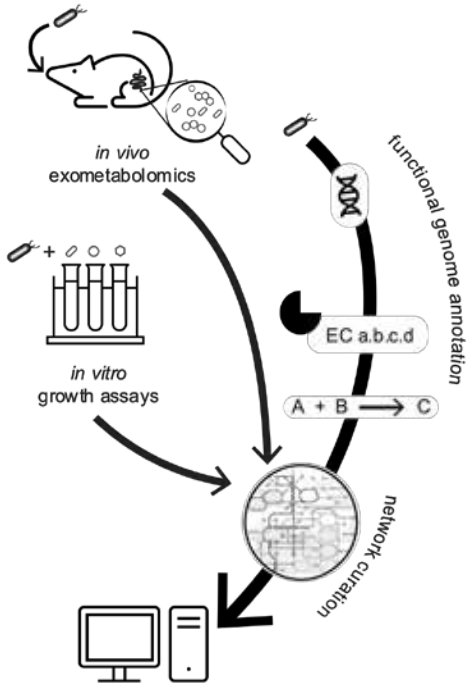

Figure 1: The workflow to reconstruct and curate the GEM of S. Typhimurium SL1344

Conclusions

Here, we introduce a context-specific and thermodynamically curated (Salvy et al., 2018) GEM of S. Typhimurium SL1344 that captures the observed physiology of the strain in the murine gut and establish a workflow (Figure 1) to produce high-quality GEMs using experimental data. Using this GEM, we will study the NTS metabolism in the murine gut.

In this contribution, we generated a draft network by functional genome annotation using the RAVEN toolbox (Wang et al., 2018) and the KEGG database (Kanehisa and Goto, 2000), as well as the published GEM of S. Typhimurium LT2 (Thiele et al., 2011). We then used experimental data and the published workflow NICEgame (Vayena et al., 2022) to curate the network. The curated model can capture experimentally observed phenotypes, i.e., the H2/fumarate respiration driven by the import of C4-dicarboxylates (Nguyen et al., 2020).

Acknowledgments

Funding for this work was provided by the Swiss National Science Foundation (SNSF): grant 200021_188623, NCCR Microbiomes, a National Centre of Competence in Research (grant number 180575) and grant 310030_192567, European Union's Horizon 2020 research and innovation programme grants: PacMen, under the Marie Sklodowska-Curie grant agreement No 72228, and ShikiFactory100, under grant agreement 814408 and the École Polytechnique Fédérale de Lausanne.

References

Gu, C. , Kim, G. B. , Kim, W. J. et al., (2019). Current status and applications of genome-scale metabolic models. Genome Biology., 20, 1–18.

Kanehisa, M. , Goto, S., (2000), January 1. KEGG: Kyoto Encyclopedia of Genes and Genomes. Nucleic Acids Research.

Kirk, M. D. , Pires, S. M. , Black, R. E. et al., (2015). World Health Organization Estimates of the Global and Regional Disease Burden of 22 Foodborne Bacterial, Protozoal, and Viral Diseases, 2010: A Data Synthesis. (von Seidlein, L., Ed.)PLOS Medicine., 12, e1001921.

Nguyen, B. D. , Cuenca V., M. , Hartl, J. et al., (2020). Import of Aspartate and Malate by DcuABC Drives H2/Fumarate Respiration to Promote Initial Salmonella Gut-Lumen Colonization in Mice. Cell Host and Microbe., 27, 922-936.e6.

Salvy, P. , Fengos, G. , Ataman, M. et al., (2018). pyTFA and matTFA: a Python package and a Matlab toolbox for Thermodynamics-based Flux Analysis. (Berger, B., Ed.)Bioinformatics., 35, 167–169.

Simonsen, J. , Mølbak, K. , Falkenhorst, G. et al., (2009). Estimation of incidences of infectious diseases based on antibody measurements. Statistics in Medicine., 28, 1882–1895.

Stanaway, J. D. , Parisi, A. , Sarkar, K. et al., (2019). The global burden of non-typhoidal salmonella invasive disease: a systematic analysis for the Global Burden of Disease Study 2017. The Lancet Infectious Diseases., 19, 1312–1324.

Thiele, I. , Hyduke, D. R. , Steeb, B. et al., (2011). A community effort towards a knowledge-base and mathematical model of the human pathogen Salmonella Typhimurium LT2. BMC Systems Biology., 5.

Vayena, E. , Chiappino-Pepe, A. , Mohammadipeyhani, H. et al., (2022). A workflow for annotating the knowledge gaps in metabolic reconstructions using known and hypothetical reactions. Proceedings of the National Academy of Sciences., 119, e2211197119.

Wang, H. , Marcišauskas, S. , Sánchez, B. J. et al., (2018). RAVEN 2.0: A versatile toolbox for metabolic network reconstruction and a case study on Streptomyces coelicolor. (Ouzounis, C. A., Ed.)PLOS Computational Biology., 14, e1006541.

Wotzka, S. Y. , Nguyen, B. D. , Hardt, W. D., (2017), April 12. Salmonella Typhimurium Diarrhea Reveals Basic Principles of Enteropathogen Infection and Disease-Promoted DNA Exchange. Cell Host and Microbe.

A computational workflow to reconstruct microbial interaction networks

Omid Oftadeh†, Asli Sahin†, Evangelia Vayena, Vassily Hatzimanikatis
Laboratory of Computational Systems Biotechnology
École Polyetechnique Fedérale de Lausanne (EPFL), Switzerland
† These authors contributed equally

Abstract: Microbial communities inhabit diverse ecological environments and significantly impact our health and environment. However, the principles that govern the formation and evolution of microbiomes remain poorly understood. Computational tools enable us to untangle the inherent complexity of the communities and improve our understanding of the system. A crucial step in studying the dynamics of microbial communities is to identify the potential interactions between the community members. Such interactions might include cooperation or competition over shared resources. Due to the size and high complexity of the metabolic network of each organism, diverse interconnections might rise between each pair of organisms, which, consequently, makes unraveling the community interactions challenging. In this study, we present our novel computational method to reconstruct community interaction networks. Our study utilizes genome-scale metabolic models (GEMs) of the member species as input. It then generates all possible interactions that might arise based on the metabolic capabilities of the member species. The presented workflow can further guide experimental studies, reveal the underlying mechanisms driving the crosstalk between the microorganisms, and provide novel insights into designing robust synthetic communities for increased functionality.

Keywords: Microbial communities, Microbial interactions, Genome-scale metabolic models, Systems biology

Introduction

Microbial communities are essential constituents of our ecosystem by their presence in, on, and around us. They are key players in many processes ranging from the biogeochemical cycles, biotechnology, and food production to human health and wellbeing (Rau and Zeidan, 2018; Qian et al., 2020). The members of the microbial community engage with each other through metabolic interactions. These interactions occur through cooperation or competition over shared resources which might lead to mutualistic, commensal, competitive, or predatory interactions (Großkopf and Soyer, 2014). Understanding these interspecific interactions is crucial for microbial ecology as they contribute to the emergent capabilities at the community level and might affect the properties and composition of the microbial community (Foster and Bell, 2012; Ponomarova and Patil, 2015). However, as each species can uptake and secrete a large number of metabolites, reconstructing this web of interactions for microbial communities is extremely challenging (Zelezniak et al., 2015). Computational tools have been previously used in this context to study competitive and cooperative, pairwise (Freilich et al., 2011) and higher-order interactions (Zelezniak et al., 2015).

In this study, we present our novel computational workflow, which employs genome-scale metabolic models (GEMs) (Gu et al., 2019) and constraint-based optimization methods (Heinken et al., 2021) to reconstruct complex interspecies connections. Unlike existing methods, our workflow systematically explores the interaction space and introduces a ranking metric based on the metabolic capabilities of each organism. Furthermore, our novel approach allows to integrate experimental data to explore context-specific interaction networks.

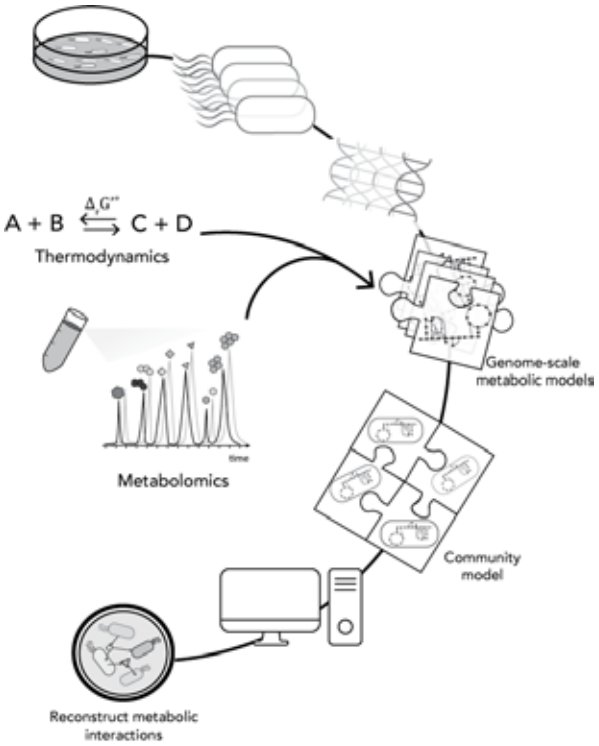

Figure 1. The workflow to reconstruct microbial interactions networks

Conclusions

In this study, we applied our novel workflow to study microbial communities of different sizes. To this end, we used automatically reconstructed GEMs through CarveMe pipeline (Machado et al., 2018) and reconstructed the metabolic interaction networks for the core bee gut microbial community. Our analysis shows that most frequently cross-fed metabolites include carboxylic acids and amino acids, and the minimal environments supporting the community's growth consist mainly of sugars, amino acids, and vitamins. Our framework can be readily applied to study other microbial communities. It can be further used to study the effect of biotic and abiotic perturbations on microbial interaction networks and capture characteristics of different communities. We envision that our workflow will accelerate the development of dynamic and spatiotemporal modeling of microbial communities. Overall, our novel approach brings us closer to a comprehensive understanding of microbial communities by shedding light on the complex network of interspecies connections.

Acknowledgments

Funding for this work was provided by the European Union's Horizon 2020 research and innovation program ShikiFactory100 under Grant Agreement No. 814408, Swiss National Science Foundation (SNSF): grant 200021_188623, NCCR Microbiomes, a National Center of Competence in Research, funded by SNSF grant 51NF40_180575 and the École Polytechnique Fédérale de Lausanne.

References

Foster, K. R. , Bell, T., (2012). Competition, not cooperation, dominates interactions among culturable microbial species. Current Biology., 22, 1845–1850.

Freilich, S. , Zarecki, R. , Eilam, O. et al., (2011). Competitive and cooperative metabolic interactions in bacterial communities. Nature Communications., 2.

Großkopf, T. , Soyer, O. S., (2014). Synthetic microbial communities. Current Opinion in Microbiology., 18, 72–77.

Gu, C. , Kim, G. B. , Kim, W. J. et al., (2019). Current status and applications of genome-scale metabolic models. Genome Biology., 20, 1–18.

Heinken, A. , Basile, A. , Thiele, I., (2021). Advances in constraint-based modelling of microbial communities. Current Opinion in Systems Biology., 27, 100346.

Machado, D. , Andrejev, S. , Tramontano, M. et al., (2018). Fast automated reconstruction of genome-scale metabolic models for microbial species and communities. Nucleic Acids Research., 46, 7542–7553.

Ponomarova, O. , Patil, K. R., (2015). Metabolic interactions in microbial communities: Untangling the Gordian knot. Current Opinion in Microbiology., 27, 37–44.

Qian, X. , Chen, L. , Sui, Y. et al., (2020). Biotechnological potential and applications of microbial consortia. Biotechnology Advances., 40, 107500.

Rau, M. H. , Zeidan, A. A., (2018). Constraint-based modeling in microbial food biotechnology. Biochemical Society Transactions., 46, 249–260.

Zelezniak, A. , Andrejev, S. , Ponomarova, O. et al., (2015). Metabolic dependencies drive species cooccurrence in diverse microbial communities (Proceedings of the National Academy of Sciences of the United States of America (2015) 112:51 (E7156)). Proceedings of the National Academy of Sciences of the United States of America., 112, E7156.

A Systematic Mixed-integer linear programming approach for the solution of large-scale metabolism and protein expression (ME-models)

O. Oftadeha, P. Salvy[a], M. Masid[a], M. Curvat[a], L. Miskovic[a], V. Hatzimanikatis[a]
[a]Laboratory of Computational Systems Biotechnology, EPFL, 1015, Lausanne, CH

Abstract: Eukaryotic organisms play an important role in industrial biotechnology, from producing fuels and commodity chemicals to therapeutic proteins. To optimize these industrial systems, a mathematical approach can be used to integrate the description of multiple biological networks into a single model for cell analysis and engineering. One of the current most accurate models of biological systems includes metabolism and expression (ME-models), and Expression and Thermodynamics FLux (ETFL) is one such formulation that efficiently integrates RNA and protein synthesis with traditional genome-scale metabolic models. However, ETFL is so far only applicable for E. coli. To therefore adapt this ME-model for Saccharomyces cerevisiae, we herein developed yETFL. To do this, we augmented the original formulation with additional considerations for biomass composition, the compartmentalized cellular expression system, and the energetic costs of biological processes. We demonstrated the ability of yETFL to capture maximum growth rate, essential genes, and the phenotype of overflow metabolism and to sample the solutions space. We envision that the extended ETFL formulation can be applied to ME-model development for a wide range of eukaryotic organisms and facilitate simulation and analysis of the impact of different perturbations at the genomic or transcriptomic level.

Keywords: Systems biology, Metabolic and expression model, Saccharomyces cerevisiae, Genome-scale metabolic models, Mixed-integer linear programming, Expression system

Introduction

Cellular expression and metabolism are interconnected (Alberts, 2002); on one side, nucleotides and amino acids, the building blocks of RNA and protein synthesis, are synthesized by metabolism. On the other side, expression produces enzymes which catalyze metabolic reactions. Thus, allocation of cellular resources to express different enzymes is important in determining the rate of metabolic reactions, and modeling expression alongside metabolism provides a more realistic image of what is happening in the cells.

Models of metabolism and expression (ME-models) explicitly account for expression limitations while simulating metabolism (Lerman, et al., 2012; O'brien, et al., 2013; Sánchez, et al.). These models can capture phenotypes that traditional metabolic networks could not capture such as the maximum growth and overflow metabolism. However, the formulation of ME-models is inherently nonlinear and the variables have different orders of magnitude. Expression and Thermodynamics Flux (ETFL) is a novel and efficient formulation to reconstruct ME-models (Salvy and Hatzimanikatis, 2020). ETFL replaces the bilinear terms by estimating growth using a piecewise linear function. Thus, the final formulation of ETFL is a mixed-integer linear programming (MILP) problem. Also, the variables are scaled to reduce the numerical difficulty of the problem. The ETFL formulation includes thermodynamic constraints to ensure thermodynamic feasibility of the solutions (Soh and Hatzimanikatis, 2014). Finally, the presence of variable for metabolite, RNA, and protein concentrations makes ETFL a suitable platform to systematically integrate various omics data, including metabolomics, transcriptomics, and proteomics.

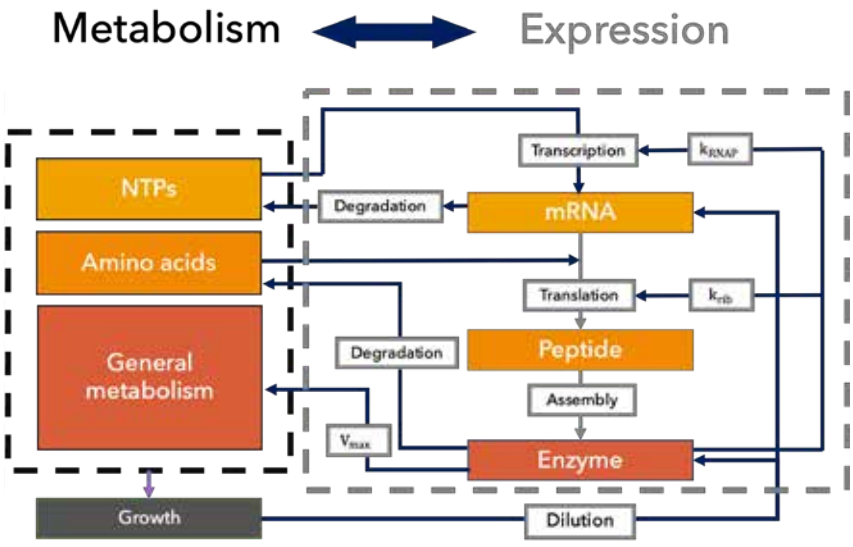

Figure 1: The inter-connection between metabolism and expression

Results

Here, we amended the ETFL formulation in three aspects: (i) we amended the energetic requirements for macromolecule synthesis in the form of growth-associated maintenance, (ii) we improved cellular resource allocation by the model through including additional constraints, and (iii) we enabled implementation of multiple RNA polymerases and ribosomes. The latter is important, as it enables reconstructing ME-models for eukaryotic organisms. We used the improved ETFL formulation to reconstruct the first ME-model for the baker's yeast, yETFL (Oftadeh, et al., 2021). We used yETFL to systematically check for essentiality of the genes. We also used yETFL to predict the maximum growth in yeast in agreement with the experimental observations. We demonstrated that yETFL could successfully capture the Crabtree effect, where the model predicted ethanol secretion and shift in O2 uptake and CO2 secretion. As the first ME-model for a eukaryote, yETFL paves the way to reconstruct ME-models for other higher-order organisms.

Conclusion

ETFL is a semi-automatic framework enabling efficient reconstruction of ME-models for a wide range of organisms. The reconstructed ME-models can be used to capture phenotypes related to protein efficiency. In addition, such models provide the possibility to calculate resource allocation alongside the phylogenetic tree. Finally, due to the mechanistic inclusion of RNA and protein expression, the impact of perturbations like RNA interference and antibiotics can be investigated using ME-models. As the first ME-model for a eukaryote, reconstruction of yETFL paves the way for reconstruction of ME-models for higher organisms.

Acknowledgments

The authors would like to thank Dr. Kaycie Butler for her help in improving the wording and structure of this manuscript. This work has received funding from the European Union's Horizon 2020 research and innovation programme under Grant Agreement No.814408 (O.O.), the Swiss National Science Foundation under Grant Agreement 200021_188623 (O.O.), the European Union's Horizon 2020 Research and Innovation Programme under the Marie Skłodowska-Curie Grant Agreement No. 722287 (P.S.), the European Union's Horizon 2020 research and innovation program under the Marie Skłodowska Curie Grant Agreement No. 675585 (M.M.), and the École Polytechnique Fédérale de Lausanne.

References

Alberts, B. Molecular Biology of the Cell: Hauptbd. Garland; 2002.

Lerman, J.A., et al. In silico method for modelling metabolism and gene product expression at genome scale. Nature communications 2012;3(1):1-10.

O'brien, E.J., et al. Genome-scale models of metabolism and gene expression extend and refine growth phenotype prediction. Molecular systems biology 2013;9(1):693.

Oftadeh, O., et al. A genome-scale metabolic model of Saccharomyces cerevisiae that integrates expression constraints and reaction thermodynamics. Nature Communications 2021;12(1):4790.

Salvy, P. and Hatzimanikatis, V. The ETFL formulation allows multi-omics integration in thermodynamics-compliant metabolism and expression models. Nature Communications 2020;11(1):1-17.

Soh, K.C. and Hatzimanikatis, V. Constraining the flux space using thermodynamics and integration of metabolomics data. In, Metabolic Flux Analysis. Springer; 2014. p. 49-63.

Sánchez, B.J., et al. Improving the phenotype predictions of a yeast genome-scale metabolic model by incorporating enzymatic constraints. Molecular systems biology 2017;13(8):935.

Dynamic studies of metabolism empowered by AI

Ljubisa Miskovic, Subham Choudhury, Vassily Hatzimanikatis
Institute of Chemical Sciences and Engineering, School of Basic Sciences
Ecole Polytechnique Fédérale de Lausanne (EPFL), Switzerland

Abstract: Nonlinear kinetic models allow us to describe the intracellular metabolic states of living organisms. However, constructing large-scale kinetic models is notoriously difficult due to the lack of data about the kinetic parameters characteristic of cellular physiology. To address this issue, we recently proposed REKINDLE (REconstruction of KINetic models using Deep LEarning), a novel generative-deep-learning-based framework for efficient parameterization of large-scale kinetic models that capture the experimentally observed metabolic responses. By leveraging the extrapolative abilities of neural networks, REKINDLE significantly reduces the extensive computational requirements of traditional kinetic modeling approaches. Within the framework, kinetic model generators (generative neural networks) designed for one study can be re-tuned and used in other studies using just a few data points. This way, REKINDLE significantly expands the breadth of applications of kinetic modeling. In this work, we present our latest efforts to bring kinetic modeling a step closer to high-throughput dynamic studies of metabolism. Kinetic models generated by the proposed frameworks can be used to study metabolic diseases, optimization of biosynthetic pathways, and sustainable production of high-added-value chemicals. The presented work will significantly reduce efforts in generating kinetic models and provide a valuable resource for advancing biological knowledge beyond the current state-of-the-art.

Keywords: Large-scale kinetic models of metabolism, nonlinear dynamics, generative deep learning.

Introduction

Nonlinear kinetic models allow us to predict the cellular responses to variations in cellular and environmental conditions. However, despite the capability of these models to reconcile a wide range of omics data in a single mathematical platform and their potential for advancing our knowledge of metabolism, large-scale kinetic models are scarce. The lack of data about the kinetic parameters characteristic of cellular physiology hampers the development of these models. Estimating the unknown kinetic parameters requires employing elaborate computational procedures, limiting kinetic models' applicability. Another aspect that impedes the widespread utilization of kinetic models is the difficulty in obtaining specific model properties required for reliable predictions. Indeed, kinetic models must be consistent with experimental observations, locally stable around the steady state they are built at, provide satisfactory dynamic behavior, and be robust to parameter variations due to changes in genetic or environmental conditions. Consequently, the kinetic parameter space satisfying all these requirements is considerably constrained. Therefore, we need to develop efficient approaches for estimating kinetic parameters accessible to a broader research community and allow using these models for a wide gamut of dynamic studies. To address these issues and accelerate the development of kinetic models, we have previously proposed iSCHRUNK (Andreozzi et al., 2016). This computational approach uses classification algorithms and ORACLE (Hameri et al., 2019; Miskovic and Hatzimanikatis, 2010) to derive values of kinetic parameters consistent with the experimentally observed physiology. Whereas iSCHRUNK has shown its utility in several studies (Miskovic et al., 2019; Tokic et al., 2020), as the number of properties we require from models increases as well as the dimensionality of the problem, it fails to capture a global nonlinear separation delineating the space with the desired kinetic models.

Methods and results

Feedforward neural networks, being universal nonlinear approximators, lend themselves naturally for characterizing the space of desired kinetic models. To this end, we have recently developed REKINDLE, a deep-learning framework based on general adversarial networks, GANs (Choudhury et al., 2022). The idea of REKINDLE is to train a GAN containing two neural networks, a generator and a discriminator (Goodfellow et al., 2014), using the parameter sets provided by ORACLE or any other traditional kinetic modeling framework (Figure 1).

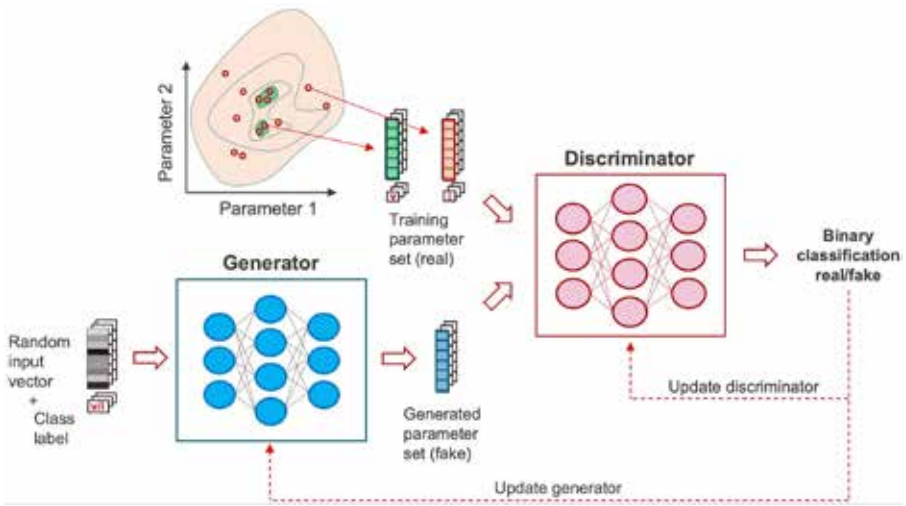

Figure 1. Concept of REKINDLE

Once the GAN is trained, we apply to the input of the Generator a vector of random variables, and if the generator is well trained, the generated parameter sets belong only to the subspace of kinetic parameters providing desired model properties (Figure 2). This way, by performing a stratified sampling, REKINDLE allows orders of magnitude acceleration in creating kinetic models. The validation tests performed for the case study of E. coli metabolism, including bioreactor simulations, demonstrate that the generated models satisfy all imposed properties. The results obtained for four conditions showed that REKINDLE improved by 38-44% the incidence of the desired kinetic models attaining a total of 97-100% of the incidence. Moreover, leveraging the well-known concept of transfer learning, we show that this approach allows us to scour the cellular metabolic states and tune the generators devised for one physiology for another physiology with just a few data points. We then go further and present our efforts in developing a method that directly generates parameters that give rise to desired models without requiring parameters from traditional kinetic modeling methods.

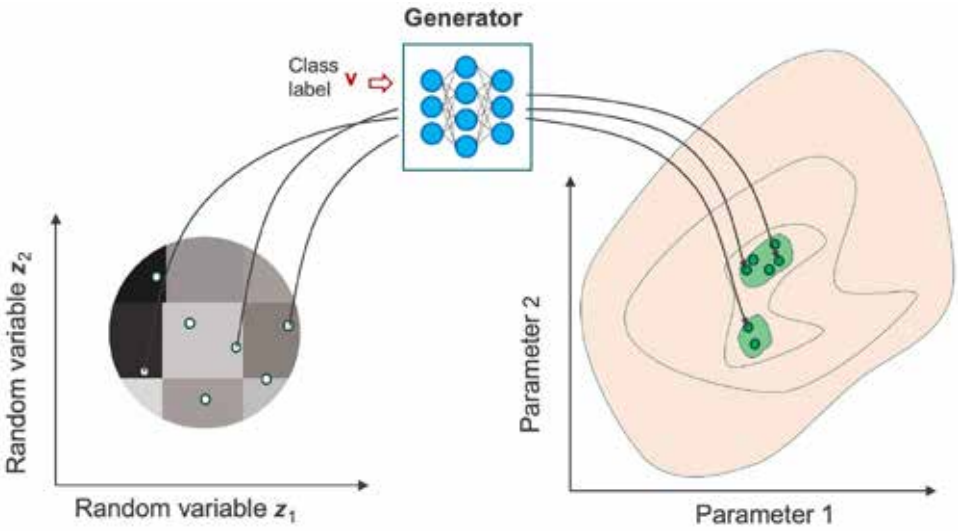

Figure 2. Generating kinetic parameter set for model with desired properties

Conclusions

Applying ML paves the way toward high-throughput metabolism studies, accelerates model reconstruction, and advances our understanding of metabolism.

Acknowledgments

This work was supported by funding from the Swiss National Science Foundation grant 315230_163423, the European Union's Horizon 2020 research and innovation programme under grant agreement 814408, Swedish Research Council Vetenskapsradet grant 2016-06160. We acknowledge the support of NVIDIA Corporation with the donation of two Titan XP GPUs used for this research.

References

Andreozzi, S., Miskovic, L., Hatzimanikatis, V., 2016. iSCHRUNK - In Silico Approach to Characterization and Reduction of Uncertainty in the Kinetic Models of Genome-scale Metabolic Networks. Metabolic Engineering. 33, 158-168.

Choudhury, S., Moret, M., Salvy, P., Weilandt, D., Hatzimanikatis, V., Miskovic, L., 2022. Reconstructing Kinetic Models for Dynamical Studies of Metabolism using Generative Adversarial Networks. Nature Machine Intelligence. 4, 710-719.

Goodfellow, I., Pouget-Abadie, J., Mirza, M., Xu, B., Warde-Farley, D., Ozair, S., Courville, A., Bengio, Y., Generative adversarial nets. Advances in neural information processing systems, 2014, pp. 2672-2680.

Hameri, T., Fengos, G., Ataman, M., Miskovic, L., Hatzimanikatis, V., 2019. Kinetic models of metabolism that consider alternative steady-state solutions of intracellular fluxes and concentrations. Metabolic Engineering. 52, 29-41.

Miskovic, L., Béal, J., Moret, M., Hatzimanikatis, V., 2019. Uncertainty Reduction in Biochemical Kinetic Models: Enforcing Desired Model Properties. PLOS Computational Biology. 15, e1007242.

Miskovic, L., Hatzimanikatis, V., 2010. Production of biofuels and biochemicals: in need of an ORACLE. Trends in biotechnology. 28, 391-397.

Tokic, M., Hatzimanikatis, V., Miskovic, L., 2020. Large-scale kinetic metabolic models of Pseudomonas putida KT2440 for consistent design of metabolic engineering strategies. Biotechnology for Biofuels. 13.

Overcoming combinatorial explosion – A Strain Design Framework Based on Nonlinear Kinetic Models

Bharath Narayanan, Daniel Weilandt, Maria Masid, Ljubisa Miskovic, Vassily Hatzimanikatis
Institute of Chemical Sciences and Engineering, School of Basic Sciences
Ecole Polytechnique Fédérale de Lausanne (EPFL), Switzerland

Abstract: Nonlinear models can capture the temporal metabolic responses of organisms to genetic and process perturbations and thus serve as a starting point for strain design. Two challenges exist in this endeavor: (i) significant structural and parametric uncertainty inherent in kinetic modeling; and (ii) no systematic approach for using these models for rational strain design. To address these issues, we have developed a framework for rational strain design that employs large-scale nonlinear kinetic models to provide robust strain design choices. Even with high-quality kinetic models, it is challenging to determine targets that meet the desired design specifications because it requires simulating the metabolic network's responses for many putative designs, which leads to a combinatorial explosion as the size of the metabolic network grows. We propose formulating an optimization problem and identifying enzymatic interventions that maintain closeness to the reference physiology while satisfying the requirements on specific productivity of target biochemicals. We applied the framework to devise targets to overproduce L-tyrosine in E. coli shikimate metabolism. We demonstrate that the obtained robust designs perform better than those devised with Metabolic Control Analysis. We anticipate that the framework will allow for high throughput, robust designs, and accelerated production in biotechnological processes.

Keywords: Large-scale kinetic models of metabolism, nonlinear dynamics, strain design.

Introduction

Modern genetic techniques allow precise manipulation of genes for improved cellular performance. However, determining how many and which genes we have to manipulate to achieve desired cellular behavior remains challenging. Devising multi-target strategies that improve the specific productivity of target chemicals while maintaining cell viability by performing experiments requires considerable resources. Researchers often use kinetic metabolic models to limit the number of strategies that will be experimentally verified. However, it is difficult to identify targets that meet desired design specifications because this task entails computing the metabolic responses for many candidate designs. For example, exhaustively exploring all possible strategies for targeting three enzymes from a metabolic network of 300 reactions requires almost 4.5 million simulation runs. In addition, one needs to verify if the designed strains are robust and meet the desired specifications. Hence, there exists a need for systematic approaches that efficiently use nonlinear kinetic models. To this end, we present a computational framework called NOMAD (NOnlinear dynamic Model Assisted rational metabolic engineering Design) that proposes metabolic engineering strategies that satisfy the desired design specifications while preserving the robustness of the engineered strain by maintaining its physiology close to the phenotype shaped through evolution and selection (Narayanan et al., 2022). We perform this task by keeping the metabolic states (metabolite concentrations and metabolic fluxes) of the engineered strain close to those of the reference strain. Moreover, we test, within the proposed framework, the performance of the designs in bioreactor simulations. We then recommend the best-performing strains from such tests for experimental validation. We employ this method for devising metabolic engineering strategies to improve tyrosine production in E. coli.

Results

We used our in-house developed ORACLE framework for the generation of large-scale kinetic models of metabolism (Hameri et al., 2019; Miskovic and Hatzimanikatis, 2010; Tokic et al., 2020), implemented in the Python toolbox SKiMPy (Weilandt et al., 2021), to generate a population of kinetic models consistent with the experimental observations acquired on the wild-type strain. The generated models contain 193 reactions and 163 mass balances for metabolites located in the cytosol and extracellular space. We next pruned the population of models for properties such as local stability, experimentally observed dominant time constants (Choudhury et al., 2022), and robustness to obtain a set of reliable models for strain design. The refined set of 28 models to perform strain design with Network Response Analysis (NRA), a MILP optimization framework for strain design (Tsouka et al., 2021) for two cases allowing 5-fold and 2-fold change in the activity of target enzymes.

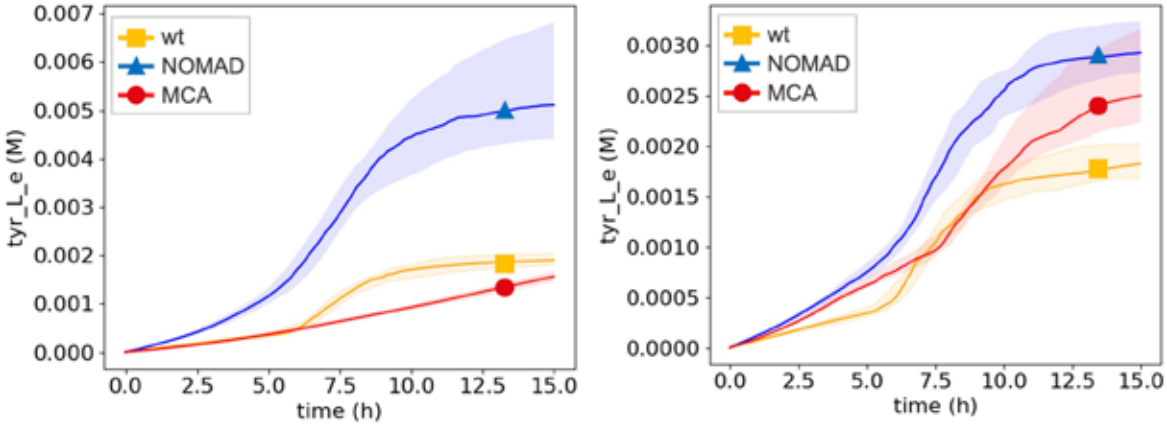

Figure 1. Bioreactor simulation runs for the allowed 5-fold (left) and 2-fold (right) enzyme activity change: time evolution of L-tyrosine titer (median and region between 1st and 3rd quartile responses of 28 models showed)

For comparison, we also devised strain designs using the well-known metabolic control analysis (MCA) (Hatzimanikatis and Bailey, 1996; Miskovic et al., 2019).

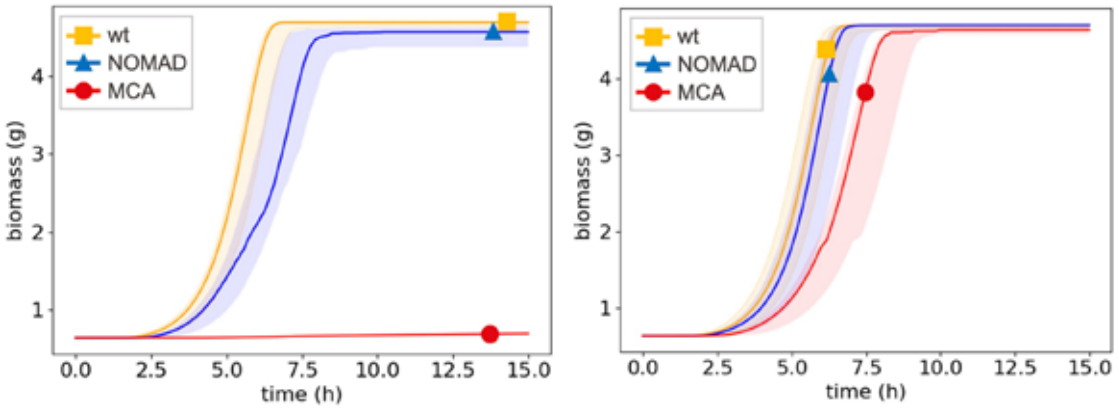

Figure 2. Bioreactor simulation runs for the allowed 5-fold (left) and 2-fold (right) enzyme activity change: growth time evolution

We then tested the strain designs in a bioreactor setting set up in such a way to provide near-real-world conditions. The obtained results from bioreactor simulations demonstrate that NOMAD provides consistently superior designs to MCA for both 5-fold and 2-fold allowed change in the enzyme activities. The final median L-tyrosine titers improved to 0.005M and 0.0029M for the NOMAD designs with 5-fold and 2-fold enzyme activity changes, respectively (Figure 1), whereas the growth remained close to the one of the wild-type strain (Figure 2). In contrast, an MCA design with 5-fold changes in enzyme activities veered far from the robust physiology with low cell viability (Figure 2). MCA designs with 2-fold changes showed improvement over the wild-type strain but were inferior to NOMAD strains. These results demonstrate the importance of maintaining physiology close to the wild-type.

Conclusions

NOMAD is a versatile framework paving the way for accelerated use of kinetic models in rational strain design.

Acknowledgments

This work was supported by funding from the Swiss National Science Foundation Synergia grant CRSII5_198543, the European Union's Horizon 2020 research and innovation program under grant agreement 814408, Swedish Research Council Vetenskapsradet grant 2016-06160.

References

Choudhury, S., Moret, M., et al., 2022. Reconstructing Kinetic Models for Dynamical Studies of Metabolism using Generative Adversarial Networks. Nat Mach Intel 4, 710-719.

Hameri, T., Fengos, G., et al., 2019. Kinetic models of metabolism that consider alternative steady-state solutions of intracellular fluxes and concentrations. Met Eng 29-41.

Hatzimanikatis, V., Bailey, J. E., 1996. MCA has more to say. Journal of Theoretical Biology. 182, 233-242.

Miskovic, L., Hatzimanikatis, V., 2010. Production of biofuels and biochemicals: in need of an ORACLE. Trends biotechnol 28, 391-397.

Miskovic, L., Tokic, M., Savoglidis, G., et al., 2019. Control Theory Concepts for Modeling Uncertainty in Enzyme Kinetics of Biochemical Networks. Ind Eng Chem Res. 58, 13544-13554.

Narayanan, B., Weilandt, D. R., et al., 2022. Rational strain design with minimal phenotype perturbation. bioRxiv.

Tokic, M., Hatzimanikatis, V., Miskovic, L., 2020. Large-scale kinetic metabolic models of Pseudomonas putida KT2440 for consistent design of metabolic engineering strategies. Biotechnol Biofuels. 13.

Tsouka, S., Ataman, M., Hameri, T., et al., 2021. Constraint-based metabolic control analysis for rational strain engineering. Metab Eng. 66, 191-203.

Weilandt, D., Salvy, P., Masid, et al., 2021. Symbolic Kinetic Models in Python (SKiMpy): Intuitive modeling of large scale biological kinetic models. bioRxiv.

A process systems engineering approach for the parallel generation of multiple condition-specific genome-scale metabolic models by integrating relative multi-omics data

David Liaskos[a], Maria Masid[a,b], Vassily Hatzimanikatis[a]
[a]Laboratory of Computational Systems Biotechnology, École Polytechnique Fédérale de Lausanne (EPFL), Lausanne, Switzerland
[b]Ludwig Institute for Cancer Research, Department of Oncology, University of Lausanne, and Lausanne University Teaching Hospital (CHUV), Switzerland

Abstract: The recent burgeoning of omics data generated requires the development of systematic methods for their accurate interpretation. Process systems engineering tools can assist in translating omics data into alterations in biological pathways and, therefore, provide insight into the mechanisms behind the observations. Although current methods for integrating omics data into genome-scale metabolic models (GEMs) can reveal many aspects of metabolic alterations, they still lack the ability to compare multiple conditions simultaneously. To compare these different conditions, we developed the REMI-X method. REMI-X is an expansion of the Relative Expression and Metabolomic Integrations (REMI) method for the generation of multiple condition-specific GEMs in parallel. In REMI, we use differential gene expression and metabolite abundance data to obtain alternative flux profiles consistent with the relative omics ratios between the two conditions of interest. Here we extend this method by allowing pairwise comparisons of more than two conditions and ensuring the same flux profiles across unique pairs of omics ratios. We applied the REMI-X method to investigate the deregulation of central carbon pathway fluxes in different types of cancer cells. Our process engineering approach is a powerful tool for systematically studying metabolic differences in multiple condition-specific models.

Keywords: Metabolic networks, Omics data, Cancer

Introduction

Continuous advances in omics technologies have enabled their ever-wide use to address various aspects of biological research (Karczewski and Snyder, 2018). However, one of the most critical points is how to translate this vast amount of omics data into biological knowledge. Towards this direction, process systems engineering tools, such as genome-scale metabolic models (GEMs), can assist in inferring mechanistic information behind the observations (Gu et al., 2019). Predictions on the mechanisms of pathway alteration can be enhanced by integrating omics data into GEMs (Machado and Herrgard, 2014). However, current methods for relative omics data integration cannot compare multiple conditions concurrently. These conditions might include different cell types, treatments, genetic modifications, abiotic conditions, or time points in the life cycle of a cell. In this work, we present the REMI-X method, an expansion of the two conditions comparison method REMI (Pandey et al., 2019). REMI-X enables the parallel generation of more than two condition-specific models by allowing pairwise comparisons of gene expression and metabolite abundance data between the pairs of omics ratios. In the REMI-X method, we formulate a mixed-integer linear optimization problem (Hatzimanikatis et al., 1996), where omics ratios are integrated into the optimization problem by flux-based constraints. The proposed method can be applied to a wide range of studies where omics data are available, either for prokaryotic or eukaryotic organisms. For example, we can use REMI-X to study metabolic changes in the physiological state of cultivation due to the abiotic conditions of the cell by integrating omics data as well as data regarding media composition. Our method also allows the comparative analysis of multiple bacterial strains in parallel to assess their robustness to scale up. In the present study, we apply the REMI-X method to investigate the metabolic profile of three cancer cell lines.

Results

Here, we investigate the deregulation of the central carbon pathway fluxes in three tissue-specific cancer cell lines. These cell lines include breast, lung, and blood cancer. First, we use the redHUMAN (Masid et al., 2020) algorithm to reduce the complexity of the human GEM Recon3D (Brunk et al., 2018). The reduced model comprises 673 metabolites, 1685 reactions, and 829 metabolic genes. Using the gene-protein-reaction rules, we map the data for gene expression (Ghandi, Huang et al., 2019) and metabolite abundance (Li et al., 2019) acquired from the Cancer Cell Line Encyclopedia (CCLE) database to the enzymes and metabolites in the reduced metabolic model. We then implement the REMI-X method to maximize the number of differential gene expression and metabolite abundance data that can be integrated into our model, and we enumerate the alternative solutions. More than 95% of the omics ratios can be integrated into our model. After integrating the consistent omics ratios, we perform thermodynamics flux variability analysis (TFVA) to define the region of feasible flux distributions for each cancer cell line. TFVA results show that metabolomics integration further constrains the flux distribution range and fixes the directionalities of numerous reactions. Once we have defined the feasible flux distributions, we then perform sampling of the solution space to obtain a set of possible flux distributions. The sampling values allow us to estimate the significance of the alterations in the metabolic flux rates between the different cancer cell lines. Finally, we compare the central carbon pathway profiles between lung, breast, and blood cancers to identify the level of each metabolic pathway deregulation (Figure 1).

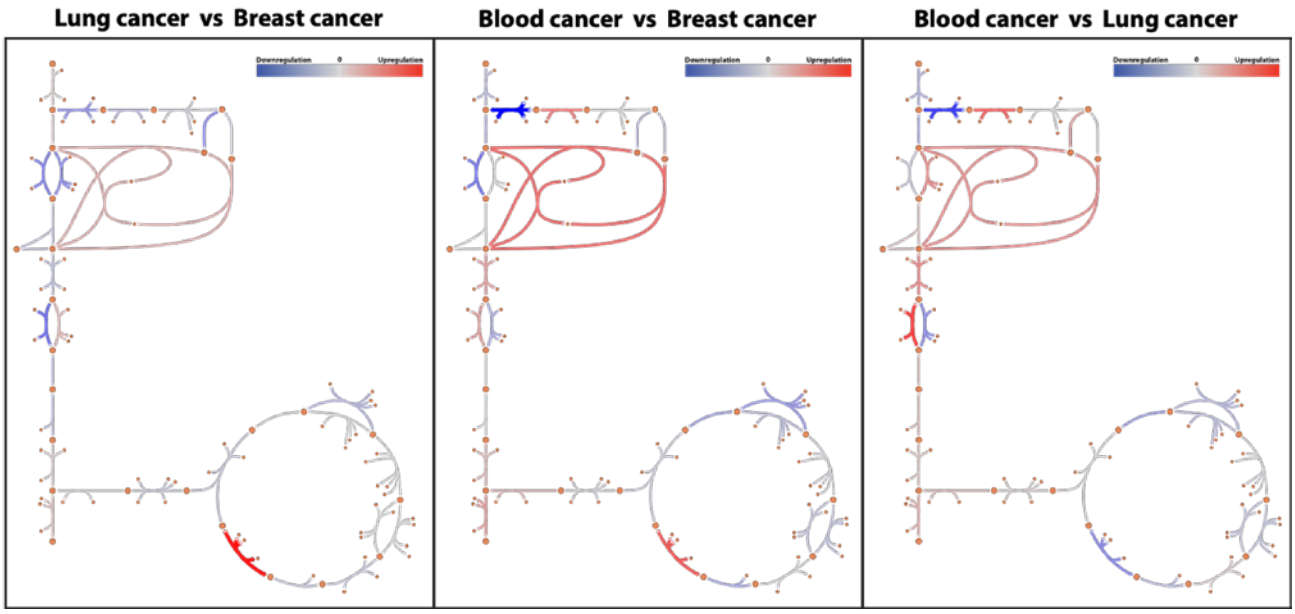

Figure 1. The central carbon pathways deregulation levels between lung, breast, and blood cancer cell lines.

Conclusions

Overall, the REMI-X method allows us to integrate multi-omics data into GEMs for the parallel generation of multiple condition-specific metabolic models. In the days of high-throughput measurements, our approach increases confidence in inferring statements for the metabolic pathways deregulation from observations made in health and disease conditions.

Acknowledgments

This work has received financial support from École Polytechnique Fédérale de Lausanne (EPFL).

References

Brunk, E., et al. (2018). Recon3D enables a three-dimensional view of gene variation in human metabolism. Nature Biotechnology, 36(3).

Ghandi, M., Huang, F. W., et al. (2019). Next-generation characterization of the Cancer Cell Line Encyclopedia. Nature, 569(7757).

Gu, C., Kim, G. B., Kim, W. J., Kim, H. U., & Lee, S. Y. (2019). Current status and applications of genome-scale metabolic models. Genome Biology, 20(1), 121.

Hatzimanikatis, V., Floudas, C. A., & Bailey, J. E. (1996). Analysis and design of metabolic reaction networks via mixed-integer linear optimization. AIChE Journal, 42(5).

Karczewski, K. J., & Snyder, M. P. (2018). Integrative omics for health and disease. Nature Reviews Genetics, 19(5).

Li, H., et al. (2019). The landscape of cancer cell line metabolism. Nature Medicine, 25(5).

Machado, D., & Herrgård, M. (2014). Systematic Evaluation of Methods for Integration of Transcriptomic Data into Constraint-Based Models of Metabolism. PLOS Computational Biology, 10(4), e1003580.

Masid, M., Ataman, M., & Hatzimanikatis, V. (2020). Analysis of human metabolism by reducing the complexity of the genome-scale models using redHUMAN. Nature Communications, 11(1).

Pandey, V., Hadadi, N., & Hatzimanikatis, V. (2019). Enhanced flux prediction by integrating relative expression and relative metabolite abundance into thermodynamically consistent metabolic models. PLOS Computational Biology, 15(5), e1007036.

THEME 6
Multi-scale energy systems engineering

Paper 35	Energy storage requirements towards net-zero emissions in Europe	106
Paper 163	Optimal Design of hydrogen supply chains under demand and resource uncertainty	108
Paper 341	Optimal Cross-sector Integrated Energy Systems to Reduce GHG Emissions Under Uncertainties in Demand, Fuel Prices, and Solar Irradiation	110
Paper 375	Modeling hydrogen applications in combined cycle heat and power plants	112
Paper 433	Combining Operational and Design Optimization Decisions with Hybrid Models for Direct Air Capture Retrofit Analysis	116
Paper 503	Optimal decarbonization routes for high density polyethylene manufacturing	118
Paper 620	Techno–economic assessment of a novel reforming process with low energy demand for high–purity hydrogen production	120
Paper 694	Prospective life cycle assessment of low-carbon heavy-duty trucks	122
Paper 700	Electrification in carbon capture and utilization: vapor recompression in green methanol	124

Energy storage requirements towards net-zero emissions in Europe

Paolo Gabrielli
Institute of Energy and Process Engineering
ETH Zurich, 8092 Zurich, Switzerland

Abstract: This study determines the role of different types of energy storage to decarbonize the European electricity system. The model follows a greenfield approach and determines the optimal installed capacity and energy dispatch for all technologies that minimizes the total annual cost of the system, while complying with targets of zero CO2 emissions in 2050. Three types of energy storage technologies are considered, namely battery, pumped hydro, and hydrogen storage. The impact of spatial resolutions, from regional to continental, on the optimal energy storage mix is investigated.

Keywords: Energy storage, zero-emissions, energy modeling, optimization, European electricity system

Introduction

The evident consequences of climate change, convinced the leaders of over 60 countries worldwide to adopt the United Nations' Paris Agreement in 2015 (UNFCCC, 2015). The central aim of the Paris Agreement is to limit global warming to well below 2 °C above pre-industrial levels by the end of this century. This calls for a transformation of all sectors of human activity, which must achieve net-zero CO2 emissions between 2040 and 2060 (IEA, 2021; IPCC, 2022). Within this context, the electricity sector is riding a wave of grand transformation through a wide deployment of renewable energy sources, mostly wind and solar (IEA, 2021).

Energy storage can offset the temporal fluctuations of solar and wind energy generation. It gives the possibility of storing energy during a period of energy overproduction, and of reusing it during periods of energy shortages (Gabrielli et al., 2018), hence removing the need for flexible fossil-based generation and its carbon emissions. Different types of energy storage can be more or less economically and environmentally viable depending on various technical, economic, environmental and geographical circumstances (Gabrielli et al., 2019; Petkov and Gabrielli, 2020; Petkov et al., 2021; Sepulveda et al., 2021). On the one hand, short-term storage technologies, like batteries, feature high round-trip efficiencies, but also high losses when storing energy for a long time (Malhotra et al., 2016). On the other hand, long-term storage systems, such as hydrogen storage, are characterized by negligible losses but relatively low efficiencies (Gabrielli et al., 2020).

Methodology

This study determines the role of different types of energy storage to decarbonize the European electricity system. It uses the Euro-Calliope optimization model to simulate the European electricity system in 2050 (Tröndle et al., 2020; Tröndle and Pickering, 2021), to achieve net-zero CO2 emissions. The model is formulated as a mixed integer linear program that determines the optimal installed capacity and energy dispatch for all technologies that minimizes the total annual cost of the system, while complying with constraints on CO2 emissions. Three types of energy storage technologies are considered, i.e., battery, pumped hydro, and hydrogen storage. A greenfield approach is adopted, hence a new system is designed independently of the incumbent energy system. The analysis focuses on the impact of spatial resolutions, from regional to continental, on the optimal energy storage portfolio.

This work improves the state-of-the-art as follows: (1) it analyses the system at various spatial resolutions, and determines the impact of spatial resolutions on the assessment of energy storage requirements; (2) it models the trade-offs between short and long-term energy storage accounting for spatial diversity, (3) it widens the scope of existing research in Europe, which focuses on either the EU-28 or aggregate countries and regions, and (4) it does not restrict its scope to a fully renewable electricity system, but it investigates the impact of different strategies to phase-out fossil fuels on the energy storage requirements in Europe. Overall, the work provides a perspective on the role of energy storage to achieve net-zero CO2 emissions in Europe.

Findings and conclusions

Findings show that different types of countries exist in Europe, where the energy storage mix is dominated by one of the different storage technologies. Overall, short-term battery storage best captures solar fluctuations, and is optimally combined with solar generation, while long-term hydrogen storage smoothen both solar and wind peak generation. Also, storage requirements depend significantly on the spatial resolution used to perform the assessment. More specifically, the comparative assessment of different spatial resolutions shows that the amount of energy storage installed, and especially the amount of hydrogen storage, depends significantly on the spatial resolution of the system. Higher spatial resolutions (regional) result in higher wind and solar energy generation, hence in higher storage capacity. Moreover, the location of the storage installations change when considering different system resolutions, possibly moving from one country to the bordering regions of another.

Acknowledgments

This research was carried out with the support of the Swiss Federal Office of Energy (SFOE) as part of the SWEET PATHFNDR project. The authors bear sole responsibility for the conclusions and the results.

References

Gabrielli, P., Gazzani, M., Martelli, E., & Mazzotti, M. (2018). Optimal design of multi-energy systems with seasonal storage. Applied Energy, 219, 408–424.

Gabrielli, P., Fürer, F., Mavromatidis, G., & Mazzotti, M. (2019). Robust and optimal design of multi-energy systems with seasonal storage through uncertainty analysis, Applied Energy, 238, 1192-1210.

Gabrielli, P., Poluzzi, A., Kramer, G. J., Spiers, C., Mazzotti, M., & Gazzani, M. (2020). Seasonal energy storage for zero-emissions multi-energy systems via underground hydrogen storage. Renewable and Sustainable Energy Reviews, 121, 109629.

IEA. (2021). Net Zero by 2050, IEA, Paris.

https://www.iea.org/reports/net-zero-by-2050

IPCC. (2022). Summary for Policymakers. In H.-O. Pörtner, D. C. Roberts, E. S. Poloczanska, K. Mintenbeck, M. Tignor, A. Alegría, M. Craig, S. Langsdorf, S. Löschke, V. Möller, & A. Okem (Eds.), Climate Change 2022: Impacts, Adaptation, and Vulnerability. Contribution of Working Group II to the Sixth Assessment Report of the Intergovernmental Panel on Climate Change

Petkov, I., & Gabrielli, P. (2020). Power-to-hydrogen as seasonal energy storage: an uncertainty analysis for optimal design of low-carbon multi-energy systems. Applied Energy, 274, 115197.

Petkov, I., Spokaite, M., & Gabrielli, P. (2021). The impact of urban district composition on storage technology reliance: trade-offs between thermal storage, batteries, and power-to-hydrogen. Energy, 224, 120102.

Sepulveda, N. A., Jenkins, J. D., Edington, A., Mallapragada, D. S., & Lester, R. K. (2021). The design space for long-duration energy storage in decarbonized power systems. Nature Energy, 6(5), 506–516.

Tröndle, T., Lilliestam, J., Marelli, S., & Pfenninger, S. (2020). Trade-Offs between Geographic Scale, Cost, and Infrastructure Requirements for Fully Renewable Electricity in Europe. Joule, 4 (9), 1929–1948.

Tröndle, T., & Pickering, B. (2021). Euro-Calliope: Pre-built models (1.1.0) [Data set]. Zenodo.

United Nations Framework Convention on Climate Change (UNFCCC). (2015). The Paris Agreement.

https://unfccc.int/process-and-meetings/the-paris-agreement/the-paris-agreement

Optimal Design of hydrogen supply chains under demand and resource uncertainty

Alissa Ganter, Paolo Gabrielli, Giovanni Sansavini
Institute of Energy and Process Engineering
ETH Zurich, 8092 Zurich, Switzerland

Abstract: The scale-up of hydrogen supply chains is essential to achieve carbon neutrality by 2050. In this work, an optimization-based hydrogen supply chain model is developed to investigate the optimal roll-out of hydrogen supply chains considering hydrogen demand and resource uncertainties. We identify biomass-based hydrogen production as the most cost-effective low-carbon hydrogen production option. However, electricity-based hydrogen production technologies via water-electrolysis increase the robustness of the solution by reducing the dependency on biomass feedstock and diversifying the technology mix.

Keywords: Hydrogen supply chains, network optimization, hard-to-abate industry, net-zero emissions pathways, decision-making under uncertainty.

Introduction

The industrial sector is currently responsible for 20% of the European greenhouse gas emissions (EEA 2022). Major contributors are cement (31%), steel (30%), and chemical industry (20%). Hence, abating the emissions of such industries is key to achieving climate goals. However, these industries inherently rely on carbonaceous feedstock in their production to provide carbon and/or hydrogen. Limited cost-competitive solutions exist to achieve net-zero carbon emissions in these industries. Therefore, these industries are often referred to as "hard-to-abate" industries. Hydrogen produced with low carbon emissions (i.e., low-carbon hydrogen) has the potential to decarbonize these industries (Gabrielli, Gazzani, and Mazzotti 2020).

Currently, hydrogen production is mostly based on steam methane reforming (SMR) of natural gas, contributing to about 3% of European greenhouse gas emissions (FCH Observatory 2022). One solution to abate carbon emissions is coupling SMR with carbon capture and storage (CCS) (Bauer et al. 2022). Other mature and economically viable solutions for low-carbon hydrogen production include water electrolysis from renewable electricity, gasification of biomass, and reforming of biogas. Furthermore, the coupling of biomass-based hydrogen production with CCS can generate net-negative process emissions. Recent evidence suggests that the scale-up of hydrogen supply chains (HSCs) is essential to achieve climate goals, such as the EU's net-zero carbon emissions target for 2050 (Seck et al. 2022).

Two quantities are key to determining the optimal design of hydrogen supply chains: (1) hydrogen demand and (2) biomass availability. However, their amount and their spatial distribution are uncertain. This work investigates the uncertainty associated with hydrogen demand and biomass availability and quantifies the impact on the optimal design of hydrogen supply chains in Europe (EU27, with CH, NO, UK) with regional spatial resolution, and for a multi-year time horizon from 2025-2050.

Method

HSCs are defined as networks of hydrogen production and consumption sites that are interconnected by hydrogen transport options. Hydrogen production can be coupled with CCS. Therefore, carbon supply chains and HSCs are co-designed to account for carbon transport from the capture to the storage site. The transport of biomass is also considered.

The model is implemented as a mixed-integer linear optimization problem that minimizes cost in compliance with climate goals, such as net-zero carbon emissions by 2050. Besides climate goals, the techno-economic performance of hydrogen production and transport technologies are accounted for, as well as spatially resolved data on feedstock availability, hydrogen demand, and available carbon storage sites. The model determines the cost-optimal type, size, and location of (a) hydrogen production, (b) carbon capture, and (c) hydrogen, carbon, and biomass transport technologies. In compliance with mass- and energy balances, the in-, and out-flows of (a) - (c), and the required feedstock amounts are computed. The decisions are time-dependent, with a yearly resolution over a multi-year time horizon from 2025 to 2050.

A scenario-based uncertainty quantification approach identifies a discrete set of scenarios, , with varying hydrogen demands and biomass availabilities. Three levels of hydrogen demand are considered: (1) constant hydrogen demands, similar to today's values, (2) moderate growth in hydrogen demands (20% increase), and (3) steep increase in hydrogen demands (50% increase). Similarly, three levels of biomass availability are considered: (1) full availability of the sustainable biomass potential (Panoutsou and Maniatis 2021), (2) reduced availability of sustainable biomass, which corresponds to about 17% of the sustainable biomass potential in Europe and is determined based on the sectoral energy demands of hard-to-abate industries in the EU reference scenario (Capros et al. 2021), and (3) no biomass availability. Based on the three levels of hydrogen demand and biomass availability nine scenarios are derived.

To determine the cost-optimal HSC design across all scenarios, we determine the optimal HSC design for each scenario and perform an out-of-sample analysis to investigate the performance of the HSC design for each scenario assuming the realization of the other scenarios. We allow the installation of additional hydrogen production and transport technologies such that hydrogen demand and climate goals are fulfilled under the new set of conditions. The additional costs quantify the robustness of the HSC design under the specific scenario. Each model contains 830000 continuous and 66000 integer variables and is solved using the commercial solver Gurobi (Gurobi Optimization LLC 2022).

The optimality of the solutions is quantified in terms of the levelized cost of hydrogen. Moreover, we determine which combinations of production

pathways, feedstocks, and energy sources increase the robustness of the solution.

Conclusion

In general, a lower levelized cost of hydrogen can be expected in scenarios with high biomass availability, and low hydrogen demands. Indeed, biomass-based hydrogen production is identified as the most cost-effective low-carbon hydrogen production technology. For sufficient levels of biomass, hydrogen is predominantly produced via gasification of dry biomass (about 70%), and biomethane reforming starting from wet biomass (about 30%), while water electrolysis only plays a minor role (less than 5%). Even in scenarios where only 17% of the total sustainable biomass potential is available, hydrogen is predominantly produced from biomass. Biomass transport capacities are expanded to overcome limitations in the hydrogen production due to the strongly reduced biomass availability. Compared to scenarios in which the full biomass potential is available, the biomass transport capacity is tenfold.

Achieving net-zero supply chain emissions by 2050 necessitates the coupling of biomass-based hydrogen production with CCS to generate the required carbon removal. If no biomass is available, the net-zero emissions goal cannot be realized. Nevertheless, an emission reduction of 70% (-35Mt) can be achieved by deploying SMR from natural gas coupled with CCS, and electrolysis, where the former enables a cost-efficient transition from natural-gas-based to electricity-based hydrogen production.

Although water electrolysis is not cost-competitive when compared to biomass-based hydrogen production and SMR coupled with CCS, installing electrolyzers can increase the robustness of the solution as it reduces the dependency on biomass feedstock. Our findings show that additional hydrogen production capacities will have to be installed in most scenarios (on average between 15% to 35%) to adapt to the conditions of the other scenarios. However, these additional installation requirements are reduced in scenarios where electrolyzers are installed (about 15%). In contrast, hydrogen and carbon transport requirements are robust across scenarios.

Acknowledgments

This work was carried out with the support of the Swiss Federal Office of Energy (SFOE) as part of the SWEET PATHFNDR project. The authors bear sole responsibility for the conclusions and the results.

References

Bauer, Christian et al. 2022. "On the Climate Impacts of Blue Hydrogen Production." Sustainable Energy & Fuels 6(1): 66–75. http://xlink.rsc.org/?DOI=D1SE01508G.

Capros, P; et al. 2021. EU Reference Scenario 2020. https://op.europa.eu/s/shWr.

EEA. 2022. Annual European Union Greenhouse Gas Inventory 1990–2020 and Inventory Report 2022. https://www.eea.europa.eu/publications/annual-european-union-greenhouse-gas-1.

FCH Observatory. 2022. "Hydrogen Supply Capacity." https://www.fchobservatory.eu/observatory/technology-and-market/hydrogen-supply-capacity (October 14, 2022).

Gabrielli, Paolo, Matteo Gazzani, and Marco Mazzotti. 2020. "The Role of Carbon Capture and Utilization, Carbon Capture and Storage, and Biomass to Enable a Net-Zero-CO2 Emissions Chemical Industry." Industrial and Engineering Chemistry Research 59(15): 7033–45.

Gurobi Optimization LLC. 2022. "Gurobi Optimizer Reference Manual." https://www.gurobi.com.

Panoutsou, Calliope;, and Kydriakos Maniatis. 2021. "Sustainable Biomass Availability in the EU, to 2050." TAPPI Journal 20(8).

Seck, Gondia S et al. 2022. "Hydrogen and the Decarbonization of the Energy System in Europe in 2050 : A Detailed Model-Based Analysis EU." Renewable and Sustainable Energy Reviews 167. https://doi.org/10.1016/j.rser.2022.112779.

Optimal Cross-sector Integrated Energy Systems to Reduce GHG Emissions Under Uncertainties in Demand, Fuel Prices, and Solar Irradiation

Ruonan Li, Vladimir Mahalec
Department of Chemical Engineering
McMaster University, Hamilton, ON, Canada

Abstract: While a high level of integration enables the reduction of GHG emissions through the coordination of energy production and consumption among subsystems, it also poses questions regarding the system performance if actual conditions differ from those employed during the system design. This work examines the flexibility of such integrated systems under uncertainties in demand, fuel prices, and solar irradiation. Case studies on an integrated system with a residential building, supermarket, confectionery plant, bakery plant, brewery, and electric vehicles show that the integrated system releases 14% less GHG emissions than the individually operated subsystems, even with uncertainties. However, uncertainties cause GHG emissions of the integrated system to increase by up to 4.5% compared to the deterministic scenario. Allowing the three plants to switch their production rates can mitigate impacts of uncertainties, where the GHG emissions are over 2.8% less than the integrated system with steady production rates.

Keywords: GHG emission reduction, Cross-sector integrated energy system, Flexible production counteracts uncertainties.

Introduction

Integrating energy systems across different sectors is an efficient method to reduce greenhouse gas (GHG) emissions associated with meeting energy demands, Li et al. (2022). Most of the prior studies investigating integrated energy systems assume that energy loads, environmental conditions, electricity prices, and natural gas prices are known or fixed. However, the exact values of these parameters are usually unclear when designing the system.

This work investigates the impacts of uncertainties on an integrated system with adjustable industrial plant production rates. It intends to explore (1) impacts of uncertainties on the performance, optimal design, and optimal operation of the integrated system; (2) benefits of allowing plants to switch their production rates in resisting the impacts of uncertainties on the integrated system.

Case study and optimization problem formulation

The integrated cluster of energy systems being studied is comprised of a bakery plant, a brewery, a confectionery plant, a residential building, and a supermarket, where the production rates of the three plants can be adjusted. Electric vehicles (EVs) are formulated as an affiliation of the residential building. It is assumed that each subsystem has options to install equipment components shown in Figure 1. The specific size and operation of the equipment are decided by solving an optimization problem.

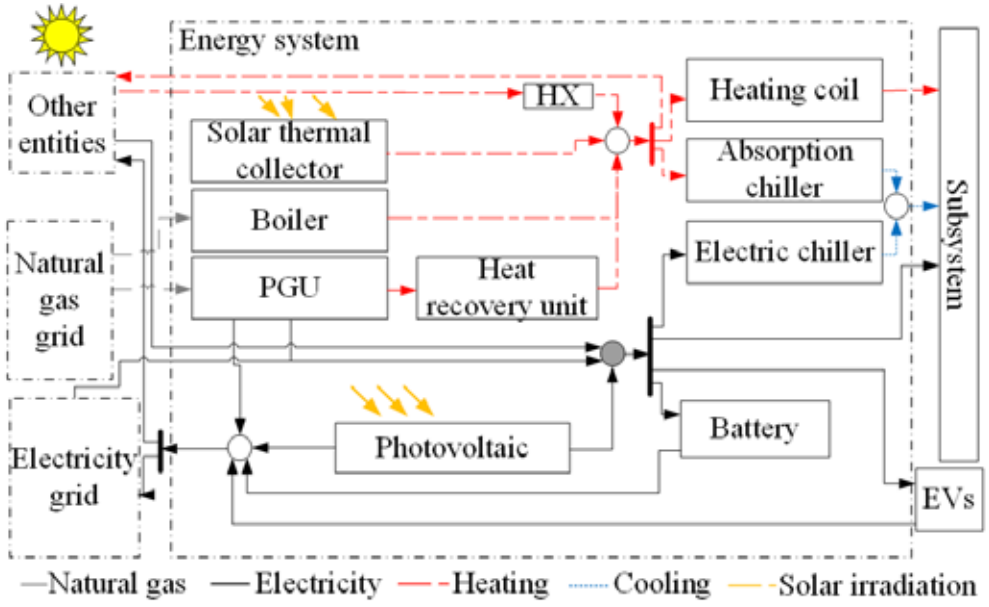

Figure 1. The energy system of a subsystem integrated into the cluster

This work considers uncertainties associated with hourly heating, cooling, and electricity demand of the residential building, natural gas price, and solar irradiation. The objective function is minimizing the total GHG emissions of all entities. It includes emissions from combusting natural gas in the power generation unit (PGU), the boiler, and using the electricity from the external grid.

Results and discussion

Compared to the non-integrated system, when considering uncertainties, the integrated system with steady production rates of plants still releases around 14% less GHG emissions than the non-integrated system. The non-integrated system stands for individually operated subsystems without energy transfer. It indicates the integrated operation can still reduce GHG emissions of the entire system under uncertainties. However, compared to the corresponding deterministic scenario, the reductions in GHG emissions are 0.6% less.

When industrial plants have flexible production rates, the impacts of uncertainties on GHG emissions reduction, grid electricity usage, and operation of the boilers can be mitigated. When considering uncertainties, the integrated system with flexible production rates releases over 2.8% less GHG emissions and uses over 44.1% less natural gas for operating the boiler compared to the integrated system with steady production rates. It is due to the adjustable production rates of plants allowing the integrated system to adjust the heating and electricity transfer facing uncertainties. Specifically, under uncertainties, electricity transfer of the integrated system with flexible production rates is around 15.8% higher compared to the system with steady production rates. Thus, more heating and electricity are generated by the PGUs instead of being generated by the boiler and purchased from the external grid.

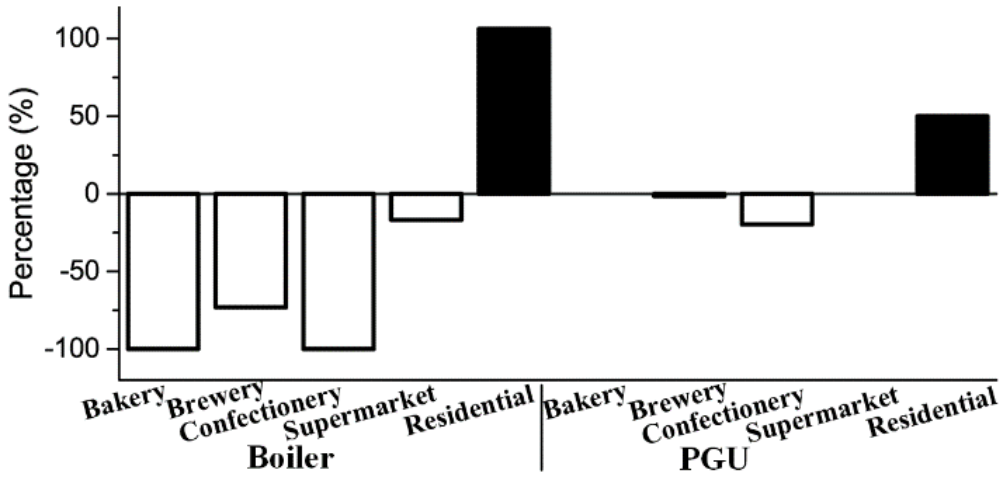

Figure 2. Changes in sizes of PGU and Boiler of the stochastic flexible integrated system compared to the stochastic steady production rate integrated system

Under uncertainties, as shown in Figure 2, the three plants of the integrated system with flexible production rates have smaller boilers (19% less) compared to the integrated system with steady production rates. However, the flexible system has smaller PGUs (4%) but larger boilers (10%) in the residential building. It is due to the system with flexible production rates increasing the operation of the PGUs in the three plants to transfer more electricity to the residential building, which also leads to more heat being generated by the PGU. Thus, using boilers to generate heat in the plants is less necessary. With more electricity being transferred to the residential building, the building needs a smaller PGU to generate electricity locally, but a larger size boiler for heating.

Conclusions

The case study shows that flexible plant production schedules are an effective way to adapt the operation of cross-sector integrated energy systems in a manner that compensates for changes due to uncertainties in heating, cooling, and electrical energy demands in residential and other civic buildings. Flexible scheduling of industrial pants production decreases reliance on supplementary equipment and supplementary energy resources under unexpected scenarios. This enables provided by the integrated operation to be maintained close to its original design performance level. Further work will investigate the vulnerability of integrated systems to failures of individual components.

Acknowledgments

The authors gratefully acknowledge the support from McMaster Advanced Control Consortium, and Ontario Research Fund.

References

R. Li, V. Mahalec V., 2022, Integrated design and operation of energy systems for residential buildings, commercial buildings, and light industries, Appl Energy, 305, 117822

Modeling hydrogen applications in combined cycle heat and power plants

Jan F. Wiegner[a], Norbert Sürken[b], Ralf Neuhäuser[b], Matteo Gazzani[a]
[a]Utrecht Universiy, Princetonlaan 8a, 3584 CB Utrecht
[b]Siemens Energy, Rheinstr. 100, 45478 Mülheim an der Ruhr

Abstract: Combined cycle heat and power (CHP) plants are expected to play an important role in balancing generation of heat and electricity from non-dispatchable renewable energy. Retrofitting a CHP plant for hydrogen combustion is a prominent option to decarbonize (part of) its electricity and heat generation. In this work, we study and optimize different options for using hydrogen in CHP plants, namely: direct combustion in the gas turbine, supplementary firing in the heat recovery boiler (duct burner), and oxy-fuel combustion of hydrogen for direct steam production.

Therefore, we first model an exemplary CHP plant in a detailed non-linear process model based on the principles of thermodynamics and fluid-dynamics. This process model provides enough load points to fit a surrogate, mixed-integer-linear model that can optimize the plant operation economically within a reasonable computation time. We validate the surrogate model and use it to study (1) economic hydrogen combustion in a combined cycle plant, and (2) evaluate the economic benefit of retrofitting the plant with a duct burner or an oxy-fuel hydrogen burner.

Keywords: Combined Cycle Heat and Power Plants, Hydrogen, Oxyfuel Combustion, Gas Turbine, Steam Turbine, Steam Generation.

Introduction

Combined cycle heat and power (CHP) plants are expected to play an important role in balancing generation of heat and electricity from non-dispatchable renewable energy. However, the increasing share of fluctuating renewable power generation poses a paradox to CHP plant operators: While they are key from a system perspective to maintain the balance between demand and supply, the increasing generation from renewable sources results in lower operating times and consequently lower profit contribution margins for their owners. Calls for decarbonization as well as rising gas and emission prices further increase the financial pressure on plant operators. Retrofitting a CHP plant for hydrogen use is a prominent option to decarbonize (part of) its electricity and heat generation; however, it does not necessarily improve the plants profitability (Bauer et al., 2022, Öberg et al., 2022, Welder et al., 2019).

In this work, we study novel and traditional options for hydrogen use at limited volumes in a CHP plant from an operator's point of view. The novel option encompasses an oxy-fuel hydrogen burner (OHB) providing an additional option for heat-input to the plant's bottoming steam cycle. In this OHB, hydrogen is burned stoichiometrically with oxygen in steam atmosphere to produce high-temperature steam that can be fed to the plant's bottoming steam cycle (Sternfeld et al., 1989, Schastlivtsev et al., 2020). Additionally, we model a hydrogen-fueled supplementary firing downstream of the gas turbine (duct burner) and the admixture of hydrogen to natural gas to fire the gas turbine. The duct burner and the OHB increase the electric and thermal capacity and provide additional operational flexibility. The plant including the retrofitting options is modelled in two different frameworks: First, in a detailed non-linear process model. Second, we use the performance estimated in the non-linear model to fit a mixed-integer linear (MILP) model, that can determine the most profitable operation of the plant over multiple time-slices (here, over a full year). As such, the contribution of this work is threefold: (i) Developing a quick-to-solve but precise model of an exemplary CHP plant; (ii) Evaluating economically hydrogen combustion in a CHP plant from an operator perspective; (iii) Evaluating the economic benefit of retrofitting an existing CHP plant with components for combustion of small amounts of hydrogen.

Process Model

The process model is a static representation of an exemplary CHP plant in an industrial complex. It comprises a gas turbine, a heat recovery steam generator (HRSG) with two pressure levels and a steam turbo-set featuring a high-pressure steam turbine and a combined intermediate and low-pressure steam turbine. Process steam for industrial applications can be extracted before the high-pressure steam turbine and upstream of the combined medium/low pressure steam turbine, respectively. The process model implements detailed thermodynamic and fluid dynamic equations for all plant components, e.g. piping, pumps, heat exchangers, compressors and turbines. As such, the model can realistically simulate the behavior of the plant for different operating points and ambient temperatures. The process model was formulated for three different configurations (CHP only, CHP+duct burner and CHP+OHB) with a single load point taking around 18 seconds to solve. The detailed model is Siemens Energy proprietary information.

Surrogate MILP Model

The MILP model includes separate equations for the gas turbine and the recovery steam cycle. The performance of the gas turbine and steam turbo-set are formulated as piecewise-affine functions with ambient temperature dependency. Additionally, minimum part-load constraints are added. An objective function is formulated to maximize total profit Π over a considered timeframe T (here: one year). The full model depicts a constrained maximization problem:

$$\max \Pi = \sum_{T} p_{\mathrm{t,el}} E_{\mathrm{t,el}} - p_{\mathrm{NG}} E_{\mathrm{t,NG,in}} - p_{\mathrm{CO2}} M_{\mathrm{t,CO2}} - p_{\mathrm{H2}} E_{\mathrm{t,H2,in}} \quad (1)$$

$$s.t. \quad CHP\,performance\,equations \quad (2)$$

$$steam\,demand = steam\,supply \quad (3)$$

Where $P_{t,i}$ and $E_{t,i}$ depict the price and generation/consumption of carrier i in time slice t and M_{t,CO_2} denotes CO_2 emissions from the combustion of natural gas. The MILP model solves in 0.33 seconds on average for a single load point, which is around 55 times faster than the detailed process model.

Validation

The validation of the MILP model against the detailed model was performed by generating a set of random load points constrained by fuel inputs, and by comparing the solution for total electricity generation of the two models. Figure 1 shows the relative error in total electricity output between the non-linear process model and the MILP model. The absolute relative error is well below 4% and we conclude that the surrogate MILP model is sufficiently precise to mimic the behavior of the CHP plant.

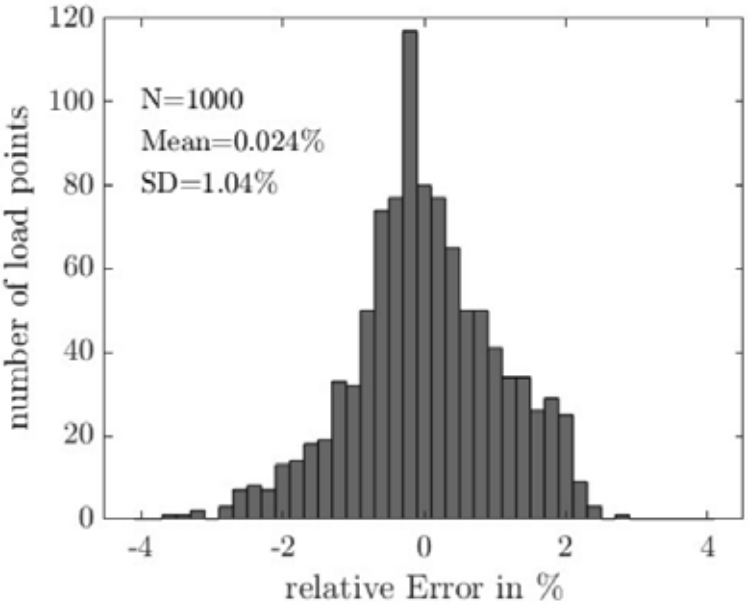

Figure 1: Model Validation. The histogram shows the distribution of relative difference in total electric output between the process model and the MILP model

Optimization Results

With the MILP model, we optimize the operation of the plant over a full year with an hourly resolution. We therefore consider ambient temperature, industrial steam demand and electricity prices on an hourly basis as well as a variety of different constant fuel and CO2 price combinations. The plant is optimized separately for the three different plant configurations (CHP only, CHP+duct burner, and CHP+OHB). The difference in profit between the retrofit configurations and the CHP only configuration is the additional profit possible with the respective retrofit option. These additional profits may be interpreted as a hypothetical acceptable annualized investment cost, the plant operator may be willing to invest for a specific retrofit option. The input data is shown in Table 1.

Table 1: Input Data

		Value	Unit
Electricity Prices	Average Std. Deviation	112 75	EUR/MWh
Natural Gas Price (range)		25 - 200	EUR/MWh
Hydrogen Price (range)		25 - 200	EUR/MWh
CO2 Price (range)		25 - 200	EUR/t
Ambient temperature	Average Std. Deviation	11.20 7.12	°C
Steam Demand (yearly sum)	High Pressure Medium Pressure	430 120	GWh

In the CHP only configuration, hydrogen use in the gas turbine is not economic unless its cost is below the cost of natural gas (including emission costs). The operation of the plant follows the electricity price profile: For high prices, the plant runs at its maximum point of operation, while for low electricity prices, it is optimal to use as little fuel as possible to supply the steam demand, resulting in a lower electricity output.
In a next step, we optimize the two additional configurations, i.e. CHP+duct burner and CHP+OHB. We report differences in key performance indicators to the CHP only case (Figure 2 shows the CHP+OHB configuration). The retrofit of the plant with either a duct burner or with an OHB increases the profit of the plant over a large range of input assumptions. This is an effect of the ability of both components to increase electric output from the steam cycle at times of high electricity prices. A surprising result is the profitable hydrogen combustion for a CHP+OHB configuration in the case where hydrogen is more expensive than the combined natural gas and emission cost (upper left triangle in Figure 2 for $p^{+}_{NG} \leq p_{H2}$). This results from the fact that the OHB can only burn hydrogen (and not natural gas) and its operation does not suffer from fuel price competition between natural gas and hydrogen. As such, the CHP+OHB configuration can increase the annual electricity output of the plant without any additional carbon emission while improving the profitability of the plant.

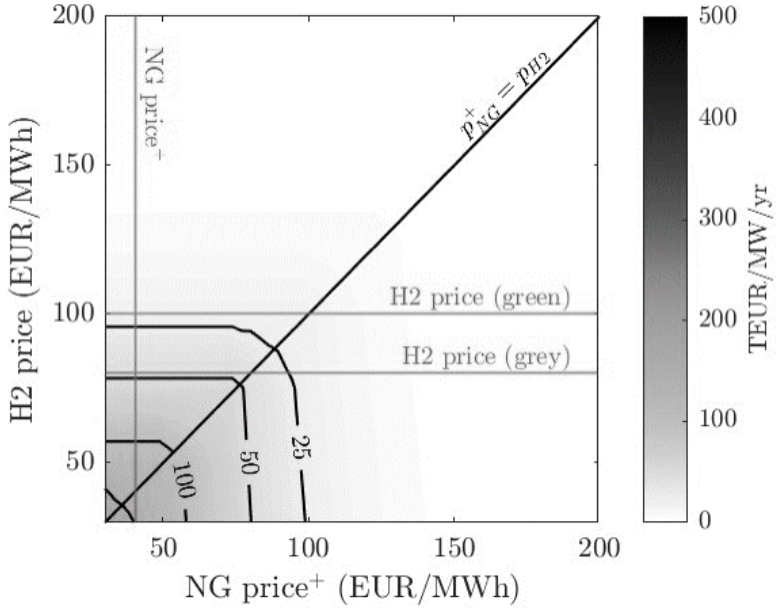

Figure 2: Additional profit (per year and MW installed) for the CHP+OHB plant configuration for different hydrogen and natural gas prices. The additional profit is calculated as the difference of total operational profit between the CHP+OHB configuration and the CHP only configuration. The natural gas price includes emission costs. Current fuel prices are indicated for reference.

The CHP+duct burner configuration has a slightly lower additional profit than the CHP+OHB configuration. This is due to the lower steam generation efficiency of the duct burner compared to the OHB.
In this work, we ignored investment costs, and the additional profits possible need to be weighed against respective investment costs. Thus, despite the duct burner resulting in a higher additional profit than the OHB, the higher investment cost associated to the duct burner might make it a less attractive retrofit compared to an OHB. Estimating valid investment costs is subject of ongoing research.

Conclusion

The mixed-integer linear model proved to be significantly faster to solve than its detailed, non-linear counterpart (0.33 vs. 18 seconds for a single load point), while maintaining a high precision (below 4% relative difference). This increase in computational performance makes the surrogate model an attractive option for multi-period, economic optimizations of the CHP plant operation.
We used the model to evaluate hydrogen combustion in a combined cycle heat and power plant and found that replacing natural gas with hydrogen to directly fire the gas turbine is not a business case at current hydrogen/natural gas prices. This changes only if hydrogen becomes less expensive than natural gas (including emission cost).
However, both a hydrogen-fueled duct burner and an OHB makes hydrogen use in a CHP a profitable business case, also at current prices. This is also true if hydrogen prices are higher than natural gas prices (including emission costs). As such, the retrofit with an OHB or a hydrogen-fueled duct burner can improve both, the environmental and the economic performance of a plant.
We currently working on a more elaborated analysis forthcoming in 2023 (Wiegner et al., forthcoming).

Acknowledgments

This publication is part of the project "Facilitating Large Scale Offshore Wind Energy Production by Developing Offshore Storage and Transport Alternatives" (with project number WIND.2019.002) which is partly financed by the Dutch Research Council (NWO). Furthermore, we thank Siemens Energy for providing data from their detailed process model.

References

Bauer, T., Prenzel, M., Klasing, F., Franck, R., Lützow, J., Perrey, K., Faatz ,R., Trautmann, J., Reimer, A., & Kirschbaum, S. (2022). Ideal-Typical Utility Infrastructure at Chemical Sites – Definition, Operation and De-fossilization. Chemie Ingenieur Technik, 94(6), 840-851.

Öberg, S., Odenberger, M., & Johnsson, F. (2022). Exploring the competitiveness of hydrogen-fueled gas turbines in future energy systems. International Journal of Hydrogen Energy, 47(1), 624–644.

Schastlivtsev, A. I., Dunikov, D. O., Borzenko, V. I., & Shmatov, D. P. (2020). Hydrogen-Oxygen Installations for the Energy Industry. High Temperature, 58(5), 733–743..

Sternfeld, H. J., & Heinrich, P. (1989). A demonstration plant for the hydrogen/oxygen spinning reserve. International Journal of Hydrogen Energy, 14(10), 703–716.

Welder, L., Stenzel, P., Ebersbach, N., Markewitz, P., Robinius, M., Emonts, B., & Stolten, D. (2019). Design and evaluation of hydrogen electricity reconversion pathways in national energy systems using spatially and temporally resolved energy system optimization. International Journal of Hydrogen Energy, 44(19), 9594–9607.

Wiegner, J.F., Sürken, N., Neuhäuser, R., Gazzani, M. & Gibescu, M. (forthcoming). Optimizing the use of limited amounts of hydrogen in existing combined heat and power plants.

Combining Operational and Design Optimization Decisions with Hybrid Models for Direct Air Capture Retrofit Analysis

Zachary Kilwein[1], Pengfei Cheng[1], Joseph Scott[1], Matthew Realff[1], Fani Boukouvala[1]
[1]School of Chemical and Biomolecular Engineering
Georgia Institute of Technology, Atlanta, USA

Abstract: In order to meet decarbonization goals, carbon capture technologies must be added to existing fossil fuel based power plants. Natural gas combined cycle plants account for a large portion of US electricity production and retrofitting these plants with carbon capture systems is key. In this work, we look at efficiently solving the multi-timescale optimization problem represented by this retrofit. Dependent design and operational decisions must be made with uncertain costing parameters (i.e. electricity prices and carbon credit). We propose to solve this multiscale integrated problem using hybrid formulations with embedded pre-trained machine learning models and derivative-free optimization solvers.

Keywords: Surrogate modeling, carbon capture, multi-scale optimization

Introduction

Natural gas combined cycle (NGCC) power plants are the single largest source of energy production in the United States (Monthly Energy Review, 2022) and even aggressive forecasts of electrification and decarbonization expect NGCC to play a key role in the upcoming decades (Larson et. al, 2020). Coupling of NGCC and post combustion carbon capture (PCC) is one way to maintain high power output through existing plants, while addressing their considerable CO2 emissions. Building off research on modular Direct Air Capture (DAC) units (Sujan et. al, 2019), researchers have proposed a retrofit design to integrate PCC and DAC to existing NGCCs, in order to create operational flexibility and take advantage of heat integration opportunities, while allowing for net-negative emissions. The modularity of DAC units also allows for adaptable retrofitting of current plants from a design perspective. Operationally, dynamic electricity prices and CO2 costing parameters heavily influence plant power output and downstream carbon capture units. While this flexibility allows for robust, market-driven decisions, the size and multiple time-scales of the resulting optimization formulation of the integrated design and operation, may lead to intractable problems.

In this work, we propose alternative approaches to solve these problems, using embedded surrogate models to replace the operational (hourly) component of the optimization problem. Fast surrogate solutions allow us to quickly estimate operational responses under various price scenarios (electricity and CO2). We combine the surrogate models with derivative-free optimization to determine the best design decisions for the retrofit of the NGCC plant.

Formulation

The underlying model to describe the DAC retrofit is summarized below in Figure 1.

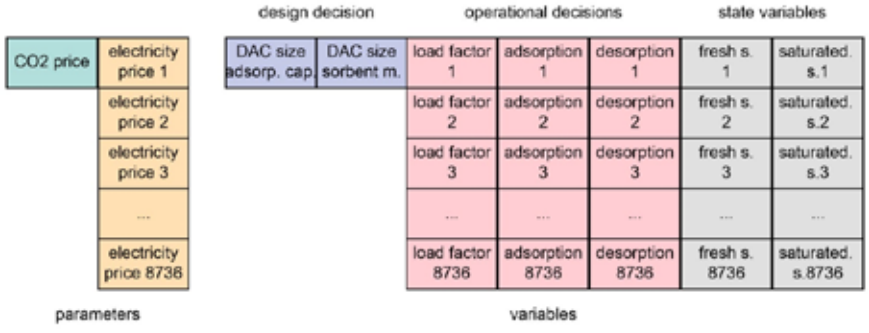

Figure 1. NGCC-DAC Retrofit Model

The two design variables DACads,cap and DACsorb,m correspond to the adsorption capacity and mass of sorbent for the DAC unit. These values are to be set for all time points and directly affect the capital cost. The other degrees of freedom in the model are discretized operational decisions such as plant load factor, amount of CO2 adsorbed ( ), and amount of CO2 desorbed ( ). These variables determine how the plant and carbon capture units operate at each hour given price signals and the overall DAC size available. Finally, state variables ( ) are calculated through linear mass balance constraints. Given all variables and costing parameters, the net present value (NPV) of the plant can be calculated. Equations 1-4 show the multi-scale formulation:

$$\max NPV(y_{DAC}, y_1, \ldots, y_T) \quad (1)$$

$$y_t = NN(y_{DAC}, x_t), \ \forall t \epsilon T \quad (2)$$

$$x_t^{fresh} = x_{t-1}^{fresh} - y_t^{adsorb} + y_t^{regen} \quad (3)$$

$$x_t^{sat} = x_{t-1}^{sat} + y_t^{adsorb} - y_t^{regen} \quad (4)$$

Here, y_{DAC} refers to the design size decisions of the DAC unit and y_t denotes the operational variables at time t. Equation 1 is the objective function (NPV). Equation 2 is the NN prediction of y_t at each time step. The states of the DAC unit include fresh, adsorb, desorb, regeneration and saturated which are related in Eq 3-4.

Results and Discussion

Surrogate Performance

To create a dataset for optimal operational decisions, the model was solved 3,696 times with the following variable parameter values: (1) the DAC size [0, 3000 tonnes], (2) the electricity price signal for a given period T (based off historical data). T was set to be 361 hours to make sure that the solution captures the sorbent inventory dynamics and is representative enough while the model can be solved fast enough. The model was solved on an Intel i9 (16 cores) 3.10 GHz processor with 32 GB RAM. The average solution time is 2.37 s. After generating the dataset described above, neural network models were trained to predict load factor, $y^{adsorbe}$ and y^{desorb} as outputs given the electricity price signal, DAC size and CO2 price. The feed-forward neural network model was trained using Tensorflow. The model consisted of two hidden layers with 100 nodes each and ReLU activation functions. Overall, the model is highly predictive and all 3 outputs show high test accuracy. The R2 values are shown in Table 1.

Table 1. Test Accuracy of ML Model

Variable	Test R^2
Load Factor	0.9313
$y^{adsorbe}$	0.9901
y^{desorb}	0.9611

Combined Optimization

To solve the multi-scale optimization problem, the trained NN surrogate is used as a feed forward prediction. Given values of the DAC design decisions a forward prediction and NPV calculation can be made in 11.3 sec. To maximize NPV, the design decisions are formulated as the degrees of freedom in a derivative-free optimization problem that we solve with the DIRECT method in Scipy (Jones et al, 1993). The advantage of this approach is that the design variables (total of 2) become the sole degrees of freedom, while the inner ML-based function becomes the "black-box" function call that generates the required output data. An alternative approach would be to directly use the inner operational optimization problem as the inner input-output generator, but in this case each sample required by the derivative-free optimizer will be an optimization problem and will have increased computational cost.

Table 2. Multiscale Optimization Results

CO_2 Price ($/tonne)	$DAC_{sorb,m}$ (tonne)	NPV (MM$)	CPU (min)
150	2731	-463	45.2
225	3000	520	47.1

Table 2 shows optimal solutions of the integrated model using ERCOT pricing data and two carbon price scenarios. The integrated model solves in less than an hour and a positive NPV is achieved in the higher CO2 price scenario.

Conclusions

Implementing carbon capture technology in existing plants is a critical need that requires cost effective solutions. The combined optimization of design and dynamic operations can be computationally intractable, so machine learning models can be used to replace the operational decisions. We show how this can be done with the DAC system and how the resulting multi-scale optimization problem is solved with derivative-free optimization. The integrated optimization solution provides optimal design decisions for various pricing scenarios allowing for flexible retrofit designs of existing NGCC power plants. Currently, we are comparing alternative hybrid and derivative-free approaches that may be applied to this problem.

Acknowledgements

The authors acknowledge support from the National Science Foundation (NSF-1944678).

References

Jones, D.R., Perttunen, C.D. & Stuckman, B.E. (1993) Lipschitzian optimization without the Lipschitz constant. J Optim Theory Appl 79, 157-181.

Larson, E., et al. (2020) "Net-Zero America: Potential Pathways, Infrastructure, and Impacts, interim report Princeton University, Princeton, NJ.

Monthly Energy Review. (2022) Technical report, US Energy Information Administration

Sujan, Achintya and Simon H Pang, Guanghui Zhu, Christopher W Jones, and Ryan P Lively. (2019) Direct co2 capture from air using poly (ethylenimine)-loaded polymer/silica fiber sorbents. ACS Sustainable Chemistry & Engineering, 7(5):5264–5273.

Optimal decarbonization routes for high density polyethylene manufacturing

Shiyu Ding[a], André Faij[a, b], Juliana Monteiro[b], Gert Jan Kramer[a], Matteo Gazzani[a]
[a]Utrecht University, Princetonlaan 8a, 3584 CB Utrecht, The Netherlands
[b]TNO, Energy Transition Studies (ETS), 1043 NT Amsterdam, the Netherlands

Abstract: In this work, we aim at presenting the structure and the preliminary implementation of a comprehensive assessment of different decarbonization routes for the production of high density polyethylene (HDPE). More specifically, we investigate possible HDPE production processes starting from renewable energy, water, and CO2-neutral carbon feedstock. While most existing studies focus either on detailed technology assessments or high-level system performance, in this work we develop a bottom-up approach that bridges technology simulation, possible production routes (e.g. bio-based vs recycling), and system evaluation. Therefore, different process modules and operation units are connected and optimized for economic and environmental performance. As a preliminary implementation, this work shows the methodology, the challenges and the benefits of this bottom-up approach using one carbon-circular HDPE route case study.

Keywords: Decarbonization routes, HDPE manufacturing, process modeling, LCA, TEA.

Introduction

High density polyethylene (HDPE) is conventionally produced from fossil fuels, which provide both the material feedstock and the required energy (EUROPEAN COMMISSION, 2007). At the end-of-life, most HDPE is combusted in incineration plants, disposed in landfills, or released to the environment (Abbas et al., 2022). From a life cycle perspective, 1 kg of HDPE emits between 1.85-4.5 kg of CO2 depending on the end-of-life route (Nguyen et al., 2020; Manfredi et al., 2009).

To make HDPE CO2-netural and transition to a fossil-free circular economy, we need to replace fossil fuels with the combination of renewable energy and CO2-neutral carbon feedstock. The latter can be supplied via biomass, non-fossil recycled carbon resources, or CO2 captured from the air. New manufacturing routes need to be designed and assessed accordingly.

Currently, HDPE decarbonization routes are either qualitatively assessed or quantitatively assessed by collecting high-level technology performance data (Belboom et al., 2016; IEA, 2018; Zhao et al., 2018). The high uncertainty of these data, which are particularly high for low technology readiness level (TRL) technologies, makes the outcome results unclear and subject to significant fluctuations depending on the specific assumptions. On a similar note, the existing assessments can hardly be directly compared because they have different scopes and assumptions. Moreover, high-level assessments are typically based on black-box technology models that are either tuned for very specific technology configurations or generic for a class/family of technologies. This makes the results difficult to compare, hardly portable to other case studies, for example with respect to different geographic regions or price/emission scenarios. It is equally important that such high-level technology assessments do not exploit the opportunity to rigorously optimize technology and process from a system perspective.

With this contribution, we will discuss a possible solution enabled by computer aided process modeling for designing and assessing the optimal HDPE decarbonization routes.

Model Description

Herein, a bottom-up approach is used to model and analyze possible production process routes that convert CO2-neutral (or low-CO2) carbon feedstock, renewable electricity, and water into HDPE. Separate process modules consisting of operation units and material conversions are linked for different HDPE decarbonization routes, for example ethylene polymerization, methanol synthesis and conversion to ethylene, carbon capture. These process modules are coupled with techno-economic and environmental assessments and optimized systematically. The approach is aided by ASPEN Plus and MATLAB software which are interfaced to achieve high consistency, transparency and flexibility of the results. By conducting a literature review, we identified three types of renewable carbon resources (biomass, non-fossil recycled carbon sources, and CO2 captured from the air), eleven HDPE decarbonization routes, and twenty technologies.

Case Study

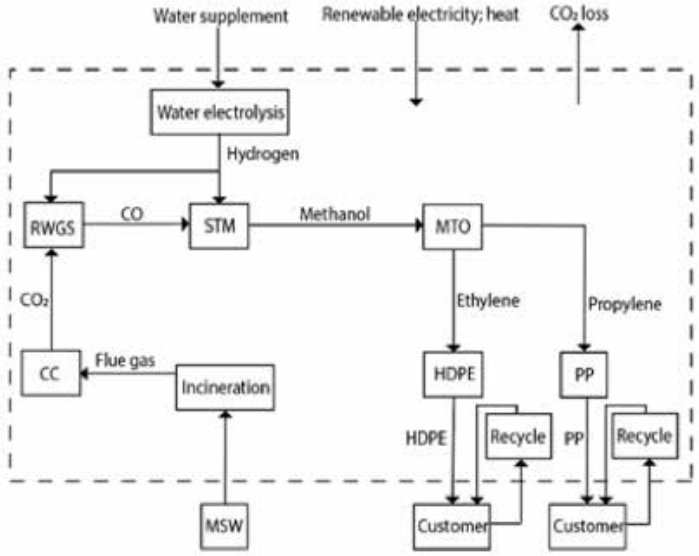

Figure 1. One example HDPE decarbonization route: the studied processes are in the dashed box and the arrows point product streams (HDPE high density polyethylene; RWGS reverse water gas shift; STM syngas to methanol; MTO methanol to olefins; PP polypropylene; MSW municipal solid waste; CC carbon capture).

In Figure 1, we showcase how one innovative decarbonization route performs within the developed framework. The showcase route is a circular carbon system: municipal solid waste (MSW) is incinerated and CO2 is removed from the produced flue gas via a carbon capture process, the CO2 product is converted into CO in a reverse water gas shift (RWGS) process, CO is fed into syngas-to-methanol (STM) unit, and the produced methanol is converted into olefins in a methanol-to-olefins (MTO) process. The main products—ethylene and propylene – are then polymerized as customer products, which are collected after being used as MSW, and MSW is again incinerated for circular carbon reuse. Finally, mechanical recycle of HDPE and PP is considered as exogenous input, i.e. it is not modeled.
The process modules and the whole HDPE production system are optimized for costs and CO2 emissions using a derivative-free method (multi-objective particle swarm, genetic algorithm, Bayesian optimization tool).

Conclusion

Several emerging routes exist for the production of CO2-neutral (or low-CO2) HDPE. However, these routes are mostly assessed independently using either very specific technology models or from a high-level perspective. It is therefore difficult to identify what are the most promising routes for decarbonized HDPE production. With this work, we show how process-level design and assessment can increase the consistency, transparency and flexibility of the results. On the other hand, the process models are non-linear equation oriented in detail, thus the route solution consisting of several process models is challenging.
For the future work, the framework will be expanded with all the identified routes and technologies, thus suggesting on the optimal decarbonization routes for HDPE manufacturing.

Acknowledgments

This work was financially supported by the TNO program 'Industrial Transformation'.

References

Abbas-Abadi, M. S., Zayoud, A., Kusenberg, M., Roosen, M., Vermeire, F., Yazdani, P, Van Geem, K. M. (2022). Thermochemical recycling of end-of-life and virgin HDPE: A pilot-scale study. Journal of Analytical and Applied Pyrolysis, 166, 105614. doi:10.1016/j.jaap.2022.105614

Belboom, S., Léonard, A. (2016). Does biobased polymer achieve better environmental impacts than fossil polymer? comparison of fossil HDPE and biobased HDPE produced from sugar beet and wheat. Biomass and Bioenergy, 85, 159-167. doi:10.1016/j.biombioe.2015.12.014

EUROPEAN COMMISSION (2007). Reference Document on Best Available Techniques in the Production of Polymers.

IEA (2018). The Future of Petrochemicals—Towards a more sustainable chemical industry.

Manfredi, S., Tonini, D., Christensen, T. H., Scharff, H. (2009). Landfilling of waste: Accounting of greenhouse gases and global warming contributions. Waste Management Research: The Journal for a Sustainable

Nguyen, L. K., Na, S., Hsuan, Y. G., Spatari, S. (2020). Uncertainty in the life cycle greenhouse gas emissions and costs of HDPE PIPE Alternatives. Resources, Conservation and Recycling, 154, 104602. doi:10.1016/j.resconrec.2019.104602

Circular Economy, 27(8), 825-836. doi:10.1177/0734242x09348529

Zhao, Z., Chong, K., Jiang, J., Wilson, K., Zhang, X., Wang, F. (2018). Low-carbon roadmap of Chemical Production: A case study of ethylene in China. Renewable and Sustainable Energy Reviews, 97, 580-591. doi:10.1016/j.rser.2018.08.008

Techno-economic assessment of a novel reforming process with low energy demand for high-purity hydrogen production

Athanasios Arampatzis[1], Theodoros Papalas[1], Andy N. Antzaras[1], Angeliki A. Lemonidou[1]
[1]Department of Chemical Engineering
Aristotle University of Thessaloniki (AUTh), Greece

Abstract: A comparative feasibility analysis between industrial steam reforming of natural gas and an intensified reforming process by combing carbonate and chemical looping was performed. The study included the design of the flow diagrams for each scenario, mass and energy balances calculations and sizing of the necessary equipment. A complete economic analysis was conducted for both cases, including calculation of the fixed capital investment and the total annual production cost. The technoeconomic calculations for the two processes highlighted the superiority of the intensified reforming process, demonstrating almost a 16% lower levelized cost of H2 production while significantly reducing the specific CO2 emissions.

Keywords: Blue H2, Sorption enhanced chemical looping reforming, Ca-Ni looping, Technoeconomic analysis.

Introduction

The environmental issues related to excessive use of fossil fuels, have dictated the necessity to improve the efficiency in the energy production sector as well as the transition towards sustainable resources. In this context, H2 is heavily supported as an energy carrier, as it is expected to play a key role in this necessary transition. Also, H2 demand as a primary industrial gas is continuously increasing. H2, however, is produced at industrial scale via steam reforming of CH4 (SMR), a particularly energy-intensive process due to the strong endothermicity of SMR and the applied harsh operating conditions. Moreover, multiple steps downstream the reformer are required to acquire a high-purity H2 stream, increasing the complexity and the cost of the process. It is clear that an intensification over H2 production is necessary.

At this direction, sorption enhanced chemical looping steam methane reforming (SE-CL-SMR) is considered as an alternative method for blue H2 production, combining chemical looping reforming with CO2 capture (Antzara et al, 2015; Antzaras & Lemonidou, 2022). In this cyclic process, the reformer contains a CO2 sorbent and an oxygen transfer material (OTM). In the first step, the OTM is reduced by CH4 and serves as the reforming catalyst. The reaction proceeds under autothermal conditions due to the heat released by the exothermic carbonation. In the second step, the saturated sorbent is regenerated, with the energy provided by the OTM re-oxidation (Fermoso et al, 2014; Rydén & Ramos, 2012).

In continuation of our computational and experimental work on the process, we report herein the economic evaluation of SE-CL-SMR at large scale. For comparison, conventional reforming was also assessed.

Methodology

The flow diagram of each process was designed in Aspen Plus V9 by selecting a fixed H2 production capacity of 4,500 Nm3/h with the lifetime of each unit set at 20 years. The conventional process was performed at high pressure (25 bar), with the reforming reactor operating at 850 °C followed by two water gas shift (WGS) reactors to convert the unreacted CO and a pressure swing absorption (PSA) unit where a pure H2 stream is separated. On the other hand, the reforming step of the intensified process operated at atmospheric pressure and 600 °C without the requirement of additional conversion or separation steps, and the sorbent regeneration took place in a second reactor at 850 °C. The final H2 stream was compressed at 25 bars in order to have a meaningful comparison with conventional SMR. The best performing sorbent and OTM, based on previous results derived from bench-scale experiments (Antzara et al, 2016), were also used in the simulation of this study. In both cases, a similar heat integration strategy was followed, with the residual energy in the product steams after feed preheating, used to generate electricity in a heat recovery steam cycle.

Kinetic equations for each reaction step were selected from literature, enabling the calculation of energy and mass balances. Simulation results were then utilized to perform a detailed economic analysis, including sizing of the necessary equipment and calculation of capital and operating expenses. Finally, the levelized cost of H2 production (LCOH) and specific CO2 emissions were determined for each unit.

Results

The main cost factors calculated for each scenario are presented in Table 1. The Fixed Capital Investment (FCI) of each production unit was calculated based on the purchased and delivered equipment cost based on literature data, by including also several direct and indirect costs, as a percentage of the equipment cost. Overall, the conventional SMR presented a higher FCI due to the requirement of additional production and separation steps, as well as the increased equipment cost due to the harsher operating conditions applied. Comparing the annual production cost of the two plants, it is observed that SE-CL-SMR presents ~17% lower cost. As in both cases, natural gas constitutes a significant fraction of operating expenses, the increased efficiency of the intensified process led to ~15% reduction in feed requirements. This is an important aspect, considering the price volatility of natural gas due to the energy crisis.

The two scenarios were compared based on their LCOH, specific CO2 emissions and feasibility in the event of volatile cost factors. For the conventional process, the LCOH was estimated at 3.21 $/kg H2, which is close to the cost reported for units with similar H2 capacities. In the intensified process, the respective cost was found ~16% lower.

Table 1. Estimation of different cost factors for conventional SMR and SE-CL-SMR

	SMR	SE-CL-SMR
Fixed Capital Investment (M$/yr)	14.20	11.84
Total production cost (M$/yr)	3000	7.65
Natural gas feed (m3/h, STP)	2,032	1,736
LCOH ($/kg H2)	3.21	2.70
Specific emissions (kg CO2/kg H2)	10.83	1.40

The most important advantage of the intensified process however is the almost 90% reduction in specific CO2 emissions compared to the conventional unit. This is clearly illustrated by comparing the LCOH for the two cases in a possible rapid increase of the carbon tax (Fig. 1). A drastic increase in the CO2 emissions tax can lead to up to 20% increased production cost for conventional SMR, while only a 4% increase is observed for the intensified process, rendering it as a more sustainable route for H2 production. Although a potentially lower performance of the materials at larger scale would narrow the gap compared to conventional SMR, SE-CL-SMR still represents an intensified, low-energy-demanding process for blue H2 production.

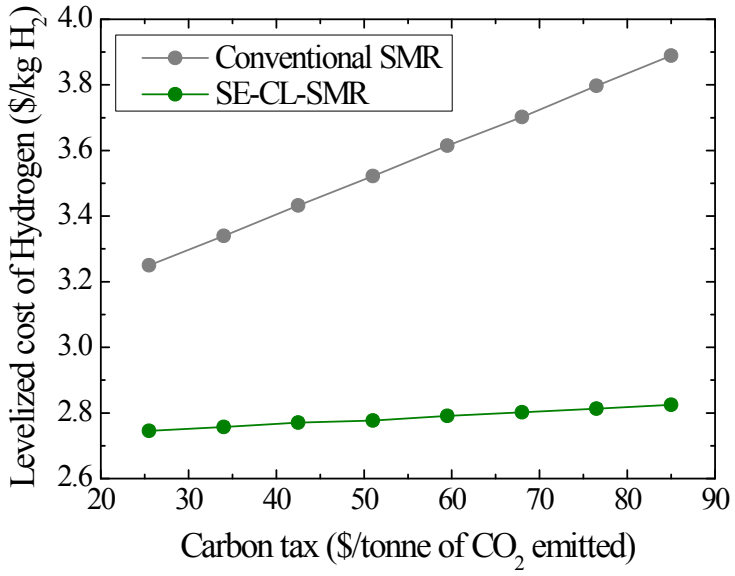

Figure 1. LCOH as a function of carbon tax

Conclusions

Intensification of SMR by introducing chemical looping and in-situ CO2 capture can lead to significantly improved efficiency, reducing the production cost and specific CO2 emissions by up to ~16 and ~90% respectively. In the transition period until green H2 is considered competitive, process intensification will be one of the most effective ways to reduce the overall carbon footprint of H2 production.

References

Antzara, A., Heracleous, E., Bukur, D.B., Lemonidou, A.A. (2015). Thermodynamic analysis of hydrogen production via chemical looping steam methane reforming coupled with in situ CO2 capture. Int. J. Greenh. Gas Control, 32, 115.

Antzara, A.N., Heracleous, E., Lemonidou, A.A. (2016). Energy efficient sorption enhanced-chemical looping methane reforming process for high-purity H2 production: Experimental proof-of-concept. Appl. Energy, 180, 457.

Antzaras, A.N., Lemonidou, A.A. (2022). Recent advances on materials and processes for intensified production of blue hydrogen. Renew. Sust. Energ. Rev., 155, 111917.

Fermoso, J., Gil, M.V., Rubiera, F., Chen, D. (2014). Multifunctional Pd/Ni–Co catalyst for hydrogen production by chemical looping coupled with steam reforming of acetic acid. ChemSusChem, 7, 3063.

Rydén, M., Ramos, P. (2012). H2 production with CO2 capture by sorption enhanced chemical looping reforming using NiO as oxygen carrier and CaO as CO2 sorbent, Fuel Process. Technol., 96, 27.

Prospective life cycle assessment of low-carbon heavy-duty trucks

Margarita A. Charalambous, Victor Tulus, Gonzalo Guillén-Gosálbez
Institute for Chemical and Bioengineering, Department of Chemistry and Applied Biosciences, ETH Zürich, Vladimir-Prelog-Weg 1, 8093 Zürich, Switzerland

Abstract: Considering the high greenhouse gas emissions caused by the transportation sector (24%), as estimated by IEA (2021), it is crucial to look into decarbonization alternatives, especially in heavy-duty road transport. This work focuses on the environmental assessment of future heavy-duty (HD) truck powertrains and fuel pathways, which are often assessed using current inventory data. To that end, we used prospective environmental inventories based on premise and sustainable integrated assessment models (IAM) to compare five decarbonization options; battery electric, fuel cells, internal combustion engines powered by the projected diesel fuel mix, e-diesel, or e-natural gas. We found that whereas the batteries and fuel cells perform environmentally better, synthetic fuels based on renewable carbon and green hydrogen can also provide substantial emission reductions for this sector. Lastly, this work shows that prospective environmental assessment could allow for a more accurate evaluation of future environmental impacts of the heavy transport sector.

Keywords: prospective life cycle assessment, transportation, heavy-duty trucks, integrated assessment models

Introduction

At present, freight road transport emits 6% of European CO2 (European Parliament and Council, 2019). To reach carbon neutrality in 2050, the EU has developed emission standards imposing CO2 reductions of up to 15% and 30% in 2025 and 2030, respectively (relative to 2020). Several powertrains and fuels will play a role in fulfilling this challenging task, including battery electric (BE) and fuel cell (FC) trucks. The uptake of these "zero-emission" powertrains is moving slowly; thus, a portfolio of technologies is needed to achieve the above goals.

Finding the right technological mixes requires conducting life cycle assessment (LCA) studies to evaluate their environmental implications. Current LCAs are often based on existing data, thereby providing limited insight into the future roles of technologies in an expected economy. Prospective LCA has recently emerged to assess the future environmental impacts of emerging technologies by combining Integrated Assessment Models (IAM) scenarios with life cycle inventories (Beltran and Cox, 2018). Sacchi (2022), introduced premise, a tool that generates prospective inventory databases by integrating IAM scenarios. This tool enables the creation of library datasets that use future projections for a more accurate assessment of technologies and future supply chains. These datasets are based on the Ecoinvent database. Here we shall apply premise to the assessment of future low-carbon heavy trucks alternatives to shed light on their future performance.

Methodology

We followed the life cycle assessment (LCA) methodology to calculate the life cycle impacts from 2020 to 2050. The goal is to compare the environmental impacts of HD truck powertrains. The functional unit was defined as 1-tonne·kilometer (tkm), and we adopted a cradle-to-wheel scope following a global attributional approach.

The life cycle inventory was calculated in Brightway2 v.2.4.2, combining data for the background and foreground systems. For 2020, background data from Ecoinvent v3.8 were used, while for 2030 and 2050, premise was used to generate prospective background inventories. The background system of Ecoinvent v3.8 is transformed using the REMIND v.3 IAM model for the sustainable SSP2PkBudg500 scenario (Aboumahboub, 2020). This sustainable IAM scenario assumes that CO2 emissions will peak at 500 Gt, which is compliant with the Paris Agreement target of atmospheric temperature increase of 1.5oC. In regards to the foreground system, the fuel pathways of hydrogen, diesel and compressed gas were developed based on literature data and process simulations. Notably, the scenarios considered in this work include battery electric (BE) trucks powered by the electricity mix, fuel cell (FC) trucks fueled with electrolytic hydrogen (H2) powered with wind power, and internal combustion engines with synthetic diesel (e-diesel) or fossil diesel that follow the business-as-usual (BAU), as well as, synthetically produced compressed natural gas (enatural gas). For the production of H2, data were taken from Bareiß (2019). For the e-diesel production, inventory data were taken from Medrano-García (2022), and lastly, for the production of e-natural gas, a process simulation was developed in Aspen Plus v.11 based on Chauvy (2020). Ediesel and enatural gas are produced by mixing CO2 and hydrogen. For this case, we consider that electrolytic H2 is powered by wind electricity and CO2 is either coming from a direct air capture (DAC) or pre-combustion capture from natural gas power plant (NG CCU). Lastly, for the business-as-usual (BAU), Ecoinvent and premise data are used.

For the life cycle impact assessment, we chose the IPCC 2013 100a as the life cycle impact assessment method to calculate the impacts. Finally, the results are interpreted, and the main conclusions are summarized.

Results and discussion

Figure 1 shows that for all the powertrains and fuel pathways, the emissions per tkm will decrease from 2020 to 2050.

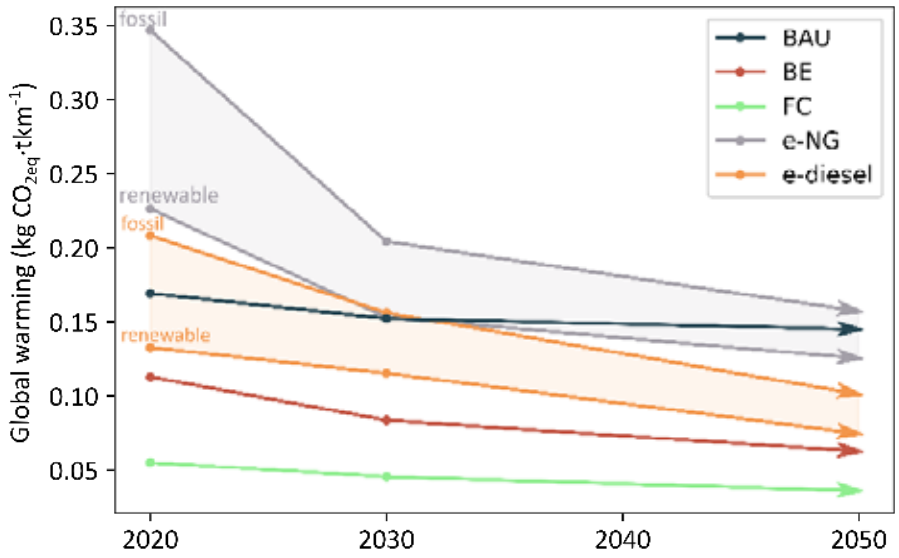

Figure 1. Global warming impacts. Five powertrains were investigated; BAU (ICE fueled by the market for diesel), BE (battery electric), FC (fuel cell), e-NG and e-diesel (produced from e-H2 powered with wind and CO2 from DAC or NG CCU)

Overall, the zero-carbon emission powertrains, FC and BE, perform better with the former being the best. The higher engine efficiency, lower H2 demand per tkm and the zero combustion emissions compared to the other powertrains set these two technologies at the top of our list.
In regards to the synthetic fuels investigated here, ediesel performs better than e-natural gas. Moreover, between the fossil CO2 and renewable CO2 there is a 0.080.03 kgCO2-eq·tkm-1 difference for e-diesel and 0.120.03 kgCO2-eq·tkm-1 for e-natural gas. Both synthetic fuels derived from fossil CO2 perform worse than the BAU until 2030, with only ediesel decreasing emissions until 2050. Notably, the emissions reduction is mostly attributed to a greener electricity mix and engine improvements.
Looking into the short-term solutions and motivated by the 30% reduction target set by the European Union for the sector, ediesel from renewable CO2 can enable alone a 24% reduction in emissions by 2030, and it could be directly fueled in already existing engines.
The environmental superiority of zero-emission powertrains is well known; however, their slow uptake calls for alternative fuels that could be easily retrofitted.

Acknowledgments

This publication was created as part of NCCR Catalysis (grant 180544), a National Centre of Competence in Research funded by the Swiss National Science Foundation.

References

Aboumahboub T, Auer C, Bauer N, Baumstark L, Bertram C, Bi S, et al. Model documentation | version 2.1.0 | REMIND - REgional model of INvestments and development. 2020.

Bareiß K., de la Rua C., Möckl M. and Hamacher T., (2019). Life cycle assessment of hydrogen from proton exchange membrane water electrolysis in future energy systems Appl. Energy. 237, 862–872.

Chauvy R., Dubois L., Lybaert P., Thomas D., and Weireld G. De (2020). Production of synthetic natural gas from industrial carbon dioxide. Appl. Energy, 260, 114249.

European Parliament and Council, REGULATION (EU) 2019/1242 of the European Parliament and of the Council, Brussels, Belgium, 2019.

Medrano-García Juan D., Charalambous Margarita A., and Guillén-Gosálbez Gonzalo (2020). Economic and Environmental barriers of CO2based FischerTropsch ElectroDiesel ACS Sust. Chem. & Eng., 10, 1175111759.

Mendoza Beltran A, Cox B, Mutel C, van Vuuren Detlef P, Vivanco David F., Deetman S, et al. (2018). When the background matters: using scenarios from integrated assessment models in prospective life cycle assessment. J. Ind. Ecol., 24:64–79.

Sacchi R., Terlouw T., Siala K., Dirnaichner A., Bauer C., Cox B., Mutel C., Daioglou V., Luderer G., PRospective EnvironMental Impact asSEment (premise): A streamlined approach to producing databases for prospective life cycle assessment using integrated assessment models, (2022) Renew. Sustain. Energy Rev, 160, 112311.

Electrification in carbon capture and utilization: vapor recompression in green methanol

Juan D. Medrano-García[1], Marina T. Chagas[1], Gonzalo Guillén-Gosálbez[1]
[1]Institute for Chemical and Bioengineering, Department of Chemistry and Applied Biosciences, ETH Zürich, Switzerland

Abstract: This work explores the further decarbonization of green methanol production, assessing the economic and environmental implications of electrifying the heating needs. To this end, we apply process simulation to model the substitution of the conventional distillation column with a vapor recompression column (VRC). We consider three renewable electricity scenarios for H2 production (wind, solar and nuclear) and compare them with and without VCR. The results show that the VRC technology slightly increases the cost of the synthesis, with wind electricity for H2 production leading to the cheapest production cost. On the other hand, nuclear H2 provides the best environmental results. This work highlights that, under the appropriate conditions, integrating the well-known VRC technology in the green methanol process can further improve its environmental appeal, especially in the future as the power mix will be gradually decarbonized.

Keywords: Green methanol, Decarbonization, Life cycle assessment (LCA)

Introduction

With over 24 % of current anthropogenic CO2 emissions, the transport sector needs to lean more heavily towards non-fossil fuels to attain the 1.5 ºC goal by 2100. Synthetic fuels are one possible alternative to curb emissions in the carbon sector. Among them, green methanol from renewable H2 and captured CO2 has gained a special interest in recent years. However, despite reducing the carbon foorprint relative to conventional natural gas-based methanol, green methanol still requires fossil energy sources to cover the heating requirements. Notably, even after heat integration, heating utilities, often supplied by steam from natural gas, are needed either in the reboiler or to preheat the reactor feed, depending on the process configuration (Pérez-Fortes et al., 2016).

Vapor recompression column (VRC) is a mature technology that consists in the compression (and consequent heating) of the top product of a distillation column in order to supply heat to the reboiler. In essence, VRC effectively transforms electricity into heating with high coefficients of performance (COP) (Kazemi et al., 2018), which allows for replacing fossil resources with electricity as energy input to the process, thereby potentially reducing costs and also emissions when low-carbon electricity is employed. Here, we shall explore this concept in green methanol production.

Methodology

Our goal is to remove all heating requirements in green methanol production. To this end, we integrate a VRC into a green methanol process flowsheet modeled in Aspen HYSYS v11. We design the VRC by compressing the vapor (methanol) that leaves the first tray of the column and then use it to exchange heat with the reboiler considering a minimum temperature difference of 10 ºC. The stream is pressurized until it reaches 6.36 bar, which is enough for the system to require no heating utilities after heat integration. Furthermore, we consider that the purged gases are combusted with electrolytic O2. The CO2 produced is recycled back to the reactor, and the energy is consumed within the system.

We study 18 scenarios resulting from the combination of three sources of electrolytic H2 (wind, solar and nuclear), three electricity mixes for the continuous operation of the plant (current global mix, future global mix, current Swiss mix), and two different process configurations, with (VCR) and without the recompression technology (base case). The CO2 used in the process is assumed to be provided by direct air capture (DAC). We compute the economic and environmental performance based on the mass and energy flows from the model (foreground system) in combination with data taken from the Ecoinvent v3.5 database (background system) using the software Simapro v9.2.0.2 and the ReciPe 2016 v1.03 methodology.

Results and discussion

The production cost of green methanol using wind, solar, and nuclear-powered electrolytic H2 for the base case and VRC scenarios is shown in Figure 1. Here, it can be seen that electrifying the column results in slightly higher production costs (2.0 – 2.7 %) in all cases, with wind H2 producing the cheapest methanol, followed by solar and nuclear. This increase results from the very different volatilities of water and methanol, since the VRC technology is optimized for mixtures with close volatilities, such as the ethylene/ethane pair. Overall, 91.90 – 94.46 % of the cost contribution is associated with H2 production (65.39 – 74.69 %) and CO2 capture (19.77 – 26.51 %), while the utilities only comprise 0.36 – 0.48 %, with electricity ranging from 2.86 to 4.50 %.

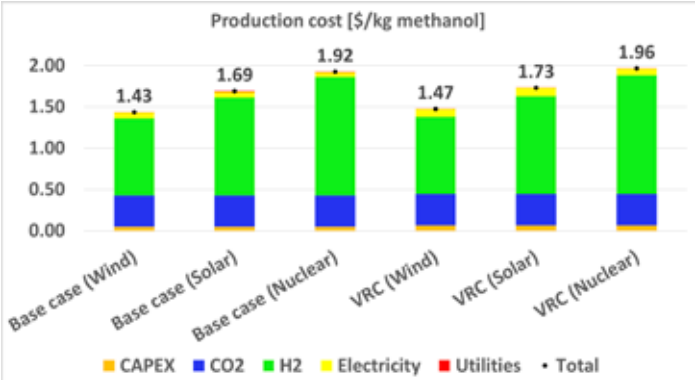

Figure 1. Green methanol production cost breakdown (current global mix scenario)

Regarding the environmental assessment, Figure 2 shows that installing the VCR technology in green methanol production reduces the carbon production footprint only when considering low-carbon electricity mixes. For instance, if using the current mix (0.151 kgCO2-eq/kWh), VRC would increase the footprint. However, for a future mix scenario in 2040 (0.042 kgCO2-eq/kWh) modeled based on the World Energy Outllok 2019, the climate change impact would decrease by 3 %. Moreover, in a mix with lower carbon intensity (0.003 kgCO2-eq/kWh), like the Swiss one, VRC would lead to an 8 % improvement in carbon footprint, four times lower than in the base case current mix scenario (– 0.44 and – 0.11 kg CO2-eq/kg).

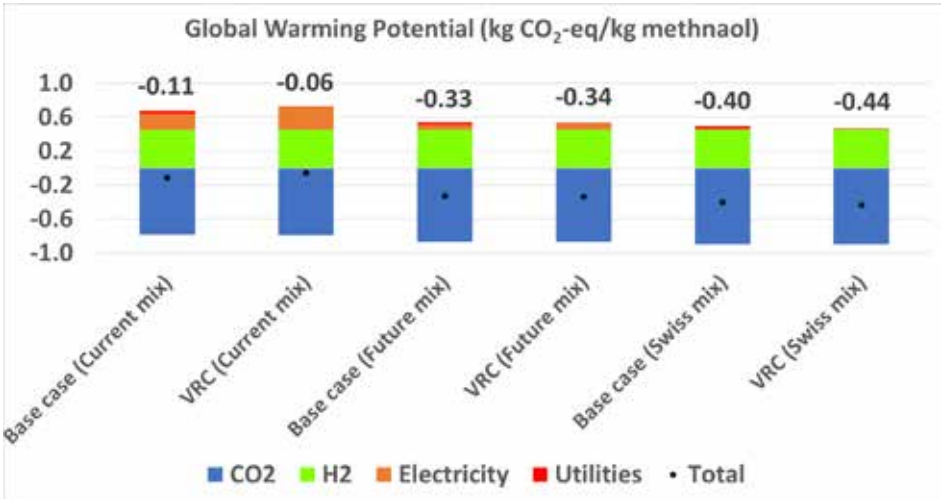

Figure 2. Green methanol production GWP impact breakdown (wind scenario)

Conclusions

In this work, we studied the complete electrification of green methanol production using the VRC technology. VRC replaces all fossil-based heating with electricity inputs, thereby reducing emissions when low-carbon electricity is employed instead of combusting fossil resources. We found that VRC leads to increased costs (~ 2 %) but a reduced carbon footprint (~ 3 - 8 %) using low-carbon electricity.
Overall, our results prove that VRC can help to electrify the methanol plant to reduce its emissions at a marginal increase in cost, even more in the future, as the mix gets decarbonized.

Acknowledgments

This publication was created as part of the NCCR Catalysis (Grant 180544), a National Centre of Competence in Research funded by the Swiss National Science Foundation.

References

Kazemi, A., Mehrabani-Zeinabad, A., & Beheshti, M. (2018). Distillation without hot utilities; development of novel distillation configurations for energy and costs saving for separation of propylene/propane mixture. Chemical Engineering and Processing: Process Intensification, 123, 158–167. https://doi.org/10.1016/j.cep.2017.10.027
Pérez-Fortes, M., Schöneberger, J. C., Boulamanti, A., & Tzimas, E. (2016). Methanol synthesis using captured CO2 as raw material: Techno-economic and environmental assessment. Applied Energy, 161, 718–732. https://doi.org/10.1016/j.apenergy.2015.07.067

THEME 7
Sustainable supply chains and ecosystems

Paper 107	Integrated strategic and tactical optimization of ethiopia's bioethanol supply chain coupled with operational plan using vehicle routing	128
Paper 385	A process modeling based eco-design framework: application to the produciton of biomethane and CO2 capture from biogas	130
Paper 799	Systematic Planning of Constructing Hydrogen Refueling Stations in Transportation Energy Systems with the Case of South Korea	132
Paper 868	Strategic and tactical planning model for the design of perishable product supply chain network in ethiopia	134

Integrated strategic and tactical optimization of ethiopia's bioethanol supply chain coupled with operational plan using vehicle routing

Tesfayesus Mamo[a,b], Ludovic Montastruc[a], Stéphane Negny[a], Lemma Dendena[b]
[a]Université de Toulouse, INP-ENSIACET, 4, allée Emile Monso, F-31432 Toulouse Cedex 04, France
[b]Addis Ababa University, Addis Ababa Institute of Technology, School of Chemical and Bio-Engineering, Addis Ababa, Ethiopia

Abstract: This work addresses a holistic approach to supply chain optimization by integrating the three decision levels (strategic, tactical and operational). To design and size the developed mixed integer liner program in a reasonable amount time, the model is decomposed in two sub-models: In the first stage, an integrated strategic and tactical optimization model is developed and in the second stage, a vehicle routing problem is developed as an operational model. To combine the optimization model with the operational model, a novel sequential iterative approach is designed. The optimization model is a mixed-integer linear programming (MILP) that maximizes the NPV of the bioethanol supply chain while the operational model is a vehicle routing problem (VRP) that minimizes the transportation cost. The capability of our approach is used for Ethiopia's scenario to offer decision support for stakeholders, investors, and policy makers to make the bioethanol supply chain economically viable.

Keywords: Integrated, Bioethanol, Optimization, Supply chain

Introduction

Even though the process system engineering community (PSE) faces a growing number of difficult problems, process supply chain design and planning continue to be a major interest offering multiple opportunities. These opportunities bring financial profitability while fulfilling customers' requests for all the network entities along the supply chain. The process supply chain is described as a complicated system due to the variety of entities with their own objectives and characteristics, as well as the diverse network flows. Through time, the scope of planning and designing supply chain has been expanded by integrating the different levels of supply chain on the one hand but also by considering the pillars of sustainability (Barbosa-Póvoa et al., 2018). Thus, process supply chain has been the subject of intensive research by the community of PSE to make a significant contribution to address complex research domain extensively. The research subject of process supply chain is primarily addressed by developing mono or multi objective methods and tools considering decisions that range from strategic to tactical and operational levels (Barbosa-Póvoa et al., 2018).

Conventionally, biofuel supply chain planning has been done hierarchically at the strategic (long-term decisions: supply network design), tactical (medium-term decisions: management of network design) and operational (short- term decisions: routing) levels (Akhtari et al., 2018). However, a recent trend in the PSE involves the integration of both strategic and tactical level in order to contribute to intelligent and coherent decision making. The problem with the previous method is using solution from one level may results in inconsistent or infeasible solution (Tesfamichael et al., 2021). This happens because each lower planning level includes variations that are not accountable for, at higher planning levels (Akhtari & Sowlati, 2020). This was shown by the study of Akhtari et al. (2018) in a case study of British Columbia where the strategic optimization solutions were not attained at the tactical level. Thus, it is required to integrate different planning levels not only to create values but also to assure that plans from higher planning levels are attainable at lower planning levels.

Another important work included in our model is the vehicle routing problem (VRP). Despite its importance and being one of the most frequently studied optimization problems in logistics in general, vehicle routing decisions is, most of the time overlooked in the literature related decision in PSE besides strategic and tactical for bioethanol supply chain. Consequently, this work will incorporate vehicle routing decisions in the optimization of biofuel supply chain besides the strategic and tactical decisions. As a result, the objective of the work is to address the strategic, tactical and operational decisions in an integrated manner and develop a hybrid optimization-surrogate model to solve the integrated problem.

The methodology is developed in a recursive optimization-surrogate approach. This approach proposes a new multi scale resolution process that decomposes the problem in both time and level of decision. Thus, the model is decomposed in two stages. In the first stage, an integrated strategic and tactical optimization model is developed and in the second stage, based on the input from the optimization model a vehicle routing problem is developed as an operational model. This decomposition allows to solve an accurate model in a reasonable computational time, while keeping quality solution. To solve the multi scale

problem, a novel iterative closed loop sequential strategy is proposed. The operational model uses the supply chain design determined by the optimization model to schedule the supply chain in order to achieve the lowest feasible transportation cost. Moreover, the operational model's output is utilized to predict the optimization model's input parameter in order to alter the supply network design based on a weekly basis. The improvement is done to make sure that the transportation cost in the optimization model is kept as minimum as possible. The optimization model is utilized as a decision-making tool for strategic and tactical design and planning in the bioethanol supply chain, with the goal of maximizing the net present value (NPV) while the goal of operational model is minimizing the transportation cost across the supply chain.

To demonstrate the proposed strategy, the developed model is applied in Ethiopia to determine the optimal bioethanol supply chain. The Ethiopia government has included the development of biofuel as one of its development strategies since 2010 as a result of the ever-rising fossil fuel prices and the environmental concerns due to the excessive consumption of fossil fuels (Tesfamichael et al., 2021). In spite of the government's strong desire to produce bioethanol from biomass feedstock, little has been done in the past decade to attain this objective (Tesfamichael et al., 2021). Table 1 displays the result of the total transport cost for each iteration . The transportation cost of the operational level is 3 times higher than the one without this level. This explains that the transport cost of the strategic and tactical models is estimated from the coarse-grained model where as in the second case it is a fine-grained model. The incorporation of the operational level to the integrated strategic and tactical decisions is an added value provided that there is a very detailed description of the decisions taken at this level.

Table 1. Comparison of the total transport cost(M$)

Iteration	Transport cost for strategic and tactical levels (M$)	Transport cost for strategic, tactical and operational levels (M$)
1	2.5	7.4
1	7.4	7.4

Conclusion

In this work a novel sequential iterative approach is designed to integrate the impacts of decisions across the different levels of supply chains. The result of the proposed model highlights the importance of a fine modelling of the operational level on the quality it has on the strategic and tactical levels. The iteration between the decision-making levels ensured the consistency of the decision and demonstrates the relevance of the proposed approach.

Acknowledgments

We would like to thank the French embassy in Ethiopia and the Ethiopian Ministry of Education (MOSHE) for funding this program.

References

Akhtari, S., & Sowlati, T. (2020). Hybrid optimization-simulation for integrated planning of bioenergy and biofuel supply chains. Applied Energy, 259, 114124.

Akhtari, S., Sowlati, T., & Griess, V. C. (2018). Integrated strategic and tactical optimization of forest-based biomass supply chains to consider medium-term supply and demand variations. Applied Energy, 213, 626–638.

Barbosa-Póvoa, A. P., da Silva, C., & Carvalho, A. (2018). Opportunities and challenges in sustainable supply chain: An operations research perspective. European Journal of Operational Research, 268(2), 399–431.

Tesfamichael, B., Montastruc, L., Negny, S., & Yimam, A. (2021). Designing and planning of Ethiopia's biomass-to-biofuel supply chain through integrated strategic-tactical optimization model considering economic dimension. Computers & Chemical Engineering, 153, 107425.

A process modeling based eco-design framework: application to the produciton of biomethane and CO_2 capture from biogas

Carlos E. Robles-Rodriguez, Eliot Wantz, Gilles Hebrard, Ligia Barna
TBI, Université de Toulouse, CNRS, INRAE, INSA, Toulouse, France

Abstract: Transition towards industry decarbonization requires the eco-design of existing and new processes to cope with the environmental policies and reduce emissions of the processes. Therefore, processes need to be assessed in terms of technology, economic feasibility and environmental footprint. Nowadays, these tools exist and allow the assessment separately. It is important, however, to bring coherence and unify these methods to be able to change and optimize conditions that can trade-off process performance. In this context, this work aims at implementing an eco-design framework based on process modeling where the tools for calculating technical and environmental performances via Life cycle assessment (LCA) are linked to simplify the analysis and identify hotspots. The here proposed framework is tested on a case study considering anaerobic digestion to produce biogas (approx., 60% CH4, 40 %CO2) and the upgrading of biogas into biomethane (96% CH4) while capturing the CO2 contained in the biogas. Two upgrading technologies were compared: chemical absorption by amines (CAA) and high-pressure water scrubbing (HPWS). This work sets the basis for further studies where simulation results could be used to optimize the hotspots and eco-design the studied technology at a proper scale.

Keywords: Eco-design, process modeling, co2 capture, biomethane

Introduction

The transition towards industry decarbonization requires to guarantee that new processes report good techno-economic performances with low environmental impacts along the phases of their life cycle. Adaptive process modeling allows to study different process scales and provides the data needed to evaluate the technical and economic performances and the creation of the inventory for environmental analysis that can be evaluated via Life Cycle Assessment (LCA). This process modeling eco-design approach has been applied to water treatment (Bisinella de Faria et al., 2016) to identify the most promising development pathways and the hotspots (e.g., unit operations) requiring further improvement and investigation. However, several technical difficulties associated with coupling or integrating process simulators into LCA software limit the scope of this approach. This work aims at presenting a proof of concept platform for eco-design. This is built upon process modeling and an interphase to connect specialized software and allow the calculation of techno-economic and environmental performances. Biogas production and upgrading to biomethane (>97%) is considered as a case study to build the platform. Two alternatives for biogas upgrading are considered: chemical absorption by amines (CAA) (Khan et al., 2021) (Figure 1A) and high pressure water scrubbing (HPWS) (Figure 1B).

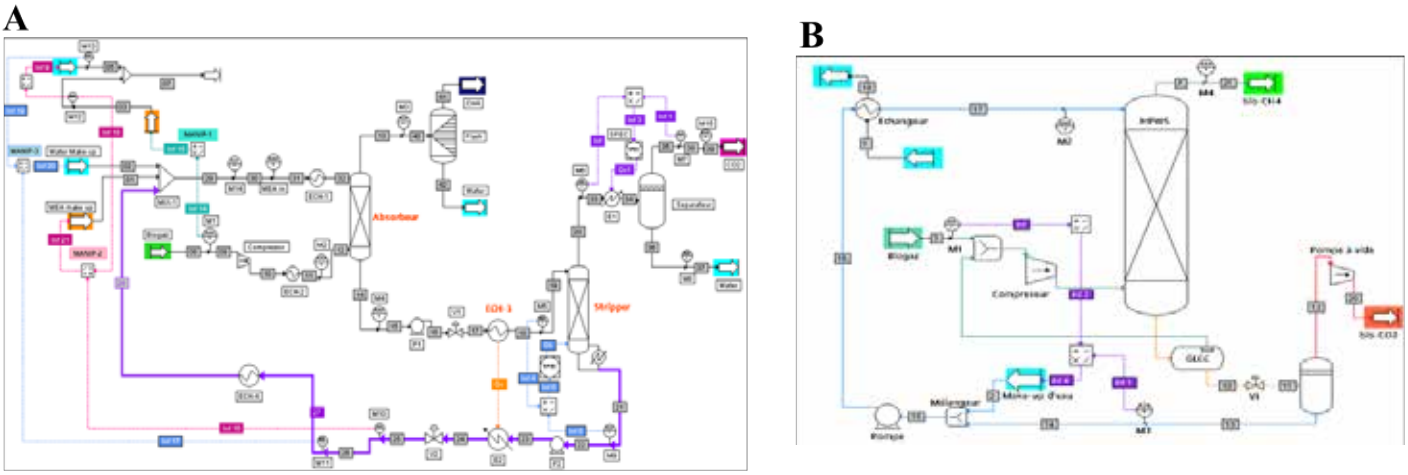

Figure 1. (A) Flowsheet of chemical absorption of CO2 by amines. (B) Flowsheet of high-pressure water scrubbing

A Python interphase has been built to connect process models and LCA software. Anaerobic digestion for biogas production was modeled via the Sys-métha conversion tool (Bareha et al., 2021) whose results for biogas flow and composition were introduced to a flow sheeting software (ProSim) that simulates biogas upgrading via HPWS and CAA. Process models were developed to handle a wide range of input flows and to consider different scales. Simulation results were exported to the Python interphase and were included in Brightway (Mutel, 2017) to perform LCA (Figure 2A).

The platform has allowed to simulate the biogas production and upgrading from the renewable resources and up to biomethane and CO2 production. Initial results have already shown that some improvements could be made to reduce environmental impacts in both studied upgrading technologies. Regarding climate change, HPWS emits less kg CO2-eq than CAA (Figure 2B). The main sources of emission were the released off for HPWS, and heat utilization followed by amine's production for CAA. Depending on CO2 utilization, CAA could be more efficient since the CO2 stream has a higher purity.

Conclusions

A simulation for biogas production from agricultural resources to the upgrading to biomethane was successfully implemented in the proof-of-concept platform coupling different software for process models and LCA. Further developments will include sensitivity analysis and optimization. Regarding the case study, other technologies for upgrading, such as membrane separation will be further considered.

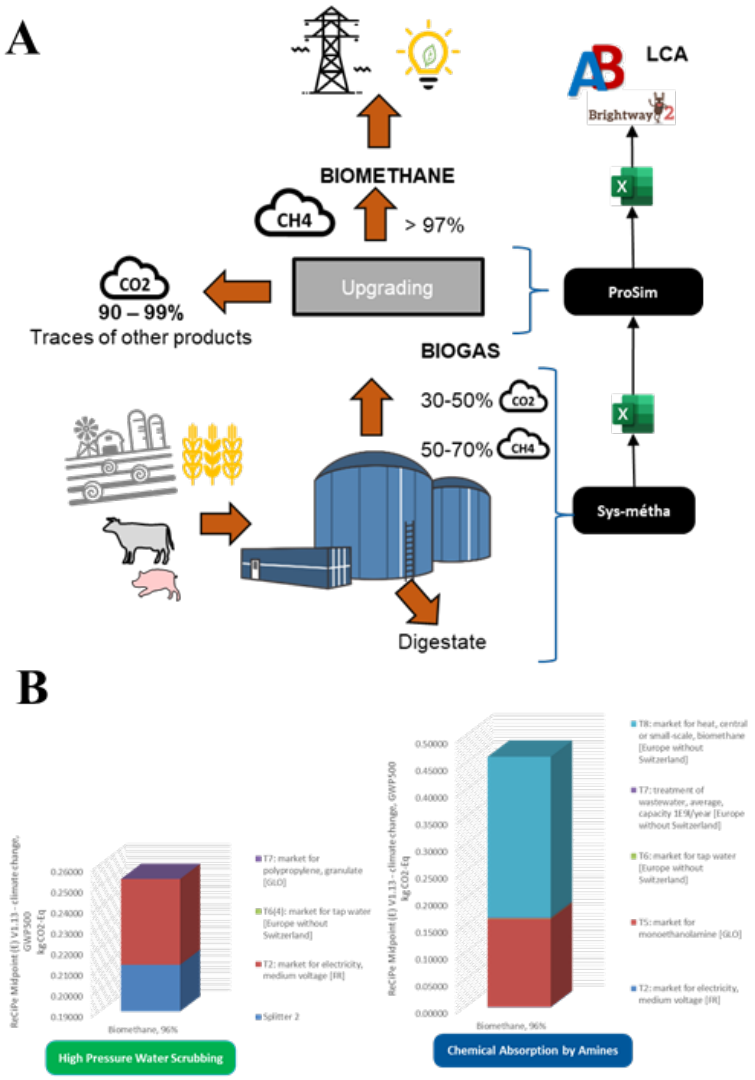

Figure 2. (A) Process model-based Eco-design framework. (B) Emissions by processes regarding the Climate Change GWP500 from the ReCiPe method V1.13.

References

Bareha, Y., Affes, R., Moinard, V., Buffet, J., Girault, R., 2021. A simple mass balance tool to predict carbon and nitrogen fluxes in anaerobic digestion systems. Waste Manag. 135, 47–59.

Bisinella de Faria, A.B., Ahmadi, A., Tiruta-Barna, L., Spérandio, M., 2016. Feasibility of rigorous multi-objective optimization of wastewater management and treatment plants. Chem. Eng. Res. Des. 115, 394–406.

Khan, M.U., Lee, J.T.E., Bashir, M.A., Dissanayake, P.D., Ok, Y.S., Tong, Y.W., Shariati, M.A., Wu, S., Ahring, B.K., 2021. Current status of biogas upgrading for direct biomethane use: A review. Renew. Sustain. Energy Rev. 149, 111343.

Mutel, C., 2017. Brightway: An open source framework for Life Cycle Assessment. J. Open Source Softw. 2, 236. 6

Systematic Planning of Constructing Hydrogen Refueling Stations in Transportation Energy Systems with the Case of South Korea

Soo hwan Kim, Jun-Hyung Ryu
Department of Energy & Electricity Engineering
Dongguk University WISE Campus, South Korea

Abstract: Hydrogen is gaining an increasing attention in the transportation sector. In order to lower its cost, it should be available as many places as possible. Hydrogen refueling station (HRS)s should be thus constructed over multiple locations. Unfortunately, it is unlikely to do so within a short time because of the heavy financial burden. It is important to develop a systematic methodology to construct them in the most efficient manner. This paper thus proposes a decision-making framework in a data-based context by using the p-median model. The case of South Korea will be presented to illustrate the applicability of the proposed methodology with some comments. Further relevant works would be followed to raise the overall performance of hydrogen supply chains with an impact on accelerating the mitigation of the global climate change in the energy systems engineering community.

Keywords: hydrogen supply chain, hydrogen refueling station, planning, optimization, p-median model.

Problem description

This problem is a hydrogen refueling station location selection problem and has an objective function to minimize the sum of the distance between the newly installed charging station and the candidate site, including the existing hydrogen refueling station. As a constraint, the maximum amount of hydrogen that the charging station can handle per day is 250kg, and the sum of the hydrogen demand at the allocated candidate site cannot exceed this. All candidate sites should be allocated to hydrogen refueling stations, and the location of existing hydrogen refueling stations should not be allocated to candidate sites for new charging stations. Number of new charging stations shall be P_n (Number of New HRS). Assuming that HRS can be operated for 14 hours a day, up to 70 hydrogen cars by assuming that 3 to 5 kg of hydrogen is charged to a car per day. The number of charged cars should be reduced when additional shutdown time should be needed to re-pressurize due to the low pressure in the storage tank. The construction cost of a HRS varies depending on the charging station's capacity, number of storage tanks, dispensers, hydrogen supply method, site, etc., and is estimated from $0.86 M to $11.8 M (Melaina and Penev, 2013). Construction costs are relatively high at 10 to 15 times the construction cost of the fossil fuel stations currently in operation. Due to the high construction cost of hydrogen refueling stations, it is impossible to build hydrogen refueling stations in all the places needed at once to meet the hydrogen demand of hydrogen cars. So the most realistic way to achieve maximum effect is to calculate the locations that hydrogen cars need first to use hydrogen refueling stations, and to build hydrogen refueling stations according to their priorities within budgetary limits. This is a very difficult problem.

The hydrogen demand (F) allocated to each candidate site was calculated by multiplying the current number of hydrogen vehicles by the average daily travel distance of 40km for drivers in Seoul and dividing the fuel efficiency of Hyundai Nexo vehicles currently distributed in Korea by 96km/kg. The calculated amount of hydrogen was again allocated by dividing by the number of candidate sites belonging to each region. In the case of Korea in 2021, most of the charging stations' facilities are 250kg/day, and if the charging capacity is ideal, up to 70 units per day can be charged based on 14 hours of operation. However, considering the failure of charging facilities, the charging of the hydrogen tank through the tube trailer is stopped, this paper limited the maximum capacity per day to 250 kg/day (C_max).

In order to calculate the hydrogen demand for Fuel cell electric vehicles(FCEV) in the case study area (Seoul), the number of hydrogen vehicles was used to estimate the minimum number of hydrogen refueling stations and hydrogen demand. In the case of Seoul, which was used as an example of Case Study, the number of registered FCEVs was 1,972 as of August 2021, and four refueling stations are in operation. Number. The amount of hydrogen required per day was calculated by multiplying the number of currently registered FCEVs presented in Table 1 by the average mileage per day and dividing it by the standard composite fuel efficiency. The calculated amount of hydrogen was used to calculate the hydrogen demand of each node and the number of hydrogen refueling stations required.

Objective

$$Minimize \quad \sum_{n}\sum_{i} D_{ni} y_{ni} \qquad (1)$$

Subject to

$$\sum_{n} y_{ni} F_n \le C_{max}\, x_i \quad \forall\, i \in I \qquad (2)$$

$$\sum_{i} y_{ni} = 1 \quad \forall\, n \in N \qquad (3)$$

$$y_n = 1 \quad \forall\, n \in P_e \qquad (4)$$

$$\sum_{i=1}^{N-P_e-1} y_n = P_n \qquad (5)$$

$$y_{ni} - x_i \le 0 \quad \forall\, n \in N,\ i \in I \qquad (6)$$

$$x_i \in \{0, 1\} \quad \forall\, i \in I \qquad (7)$$

$$y_{ni} \in \{0, 1\} \quad \forall\, n \in N,\ \ i \in I \qquad (8)$$

Table 1. Font sizes and styles

Number of HRS	Sum of distance between HRS and hydrogen demand(m)	Average distance between HRS and hydrogen demand(m)
1	2,569,950	4,707
2	2,305,971	4,223
4	1,879,251	3,442
6	1,606,200	2,942
58	1,414,023	2,590

Conclusion

In this study, we proposed the location of a HRS, a new energy source, using an existing fossil fuel gas station as a candidate site. Existing fossil fuel vehicle users are those who are likely to use vehicles that use next-generation energy sources in the future. Therefore, the existing gas station network can be converted to a hydrogen refuelling network. As of August 2021, there are 546 gas stations in Seoul and 4 hydrogen refuelling stations. Based on the current number of FCEVs, the future hydrogen demand was calculated and analysed as 25%, 50%, 100%, 150%, and 200%. The number of HRSs to be built in the future was calculated as 1, 2, 4, 6, and 8 locations. As the number of HRSs increased, the average mileage when one was built was 4,707 m, but if eight additional stations were built, it decreased by 55% to 2,590 m.

Acknowledgments

This research was supported by the Basic Science Research Program through the National Research Foundation of Korea (NRF) funded by the Ministry of Education (NRF-2020R1I1A3A04038008).

Strategic and tactical planning model for the design of perishable product supply chain network in ethiopia

Asnakech Wondimu[a,b], Ludovic Montastruc[a,b], Stéphane Negny[a,b], Shimelis Admassu[b]
[a]Laboratoire de Génie Chimique, Université de Toulouse, CNRS, INPT, UPS, Toulouse, France
[b]Addis Ababa University, Addis Ababa Institute of Technology, School of Chemical and Bio Engineering, Addis Ababa, Ethiopia

Abstract: Perishable raw materials are commonly used in process (agro-food, pharmaceutical) but the quality of these materials decrease over time, often over a short period until they become rotten. This issue raises a key concern in supply chain during storage, transportation and processing. Indeed, perishable raw materials cause huge amount of waste resulting in economic looses and environmental damages due to the increase of natural resource consumption (overproduction). To limit these losses, suppliers use quantity discount, but this strategy has also an impact on raw material deterioration due to limited production capacity. In this study, we propose a supply chain model dedicated to perishable raw materials with the goal to analyze the impacts of quantity discounts on the optimal solution. The capabilities of the model are shown through a real case study concerning the tomato supply chain in Ethiopia.

Keywords: Perishable Food Supply Chain (PFSC), Quantity discount and Supply uncertainty.

Introduction

The current world population of 8 billion and is projected to reach 9.7 billion by 2050 according to a United Nations report, in 2022.This signifies an undeniable global challenge requiring integrated food supply chain management. The food industry plays a vast role in making a significant contribution to overcoming such a challenge by providing processed food to feed 9.7 billion people within 28 years. In developing countries, such as Ethiopia food insecurity has been a severe problem since the 1970s (Brasesco et al., 2019).

Evaluating the configuration of agro-food supply chains is the best strategy to solve the supply chain inefficiencies as well as to enhance its sustainability (Barbosa-Povoa et al., 2018). However, most of the operational research focuses on tactical and operational decision levels (Soto-Silva et al., 2016). One of the recent contributions (Buiki et al., 2020) addressed strategic, tactical, and operational-level decision problems, despite the fact that supply-side uncertainty is not considered. Supply chain network resiliency improved by considering the perishability of the product after harvest (Kusumastuti et al., 2016). Quantity discount has been used to maintain the uncertainty present in the PFSC. Aside from this, (Liu et al., 2021) investigate a single-echelon supply chain considering quantity discount and its influence on the environment without considering the cost associated with an increased in processing capacity. Thus, the impact of raw material quantity discount on multi-echelon supply chains and its consequent impact on the objective function values and perishability-related issues is not considered so far.

This opens up an opportunity for the modernization of the sector, moving towards efficient supply chain management by creating a link between the farmers and agricultural companies. To address the above problems, this study uses decision support tools, MILP that minimize the overall costs of PFSC while considering the impact of quantity discount and processing capacity on the overall cost of the supply chain. Thus, increasing quantity discount while increasing processing capacity increases the overall cost but there is a need to establish a tradeoff between the cost associated with the loss of vegetables due to deterioration and cost increment due to an increase in processing capacity.

Problem statement and Model Formulation

The superstructure of the perishable food supply chain model in this work is depicted in Figure 1. The vegetable obtained from farm locations is transported to an inventory facility for preprocessing and handling. When the vegetables arrive at the inventory facility, split into two streams: one for packaging fresh vegetables, and the other one to transform them into final products to increase their shelf life. Once fresh vegetables are packed, they are directly transported to distribution centers. Part of the vegetable transported to manufacturing centers inventory is processed at location i through a process with a specific technology and capacity e for the production of the final product p. The final products could be stored at manufacturing centers and/or shipped to distribution centers. The final products that arrive at distribution centers are delivered to the customers. The assumptions made to define the problems are: locations of facilities and, their capacities are predefined (set of potential sites and, capacities for transformation processes and storages, except for the customers for which the sites are fixed), the demand is fixed, and raw material location, availability and perishability are given. Concerning the output data, the model gives: the supply chain network design, the locations and capacities of production processes and capacities, inventory levels (both for fresh vegetables and products) and, flows between the different sites.

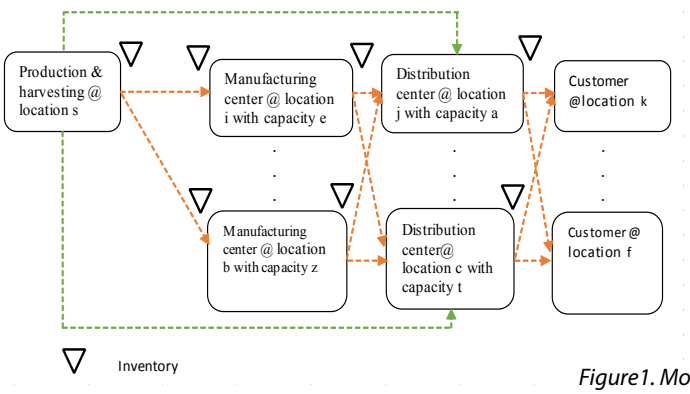

Figure1. Model Superstructure

The design of the supply chain network also gave attention to constraints and uncertainties which could affect the product's perishable characteristics. As a result, the decision variables are: location and process capacity for each possible site, the quantity of fresh vegetables obtained at suppliers, the amount of product produced in each location, shipped quantity between each stage, location and inventory level for each storage. The decision variables must respect the following constraints: Vegetable availability, mass balances at each stage both for the fresh vegetable and the final products. Aside from this, the model also considers product perishability, the fulfilled demand, capacity constraints and, unicity for storage and production process. The objective is aimed to minimize the total annual operating cost. As a result, we obtain a MILP problem solved with CPLEX.

Case study, Result and Discussion

The model capabilities were tested with a real case study, i.e. the tomato supply chain in Ethiopia considering the existing production capacity. The model for this case study had 2870 constraints and 2354 decision variables.

One of the main results of the optimization is that there is no fresh vegetable and product storage at the manufacturing and distribution centers respectively. This solution is very risky because a supply disruption is highly probable. Thus, constraints on a lower bound for storage are added. But increasing storage level enhance decay of raw material. To avoid economic losses and to reduce waste due to this deterioration, suppliers sometimes use discount to enhance sales of raw material. But quantity discount also causes deterioration of raw materials due to limited production capacity (Liu et al., 2021). Thus, there is a tradeoff between profit (increase of OPEX and CAPEX to increase production capacities) and waste due to deterioration. Figure 2. shows the impact of processing capacity on the value of objective function considering different upper value quantity discounts. The value of the objective function f1 is the cost obtained when the manufacturer bought minimum upper value quantity to satisfy the demand. Similarly, the objective function value f2 resulted when the manufacturer bought vegetable at maximum upper value based on the available vegetable.

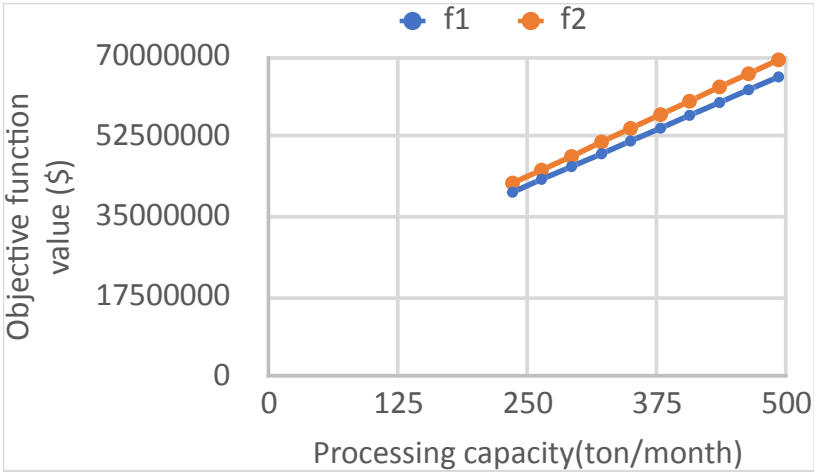

Figure 2. The impact of processing capacity on objective function

Conclusion

The suggested model is crucial to use as a platform for decision maker that addresses tradeoff between the added cost due to an increase production capacity and loss of food due to deterioration. Further studies of this work will encompass the integration of quality of food product and social dimensions.

References

A.P. Barbosa-Póvoa, C. Silva, A. Carvalho (2018). Opportunities and challenges in sustainable supply chain: An operations research perspective. European Journal of Operational Research 268, 2, 399-431.

Biuki, M., Kazemi, A., & Alinezhad, A. (2020). An integrated location-routing-inventory model for sustainable design of a perishable products supply chain network. Journal of Cleaner Production, 260, 1-14.

Brasesco, F., Asgedom, D., Casari, G. (2019). Strategic analysis and intervention plan for fresh and industrial tomato in the Agro-Commodities Procurement Zone of the pilot Integrated Agro-Industrial Park in Central-Eastern Oromia, Ethiopia. Addis Ababa.

Kumastuti, R.D., van Donk, D.P., & Teunter, R. (2016). Crop related harvesting and processing planning: a review: International Journal of Production Economics,174,76-92.

Liu L. Zhao Q., D.R., Ernesto, G.Santibanez,X.Xunzhuo (2021).Sourcing and production decisions for perishable items under quantity discounts and its impacts on environment. Journal of Cleaner Production 317,1-13.

Soto-Silva, W. E., Nadal-Roig, E., González-Araya, M. C., & Pla-Aragones, L. M. (2016). Operational research models applied to the fresh fruit supply chain. European Journal of Operational Research, 251(2), 345–355

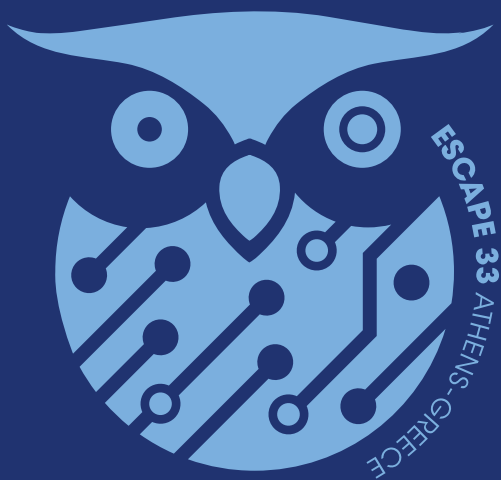
ESCAPE 33 ATHENS-GREECE